The comparative performance and behaviour of concrete elements containing glass-fibre reinforced plastic reinforcing bars.

ULAS, Esref M.

REFERENCE

The comparative performance and behaviour of concrete elements containing glass fibre-reinforced plastic reinforcing bars

Eşref Muzaffer Ulaş

A thesis submitted in partial fulfilment of the requirements of Sheffield Hallam University for the degree of Master of Philosophy

November 2001

^ g t PHAL*LAKuj*^ *?*

ABSTRACT

Corrosion of steel reinforcement is a major concern in concrete construction, particularly in aggressive environments. Therefore corrosion resistant materials such as fibre composites are becoming increasingly feasible as an alternative concrete reinforcement. There are relatively few reported design guidelines for fibre composites in concrete. Hence, there is an urgent need for research and development to extend existing guidelines and standards such as those produced by the UK Institution of Structural Engineers and the ACI Committee (US), to encourage the wider use and acceptance of fibre composites as an alternative to steel in reinforced concrete elements.

This investigation compares the behaviour and properties of a range of reinforced concrete beams under two point loading comprising different concrete grades and types using both steel and Glass Fibre Reinforced Plastic (GFRP) as primary and secondary reinforcement. A variety of conventional and 'novel' rebar configurations were used to assess their effect upon material efficiency and load capacity. Compressive and tensile strength and elastic moduli of all component properties were measured together with load, deflection, rebar and concrete strains on the reinforced concrete beams. Health and safety concepts through a risk assessment process were introduced for the testing at an early stage of the investigation.

Principal measures of beam performance include the ultimate load capacity, stiffness and failure modes together with a 'performance quotient'; a mathematical expression derived as an efficiency comparator for beams of different types and composition. Photographic and video records were also used to monitor behaviour throughout. Experimental measurements generally showed good agreement with the corresponding theoretical, quasi-theoretical and design based values although the latter tended to overestimate the structural performance of the beams. In general, load capacity increased with increase in main rebar area but was affected to a lesser extent by concrete strength. The beams reinforced with steel had a greater load capacity than those reinforced with GFRP. However, GFRP reinforced beams generally displayed a greater capacity to absorb energy than steel but exhibited reduced stiffness at any given load although this was enhanced by the inclusion of glass fibres in the mix. Cracks in the GFRP reinforced beams were usually larger and deeper compared with those in the equivalent steel reinforced beams. Failure of the more lightly reinforced steel beams, including one GFRP beam, were predominantly in 'flexure'. The more heavily reinforced steel and the remainder of the GFRP reinforced beams exhibited mostly 'shear-bond' type failure. The 'novel' rebar geometry proved to be a simple, efficient and viable alternative to conventional rebar configurations in terms of load capacity and preferred mode of failure.

It is suggested that further developments and applications could focus on small reinforced concrete elements such as lintels in aggressive environments and further refinement of the 'performance quotient' concept.

DEDICATION

To my precious mother Ayşe Aysel and my father İbrahim Mesut for their love, support and prayers...

'Pek Değerli annem Ayşe Aysel ve babam İbrahim Mesut'un sevgi, destek ve dualarma hitaben...'

Declaration

I hereby declare that no portion of the work referred to in this thesis has been submitted in support of an application for another degree or qualification of this or any other university or other institution of learning. All sources of information have been duly acknowledged.

Eşref Muzaffer Ulaş

November 2001

ACKNOWLEDGEMENTS

Firstly, the Author would like to express his deep and sincere gratitude to his supervisor, Mr Clifford Ellis for his continuous supervision, encouragement, support and valuable suggestions throughout the preparation of this work.

The Author would like to thank Prof. Pritpal S. Mangat for recommending him to undertake this research and recognising his potential in this field. The Author also would like to thank Dr. Fethi Al-Shawi for his help.

The Author appreciates the assistance of the IT and the technical staff, David Flatt, Howard Skipworth, Simon Outhwaite, Robert Skelton, Geoff Harwood, John Bickers, Peter Lonsbrough and Kevin Mason of the School of Environment and Development (former School of Construction).

The Author is very grateful for financial supports through teaching and the research studentship over the years provided by the school at Sheffield Hallam University.

Thanks also go to all my past and present colleagues and friends at Sheffield Hallam University in particular, my comrades Miles Seaton, Finbar O'Flaherty and Feridun Duman, my mentors Sophie Maluski and Marinela Colina, Margaret Godwin (the best PA), Edita Varga, Shirley Gunee for their help and many happy memories over the past years. I wish them and their families more happiness in the future.

The Author would like to especially thank to a very special person, Patricia Dobson (tennis champion of Bahamas in 1980s) for her love, encouragement, patience, teaching me tennis and being my scuba diving 'buddy'. You are my best friend!

Table of Contents

LIST OF PUBLICATIONS

1. A paper published in the 'Proceedings of International Conference, Concrete in Mankind', Dundee, Scotland, 1996.
2. An abstract published in 'The Institution of Structural Engineers Young Researcher's Conference', London, UK, 1999.
3. A poster presented in 'Science & Engineering Technology (SET2000) in House of Commons', London, UK, 2000.

List of Tables

List of Figures

NOTATION

The definitions of the symbols used in the thesis are given below.

$\sigma_{st/gfrp\ actual\ cr}$: experimental stress in the reinforcing bars at the cracked section (MPa)

$f_{st/gfrp}$: stress in the reinforcing bars obtained from tensile test (MPa)

f_{yv} : charecteristic strength of mild steel stirrups (MPa)

$v_{max\ theo}$: theoretical ultimate shear strength of the beam (MPa)

$v_{s\ actual}$: actual ultimate shear strength of the beam based on shear force diagram (MPa)

f_c : concrete cube strength (MPa)

$E_{st/gfrp}$: modulus of elasticity of the reinforcorcing bars (GPa)

E_c : modulus of elasticity of the concrete (GPa)

$\varepsilon_{st/gfrp\ theo\ uncr}$: theoretical strain in the reinforcing bars at the uncracked section

$\varepsilon_{st/gfrp\ actual\ uncr}$: experimental strain in the reinforcing bars at the uncracked section

$\varepsilon_{st/gfrp\ theo\ cr}$: theoretical strain in the reinforcing bars at the cracked section

$\varepsilon_{st/gfrp\ actual\ cr}$: experimental strain in the reinforcing bars at the cracked section

ε_{co} : the maximum concrete compression strain

ε_{c1} : measured strain at the first DEMEC disk

ε_{c2} : measured strain at the second DEMEC disk

ε_{c3} : measured strain at the third DEMEC disk

ε_{c4} : measured strain at the fourth DEMEC disk

ε_m : difference between measured strains at the fourth and the third DEMEC disks

$M_{theo\ uncr}$: theoretical bending moment at the uncracked section (kNm)

$M_{actual\ uncr}$: experimental bending moment at the uncracked section (kNm)

$M_{theo\ cr}$: theoretical bending moment at the cracked section (kNm)

$M_{actual\,cr}$: experimental bending moment at the cracked section (kNm)

$F_{initial}$: the initial visible crack load of the concrete beam (kN)

F_{max} : the failure load of the concrete beam (kN)

w : distributed load (kN/m)

$\Delta_{theo_{uncr}}$: theoretical deflection at the uncracked section (mm)

$\Delta_{theo_{cr}}$: theoretical deflection at the cracked section (mm)

$\Delta_{actual_{uncr}}$: experimental deflection at the uncracked section (mm)

$\Delta_{actual_{cr}}$: experimental deflection at the cracked section (mm)

c_{min} : minimum cover to the reinforcing bar (mm)

$w_{max_{theo}}$: estimated maximum crack width based on the theoretical formula (mm)

w_{L_1} : crack width based on measured strain at the third DEMEC disk (mm)

w_{L_2} : crack width based on measured strain at the fourth DEMEC disk (mm)

$w_{L_{average1}}$: average maximum crack width (mm)

$\chi_{theo\,uncr}$: theoretical neutral axis depth at the uncracked section (mm)

$\chi_{actual\,uncr}$: experimental neutral axis depth at the uncracked section (mm)

$\chi_{theo\,cr}$: theoretical neutral axis depth at the cracked section (mm)

$\chi_{actual\,cr}$: experimental neutral axis depth at the cracked section (mm)

a_1 : fixed distance from top edge of the beam to the first DEMEC disk (mm)

a_2 : fixed distance from top edge of the beam to the second DEMEC disk (mm)

a_{cr} : diagonal distance from the bottom edge of the beam to the edge of the reinforcing bar (mm)

b : width of the concrete section (mm)

d : effective depth of the concrete section (mm)

h : overall depth of the concrete section (mm)

D : diameter of reinforcing bar (mm)

e : fixed distance between the two loading points (mm)

L_s : fixed distance for span (mm)

L : fixed distance from the loading point to the end of the beam (mm)

s_v : spacing of stirrups along the beam (mm)

$s_{v_{max}}$: maximum spacing of stirrups along the beam (mm)

$A_{st\,/\,gfrp}$: area of reinforcing bars (mm^2)

A_{sv} : the cross sectional area of the two legs of the strirrup (mm^2)

$I_{theo\,uncr}$: theoretical second moment of area of the uncracked section (mm^4)

$I_{actual\,uncr}$: experimental second moment of area of the uncracked section (mm^4)

$I_{theo\,cr}$: theoretical second moment of area of the cracked section (mm^4)

$I_{actual\,cr}$: experimental second moment of area of the cracked section (mm^4)

$\left(\frac{1}{r_b}\right)_{theo_{uncr}}$: theoretical curvature of the beams at the uncracked section (1/mm)

$\left(\frac{1}{r_b}\right)_{theo_{cr}}$: theoretical curvature of the beams at the cracked section (1/mm)

$\left(\frac{1}{r_b}\right)_{actual_{uncr}}$: experimental curvature of the beams at the uncracked section (1/mm)

$\left(\frac{1}{r_b}\right)_{actual_{cr}}$: experimental curvature of the beams at the cracked section (1/mm)

$\rho_{concrete}$: density of concrete (kg/m^3)

ρ : tension reinforcing bars ratio (%)

k_1 : a constant value (1) given in BS8110

k_2 : a calculated value $\left(\frac{f_c}{25}\right)$ given in BS8110

α_e : modular ratio

K : a constant value based on the shape of bending moment diagram

Q_p : performance quotient

n_s : number of stirrups

CHAPTER 1

1. Introduction

1.1 Background

The development and innovations that have been achieved in the application of concrete over the centuries are remarkable. According to the archaeological excavations in former Yugoslavia it has been found that the earliest application of concrete was in floors and it is dated 5600 BC[1]. The Egyptian, Greek and Etruscans civilisations produced concrete in lime mortar composition before the Romans introduced and developed Pozzolonic cement in 75 BC from a red volcanic powder near Naples. The invention of Ordinary Portland Cement (OPC) which is widely used in today's concrete structures, was in 1824 by an English man, Joseph Aspdin.

The presence of bronze strips and rods as reinforcing material in some concrete constructions is dated between 300BC-500AD, and may suggest that the Romans had first observed the limitation of concrete i.e. being strong in compression and weak in tension. A degree of enhancement in the tensile strength of concrete by using bronze reinforcement was achieved but the Romans soon realised that the structure had started having cracks and spalling had occurred. This was principally due to the higher coefficient of thermal expansion of bronze compare to concrete[2]. The practice of Reinforced Concrete (RC) using a mesh of iron rods and wires became clear in early 1830 and became common between 1848-1897. Eugene Freyssinet (France) discovered another way to overcome the shortcoming of concrete for sustaining flexural loads and introduced prestressed concrete to the construction industry in 1930. The use of prestressing on any scale in Britain was after high strength tensile steel became readily available in the 1940s.

The construction methods and speed of building of structures improved over the years. Today, RC is claimed to be the major construction material in most civil engineering structures and bridgeworks. However, as the quantity of RC increased so did the scale of the problems associated with durability of the material. These problems can be separated into two categories. The ones in relation to the defects that develop in the

actual structure and the substructure because of the use of inferior materials or poor workmanship.

The other one, which is the major problem in structural concrete, is the corrosion of steel reinforcement. This occurs when RC is exposed to weathering and it progresses quickly particularly in salt contaminated concrete structures i.e. in marine and coastal, highways and bridges when salt and de-icing chemicals are used or in chemical plants.

The complete discussion of the processes of corrosion together with the techniques available to control corrosion is beyond the scope of this research considering the processes and the techniques are subjects for investigation themselves. Therefore, they will be described in brief for comprehending and appreciating the complexity of the problem.

The corrosion or rusting of steel is a complex electro-chemical process that occurs with a flow of current from the reactive anodic region to the un-reactive cathodic region of steel. The sum of these reactions is given by the following equation:

$$4Fe + 3O_2 + 2H_2O = 2Fe_2O_3\ H_2O \quad ^{3}$$

i.e. (Iron/Steel) + (Oxygen) + (Water) = (Rust)

It can be seen from above that the corrosion occurs when oxygen and water are present. This means that the rate of corrosion is directly related to the oxygen and water i.e. as the availability of oxygen and water increases, the rate of corrosion increases as well. The presence of atmospheric contaminants such as carbondioxide, chlorides and sulphates also has major effects on corrosion rates.

Carbonation caused by the steady diffusion of carbondioxide (CO_2) into the concrete, takes place very slowly, if concrete has low permeability. This can be achieved by well-compacted concrete, which has a low water/cement ratio. The depth of carbonation in a good quality concrete is between 10 and 20mm after years of exposure[4]. Chlorides and sulphates both increase steel corrosion rates. Chlorides put

steel reinforcement at risk quicker than carbonation[5]. The main source of chlorides comes from salt. This means that the highly aggressive environments such as marine and coastal structures together with highways where de-icing salt used, are more susceptible to corrosion.

The source of sulphates comes from the ground. When they react with water they become active and produce acidic solution which destroys the passivity of steel in the concrete. The most common places where a high level of sulphates attacks concrete are industrial environments.

The concrete cover plays an important role in the protection of steel against corrosion. If the concrete cover is insufficient the steel rusts with a loss of some of the cross-sectional area. This leads to disruption and spalling of concrete. The corrosion of steel usually gives warning through cracks, which appear, along the location of reinforcement in the concrete with rust staining. However, in some cases the corrosion of steel spreads throughout the structure without any warning resulting in collapse[6]. The damage caused by the corrosion of steel is usually localised and repair is possible but very expensive. It has been reported that approximately £500M is spent each year on concrete repair in the UK[7] and 42% of bridges in the USA need to be repaired[8]. The estimated cost of the repair bill on parking structures in Canada is $4 to $6 billion and on highway bridges in the USA is $50 billion[9]. This clearly illustrates the scale of the problem.

A considerable amount of research has been carried out by different groups and organisations around the world in finding out a better way of avoiding concrete deterioration caused by the corrosion of steel. Initially, improving the concrete by using high cement content and designing low water/cement ratio mixes together with improved quality control during and after the concrete placement play a very important part in providing adequate durability of concrete.

There are several techniques available for controlling the corrosion of steel reinforcement. In the 1970s, the surfaces of concrete bridges in Germany and USA were coated with silanes to prohibit water[10]. Epoxy-coated reinforcement has been

used in bridges in North America since 1973[11] and has been studied and used in Europe including Britain, Norway and Holland since the 1980s[12]. The cathodic protection techniques have been developed and applied to a number of bridges in the USA and Canada[13]. Stainless steel has been developed in the UK and USA since 1910 and used in many structures[14].

All these present techniques have inherent problems in relation with their use and application. Most of them are expensive and need continuous maintenance. Besides, whichever technique is employed the core material which is vulnerable to corrosion is still present and that is steel reinforcing bar.

Therefore, it seems reasonable to seek a solution which involves the substitution of conventional steel with a material that is immune to corrosive environments and is able to extend the service life and lead to lower maintenance costs. Fibre Reinforced Plastics(FRP) are ideal candidates for this substitutional material. These composites have been developed and used in the aerospace industry for more than 30 years as a substitute for metals and alloys. Research and development was first realised in the early 1950s by German Ministry of Defence engineers exploring the possible uses of glass fibre reinforcement for civil engineering[15]. Since then, one area of international research and development is the use of fibre composites in the form of corrosion resistant FRP reinforcing bars primarily used in prestressing to make use of their high tensile strength[15]. International works suggest that unstressed systems have been explored, but the mechanical behaviour of FRP reinforcement in concrete is still not well known. The contribution of these bars to the flexural and shear capacities of concrete needs to be defined. Therefore, determination of their behavioural characteristics is essential for enhancing the performance and the efficiency of concrete elements reinforced with FRP rebars.

1.2 Research Aims and Objectives

The overall investigation is based on the feasibility of using a relatively low cost glass FRP (GFRP) bar, of a type, which has been successfully applied to prestressed concrete, as reinforcement in concrete.

Principal Aims

The principal aims of this work is to:

- review the practice of using GFRP as a reinforcement in concrete elements and structures and investigate the scope for improving its performance
- postulate simplified novel rebar configurations and compare their performance with that of conventional ones for a range of concrete grades and types
- evaluate and compare the material/performance efficiency over an optimal range of configurations rebar types and concrete grades tested in the investigation
- test the validity of existing design criteria for assessing and predicting the performance of GFRP reinforced elements

Objectives

The objectives of this work cover the following aspects:

- Review previous research, applications and limitations of FRP and GFRP as reinforcement for concrete
- Review existing test methods and assessments of performance
- Compare the fundamental behaviour of high tensile steel and GFRP as simple reinforcement configurations for a range of concrete grades
- Investigate the use of simple novel rebar geometries to enhance performance
- Apply an idealised rebar geometry to a given concrete for optimising efficiency
- Assess and compare the performance of conventionally reinforced concrete beams using GFRP and high tensile steel rebar singly and in combination
- Compare and contrast the performance and material efficiency of the range of concrete elements tested
- Identify key modifications to design parameters for application to GFRP reinforced elements

Although, FRP reinforcing bars have already been used in structural applications the performance of FRP reinforced concrete is not fully understood. In order to establish the objectives above, firstly, it was clearly necessary to identify the differences in mechanical properties of both conventional steel and the FRP bars. Secondly, it was also necessary to select certain criteria such as load and deflection capacities, failure mode together with the cross section of the concrete element to give a proper definition of performance.

1.3 Thesis Layout

The thesis is divided into 8 Chapters. It presents a comprehensive literature review on the subject in Chapter 2. Previous research referred to in this thesis (wherever possible) is listed at the end of each Chapter. An introduction to the thesis is given in Chapter 1.

Details of the experimental programme including the equipment and instrumentation used to monitor 'two-point loading' tests in the laboratory are given in Chapter 3. The comparative data based on the mechanical properties of steel and FRP is also included in this Chapter.

The results obtained from the 'two-point loading' tests on the simply supported concrete beams, the analysis of all data and the discussions are included in Chapters 4, 5, 6 and 7 respectively.

Conclusions and proposals for future research presented in Chapter 8 and publications and presentations to date arising from the results of this research programme are given at the end of the thesis.

1.4 REFERENCES

[1] Cement and Concrete Association, Highlights in the History of Concrete, pp1-43.

[2] Doran D K,Construction Materials Pocket Book, ISBN 0750616660, pp80-134.

[3] The Prevention of Corrosion on Structural Steels-BSC Publication, 1985.

[4] Illston J M, Dinwoodie, J M & Smith, A A, The Nature and Behaviour of Structural Materials, ISBN 0-442-30144-6, 1979, pp553-615.

[5] Leeming M B, Concrete in the Oceans: co-ordinating report on the whole programme, Offshore Technology Report OTH 87, 248, HMSO, 1989.

[6] Clarke J L, The Need for Durable Reinforcement, Alternative Materials for the Reinforcement and Prestressing of Concrete, ISBN 0751400076, 1993, pp1-33.

[7] Swiss Bank Corporation (STOCKBROKERS), Quarterly Building Bulletin, 26 January 1989, London, pp5-7.

[8] Chartier G, People Who Drive on Glass Bridges, NEWS http://www.nsf.gov/od/lpa/news/press/pr9569.htm, 1995, pp1-2.

[9] Bedard C, Composite Reinforcing Bars: Assessing Their Use in Construction, Concrete International, January 1992, pp55-59.

[10] Prenchio W F, Durability of Concrete Treated with Silanes, Concrete International, V8, November 1988.

[11] McKenzie M, The Effects of Defects on the Durability of Epoxy-coated Reinforcement, Transportation Research Board/National Research Council, No 403, March 1993, pp17-28.

[12] Schiessl P & Reuter C, Epoxy-Coated Rebars in Europe:Research Projects, Requirements and Use, Transportation Research Board/National Research Council, No403, March 1993, pp29-45.

[13] Weyers R E & Cady PD, Cathodic Protection of Concrete Bridge Decks, Journal of American Concrete Institute, Nov-Dec 1984, pp618-622.

[14] Leffler B, Stainless Steels and Their Properties, Avesta Sheffield AB Research Foundation, 1996, pp1-36.

[15] Rehm P et al, High Performance Glass Fibre Composite Bars as Reinforcement in Concrete and Foundation Structures, Strabag-Bayer.

CHAPTER 2

2. LITERATURE REVIEW

2.1 Fibre Reinforced Plastic(FRP) Reinforcement

2.1.1 Fibre Types & Forms

Definition of fibre: A fibre may be defined as a linear filament of material with a more or less uniform, small cross-section of thickness or diameter less than 100μm and aspect ratio (ratio of length to thickness or diameter) greater than 100[1]. The typical tensile properties of fibre materials are shown in *Appendix 1*[1]. The classifications of the fibres are shown in *Figure 2.1*.

Background

The natural polymer fibres (wool, silk, and cotton) have been known and used extensively in the textile industry for thousands of years. The FRP industry started in 1940 due to the electronic needs of World War II in respect of manufacture of the radars for military aircraft[2]. Carbon Fibre Reinforced Plastic (CFRP) and Aramid Fibre Reinforced Plastic (AFRP) were developed and used mainly in the aerospace industry. They have been introduced to concrete structures as reinforcements subsequently.

Composites can be split into two categories: those with long fibres (continuous fibre-reinforced composites) and those with short fibres or staples (discontinuous fibre-composites). Fibre composites contain two components, fibre and resin. Those of commercially available fibres used in the production of grids, rods, plates and ropes for concrete reinforcement cover the following range:

- Carbon
- Aramid
- Glass

Figure 2.1 The classification of the fibres by type.

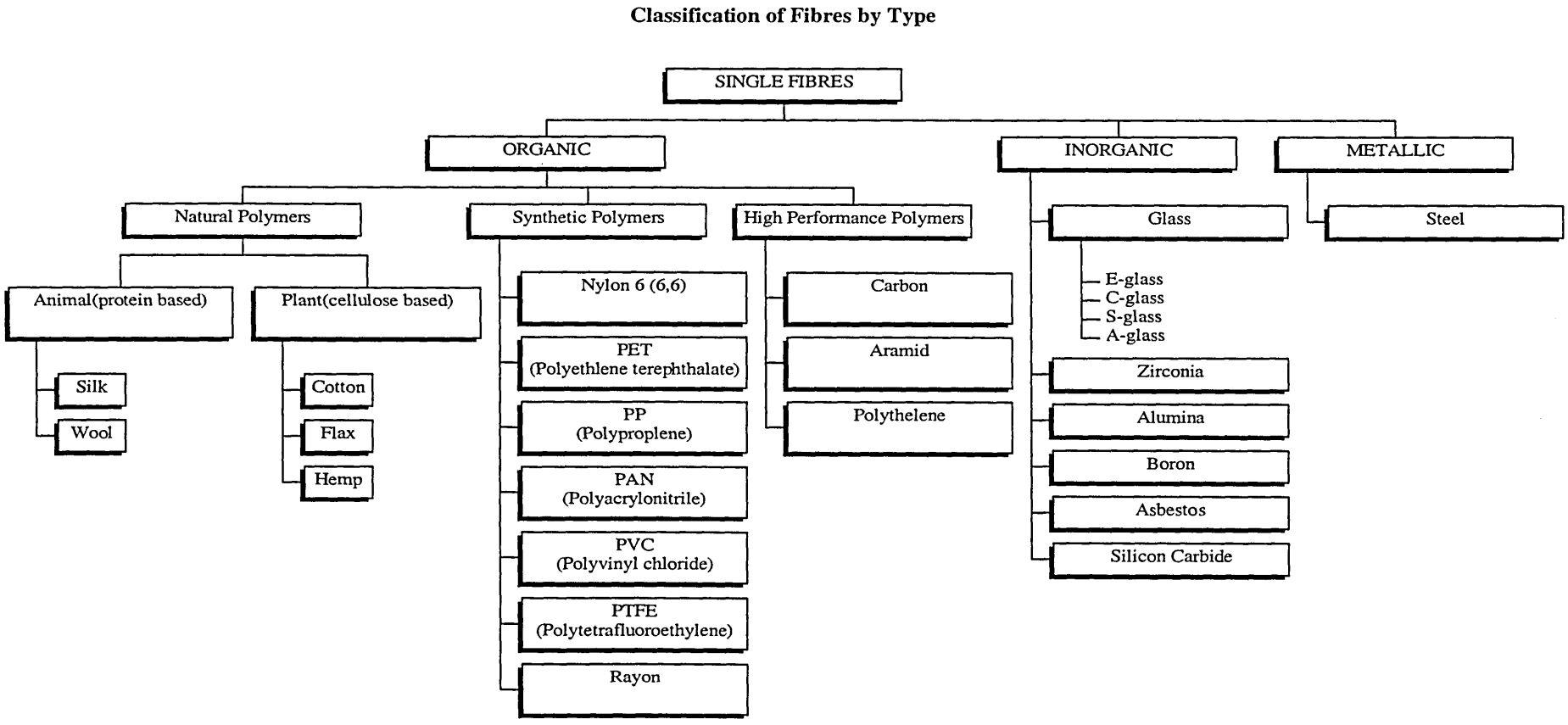

2.1.1.1 Carbon Fibres

Background

Carbon fibres are black colour and are produced from organic cellulose based precursors such as cotton, rayon, PAN (Polyacrylonitrile) being carbonized without melting followed by graphitisation at high temperatures of 1000 °C -2000°C and of 2500 °C -3000°C respectively. Apart from offering higher modulus and strength than all reinforcing fibres, carbon fibres are not affected by stress corrosion at room temperature unlike glass and polymeric fibres. Thomas Edison first achieved the transformation of cotton and bamboo strips in to carbon fibres to use as filaments in incandescent electric lamp[3].

Applications of Carbon Fibres

Carbon fibres were mainly developed for the aerospace industry and have been used in automotive, mass transportation (railways), chemical industry (water pipelines) and medical (bone plates)[4].

2.1.1.2 Aramid Fibres

Background

Aramid fibre is a generic name for synthetic organic fibres called aromatic polyamide fibres. Trade name of Kevlar was commercialised by Du Pont Company in 1972 in the USA and it is the most commonly used fibre throughout the world. Several other commercial aramid fibres are namely Nomex (USA), Teijinconex and Technora (Japan) and Twaron (Holland)[5]. Kevlar fibres are bright yellow colour and are in different types such as Kevlar (used as rubber reinforcement), Kevlar 29 (used for ropes, cables, coated fibres, architectural fabrics and ballistic protection fabrics, Kevlar 49 (used as reinforcement for epoxy, polyester, and other resins).

Applications of Aramid Fibres

Kevlar fibers have been produced in many industries to use in applications such as bullet-proof vests, industrial gloves, ropes and cables, tyres, pressure hoses, conveyor belts, boat hulls, friction products, various forms of composites[6].

2.1.1.3 Glass Fibres

Background

Ancient Egyptians were the first civilisation, which made glass. The idea of fibre glass was first described by Robert Hooke in 1665 and the modern industry started recognising the use of it as plastic reinforcement, in the 1930s when the Owens-Corning Fibreglass Corporation was set up in the U.S.A[7]. Glass fibre is a generic term like carbon fibre or steel. Common glass fibres are silica based (50%-60% SiO_2) and contain a host of other oxides of calcium, boron, sodium, aluminium and iron. *Table 2.1* contains the compositions of some commonly used glass fibres. In borosilicate E-glass, E stands for electrical and it was originally developed for electrical insulators having a good strength and reasonable elastic modulus and better resistance to water and to acids than the standard alkali soda lime silica glass (A-glass) as used in windows or containers. In C-glass, C stands for corrosion and it has a better resistance to chemical corrosion than E-glass. In alumino-magnesium silicate S-glass, S stands for the higher silica content and it has higher strength and elastic modulus than other types plus it is able to withstand higher temperatures than other glasses but also is more expensive.

Table 2.1 Approximate chemical compositions of some glass fibres (wt %)

	A-glass	C-glass	E-glass	S-glass
SiO_2	72-72.5	60-65	52-56	64.3-65
Al_2O_3	0.6-1.5	2-6	12-16	24.8-25
CaO	9-10	9-10	16-25	0.01
MgO	2.5-3.5	3-4	0-6	10-10.3
Na_2O	13-14.2	7.5-12	0-1	0-0.27
B_2O_3	-	2-7	8-13	-

The most often used glass composition is E-glass and it is available in a variety of forms and is the least expensive. C and S glasses are used when high chemical resistance, stiffness and strength are the main requirements.

Applications of Glass Fibres

Glass fibres have been used in the automotive, electronic and aircraft industry. Their use in civil enginering started in the mid 1980s. The main application of glass fibres in forms of plastic reinforcing bars and grids are in marine structures, chemical plants, bridge decks and precast highway traffic barrier walls.

2.1.1.4 Steel Fibres

Background

Steel fibres were first patented in the USA in 1962[8]. They are usually manufactured by three processes (1) by cutting cold drawn wire, (2) by slitting steel sheet, (3) by extracting them from a pool of molten steel (melt extract) for producing straight or deformed shapes having circular, rectangular or irregular cross sections.[9] [10] Depending on their grade, the tensile strengths of steel fibres range from 345MPa to 2070 MPa. Their sizes range from 13 x 0.25mm to 64 x 0.76mm. Many researchers worked on using steel fibres in concrete in order to reduce cracking by making the concrete tougher (enhanced energy absorption) and more ductile. Also, using steel fibres substantially increases shear and tensile strength of concrete[11].

Applications of Steel Fibres

The proven applications of steel fibre reinforced concrete include shotcrete, precast concrete, slabs and floors, pavements, seismic structures and repairs.

2.1.1.5 Comparison of Carbon, Aramid and Glass Fibres

The Table in *Appendix 2* adopted from *Yang*[5] shows the comparison of selected high performance fibres. Fibre flexibility is associated with modulus of elasticity and the diameter. The diameter becomes the dominant parameter controlling the flexibility in high-modulus fibres. For a given E value, the smaller the diameter the more flexible it is.

Kevlar aramid fibres have rather poor strength properties in compression compared with those in tension although this can be solved by utilising cost effective (based on specific properties) advanced hybrid composites such as Kevlar/carbon or Kevlar/glass.

Carbon fibres offer the highest strength and elastic modulus amongst all reinforcing fibres. They are not susceptible to stress corrosion or stress rupture failure at room temperature unlike glass and polymeric fibres.

Glass fibres are not moisture absorbent and are not degraded by exposure to sunlight. They have a very high resistance to chemicals and can be used up to 500 °C and will not burn. They are the least expensive fibres compared to carbon and aramid fibres.

Kevlar aramid and high strength polyethylene fibres are employed for both rigid and flexible structures whereas carbon and glass fibres are mostly limited to the reinforcement of rigid composites. Glass and carbon fibres are definitely the first choice for applications at exteremely high temperatures. Another important characteristic of these high performance fibres is their rather low values of strain (generally less than 2-3%) to fracture. For this reason, it is necessary to distribute these low ductility slender fibres into a binding medium called a resin matrix. The function of the matrix is not just for holding the fibres together but also for transmitting the applied loads to the fibres. The nature of fibre and resin matrix bonding also influences the strength and toughness of a composite.

2.1.2 Resin Types

Fibre composites are formed in a resin matrix, which can be either:

- thermosetting (e.g. epoxy-Araldite, phenolformaldehyde-Bakelite, polyester, vinlyester, polyaromatic, urea formaldehyde).
- thermoplastic (e.g. polycarbonate, polythelene, polypropylene, polystyrene, polyvinyl chloride (PVC), polytetrafluoroethylene (PTFE), polymethyl methacrylate (Perpex or Plexiglass), polyamides (Nylon).

Background

Thermosetting resin phenolformaldehyde (PF) as Bakelite was the earliest one (1907) which was developed in the modern thermoplastic resin industry dating from the 1920s[12]. The selection of a resin for FRPs depends upon the requested composite performance. In this case, there are several factors to be considered including cost, density, interfacial bonding, tensile, compressive and flexural properties, compatibility of thermal expansion, environmental resistance to solvents, moisture, temperatures and processability. Resins are often selected on the basis of their modulus of elasticity. In general terms, the characteristics of low elastic modulus resins (soft

resins) are relatively high breaking strain, good flexural properties and good bonding whereas high elastic modulus resins (rigid resins) offer high compressive strength, brittleness and relatively poor bonding. In general, the resin matrix should bond well with fibres, protect the fibres from permanent damage and be capable of transferring large forces as a result of high shearing strength[13].

2.1.2.1 Thermosetting

Thermosetting resins supplied as liquids, pastes and solids harden upon application of heat. They display good resistance against creep and severe environmental conditions (heat, cold, radiation, humidity and chemical atmospheres)[14]. Typical physical and mechanical propertis of commercial matrix materials[15] are given in *Table 2.2.*

Table 2.2 Typical physical and mechanical properties of thermosetting resins

	Polyester	Epoxy	Vinylester
Tensile strength(MPa)	20-100	55-130	70-80
Tensile modulus(GPa)	2.1-4.1	2.5-4.1	3-3.5
Ultimate strain(%)	1-6	1-9	3.5-5.5
Poisson's ratio	-	0.2-0.33	-
Density(kg/m^3)	1000-1450	1100-1300	1100-1300
T_g(°C)	100-140	50-260	90-140
Coefficient of Thermal Expansion CTE (10^{-6}/°C)	55-100	45-90	21-73
Cure shrinkage(%)	5-12	1-5	5.4-10.3

Comparison of Polyester, Vinylester and Epoxy Resins

Both polyester and vinlyester resins have low viscosity and they cure fast so that they are well suited for manufacturing FRPs. Polyesters are resistant to fire, moisture, acids, and alkalines, but are degraded by chlorinated solvents. Vinylester resins have advantages over polyester resins in terms of chemical resistance and high temperature resistance. They are easier to handle during processing than polyester and epoxy resins, and have better resilience than polyester but they are more expensive than polyester resins. Epoxy resins which can be used in all FRP manufacturing processes, have high strength and creep resistance, strong adhesion to fibres, chemical and solvent resistance, good electrical properties, high glass transition temperature, and low shrinkage and volatile emission during curing. Epoxy resins are most often used

in combination with Kevlar aramid fibres. Thermoset composites are generally stiffer, more thermally stable and brittle than thermoplastic composites.

2.1.2.2 Thermoplastic

Thermoplastic resins are those that melt or soften upon application of heat. They are also available in the form of liquids, pastes and solid. In contrast to thermosettings, thermoplastic resins display weakness against creep and severe environmental conditions. Their strength and stiffness are lower than thermosetting resins. They are employed for fast assembly packaging materials and plastic film laminates. Thermoplastic resins are more compatible with aramid fibres. Nylon is the most often used thermoplastic in Kevlar aramid fibre composites.

Table 2.3 Typical physical and mechanical properties of common thermoplastic resins[16]

Property / Fibre Type	Glass trasition temperature (^{0}C)	Density (kg/m^3)	Coefficient of Thermal Expansion (x10^{-6} ^{o}C)	Tensile Strength (MPa)	Tensile Elastic Modulus (GPa)
Polyethylene	-120	920	220	8	0.5
PTFE	-120	2100	110	20	0.5
Polyproplene	-27;10	900	110	30	1.3
Nylon 66	57	1140	90	70	2.6
Polycarbonate	150	1220	55	60	2.7
Polymethylmethacrylate	80-100	1180	65	70	2.9
Polystyrene	80-100	1050	70	50	3.0
Polyvinylchloride	80	1400	70	50	3.2

2.1.2.3 Manufacture of Different Type and Size of FRP Reinforcements

Regardless of the manufacturing technique, there are three stages common to construction of FRP composites: (1) deciding which type of resin will be used with which type of fibre, (2) forming resin and fibre into the required shape, (3) shaping and curing of the composite material into its final geometry.

The manufacturing process affects the mechanical properties of FRP composites. However, it possible to achieve the best mechanical properties through using strong fibres, tough resin, long fibre geometries and high volume fibre densities. Nevertheless, this is often not possible or very expensive to apply using available techniques. There are several techniques for manufacturing of FRP composites[17 18].

Table 2.4 adopted from *Ellyin*[18] shows the types of FRP composite manufacturing techniques and the suitable resins used for each technique. It can be seen that the thermosetting resins can be used in the majority of the techniques. The Table also indicates that the polyester and epoxy resins are suitable for the pultrusion process.

Table 2.4 The common type resins used in diffrent manufacturing technique

	Thermosets					Thermoplastics									
	Polyester	PolyesterSMC	PolyesterBMC	Epoxy	Polyurethane	Acetal	Nylon6	Nylon6/6	Polycarbonate	Polypropylene	Polyphenylene	ABS	Polypheneylene Oxide	Polystyrene	Polyester
Hand Lay-Up	*			*											
Spray-Up	*			*											
Filament Winding	*			*											
Pultrusion	*			*											
Compression Moulding	*	*	*	*	*										
Resin Transfer Moulding	*			*											
Reaction Injection Moulding	*			*	*	*									
Injection Moulding	*		*	*	*	*	*	*	*	*	*	*	*	*	*
Braided Preform	*			*											

The pultrusion process has been in use since the 1950s and it has been widely accepted by civil engineering, architectural and construction industries due to its fast speed of operation and good quality control at a relatively low cost. The mechanical and physical properties of final product are dependent on the process variables such as fibre volume, pulling speed and temperature inside the die zone which contains three parts in which temperature increases gradually to provide temperature gradient from the surface of the product to its core[19]. A two-point loading test conducted on a rectangular shape pultruded product made of graphite fibre and epoxy resin *by Lackey and Vaughan* showed that the higher the percentage of fibre (63.9% in their case) and the pull speed (40.6cm/min) the higher the flexural strength of the product[20]. Pull force measurement technique[21] contributes to the quality control of the process by monitoring the resin blockage problem (if any) developing in the die zone (curing process) through the changes in pull force. In this way, it is possible to take corrective action before the problems get accumulated. Typical values of pull forces given by

Lackey in another paper are 9.08-18.16kN for graphite/epoxy pultrusion and less than 4.54kN for glass/epoxy[22].

The pultrusion process is particularly suitable for manufacturing composite components with continuous, constant cross-section profiles. The combination of glass fibre and polyester resin is the most common composition of FRP products used in this technique. The GFRP rebars supplied by the manufacturer in the USA and used in this investigation were also produced by pultrusion process. Pultruded composites offer relatively better physical properties. This can be combined with reduced cost and durability. They have a better surface finish and close tolerances compared to other composite manufacturing processes due to the axial nature of the process. Researchers have investigated the pultrusion process for many years. Although the manufacturing process is not complicated, the effects of different process parameters and their complex interactions are critical for obtaining an optimum product[23].

Kevlar or carbon fibres combined with epoxy or thermo plastic resin have also been successfully used in this process for manufacturing FRP reinforcing bars. In contrast with steel bars, there are no standards for the size of FRP reinforcing bars so they are manufactured in a wide range of sizes. Hooks and bends can be shaped on FRPs depending on the type of resin used. It is important to note that if a thermosetting resin is used, it is not possible to bend composite reinforcing bars after the fabrication process is completed[24].

2.1.3 Comparison of FRP Reinforcements compared to Conventional Steel Reinforcements

Besides its corrosion resistance, potential advantages of FRP reinforcements compared to steel are:

- High strength
- Fatigue characteristics of high performance fibres are three times higher than steel
- High energy absorption
- Low density
- Low conductivity and electrical interference
- Lower concrete cover in concrete applications such as cladding panels[25]
- Low maintenance cost

However, potential disadvantages exist for FRP reinforcements and these are:

- High cost (5 to 50 times more than steel, however cost of stainles steel also high approximately 6 times more than steel)
- Low modulus of elasticity
- Glass fibre deterioration by alkaline attack (this may be counterbalanced by using alkaline resistant glass fibres and polyester or vinylester resins[26])
- Anchorage for prestressing FRP tendons needs special attention
- Long-term strength of FRP reinforcement can be lower than short-term static strength (it has been reported by *Saadatmanesh*[26], that the long-term strength of glass FRP is approximately 70% of its short-term strength)
- FRP reinforced element is difficult to modify and recycle once it is erected[27]

2.1.3.1 Manufacturers of FRP Composites for Concrete

Summary of products and manufacturers of FRP composites for concrete are given in *Table 2.5*. It shold be noted that the information gathered in the Table is up to year of 1993.

Table 2.5 Manufacturers of FRP composites [25 28]

TRADE NAME	MANUFACTURER	USE & FORM	MAKE UP
KODIAK	IGI International Gratings, USA	Rebar	Glass fibre reinforced plastic and polyester resin
POLYSTAL	Stabag and Bayer AG, Germany	Rebar and prestressing tendon	Glass fibre reinforced plastic and polyester resin
ISOROD	Pulltall Inc., Canada	Rebar	Glass fibre reinforced plastic and polyester resin
IMCO	IMCO Reinforced Plastics Inc., USA	Rebar	Glass, carbon or aramid fibre reinforced plastics
JITEC	Cousin Frere, France	Rebar	Glass or carbon fibre reinforced plastic and vinylester resin
DYWIDUR	DYWIDAG-Systems International, Germany	Rebar	Glass fibre reinforced plastic and epoxy resin
NEFMAC	Nefcom Corporation, Japan	2D & 3D reinforcing grids	Glass, carbon or aramid fibre reinforced plastics
PARAFIL ROPE	ICI Linear Composites, UK	Prestressing strands	Aramid fibre reinforced plastic
FIBRA	A-ICS Corporation/Mitsui Construction Co.Ltd., Tokyo, Japan	Rebar & prestressing strands	Aramid or/and carbon fibre reinforced plastics and epoxy resin
ARAPREE	AKZO and Hollandsche Beton Groep nv, Holland	Rebar & prestressing strands	Aramid fibre reinforced plastic and epoxy resin
TOKYO ROPE	Tokyorope/Toho Rayon, Japan	Prestressing strands	Carbon fibre reinforced plastics

2.2 Mechanical Properties of FRP Composite Reinforcements

It should be borne in mind that the mechanical properties of FRPs are entirely based on the factors such as volume and type of fibre and resin (contains large amounts of carbon, nitrogen and hydrogen), fibre orientation and quality control during manufacturing. Therefore, they differ from one product to another. In addition to that, pultruded FRP reinforcements are anisotropic with the highest values of their tensile strength obtained along the fibres.

2.2.1 Tensile Strength

Unlike steel, all types of FRP materials exhibit linear elastic behaviour right up to failure under tension. However, it has been suggested that it is possible to change the linear behaviour into a more ductile manner close to the failure by using FRP rebars containing low modulus fibres inside and high modulus fibres outside or alternatively producing braided FRP rebars with foam plastic at the centre[29]. Also, as *Neale and Labossiere*[30] pointed out that many polymers behave linear elastically under low tension stresses but under high stress levels they behave as viscoelastic materials. If this is to be considered, the stress-strain curve deviates slightly from linearity at some point after loading. This is due to the combinaton of microdamage in the resin matrix and debonding between the fibres and the resin matrix[30]. Typical tensile strengths of FRPs are given in *Table 2.6.*

Table 2.6 The range of tensile strengths of different type of FRP composites

	GFRP	CFRP	AFRP	Hybrid (Glass+Carbon)	Hybrid (Aramid+Carbon)
Tensile Strength (MPa)	470-1910	628-2400	1120-3000	520-797	1050-1350

Warring[31] draws attention to the fact that when the glass and resin are combined FRPs do not produce a material with the full strength of the glass since the relatively weaker strength of the resin bond will lower the ultimate performance under load. He points out that the strength is more or less directly proportional to the glass:resin ratio.

out that the strength is more or less directly proportional to the glass:resin ratio. *Clarke et al*[32] also draw attention to the fact that the mechanical properties of the composite will be less than those of the fibres themselves and will depend on the type and percentage of fibres used. The authors point out that this could be due to the molecular structure of the fibres on their own are not distorted so that the ultimate strength is higher than the composite.

Dervaux & Tousseyn[33] state that the unidirectionally reinforced composite bars containing a reasonably high percentage of fibres lose 40% and 50% of their short term stiffness over 50 and 30 years respectively. However, the composite bars containing continuous fibres and loaded in the direction of fibres may show rather more favourable characteristics.

Ueda et al[34] studied the failure criteria of braided aramid fibre rebars with diameters of 8 and 50mm subjected to a combination of tensile and shear forces. The modulus of elasticity of these rebars is 66GPa with a Poisson's ratio of 0.30. They also used 6mm diameter aramid fibre reinforced stirrups. They observed that the tensile strength of the FRP rod reduces at the crack intersection under a combination of tensile and shear forces and at the bend of stirrups under tensile forces. They also stated that it is possible to quantify the strength reduction at those locations via finite element analysis.

A model consisting of long parallel fibres embedded in resin and stressed in tension along the fibre direction can be considered in order to obtain tensile strength and tensile load capacity of a composite with assumptions being; (1) Poisson's ratio effects are neglected (2) breaking strain of the resin is less than that of the fibre then the composite will fail at a stress given below[35],

$$\sigma_o = \sigma_f V_f + \sigma_r V_r$$

σ_o: the total tensile stress of FRP composite
σ_f, σ_r: tensile strength of fibre and resin respectively
V_f: volume fraction of fibres (%)
V_r: volume fraction of resin (%)

2.2.2 Tensile Modulus of Elasticity

The tensile modulus of elasticity of FRPs can be obtained from the stress-strain curves of FRPs. *Agbim*[36] points out that the E value of a glassfibre rod based on the gross sectional area lies theoretically between two limiting values: 74GPa for the glass fibres themselves and 3.51GPa for most resins. The greater the proportion of glass fibres in a rod, the higher its E value. There is, however, a practical lower limit to the amount of resin in a rod, below which tensile strength of a rod shows a sharp drop due to the local overstressing. The E value of glassfibre rods is therefore usually below 49GPa.

Due to the low modulus of elasticity of FRPs compared to steel, *Bedard*[28] points out that this may severely limit the use of composite bars in flexural members unless there is a substantial increase in the cross section depth or in the quantity of reinforcement used in the members to control deflection and cracking.

The reinforced plastic composite consists of two main components, fibre and resin. *McCrum*[35] has drawn attention to the fact that other components cannot be neglected e.g. the size, the presence of minute and unwanted voids. The principal purposes of fibre reinforcement are to increase modulus and to increase strength. The fibre length and fibre diameter are important parameters in determining both composite modulus and strength. This means if the aspect ratio (l/d) is high, the mean stress and the tensile modulus of the fibre will also be high. On this count continous fibres are an advantage over discontinous fibres.

Bruce[37] gives an equation for calculating elastic modulus of fibre reinforced plastic composite containing longitudinal fibres only in tension and compression. These equations are from a simple model which is called the rule of mixture or homogeneous strain and are assuming that the geometry, arrangement and distribution of the phases are the same, also there is a perfect bond between fibre and the matrix material, no difference between the Poisson's ratio of the fibre and the matrix material and finally that there is no creep within the polymeric matrix.

$E_o = E_f V_f + E_m V_m$

E_o: modulus of GRP
E_f: modulus of glass fibre (e.g. 70GPa glass)
E_m: modulus of plastic resin (e.g. 3.5GPa polyester)
V_m: percentage content of resin (e.g. 29%)
V_f: percentage content of fiber (e.g. 71%)

2.2.3 Compressive Strength

FRPs are weaker in compression than in tension and this with their brittle fracture limits their use in concrete elements, which are subjected to compression forces. The information pertaining to compressive properties of FRPs has not been reported widely in the literature. *Wu*[38] and *Ehsani*[24] reported that the compressive strength of GFRP having a tensile strength of 550-990 MPa, range from 320MPa to 470 MPa. *Petrina & White*[39] reported compressive strength values 1140MPa for GFRP and 1656MPa for CFRP having tensile strengths of 1580MPa and 1860MPa respectively. *Chaallal & Benmokrane*[40] reported 540MPa compressive strength for GFRP having a tensile strength of 700MPa.

2.2.4 Compressive Modulus of Elasticity

Petrina & White[39] give the same value of 48.3GPa for GFRP and 148GPa for CFRP as their tensile modulus of elasticity. However *Chaallal et al*[40] and *Benmokrane et al*[41] give the compressive modulus of elasticity value of 40 GPa for GFRP bars having a tensile modulus of elasticity of 45GPa. In *Wu's* report[38] this value is 36-47GPa for GFRP bars having a tensile strength of 41-55 GPa. In general, compressive modulus of elasticity of FRPs is lower (~30%) than their tensile modulus of elasticity.

2.2.5 Poisson's Ratio

It is assumed[35] that the axial strains in the fibre direction and in the matrix are equal to the strain in the composite and both constituents exhibit linear elastic behaviour i.e. $\varepsilon_f = \varepsilon_r = \varepsilon$ the Poisson's ratio (ν) of composite can be calculated from a rule of mixtures law similar to the one derived for the modulus of elasticity (E). Therefore;

$\nu = V_f \nu_f + V_r \nu_r = V_f \nu_f + (1- V_f)\nu_r$

ν_f: poisson's ratio of fibres
ν_r: poisson's ratio of resin
V_f: percentage content of resin
V_r: percentage content of fiber

In the literature, the average Poisson's ratio of GFRP, AFRP and CFRP rebar products is given as 0.27, 0.48 and 0.3 respectively.

2.2.6 Shear Strength

Bank[42] points out that the information on shear moduli and strength are not usually given by manufacturers and they are needed in design of structures when considering local buckling, web crippling and connection details. In general, composites have low shear strength owing to the fact that they are cut easily through transverse direction with a hacksaw. Shear strength of GFRP reinforcing bars given in the paper published by *Masmoudi et al*[43] and *Kodiak*[44] bars data sheet as 180MPa for 20mm diameter and 58.60MPa for 15.87mm diameter bars respectively.

2.2.6.1 Determination of Shear Properties

Determination of shear properties of isotropic materials was introduced by *Iosipescu*[45] in 1960s through a test method which produces pure shear loading by generating a shear force in the zero-moment section of a straight beam. The method was successfully applied to railway weldments, rolled metals e.g aluminium alloys, mild steel, brass as well as various cast metals e.g. zinc, cast iron, cast brass, bronze and cast aluminium by Iosipescu. However, it was found that the method can be applied also to anisotropic solids, including polymers and randomly oriented fibre reinforced composites[46]. *Walrath & Adams*[46] mention several other shear test methods and they are namely, off-axis tensile tests, picture frame and rail shear test, cross sandwich beam test, slotted tension shear test, plate-twist test, short beam shear test[47]. 90 degree angular notches of depths equal to a quarter of their height are applied to the test specimen and placed at midspan. It should be noted that the composites are less susceptible to effects of stress concentrations such as those caused by notches, holes etc than metals[48]. The test set up and the geometry of test specimen are shown in *Figure 2.2.*

Figure 2.2 Shear test set up

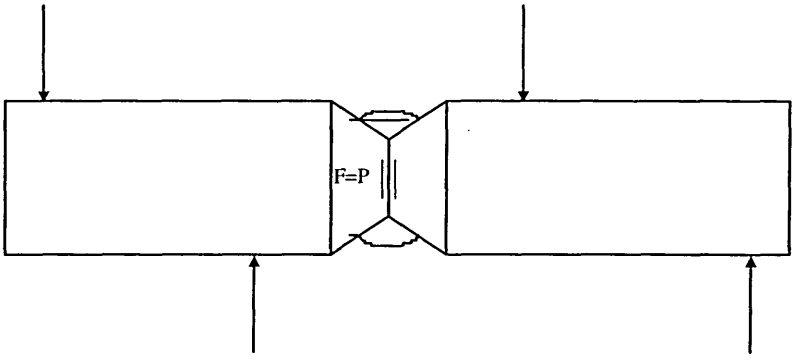

Weinberg[49] carried out Iosipesu shear tests on numbers of different composite materials. The shear strength and modulus of graphite/epoxy specimen were reported as 93.7 MPa ±9.58 and 7.10GPa ±0.568. He points out that the shear properties are strongly dependent on both the fibre/matrix bond and the matrix itself. The average ultimate shear strength of GFRP vinylester specimens obtained through the losipescu test method is 77.8+/-4.8 MPa and 65.7+/-4.4 MPa for the GFRP polyester specimens[42]. Besides the method's more realistic approach for creating pure shear stresses across the section, all authors claim that the method is easy to conduct with, less time spend on preparation and fabrication of the test specimen.

2.2.7 Relative Density

The specific gravity of FRPs range from 1.25 to 2 which is approximately four to six times lighter than steel. This provides easy transportation and less effort for handling on site together with installation compared to steel.

2.2.8 Coefficient of Thermal Expansion

The coefficient of thermal expansion of GFRP rebars is reported as 8.39 x 10^{-6} °C for volume fraction of 41% hybrid fibres (E-glass and carbon) impregnated in vinylester resin[50] and 9 x 10^{-6} °C for volume fraction of 73 to 78 % E-glass fibres impregnated in polyester resin[51]. *Ehsani*[24] reported the coefficient value for FRP as 10 x 10^{-6} ^{0}C.

2.3 Factors Affecting Performance of FRP Reinforcements

2.3.1 Void Content

McCrum[35] emphasizes the effects of microvoids (an average cross sectional diameter of less than 50μm) present in the composite on mechanical properties including shear strength, compressive strength, fatigue life and, to a lesser extent, modulus of elasticity. A volume fraction of void below 0.01 is considered to be a low void content.

2.3.2 Fatigue

Long fibres used in the composite materials exhibit good fatigue resistance. It has been reported that after so many millions of cycles (10^7) carbon FRP, aramid AFRP and glass FRP materials can conserve up to 80%, 40% and 25 % of their static strengths respectively[30]. *Mandell et al*[52] reported that the fatigue degredation rate of either unidirectional or injection moulded glass fibre/thermoplastic composites is the same and that is approximately 10% loss in their tensile strength per decade of fatigue cycle.

2.3.3 Creep

Creep is time dependent deformation under a constant load. Long term deformation due to creep is a significant phenomenon for composite materials including concrete. The parameters such as type of fibre and resin, fibre volume, stress levels, type of loading, the ambient temperature and moisture affect the creep behaviour of composites. It is reported by *Ehsani*[24] that for a high quality GFRP rebar, the additional strains caused by creep are estimated to be only 3% of the initial elastic strains. It is also reported that the results of creep tests conducted in Germany using different bar diameters of GFRP rebars at 20°C indicate that the stress rupture reduces if the constant loads are limited to 60% of the short term strength of rebar.

Gerritse, A & Den Uijl[53] studied the long term behaviour of aramid fibre/epoxy resin (ARAPREE) pretensioned tendons having 20mm width and 1.5mm thickness including creep and relaxation in an alkaline environment with pH 13 at 20 and 60 °C.

They observed that creep and relaxation are not sensitive to temperature and do not differ at temperatures at either 20 or 60 °C after 42 days with a constant load of 30 kN applied. 40% more relaxation occures in an alkaline solution than in air proving that the moist environment affects relaxation as well as creep.

Rahman et al[50] studied the creep behaviour of two types of vinlyester resin FRP (one is a mixture of E-glass and carbon fibres and the one carbon fibres only) which are in a form of 2-D mesh (NEFMAC) over 417 days. They applied five levels of tension 10%, 25%, 40%, 60%, and 75% of the ultimate tensile strength. After 417 days in air and, stressed up to 75% of the ultimate tensile strength both types of bars showed negligibily small creep. Both types retained their full tensile strength capacity under the above conditions. Neither creep strain nor residual tensile strength were affected too much by the elevated temperature of 50°C.

Uomoto et al[54] studied and evaluated the creep and the fatigue strength of three types of 6mm diameter, 400mm FRP rods which have 55% fibres by volume, GFRP, AFRP and CFRP. They obtained tensile strengths of 1491MPa, 1658MPa and 1364MPa for GFRP, AFRP and CFRP respecively from the tensile tests. The applied tensile stress was sustained at 67% and 95% of GFRP tensile strength, 70% and 90% of AFRP tensile strength and 96% and 101% of CFRP tensile strength for the creep test. The applied tensile stress was 20% to 100% of their static tensile strength for the dynamic fatigue test. From the creep test at the same applied stress they obtained the time for failure approximately 21 days for CFRP, 2days for AFRP and 10 hours for GFRP. The fatigue strength of CFRP (more than 4 millions fatigue cycles) is higher than GFRP and AFRP.

2.3.4 Environmental factors

Many types of materials used in certain applications are often subjected to environmental factors that can lead to the degradation of their properties, loss of tenacity and expected performance and eventually failure at an early stage of their use. These factors include, moisture, incompatible chemicals, weather, stress corrosion, fire, temperature and ultraviolet rays.

2.3.4.1 Moisture & Incompatible Chemicals

An excessive degree of water absorption should be avoided in composites since it has a plasticizing effect on the material resulting modifications in the mechanical properties of the resin as well as the modulus of elasticity of the composite. It is reported by *Neale & Labossiere*[30], that moisture causes a reduction of properties by as much as 25% to 30% of those for dry composites.

The strength of glass fibres depends critically on the presence of water at the surface[35]. Since water is absorbed by and diffuses through the vast majority of polymeric solids at measurable rates at ambient temperatures and humidities it is clear that the glass fibres will be exposed to molecular water. The attack of water will be on the resin, the interface or on the fibres. It is recommended to use water-resistant resins and alkali resistant fibres in composites which are exposed to continuous wet condition.

Aslonova & Resnyansky[55] studied corrosion resistance of mineral (glass, basalt) and chemical (carbon, aramid) fibres exposed to an acidic environments. as well as the contribution of final coating applied to the fibre rebars to the resistance of corrosion. They stated that the most chemically resistant fibres are zirconium-containing glass fibres and aramid fibres. The glass fibre reinforced plastic with the aluminoborosilicate fibre has less resistance in acidic and alkaline media than the zirconium-containing fibre reinforced plastic and the basalt fibre reinforced plastic. They observed that the basalt fibres have good corrosion resistance in an alkaline medium and as a result of this they suggest to use of basalt fibres as a reinforcement in concrete. They also observed the carbon fibres completely dissolving in the alkaline medium.

Katsuki & Uomoto[56] investigated the alkali penetration at 40 °C of AFRP, CFRP and GFRP vinylester resin matrix, using 6mm round rods containing 55%fibre by volume. They observed that the alkali solution penetrates GFRP (low alkali resistance) rods however does not penetrate AFRP or CFRP (both high alkali resistance) after 120 days of exposure. The authors carried out tensile tests on 200mm long specimens, which had been immersed in alkaline solution (NaOH). The results showed that the

strength loss of GFRP is 25% at 7days, 46% at 30days, 67% at 90days and 72% at 120days. No loss of strength occurred for AFRP and CFRP at 30 and 120 days.

Zayed[57] examined marine structural environments on physical and mechanical performance of unidirectional E-glass fibre impregnated in a polyester resin matrix FRP bars. The bars were exposed for 140 days to: saturated calcium hydroxide solution (as in concrete), 3.5 w% sodium chloride and saturated calcium hydroxide solution mixture (as in marine environment) respectively. The following conclusions were drawn from his work. A high level of weight was gained as a result of exposure to alkaline environments with salt. There is negligible effect on the strain and the elastic modulus with average values of 3.2% and 43GPa ($6.3x10^6$psi) respectively under the selected exposure of the environments. Also a 15% loss in the ultimate strength was observed after the bars were exposed to a calcium hydroxide-sodium chloride environment. The author recommends that future studies should cover longer exposure time to be applied on FRP bars supplied by different manufacturers within identical environments.

Tannous and Saadatmanesh[58] investigated the effect of corrosive chemical solutions on 10mm and 19.5mm diameters rebars made of E-glass fibre embedded in either vinylester or polyester resin. The authors also conducted flexural tests on 10 concrete beams having dimensions of 200mmx405mmx2400mm. The beams were reinforced with two 10mm dia, GFRP rebars and 10mm steel strirrups. They were subjected to deicing salt solution and were tested after one and two years. The authors pointed out that there is a significant loss of strength on rebars as well as the beams when they are exposed to chemical solutions.

2.3.4.2 Temperature

Changes in temperature create deterioration in composites[30]. It is important that the enviromental conditions should be sound during the curing process of composite material since it shrinks as the concrete. Resin usually changes its colour at high temperatures. Since resin and fibre have different coefficients of thermal expansion, any changes in temperature will affect the bond between the fibre and the resin.

Temperature variations can result in relatively high thermal stresses in concrete structures. The stresses due to temperature may produce cracking that can seriously affect the serviceability and the integrity of structures. *Abdalla and Elbadry*[59] considered this aspect and carried out experimental work on the concrete beams (250mmx500mmx3350mm) reinforced with FRP and compared with steel reinforced beams. The beams were subjected to initial equal end moments before heating. Test results showed that the maximum width of cracks in GFRP reinforced beams are 20% wider than in the steel reinforced beams at the temperature difference (ΔT) higher than 100 ^{0}C. The results also showed that the high transverse coefficient of thermal expansion of the GFRP creates bursting stresses within the concrete around the rebars at high temperature. This results in a loss of bond between the concrete and the GFRP consequently, a reduction in the tension stiffening of the concrete and increase in deflection.

2.3.4.3 Stress Corrosion/Environmental Stress Cracking

First observation of static fatigue (stress corrosion) was made in 1899; the strength of glass depending on load duration[35]. The rate of static fatigue in fibres is not essentially different to the rate of static fatigue in bulk glass. The assumption is that the static fatigue arises from the growth of minute cracks in the surface of the specimen, under the influence of stress and the attacking medium. When the crack has grown to a size that the applied stress causes rupture instantaneously. Static fatigue causes loss in strength and modulusof elastcity of glass fibres. Stress cracking is the long-term brittle failure of a material under a tensile stress appreciably below the limits of its short time strength; it is frequently accelerated by the presence of an active environment (stress corrosion cracking) and by triaxial stress.

It should be noted that the stress corrosion appears not only to be a problem with fibre-resin composites but also with steel reinforcement. *Page & Anchor*[60] reported a brittle fracture due to the stress corrosion of stainless steel wire hangers, which were used to support the light suspended ceilings above a swimming pool in the UK. They point out that the environmental factors associated with stress corrosion of stainless steel are the presence of significant concentrations of chloride ions and elevated temperatures. In another paper, it has been reported that a similar incident occured in

Switzerland, heavy concrete ceiling reinforced with stainless steel above a swimming pool resulted in fatal collapse in May 1985 after 13 years of service life[61].

2.3.4.4 Fire

The resin matrix of a composite is more susceptible to fire due to its high content of flammable carbon, hydrogen and nitrogen constituents. When the resin matrix burns off, it creates a dense black smoke, which can be very toxic. It is possible to improve the fire resistance of a resin matrix by using additives. *Ehsani*[24] reported an investigation carried out in Germany involving E-glass plastic rods which have been stressed to 50% of their tensile strength, could maintain 85% of their room temperature strength after 30 minutes fire exposure at 300°C. The author also reported that GFRP rebars could maintain 50% of their tensile strength at 500°C. However, when FRP rebars are used in concrete elements and exposed to fire, the concrete acting as a barrier, will protect the rebar from direct contact with fire. This means that the performance of FRPs in concrete at elevated temperature is an important factor to be considered for concrete elements such as cladding panels which are very likely to be exposed to fire.

Tanano et al[62] investigated the residual flexural strength of 200x300x3000 mm concrete beams reinforced with either carbon, aramid or glass fibre reinforced plastic rebars and compared it with steel reinforced beams. The authors reported that the residual strength of FRP reinforcement decreases as the temperature increases and the failure mode changes from crushing failure of the concrete to rupture of the reinforcement. They also observed that the stiffness of the FRP reinforced beams decreases at 250°C. However, the decrease in strength is very small. The tests carried out on steel reinforced beams showed that approximately 87 % of yield and maximun strength of the beams were maintained at 450°C. *Table 2.7* shows the melting points of different materials.

Table 2.7 The melting points of different materials[63]

Material	Temperature (approx.) °C	Effect
Polythelene	110	melts
Cellulose (cotton, wood)	260	decomposes
Zinc (galvanizing)	410	melts
*Steel	550 1500	becomes non-load bearing melts
Pyrex glass	550	annealing
Aluminium	650	melts
Brass	900	melts
Copper	1050	melts

*Regarding the strength of structural steels, the carbon content which is about 1-2% has next to no influence at elevated temperatures. Reinforcing bars which can have up to 3% carbon has little effect but since it is insulated by concrete will not get that hot. The main influencing factors at elevated temperatures are niobium and vanadium. Carbon does, however, have a slight influence over the specific heat where it rises as the carbon content rises but not by a great deal.

Fujisaki et al[64] carried out fire resistance tests on 3600mm high, 1500mm width and 150mm thick lightweight concrete panels reinforced with grid shaped carbon, glass and hybrid (carbon and glass) fibres impregnated by vinylester resin produced by a filament winding process. The results showed that the panels could take a temperature of approximately 800°C after 30 minutes of fire exposure.

Okamoto et al[65] studied the fire resistance of precast partially prestressed concrete (PPC) beams which were used for the upper foundation of a seismic base-isolated storey, containing braided aramid fibres impregnated with epoxy resin. The authors point out that there is no necessity for obtaining fire resistance of beams in design where a foundation is involved. They suggest that the beams can resist fire after two hours exposure. The residual tensile strength of aramid fibre rebars were measured at 400°C showing 40% and 59% maintenance of their original tensile strengths respectively.

2.3.4.5 Ultraviolet Rays

Ultraviolet rays present in sunlight cause damage to composites. The action of the rays causes chemical reactions in the polymeric matrices leading to a deterioration of their properties. Although, it is possible to prevent the deterioration by using carbon or special additives, which prefentially absorb the rays and convert it to less harmful

thermal energy[1]. However, this kind of damage is not particularly important, if FRP reinforcements are used inside the concrete.

2.4 Bond Performance of Reinforcements

Bond between reinforcing bars and concrete is an important factor and it should be adequate for satisfactory performance of reinforced concrete structures. For development of the bond strength, the main influential parameters are concrete strength, embedment length, concrete cover, type of rebar and rebar spacing. This section contains the bond performance of steel and FRP rebars in concrete studied by others.

2.4.1 Steel rebars

Bond stress is described by *Kong & Evans*[66] as the shear stress acting parallel to the reinforcement bar on the interface between the bar and the concrete. Adhesion, friction and mechanical interaction betweeen concrete and steel (bearing) are the typical components of bond. Steel reinforcing bars having ribbed surface texture have better bond than smooth surface textured rebars (plain rebars). It has been reported that the bigger the rib area the higher the magnitude of the bond stress of steel bars[67]. Bond of plain rebars is dependent on adhesion and friction whereas bond of ribbed rebars primarily depends on the mechanical interlock. The effect of adhesion is small and friction does not occur up until the slip occurs between rebar and concrete. Concrete bearing stresses against the ribs generate radial stresses together with circumferential tension in the concrete around the rebar resulting in longitidunal splitting of the concrete along the rebar, and bond failure. Using high strength concrete, heavier shear links and larger concrete cover to the rebars help to prevent such splitting. The other type of bond failure is the pullout failure where the rebar is pulled out and leaves the surrounding concrete intact.

Average bond stress can be calculated using the equations given in *BS8110*[68].

$$f_b = \frac{F_s}{\pi \phi l} \qquad F_s = f_s \frac{\pi \phi^2}{4}$$

f_b : bond stress between the steel and the concrete

F_s : force in the rebar or group of rebars

ϕ : effective rebar size

l : anchorage length

f_s : steel stress

$f_{bu} = \beta \sqrt{f_{cu}}$

f_{bu} : design ultimate bond stress

f_{cu} : concrete stress

β : bond coefficient (0.28 for plain rebar in tension, 0.50 for ribbed rebars in tension)

Failure mode of plain rebars is normally by pullout, once the adhesion and friction mechanisms no longer exist. If the cover/rebar diameter ratio (c/d) is less than 1.0, splitting failure may occur for plain and ribbed rebars. If the cover/diameter ratio is large or heavier shear links are present then the failure mode changes from splitting failure to shearing of concrete. The specimens having pullout failure result in higher bond stress than the specimens failed in splitting.

Traditional bond test methods are based on the concept of pullout failures giving an ultimate bond strength. *Chana*[69] argues that this concept is valid for mild steel (plain) bars but for ribbed steel bars, tests of this kind will give misleading results for most practical situations, where failure is caused by splitting of the concrete cover. Therefore, assessing the pullout test method for bond strength is based on the type of specimen used. The author compared the bond test methods and their results given in *BS4449*[70] and *RILEM*[71] standards. The author has drawn attention to the fact that neither British nor RILEM standards based on bond test are measuring the value, which can be directly related to a real life situation. However, these test standards can be useful for investigating basic pheneomena in relation to bond and for obtaining load-slip behaviour of steel rebars. A pullout test specimen in BS4449 consists of straight reinforcing rebars embedded in the centre of a concrete prism with links. This results in bond stresses having a very high value, 10-20 MPa. In BS8110[68] and BS5400[72] the value of ultimate bond stress lies between 1MPa and 4MPa which are representative values for members with a low cover. These values in BS8110 and BS5400 are not derived from any standard bond test. The RILEM test specimen

consists of a standard cube with the test rebar incorporated on its axis and as with the British Standard, this also gives higher values of ultimate bond stress. The author claims that for a realistic bond stress which can be used for design purposes, a specimen giving a splitting failure should be used. Therefore, the author proposes a test specimen, which can be used in a bond test. Two plain and two ribbed 16mm diameter steel rebars without links were cast in top and bottom regions of a 300mmm x 300mm x 200mm concrete block with 25mm cover (c/d=1.5). The specimen enables the bond strength to be determined for both top and bottom cast conditions. The sketch of the loading arrangement and the specimen are shown in *Figure 2.3.*

Figure 2.3 The loading arrangement for bond test

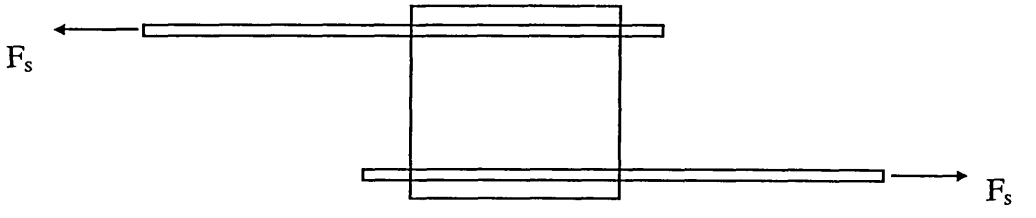

Table 2.8[73] shows the comparison between the experimental bond stress values and the characteristic values of BS8110 based on f_{cu}>40 MPa. The experimental results agreed with BS8110 standard. It can be seen in Table that the bond stress of top cast bars is higher than the bottom cast bars. It is suggested by *Azizinamini et al*[73] that this is due to the fact that bleeding of the concrete results in lower quality concrete underneath the top reinforcing bar and this limits the bearing capacity that each rib can provide. Therefore, this reduction in bearing capacity allows crushing of concrete adjacent to the ribs.

Table 2.8 The comparison of bond strength of steel rebars in concrete through experimental results and BS8110.

f_{cu} (MPa)	Rebars	Experimental values (MPa)	BS8110 characteristic values (MPa)
30.1	Plain: Top cast	1.83	1.53
	Bottom cast	2.22	2.14
	Ribbed: Top cast	1.90	1.56
	Bottom cast	3.34	2.19
41.0	Plain: Top cast	-	1.79
	Bottom cast	2.56	2.50
	Ribbed: Top cast	2.76	1.83
	Bottom cast	3.88	2.56
52.6	Plain: Top cast	1.14	2.02
	Bottom cast	3.16	2.83
	Ribbed: Top cast	3.51	2.07
	Bottom cast	3.64	2.90
59.5	Plain: Top cast	1.85	2.15
	Bottom cast	4.12	3.01
	Ribbed: Top cast	3.40	2.21
	Bottom cast	5.15	3.09
77.0	Plain: Top cast	1.07	2.44
	Bottom cast	3.83	3.42
	Ribbed: Top cast	4.48	2.51
	Bottom cast	5.19	3.51

It has been reported that the plain bars cast in a horizontal position exhibit lower bond resistance than vertical bars[74]. The effect of direction of casting of the pullout test specimen on bond performance of steel bars is also emphasized by Menzel[75]. The author's experimental results showed that the best performance was observed for vertical bars pulled against the direction of casting and furthermore the bigger the depth of concrete under the bar, the more the bleeding water accumulates under the bar resulting in weakness in the bond resistance.

It has also been reported that keeping the curing conditions the same for all specimens is an important factor to be considered, since the pullout behaviour of test samples is strongly affected by shrinkage of the concrete[76].

Mohamed & Clark[77] studied the bond behaviour of 16mm diameter plain and ribbed steel rebars with and without links (6mm links diameter) of low strength concrete (5MPa concrete strength) using the same set up and the dimensions of concrete block suggested in *Chana's*[69] paper. It is reported in the paper that the bond stress of plain and deformed rebars in low strength concrete should be calculated as (the values include a partial safety factor of 1.4):

$f_b = \beta_1(0.5 + c/\phi)f_t + 6.4A_t / s\phi \leq \beta_2 f_t$

A_t: area of link

c: cover to the main rebar

f_b: bond strength

f_{cu}: cube strength of concrete (100mm cube)

f_t: splitting tensile strength of concrete (it can be assumed that $f_t = 0.3\sqrt{f_{cu}}$

s: spacing of links

ϕ: diameter of main rebar

β_1: 0.30 (for bottom cast rebars), 0.21 (for top cast rebars)

β_2: 0.90 (for bottom cast ribbed rebars), 0.63 (for top cast ribbed rebars)
0.45 (for bottom cast plain rebars), 0.32 (for top cast plain rebars)

The authors pointed out that the design values of bond strength in BS8110 can be used to assess the bond strength of ribbed rebars in low strength concrete but, 30% reduction should be applied to the values in BS8110 for assessing the bond strength of plain rebars. The ribbed rebars with covers of twice the c/d and /or links cause shear cracks in the specimen before bond failure and this lowers the bond strength. The authors suggest that this should be alerted when assessing the bond strength of a ribbed rebar in a region of high shear force in a low strength concrete structure.
Bond strength tests have been conducted for ribbed rebars in lightweight aggregate concrete by *Clarke & Birjandi*[78]. Three different methods were used i.e. BCA (adopted from *Chana's*[69]), BS4449 and RILEM and the bond stress values obtained from each one were compared. *Table 2.9* shows the bond stress of steel rebars to concrete based upon three different methods. Three different failure modes, splitting, pull out and shear were observed. The advantage of using lightweight aggregate is the reduction in self-weight, which are about 20% less than normal weight concrete. It has been reported that in various countries lightweight concrete has been used in a variety of structures, resulting in overall savings in total cost of 10-20% over the

normal weight concrete structures. It is suggested to use bond coefficient (β) of 0.28 for top cast rebar and 0.40 for the bottom cast rebar embedded in lightweight concrete.

Table 2.9 Comparison of bond stresses measured using three methods

Aggregate	Bar dia. (mm)	f_{cu} (MPa)	Bond Stress (MPa)		
			BCA	BS4449	RILEM
Pellite	16	41.7	3.6	13.9	14.7
Pellite	10	41.7	3.3	14.0	15.8
Pellite	16	23.2	3.0	12.7	10.3
Pellite	16	48.5	3.5	14.3	12.4
Leca	16	24.7	2.5	12.8	8.4
Fibo	16	25.3	2.3	12.9	7.0

As it can be seen in the Table that the values obtained from BS4449 and RILEM are 4 to 6 times of the values obtained from the BCA method.

Tensile bond strengths of ribbed rebars embedded in high strength concrete beams have been studied by *Hwang et al*[79]. The use of high strength concrete in high buildings, bridges, offshore structures and pavements has been very common since the mid-1980s. The authors conducted flexural tests on 20 concrete beams. Ten of them had dimensions of 300 x 250 x 2850mm which were cast to investigate lap-splice strength (splice length series - see *Figure 2.4*) and the other 10 of which had dimensions of 450mm x 250mm x 1850mm to investigate development strength (developed length series). Some of the beams from the two series contained links.

Figure 2.4 Loading and reinforcement arrangements of the beam specimens

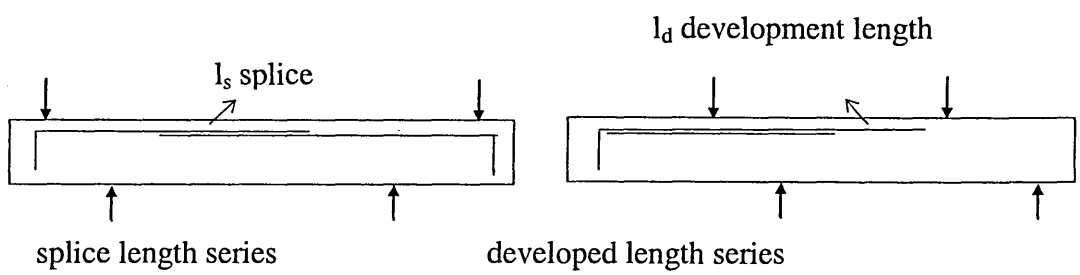

Failure mode of all the beams was splitting of concrete before the rebars yielded. Concrete strength obtained from cylinders ranged from 40 to 70 MPa. The concrete of grade 60 and 28.7mm diameter ribbed steel rebars having yield strength of

518.6MPa, were used throughout the investigation. The concrete cover was 50mm for all the beams. The formula used below is for calculating the uniform average bond strength of steel rebars to concrete. The authors concluded that the bond performance of high strength concrete is similar to the normal weight concrete for either case i.e lap-splice or developed length.

$$u_{test} = \frac{d_b f_s}{4l}$$

d_b: nominal diameter of anchored rebar
f_s: steel stress of the anchored rebar at failure
l: splice or developed length

Note that in the majority of the American papers concrete strengths are obtained from the compression tests carried out on the cylinders instead of cubes. Therefore, the Author feels that it is useful to include the relationship between the concrete cylinder and the cube strength given in *Al-Shawi et al's*[80] paper.

$$f_c^{'} = 0.563(f_{cu})^{1.102}$$

$f_c^{'}$: compressive strength of cylinder (MPa)
f_{cu} : compressive strength of cube (MPa)

The effect of bar diameter on the bond strength of steel rebars embedded in high strength concrete (95 MPa) containing silica fume and normal weight concrete (42MPa) was studied by *Larrard et al*[81] using RILEM beam test standard. The authors concluded that the high strength concrete containing silica fume enhances the bond strength by 80 % for 10mm bars and by 30 % for 25mm bars.

Using silica fume in concrete mixes enhanced the bond between aggregates and the concrete matrix associated with low porosity concrete resulting in high strength concrete[82 83]. *Gjorv et al*[83] also reported that adding condensed silica fume to concrete mix up to 16 % by weight of cement shows improvement in the pullout strength, especially in the high compressive strength range of concrete.

Bond of ribbed rebars reinforced in steel fibre reinforced concrete has been studied by

Soroushian et al[84] studied the effects of rebar confinement and compressive strength of concrete on local bond performance of deformed bars in reinforced concrete joints. They found that the confinement of concrete by transverse reinforcement does not directly influence the local bond behaviour of deformed bars in joint conditions where the vertical bars in the columns are sufficient to restrain the widening of bond splitting cracks. The authors also reported that the variations in concrete compressive strength do not influence the bond stress and slip relationship, however, ultimate bond strength increases almost proportionally with the square root of the concrete compressive strength.

21 beams reinforced with epoxy coated ribbed rebars with lap splices have been tested and compared with uncoated ribbed steel rebars for bond by *Treece & Jirsa*[85]. The authors concluded that the bond strength reduced with epoxy coated rebars compared with uncoated rebars, due to loss of adhesion between the ribs and the concrete. The loss of adhesion between concrete and the rib also means loss in friction capacity. The failure hypothesis of bond explained by the authors. When the rib of the rebar bears against the surrounding concrete, the concrete key tends to slide up the face of the rib causing splitting of concrete cover. The friction between the concrete and steel along the face of the rib acts to prevent the concrete key from sliding relative to the rib. If the friction between concrete and steel is lost, the only component of the bond strength is the force perpendicular to the face of the rib. The magnitude of the bond force is controlled by the amount of radial pressure the concrete cover can resist before splitting. This is the vertical component of the resultant forces in *Figure 2.5*. The horizontal component of the resultant is the effective bond strength. If the capacity of the cover is the same for either case, the bar with no friction will have a much smaller bond capacity than the bar, which is ribbed. In a pullout failure, friction should be much less important than in a splitting failure. A pullout failure usually occurs when the steel is well confined by concrete cover or transverse steel, preventing a splitting failure. In this case, the bond strength should be controlled primarily by the capacity of the concrete in direct shear.

Figure 2.5 The resultant forces of bond on the bars

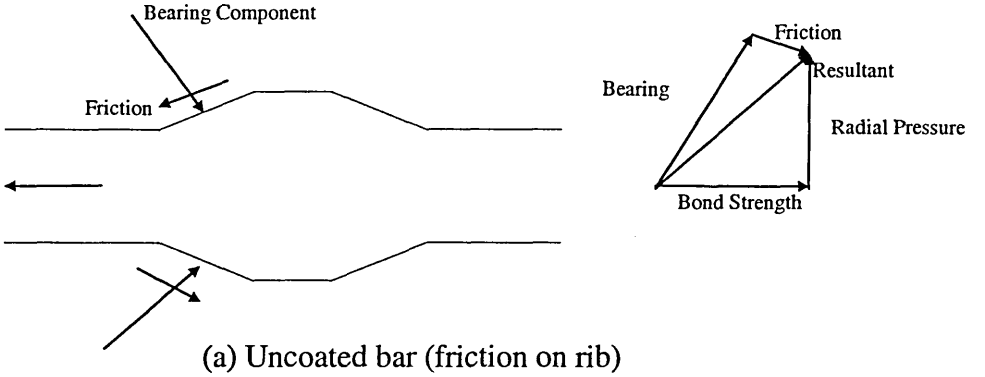

(a) Uncoated bar (friction on rib)

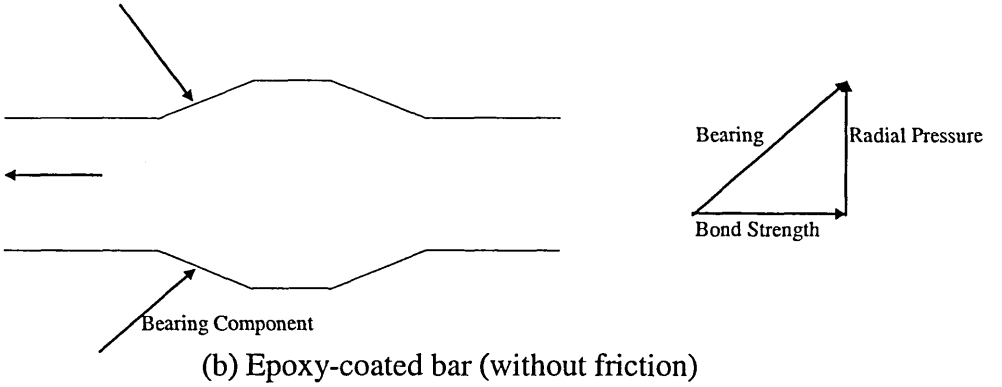

(b) Epoxy-coated bar (without friction)

It has been reported that the bond strength of a coated rebar to that of an uncoated rebar with an identical rib geometry reduces with increasing relative rib area[86]. *Cairns & Abdullah*[87] suggest that the improvement in bond strength can be achieved by using steeper rib face angles and a more heavily ribbed deformation pattern.

Clearly & Ramirez[88] studied the bond of epoxy coated ribbed steel rebars within the splice length, to concrete by testing slab-type member under three point loading. Splitting bond failure occurred for all the specimens. The comparison for bond made between epoxy-coated and uncoated ribbed rebars is approximately 15 % less than the uncoated ones. Although, epoxy coating technique is for protecting steel from corrosion, the authors stated that the members reinforced with epoxy coated rebars have fewer but wider cracks which can be a problem with the members exposed to cold weather. They also point out that the deflection is not significantly different from that with members reinforced with uncoated rebars.

Ghaffari et al[89] have drawn attention to the effects of cover, casting position (top or bottom cast rebars) and slump of concrete on bond strength of epoxy coated ribbed steel rebars. The authors stated that the casting position of a rebar affects its bond strength. The greater the amount of concrete cast below a rebar, the greater the effects of settlement and bleeding and the lower the bond strength. The results obtained from their tests show the the top-cast rebars exhibit a lower bond strength than the corresponding bottom-cast rebars, and rebars cast in high slump (203mm) concrete exhibit a reduced bond strength if the concrete is not vibrated. The top cast rebars in high slump concrete, whether vibrated or not, have a lower bond strength than the top-cast rebars in lower slump (64mm) concrete. They also reported that the bond strength of both coated and uncoated rebars increases, regardless of casting position, bar size or rib pattern. The bond strength of rebars cast in low slump concrete is higher than the ones cast in high slump concrete for the same compressive strength of concrete. Lack of vibration (consolidation) of high slump concrete effect the bond strength of coated or uncoated top or bottom cast rebars. It is more detrimental for coated rebars than for uncoated rebars.

In general, the reduction in bond strength of epoxy coated steel rebars reported by different researchers is between 6% and 35 %. This could be due to the fact that different rib geometry rebars have been used. Details of rib geometry of test rebars have not often been reported. *Swamy & Koyama*[90] reported different reductions in bond strengths of coated steel rebars having three different rib geometries, perpendecular, diagonal and double-diagonal. The authors used a pull-out type specimen with a confining helix of reinforcement around the test bar and reported the reductions of 3.9, 13.7 and 31.4% in bond strength with a free end slip of 0.05mm.

2.4.2 FRP rebars

There are no available design guidelines for bond behavior of GFRP rebars in concrete. However, numbers of people have conducted bond tests based on bond testing methods currently available for steel rebars.
Development length is defined as the minimum embedded length required to develop the ultimate tensile force of the rod and it is recommended that the development length can be taken as approximately 20 times the bar diameter for both normal and

high strength concrete. *Ehsani et al*[91] developed design recommendations for anchorage of straight and hooked GFRP rebars to concrete. A total number of 48 beam specimens, 18 pullout specimens and 36, 90° hooked rebar pullout specimens were tested. The mean concrete strengths were 28 and 56 MPa, and the GFRP rebars were made of 72% E-glass and 28% polyester resin by volume. The results showed that the bond strength and slip are greater with pullout specimens due to the absence of concrete flexural cracks. The authors state that it is more reliable and realistic relying on beam test data for determination of development length. They point out that the lower modulus of elasticity of GFRP rebars gives greater elongation which contributes to the loaded-end slip. In addition, the ribs on GFRP rebars are shallower than steel rebars which means that the rebars cannot resist large bond stress resulting in greater slip on both loaded and free ends. The bond stresses were calculated using the formula;

$$u = \frac{T}{\pi d_b l_d}$$

u : bond strength
T : applied tensile force
d_b : bar diameter
l_d : embedded length

Nanni et al[92] carried out pull-out tests by embedding the FRP and deformed-steel reinforcing bars into 150mm side concrete cube specimens in order to determine the bond performance of the two types of rods. Types of FRP rods used were glass-FRP vinylester, carbon-FRP vinylester and carbon-FRP epoxy resin having smooth and deformed surface texture. They concluded that the concrete strength does not have any influence on the bond strength and the failure mechanism of FRP rods. They also concluded that smaller diameter (6.3mm) FRP rods have higher bond strength than larger diameter (12.7mm). Test results showed that two deformed steel rods having diameters of 9.5 and 12.7mm have higher bond strength than smooth FRP but lower bond strength than deformed FRP rods.

Hattori et al[93] studied the bond creep behavior of 7.5mm diameter epoxy resin twisted carbon (PAN) fibre cable and 6mm diameter vinylester resin spiral wound aramid (Technora HM 50) round bar embedded in concrete having strengths ranging from

26.6 to 47.7MPa. They compared the two types of FRP reinforcement with 10mm diameter deformed mild steel bar. The authors initially carried out pull-out test using two 100mm side concrete cubes in which the bars were horizontally embedded in a bond length of 64mm from both sides. The average bond stresses of the bars are 1.6, 7.3 and 7.3 MPa for carbon cable, aramid bar and steel bar respectively. After 11 months, pull out creep test results showed that the bond slip (free end slip) of aramid fibre is more than steel bar and carbon cable. Carbon cable gives less value of bond slip than steel bar. They concluded that the bond slip behavior of the types of FRPs used in their study influenced by the mechanical properties of resin type in the long term. After collecting numbers of people's work on bond characteristic of different types of FRP bars, which have different surface texture, the authors stated that the bond performance of FRP bars depends on the surface texture and manufacturing process. Nevertheless, it is possible to manufacture FRP bars having similar or greater bond strength than steel bars[94].

Taerwe & Pallemans[95] carried out tests on prestressed 1m long concrete prisms using AFRP-Twaron IM (ARAPREE) bars having diameters of 7.5 and 5.3 mm to determine the critical concrete cover. They concluded that the sand coatings applied on the bars and the use of high strength concrete plus the addition of fibres reduces the critical concrete cover.

Jerrett & Ahmad[96] conducted short-term bond tests on 8mm diameter CFRP rods which have smooth and deformed surface texture embedded in concrete. The average bond strength of deformed bars associated with the maximum load was 7.4MPa and 0.42MPa for smooth bars.

The fiberglass reinforced bars have a lower tensile strength and MOE, but better bond strength than the aramid (Kevlar 49) reinforced rods[97]. Four pull-out tests were done with 6.4mm bars, 19 tests with 9.5mm bars, and 21 tetsts with 12.7mm bars. Bond strength tests were conducted on 27 tests samples. Of these, 22 can be considered 'good' failure. A 'good' failure for the bond strength test is one where the rod actually pulled out of the concrete before the concrete or rod broke. A bad failure would be one where the rod broke at the grip or the concrete crushed.

GangaRao & Faza[98] showed that, in order to develop good bond strength between FRP rebars and concrete, different surface conditions for rebar were developed. Among them, 45 degree angular wrapping or helical ribs produce a deformed surface on the rebar. Coating FRP rebars with epoxy and rolling them in a bed of sand creates a roughened surface and is one of the alternatives that will improve bond strength.

Benmokrane et al[51] studied the bond strength of GFRP and steel rebars using bending and pull-out test methods[99]. The results indicate that the diameter effect on bond observed for steel rebars is also present for GFRP rebars i.e. the average bond strength of GFRP rebars decreases as the rebar diameter increases[100]. This could be explained by the bleeding of water in concrete[101]. The bigger the diameter of the rebar, the higher the quantity of bleeding water gets trapped beneath the rebar, creating a greater void. This void reduces the contact surface between the rebar and the concrete and hence the bond. The bond strength obtained from the pull-out tests is approximately 5% up to 82% higher than that obtained from the rectangular beam tests. It is concluded that the bond strength of GFRP rebars is approximately 60 to 90 percent lower than that of steel rebars depending on rebar diameter[102]. This is comparable to epoxy coated steel rebars whose bond strength varies from 62 to 84 percent of that of deformed steel rebars[40]. Approximately 80% increase in bond strength can be achieved with sand coated GFRP rebars compared to the uncoated rebars. It is also reported that the contribution of reduced pitch of ribbed FRP rebars is not significant.

2.5 Field Applications of FRP Reinforcements

The development and the field applications of FRPs have been increasing since the 1970s[103]. It has been reported that the use of FRPs such as GFRP, AFRP and CFRP in highway and pedestrian bridges built in Europe, China, Canada and the USA, has increased significantly in recent years[25 104]. It has also been reported that, in Japan, continuous fibres are being used both in actual practice and experimentally as prestressing tendons, reinforcing bars and mesh for both new construction and retrofitting. CFRP and GFRP grids have been used in the lightweight concrete curtain walls outside buildings[105].

Potential applications of FRP reinforced concrete structures have been categorised by *Chaallal et al*[106]. Structures subjected to de-icing salts; including multi-storey parking facilities, pavement slabs, concrete bridge decks, retaining walls etc and other corrosive environments; including water treatment plants, chemical factories, paper mills, liquid gas and oil reservoirs and pipelines, chimneys and nuclear plants, foundation slabs etc. or those in which a low thermal or electrical conductibility is required; including aluminium plants, radio and T.V transmission towers, airport control towers, military structures (invisibility to radar).

Neale & Labossiere[30] give the current applications where FRPs are used, in their paper. These are namely, roof lights and dome lights, domes and other roof structures, cladding, tanks and cisterns, pipes and ducts.

The bridges where GFRP reinforcements are used are set out by *Meier*[107] in chronological order.

Pedestrian Bridges

- Tel Aviv (Israel) - 1970s
- Virginia (USA) - 1971
- Westminister Cathedral Footbridge (UK) - 1970s
- The Chongquing Cable Stayed (China) - 1986
- Shinmiya Bridge (Japan) - 1988[108]
- The Marenfelde (Germany) - 1989
- Hakui Bicycle Bridge 1 & 2 (Japan) - 1991 & 1992[108]
- Parafil Tendon Footbridge (Hertfordshire, UK) - 1994[109]
- The Chalgrove (UK) - 1995[110]

Highway Bridges

- The Paper Reinforced Plastic (USA) - before 1970
- The Lunen'sche Gasse (Germany) - 1980
- The Ginzi (Bulgaria) - 1982
- The Miyun (China) - 1982
- The road Bridge (Japan) - 1990[111]
- Rapid City Road Bridge (USA) - 1991[112]
- Notsch Road Bridge (Austria) - 1992[113]
- Beddington Trial/Centre Street Bridge (Canada)[114]
- The McKinleyville Road Bridge (USA) - 1996[115]
- The Taylor (Canada). - 1997[116]

Field applications have also been carried out using the method of wrapping FRP sheets to repair the damaged structure resulting in enhanced seismic and fatigue resistance. These applications are;

- The Ibach Bridge, (Switzerland) - 1991[117]
- The covered wooden Bridge (Sins, Switzerland) - 1992[117]
- The multi-storey parking garage (Flims, Switzerland) - 1993[117]
- Retrofitting of earthquake damaged brick walls in buildings (California, USA) – 1994[118].
- The Nikkureyama tunnel repair (Japan) - 1994[119].
- Two building columns (Canada) - 1995, University of Sherbrooke's Faculty of Business entrance[120]
- Highway ten overpass columns (Quebec, Canada) - 1996[120]
- Champlain bridge piers in St. Lawrence River (Montreal, Canada) - 1996[120]
- Numbers of columns and beams in Webster Parkade parking garage structure (Sherbrooke, Canada) - 1996[120].
- CFRP strips to strength the roof structure of the North End Water Pollution Control Center (Manitoba, Canada) - 1996[121].

Wrapping FRP straps around existing columns to increase their ductility and shear capacity, is another alternative application for FRP composites[122]. The authors stated that the glass tendons are economical alternatives in rock engineering and tunnelling and carbon fibre tendons as stay cables[123].

2.6 Cost Considerations

In cost comparison, one should certainly consider the other expenses in relation to durability, rehabilitation, transportation and handling on the site, and not only the initial cost of the material.

Costs should be compared on the basis of the total cost of the finished structure and not the particular material chosen. For instance, the additional cost of using an alternative material will be a small percentage of the total cost of the structures, though the reinforcing bar itself is considerably more expensive than conventional steel. In addition, where corrosion is a significant factor, the extra cost of the alternative material should be set against the cost of protecting conventional steel, or possibly the cost of replacing it during the life of the structure.

Several people have already made cost comparisons. In terms of cost, the price per linear foot of FRP rebar is approximately twice that of steel and approximately equal to that of epoxy coated rebars[124 125]. FRPs are expensive compared to steel but they provide a solution to the deterioration of concrete bridges, eliminating the steel corrosion problem. Experience has shown that corrosion related problems in some structures become apparent only five years after construction[106]. The cost of repairs can be, after a few years, as much as actual construction. Thus repair policies based on initial costs can be reviewed in favour of a more realistic policy based on long term costs. It has been reported that the overall cost of FRP bridges is less than steel bridges of the same type. Test results indicate that the FRP structures are maintenance free for 40 years, except in especially bad environments[37]. Membranes wear out or crack with time, sealers must be re-applied every few years, and even epoxy-coated steel bars have lost their corrosion resistance after less than 10 years of service in some cases[28].

Ehsani[24] finds the price comparison based on weight or volume of materials meaningless. This is because most manufacturers add a premium for special shapes which are more labour intensive such as hooks, stirrups, spirals and the author also thinks that since FRPs are stronger than steel bars, consideration should be given to the reduction in the required area as a saving on cost. As an example, the prices per linear foot of straight rebars for Kodiak which is in use for this project ranges from $0.27 (1992) for a No 2(6mm) rebar to $2.05 (1992) for a No 9(29mm) rebar.

Basically, the initial cost of FRPs needs careful consideration to be given to all advantages of these rebars, including high strength, light weight, non-conductivity, corrosion resistance and long term savings in repair and maintenance cost, in order to be easily justified. However, more research must be conducted for defining the appropriate factors of safety and performance of FRP reinforced concrete elements under different applications and conditions[31].

2.7 FRP Reinforced Concrete Elements

There is a growing interest in the use of fibre composites. This section outlines the research carried out by other people on the potential areas where FRP can be utilised.

2.7.1 Externally Reinforced Concrete Elements Using FRP Composites

The behaviour of concrete beams externally reinforced with steel plates has already been studied. It has been reported that substantial improvements in performance with the right epoxy used, could be achieved in terms of ultimate load, crack control, and stiffness[126 127]. Bonding of steel plates to concrete has been shown to be an effective upgrading method when three important practices are followed.

1. The surfaces to be bonded must be clean-sandblasting for the steel and the concrete surfaces being preferred.
2. The epoxy should have a bond strength of at least that of the concrete (failure should occur in the concrete)
3. Plates must be long and thin to avoid an undesirable brittle plate separation failure, although additional anchorage at the ends of the plate can also be used to avoid this type of failure.

Steel plate bonding technique to the tension face of concrete elements has been used in Australia, Japan, Switzerland and South Africa since 1960s[126]. The technique offers advantages of being economical and fast to apply without or with very little disturbance to the structure operation together with non alteration of the configuration of the structure. The major disadvantage of this technique is the corrosion of steel plate, which damages the bond and results in failure of the structure. Therefore, the use of corrosion resistant fibre composite plates in lieu of steel is desirable because it eliminates the likehood of bond failure as a result of corrosion of steel. However, one has to be aware of brittle failure of FRP plates as well as the risk of fire, vandalism or accidental damage unless the strengthening is protected[128].

It has been reported that wrapping a column with fibre composites significantly increases the column capacity and the method is most effective on circular columns[129].

Sadaatmanesh and Ehsani[130] reported that about one half of the approximately 600 000 highway bridges in the US are in need of replacement or rehabilitation. Bonding steel plates on the tension face of a concrete member is a repairing and strengthening technique, which was used in the USSR in 1974 for a deteriorated 60-year old continuous-span reinforced concrete bridge. The authors studied the behaviour of four concrete beams externally reinforced with GFRP plates using four different types of epoxies, under two point bending. They stated that the selection of a suitable epoxy is very important in the success of this strengthening technique. They suggested that the rubber-toughened epoxies are particularly suitable for this application. It concluded that the flexural strength and stiffness of concrete beams can be increased by bonding GFRP plates to the tension zone using epoxy, and the behaviour of beams strengthened in this way is very similar to the behaviour of beams strengthened with steel plates.

The effectiveness of external strengthening using FRP plates was investigated by *Ritchie et al*[131]. Sixteen under-reinforced beams were tested under two point bending. Plates of glass, carbon, and aramid fibers were bonded to the tension side of the beams using a two-part epoxy. Contribution to the shear strength was achieved on some of the beams where side plates were used for end anchorage. It has been demonstrated that bonded plates of FRP are indeed a feasible method of upgrading the strength and stiffness of a reinforced concrete beam. This is also valid for concrete slabs[132].

Eight reinforced concrete beams with epoxy-bonded fiberglass reinforced plastic (FRP) plates is experimentally investigated by *Alfarabi et al*[133]. The RC beams are initially loaded to 85% of the ultimate flexural capacity and subsequently repaired with FRP plates, bonded to the tension face of the beam. The results generally indicate that the flexural strength of the repaired beams is increased. The use of an I-jacket plate provided a proper anchorage system and improved the ductility of beams repaired with plates of large thickness.

An et al[134] studied the behaviour of reinforced concrete beams having rectangular and T cross section together with epoxy bonded FRP plates to their tension face. They observed increase in stiffness, yield moment and ultimate moment of the beams and

reduction in the curvature at failure. They suggest that the strengthening technique is particularly effective in beams with a relatively low steel reinforcement ratio. Using a high strength concrete beam combined with epoxy bonded FRP plate on the tension face increases the ultimate moment of the section.

For achieving full flexural capacity and ensuring ductility at failure for concrete beams strengthened with either steel or glass, glass-carbon and aramid FRPs it is recommended by *Swamy et al*[135] that width to thickness ratio (b/t) of a plate should not be less than 50.

Arduini et al[136] reported typical failure types observed for plain concrete beams which are externally reinforced with GFRP and AFRP plates bonded to their tension zone. Plate peeling close to the plate end, shear cracks starting from the plate ends, flexural tensile cracks in concrete with rupture of FRP plate and flexural tensile cracks in concrete with also concrete crushing in the compression zone are the typical failures. The authors point out that using fully connected bottom and side plates (L-shape) helps to avoid plate peeling and shear failure.

Wight et al[137] conducted two point bending tests on four 300mm x 575mm x 5000mm concrete beams containing tension and compression steel reinforcements. One of the beams was a control specimen, another one was reinforced with non-prestressed carbon fibre sheets and two of them reinforced with prestressed carbon sheets. The CFRP sheets used in their study contained a volume fraction of 65% with thickness of 0.2mm and width of 300mm. The composite sheets were bonded to the tension zone of the beams. The authors point out that the labour and material cost of prestressing FRP sheets is very expensive. However, prestressed sheets are slightly more effective strengthening than unstressed sheets in terms of reduction in crack widths and delaying the initial cracking stage. The reduction in cracking provides smaller deflection for prestressed sheets. Both non-prestressed and prestressed sheets, which were externally bonded to concrete beams showed higher load capacity compared to the control specimen which contained no externally bonded FRP sheets.

Green et al[138] studied freeze-thaw behaviour of twenty-one rectangular steel reinforced concrete beams (100mmx150mmx1220mm) with CFRP sheets attached to their tension zone. The beams subjected to freeze-thaw cycles for 16 hours were placed in a room where the temperature kept at -18^{0}C overnight and thawed 8 hours in a water bath (15^{0}C) during the day. After exposure to freeze-thawing conditions for the period of 50 days, the beams were tested under two-point loading. The authors observed that the cracking load of the beams subjected to freeze-thaw conditions was reduced. This is due to the fact that, the freeze-thaw action affects the properties of concrete and therefore concrete gets damaged slightly. The main failure mode of the beams was peeling of the CFRP sheet. The concluded that CFRP sheets are effective at strengthening reinforced concrete beams in both flexure and shear. Their results showed that the beams strengthened with CFRP sheets did not appear to be damaged by exposure to up to 50 days.

2.7.2 FRP Grid Reinforcements Used in Concrete Elements

There is very little information on the use of three dimensional fibre fabrics in structural concrete. For the purpose of improving the durability of reinforced concrete two- or three dimensional grid shape New Fibre Composite Material for Reinforcing Concrete (NEFMAC) which is composed of glass or carbon FRPs, have been developed and used in tunnel structures in Japan since 1986[139]. *Sekijima et al*[140] constructed a pedestrian bridge reinforced with prestressed NEFMAC grid reinforcement. The application is a success considering the bridge is already in use.

Zia et al[141] examined the flexural and shear behaviour of concrete beams reinforced with 3-D continuous carbon fiber fabric having 1.79 specific gravity, 3430MPa tensile strength and 235.2GPa elastic modulus. Conventional steel reinforced beams have also been tested under two point bending for a comparison. Their results showed that both types of beam developed the same ultimate strength as designed and reached the same deflection at failure. *Bank & Xi*[142] also have expressed similar conclusions. The closely spaced vertical carbon fibre elements served very effectively as shear reinforcement to prevent shear failure.

Ahmad et al[143] conducted punching shear tests on four carbon fibre reinforced (CFRP) and two mild steel reinforced concrete slabs. The load applied on all slabs was monotonic and was at the centre. The test results showed that CFRP reinforced slabs behaved in a more ductile manner than that of steel reinforced ones resulting from a non-linear behaviour in the post-cracking stage.

Bank et al[144] suggested that the potential for developing three-dimensional FRP cages for reinforcing concrete elements is high. The authors studied flexural behaviour of 200mm x 300mm x 3000mm (2400mm span) concrete beams reinforced with cages containing pultruded glass fibres with polyester resin. The beams containing the steel cage have also been cast for comparison. The failure mode observed for all beams was a brittle one, which took place in the tension zone of the beam. They point out that this type of failure is not desireable for serviceability design considerations. The authors noted that the number of flexural cracks in FRP reinforced beams were less than the steel reinforced beams. They also observed wider cracks in FRP cage reinforced beams than the steel cage reinforced beams. However, in terms of load capacity, the FRP cage reinforced beams performed well.

2.7.3 Prestressed Concrete Beams Using FRP Tendons

In the prestressing process beneficial stresses are deliberately introduced into a structure. This way, longer linear elastic behaviour of a concrete element at service load can be achieved. It is usually applied to materials, which are strong in compression but relatively weak in tension, such as concrete and sometimes brickwork. Highly tensioned cable or tendon is passed through the member and then securely anchored at the ends. This puts the member into compression before any external loads are applied and gains the elimination of cracks.

It is suggested, if FRPs are used as prestressing tendons for prestressed concrete instead of high strength steel, the loss of prestress caused by creep, shrinkage, elastic strain, and temperature changes in the concrete, is expected to be small due to the low elastic modulus of FRP compared to steel[145 146]. Research by *Kajfasz*[147] suggests that fibre-glass tendons in the form of stiff rods in which the fibres are glued together with

polyester resin would prove to be more efficient for prestressing. Longitudinally prestressed Polystal (68% glass fibre glued together with polyester resin) tendons have already been used in a bridge and a tunnel in Dusseldorf in Germany in 1980[148].

Somes[149] stated that if FRP tendons are used in concrete for prestressing, consideration should be given to the aspects, such as the design and manufacture of anchorages, avoidance of surface damage to the tendons at casting and the choice of correct tensioning stress. The author conducted two point bending tests on eight FRP tendon reinforced prestressed beams that showed failure of concrete in compression.

However, *Iwaki et al*[150] pointed out that in most cases prestressed concrete beams can fail in a catastrophic way i.e. brittle flexural failure due to elastic rupture of the FRP used. This type of failure mode is undesirable from the view point of the maintenance and hazard anticipation of structures. They suggest that an appropriate combination of bonded and unbonded tendons with different amounts of tensioning force will satisfy the required ductility i.e. elimination of catastrophic failure.

Mutsuyoshi et al[151] pointed out that prestressed concrete structures with an external steel cable system have been applied to real life structures mainly in Europe. The authors carried out two point bending tests on T-shaped beams having 3000mm length 400mm overall depth. The beams were reinforced with steel rebars and stirrups. For each beam externally prestressed stranded steel cable, AFRP and CFRP cables were longitudinaly fixed on opposite sides. The prestressing force applied on steel, AFRP and CFRP cables was 63%, 58% and 52% of their ultimate tensile strengths. Failure mode of concrete compression failure was observed for steel and AFRP beams whereas CFRP beams were failed simultaneously both in compression failure of concrete and breaking of cables. It should be noted that in their study the breaking load of CFRP cables is smaller than the others with the same amount of prestressing force (70kN) applied on all cables. This could be considered as a reason for breaking of CFRP cables. Test results based on the load deflection relationship showed that the beams reinforced with FRP indicate almost the same behaviour as the steel reinforced beam. They claim that FRPs can be applied to actual prestressed concrete as external cables.

Currier et al[152] studied the deflection of nine concrete beams having dimensions of 127mm x 254mm x 5490mm reinforced with prestressed epoxy/earbon, epoxy/aramid and glassfibre tendons for a period of one year. The authors stated that the current methods available for determining the long-term deflections underestimate the deflections of members prestressed with FRP tendons.

2.7.4 Unstressed Concrete Beams Reinforced with FRP Composites

The beam is probably the most common structural element and is subjected to bending which causes curvature of the member. Steel reinforced concrete elements have been studied for years and their design equations and standards are well established. However, the current design methodology for steel reinforced concrete beams cannot be applied directly to FRP reinforced concrete beams[153]. However, the others state that the classical theories employed for analysing steel reinforced beams can be used for accurately predicting the behaviour of GFRP reinforced concrete beams[125]. *Clarke*[154] states that there are two approaches when introducing a new type of reinforcement, which have very different properties. Either adapt the existing method or formulate new design rules. Fortunately, the first is the most feasible option, as it will cost less and is quicker.

Nawy and Neuwerth[155] investigated the flexural behaviour of concrete beams reinforced with GFRP bars. They used chopped wire in the concrete mix for some of the beams to increase the shear capacity. Test results showed that at ultimate load, the deflection of GFRP reinforced beams was approximately three times greater than that of the corrosponding steel reinforced beams. A larger number of distributed cracks were observed in GFRP reinforced beams than in the steel reinforced beams. This indicates a good mechanical bond between the bar and the concrete. The test results also showed that the behaviour of the beams regarding cracking, ultimate load and deflection could be predicted with the same degree of accuracy as for steel reinforced concrete beams.

Pre-and post-cracking deflection behaviour of twenty-five rectangular concrete beams reinforced with FRP rebars were designed and tested under bending by *Faza et al*[153].

Test variables included concrete strengths (29-69 GPa), type of FRP rebar (smooth, ribbed, sand coated), and rebar size. The test results showed that the use of sand coated FRP rebars with high strength concrete improves the load deflection behaviour of concrete beams. The authors found that the theoretically predicted deflections of GFRP reinforced beams were underestimated using an effective moment of inertia (Ie), as specified in the ACI 318 Building Code[156].

Behaviour of concrete beams reinforced with GFRP bars and stirrups was experimentally investigated by *Saadatmanesh and Ehsani*[130]. Three beams were constructed with GFRP longitudinal rebars and conventional steel stirrups; the other three were constructed with longitudinal steel rebars and GFRP stirrups. The results indicated that GFRP stirrups effectively resisted the shear forces in all beams, considering none of the beams failed in shear. The number and pattern of shear cracks observed was similar to the beams that had conventional steel stirrups. Based on the observation of a large number of uniformly distributed cracks, it was concluded that a good mechanical bond was developed between the GFRP bars and concrete. The authors stated that deflection might become the limiting design criterion for specific structural elements due to the low modulus of elasticity of GFRP rebars.

Chaallal et al[106] investigated the effect of temperature on the flexural behaviour of simply supported rectangular concrete beams, four reinforced with 2No 9.3mm GFRP and three with 2No 11.3mm steel rebars. 30MPa strength concrete beams were tested under two point bending at two temperatures, 20^{o}C and -30^{o}C. Flexure tests also were carried out on 30MPa concrete beams reinforced with steel and with NGFR (New Glass Fibre Reinforcement) rebars for two temperatures: 20 and -30 C. It was observed that GFRP beams performed in a similar manner to steel beams at low temperature (-30 C) which did not affect the overall strength of concrete beams reinforced with GFRP rebars.

Benmokrane et al[157] investigated the flexural behaviour of concrete beams containing FRP rebars and identical conventional steel rebars. An experimental and theoretical comparison was made between the beams, in terms of cracking behaviour, load-carrying capacities and modes of failure, load-deflection response, flexural rigidity,

and strain distribution. Experimental strain distributions demonstrated the perfect bond between FRP bars and the surrounding concrete. The authors stated that ACI Code formulae for predicting deflection response, cracking-ultimate moments, and cracked-effective moments of inertia could easily be adapted for modelling the flexural behaviour of concrete beams reinforced with FRP reinforcing bars if appropriate modifications are made.

Larralde et al[124] conducted bending tests to investigate the behaviour of concrete beams reinforced with FRP rebars and FRP in combination with steel bars. The results showed that the calculated ultimate loads differ from the experimental values. The deflection values are fairly well predicted at load levels of approximately 30% of the ultimate load.

Satoh et al[158] conducted flexural tests on four 100/150/1200mm concrete beams reinforced with conventional steel, AFRP, CFRP, GFRP straight bars and steel strirrups as well as on four polymer mortar repaired beams containing the same type of reinforcement. The results showed that tensile stress in the main reinforcement, the concrete crack width and the central displacement of FRP reinforced beams agreed with the calculated values. Those parameters showed decreased values for repaired reinforced concrete beams.

In *Okamura et al*'s[159] paper, the design concept of concrete members reinforced with continuous fibre reinforcing materials is discussed. For the design concept they point out the following for reinforced concrete:

- Shear failure which could be brittle failure of concrete in the compression zone or breaking of FRP rebars
- Flexural failure which could be brittle failure of concrete crushing in the compression zone and the rupture failure of FRP

Both concrete and FRP are brittle materials and hence the failure of the FRP reinforced members is influenced by the least ductile element within the member

resulting in catastrophic failure. Research by the authors suggests that to deal with this issue two concepts need to be adopted:

1. An enhanced materials factor(γ_m) should be used to increase the safety factor for FRP materials i.e. $f_d=f_k/\gamma_m$

   f_d: design strength

   f_k: chararecteristic strength of the reinforcement

γ_m of FRP is suggested to be higher than γ_m of steel which is 1. For FRP it may be taken to be between 1 and 1.3.

2. The design capacity of the member cross section R_d should be determined as below in order to obtain sufficient safety of concrete members by using an appropriate member factor:

   $R_d=R/\gamma_b$

   R: calculated capacity of member cross section

   γ_b: member factor (1.15 for steel, it may be taken as between 1.15 to 1.3 for FRP. (Note that in the latest ammendments of BS8110, this factor is given as 1.05)

In this paper, the authors also suggest limits for allowable crack widths being between 0.3 and 0.5mm in the case of combined use of FRP and steel, and the material coefficient for static fatigue (1 for steel) may be taken as between 1.2 and 1.3.

Al-sayed et al[160] studied the flexural behaviour of concrete beams. The authors tested nine beams, three of which were reinforced with 3ϕ14 steel bars at an effective depth of 160mm having the dimensions of 200x210x2900mm. The other three were reinforced with 4ϕ19 GFRP bars at an effective depth of 157.5mm, having the same dimensions as above. The last three beams were reinforced with 4ϕ12.7 GFRP bars at an effective depth of 210.7mm, having the dimensions of 200x260x2900mm. All the beams were provided with ϕ8 steel links at 120mm centres, tested simply supported over a span of 2700mm and loaded by two concentrated loads. The compressive strength of concrete was 31.3 MPa obtained from a w/c of 0.5. The tension steel had a yield stress of 553MPa, the 12.7mm GFRP bars had an ultimate stress of 740MPa,

and the 19mm GFRP had an ultimate stress of 620MPa. The authors concluded that the GFRP reinforced beams can be flexurally designed using the ultimate design method for over-reinforced sections. However they point out that the deflection at service load for such beams may control the design of many GFRP reinforced structures. They also point out that the minimum cost criteria, which connects to an optimum design can be achieved by simply increasing the depth of cross section by 24%. This increase reduces the GFRP bars by 55%, increases the flexural capacity by 40 %, reduces the deflection at service load by 34% and at an ultimate load by 13%, decreasing the overall cost by 40%. They also suggest that for relatively ductile types of concrete, compression failure of GFRP reinforced beams can be obtained by using a 1.5 factor of safety against the possibility of experiencing tensile failure of GFRP bars.

In *Mikami H et al*'s[161] paper, fatigue characteristics of reinforced and prestressed concrete beams reinforced with braided AFRP rods (aramid fibres are 65% by volume) are discussed based on laboratory experiments. Rods were used as tendons, tension reinforcement and spirally-formed shear reinforcement in rectangular beams having dimensions of 200mmx250mmx2400mm. The ratio of shear span to effective depth of the beam was taken as 3. Before casting the concrete, tendons were stressed at about 45% the ultimate tensile force of AFRP rod. Shear reinforcement consisted of either deformed bars (6mm dia. links) or braided AFRP spiral (6.9mm dia.) reinforcement. MOE of deformed (19.1mm and 6.3mm), braided, straight spiral bars (15.9mm-straight and 6.9mm-spiral) were 196GPa, 63.76GPa and 59.84GPa respectively. Concrete strengths varied with values of 32, 22 and 39MPa. None of the specimens had failed up to 2million cycles. It was concluded that for the restraint of incremental beam deflection, AFRP tendons offer the same efficiency as deformed steel bars. Also, beam test results for fatigue of concrete can be predicted conservatively by the equation given in the Japaneese Standard[162] but the beam test results for fatigue of AFRP tendons are not in good agreement with the equation proposed by the author.

Ozawa et al[163] studied the static and flexural fatigue behaviour of concrete beams reinforced with FRP longitidunal bars and stirrups, which were formed in one body

and was placed in the concrete beams. FRP reinforcements consisted of continuous glass and carbon fibres impregnated with resin and formed in one body by the filament winding method. 10 specimens were tested under two-point bending; two of them were statically loaded and the other eight were fatigue loaded. The authors' static test results showed that compared with a steel reinforced concrete beam, the lower stiffness of FRP reinforcement leads to higher location of neutral axis, lower flexural rigidity of the beam and larger stresses in the bottom longitidunal bar after initial flexural cracking. Also, their experimental results agree with the calculations by the elastic theory in which total cross sectional area is effective before flexural cracking and approach the calculation by the beam theory in which tensile stress in concrete is ignored after cracking. After appearance of diagonal cracks, however, the measured deflection becomes larger than the calculated one because of the assumption that shear deformation of the beam is neglected. The authors point out that the their fatigue results were varied. Fatigue failure of the bottom longitidunal bars in the constant moment region or that of the longitidunal bars and stirrups in the shear span caused the failure of all specimens. The rupture of FRP reinforcement occurred at the cross point of longitudinal bar and stirrup near cracks. Most flexural cracks propagated along the stirrups and a few between stirrups.

Clarke et al[32] carried out two-point bending test on the beams having the dimensions of 150mm x 250mm x 2500mm and shear spans of 787mm. The main variables are reinforcement type, surface texture and cross-sectional shape of the bars, stirrup spacing and main reinforcement areas. The authors outlined the points based on the test results:

Bond failure: The bond characteristics of textured FRP pultruded rods are dominated by the shear strength of the resin matrix at the surface. Suitable pultrusion resins have a shear strength higher than that of concrete and, hence, bond failure of textured rods is expected at the concrete interface. Deformations on the surface of FRP rods similar to the ones found on deformed steel rebars cannot theoretically enhance the bond characteristics in the same way, since shear failure could occur through the composite.

The stress levels in FRP reinforcement: The overall stresses developed in the FRP rods at failure of the beams were well below the theoretical predicted values. This is a consequence of the fact that FRP reinforced elements tend to be over reinforced, leading to the failure of the concrete in compression. However, such premature failures do not help establish the maximum bond and tensile stresses that can be developed in FRP rods. As a result, some experiments were designed aimed at pushing the stress in the FRP rods to as high a level as possible. This was achieved partly by designing the section with relatively small areas of reinforcement and partly by enhancing the strain potential of the concrete in compression.

Shear failure and deformation: Combinations of steel and FRP reinforcement were used as main and link reinforcement in order to differentiate the effects. FRP shear links designed to resist specific stress levels were also demonstrated to perform well and to prevent shear failures without increasing the overall deflections significantly. Analytical work carried out in parallel with the experimental work gives good predictions of the behaviour of FRP and steel reinforced beams and validates the assumption that plane sections remain plane. This is very important from the design point of view, since it means that established design equations can be used with only minor modifications.

Serviceability: due to the lower stiffness, deflections and crack widths may become dominant criteria. For a given load, cracks in a FRP reinforced beam will generally be wider than for equvalent steel reinforced beam. However initial studies have shown that existing formulae may be used to predict crack widths.

Ngo & Scordelis[164] claim that the finite element analysis (FEA) offers a complete picture of the stress distribution in the entire beam, which cannot be usually obtained by other analytical or experimental methods. However, the authors have drawn attention to the fact that there are several factors that should be kept in mind regarding the use of the FEA method. The method is an approximate analytical procedure whose accuracy depends on the fineness of the mesh size. Furthermore, the accuracy of the analytical results, when referred to actual RC members, all dependent on (including all of the major influences) the analytical idealization of the actual member.

The other important thing is the computational effort of the method i.e. the consideration of time which takes quite a bit to solve the problem and the storage capacity of the computer. However, nowadays, the storage capacity of the computers is not a problem.

Alsayed & Al-Salloum[165] present a minimum cost design and behavioural assessment for simply supported beams reinforced with FRP and steel beams. They emphasized that due to no yielding plateau with FRP reinforced concrete beams, it is expected that a concrete member reinforced with FRP materials may have brittle failure, higher initial cost and higher deflection under service load conditions.

The proposed formula for the initial cost of the beam per unit length for a given cross section is as follows:

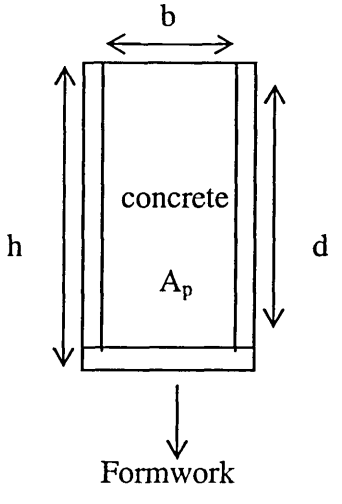

$$Z(\rho, d)=[b(d+d_1)-\rho bd]C_c+\rho bdC_p+[2(d+d_1)+b]C_f$$

ρ: reinforcement ratio
d_1:concrete cover
C_c:cost of concrete per unit sectional area of concrete per unit length of beam
C_f:cost of formwork per unit peripheral length around section (sides and bottom) per unit length of beam
C_p:cost of fibre plastic rebars per unit of area of material employed in section per unit length of beam
C_s: cost of steel rebars per unit area of material employed in section per unit length of beam

Some researchers have recommended reduction factors to be applied to the FRP ultimate tensile strength, to minimize the failure due to breaking of FRP rebars which is more brittle than failure due to crushing of concrete[166].

Faza & Gangarao[167] recommended that the maximum permissible strength be 0.80 of the design strength. *Nanni*[168] suggested that the strength reduction factor to be taken as 0.70.

Kobayashi & Fujisaki[169] conducted tests on concrete prisms having the dimensions of 100mm x 100mm x 650mm subjected to compressive forces. They point out that the

aramid FRP rebars failed earlier than their ultimate compressive strength. This suggests that the aramid FRP reinforcements may not be suitable for columns. *Faza & GangaRao*[170] conducted two-point bending tests on twenty-two beams having the dimensions of 152mm x 305mm x 3000mm, reinforced with straight FRP rebars and FRP stirrups. The concrete cylinder strengths of the beams were 29MPa, 35MPa, 45MPa and 52MPa respectively. The size of the rebars and the stirrups is not clearly specified in the paper. They reported that the ultimate moment capacity of concrete beams having 52MPa of concrete strength was increased by 90% when FRP rebars of ultimate strength of 869MPa were used instead of mild steel rebars. The authors refer to 52MPa concrete as a high strength concrete and also conclude that the cracking moment of the high strength concrete beams was increased with noticeable reduction in crack widths. The failure mode observed was a shear failure followed by secondary compression failure.

The principal factors that influence the short-term deflection of a member under load are the magnitude and distribution of the load, span and conditions of restraint, section properties including reinforcement percentages, material properties, number and extent of flexural cracking[171].

Alsayed[172] studied the predicted and measured load deflection relationships for 12 concrete beams reinforced with steel and GFRP reinforcing bars and steel stirrups. In this study he used ACI318 Code and proposed a modified effective second moment of area, I_m i.e. I_m replaces I_e effective second moment of area. The author concluded that the current ACI model for predicting the load-deflection relationship for steel RC beams underestimates the actual deflection of GFRP RC beams. However, replacing I_e with I_m improves the prediction of the service load deflection of GFRP RC beams.

Nawy & Neuwerth[173] used Branson's deflection equation for evaluating the effective moment of inertia of the cracked section: The beams tested contain FRP rebars (6.3mm dia.) in the tension zone of the concrete beams.

$$I_e = \left(\frac{M_{cr}}{M_a}\right)^3 I_g + \left(1 - \frac{M_{cr}}{M_a}\right)^3 I_{cr}$$

$$I_m = \frac{23 I_{cr} I_e}{[8 I_{cr} + 15 I_e]}$$

I_e : effective moment of inertia

I_m : proposed effective moment of inertia

I_{cr} : cracked section moment of inertia

M_{cr} : cracking moment as observed in the tests of the beams

M_a : moment of deflection level sought

Deflection :

$$\Delta_{max} = \frac{Pa}{24 E_c I_e}(3L^2 - 4a^2)$$

a : distance from the loading point to the support at each end (mm)

P : concentrated load (kN)

L : span (mm)

E_c : the concrete modulus modulus of elasticity(GPa)

The authors point out that the values of deflection for beams (ACI 318-71C) reinforced with FRP rebars underestimates I_e for low percentage of GFRP reinforcement. Therefore, calculated deflections are lower than observed values.

Masmoudi[174] studied the effects of the reinforcement ratio on the concrete and FRP reinforcement strains, neutral axis depth and ultimate moment capacity. The dimensions of the simply supported beams tested under two-point loading were 200mmx300mmx3300mm. The FRP rebars used in the study were E-glass fibres impregnated in a thermoset polyester resin. The beams were reinforced with 2Ø12.7, 3Ø12.7, 4Ø12.7, 6Ø12.7 FRP rebars respectively. The beams also contained 32Ø10 steel strirrups. The experimental results showed that immediately following the first crack, the neutral axis was close to the extreme compression fibres and then moved down as the applied moment increased. The authors believe that this is due to the unstable propagation of first cracks. The effect of the reinforcement ratio on neutral axis depth was simply, as the reinforcement ratio increased, the neutral axis moved away from the extreme compression fibres. When the ratio of the reinforcement increased, the strain of concrete and that of the FRP rebars decreased for a given load level. Finally, ultimate moment capacity of the beams increased with increase in the

reinforcement ratio. This is also confirmed by *Theriault et al*[175]. The authors carried out two-point loading tests on the concrete beams (130mmx180mmx1800mm) reinforced with ∅12.3 GFRP rebars and ∅6 smooth steel compression rebars and stirrups. The authors focused on the effects of the concrete strength and the reinforcement ratio on the behaviour of concrete beams including cracking and deflection. The results showed that the higher the concrete strength, the wider the crack for the same applied moment. The authors pointed out that this could be tempered by a higher reinforcement ratio. They also observed that the stiffness of the tested beams stayed about the same whether the beams loaded statically or cyclically. The stiffness also did not change much with the concrete strength but, it was higher for the beams containing more rebar area than the ones less rebar area.

2.8 Conclusions

The literature review carried out by the Author describes fibre composites and their types, manufacturing techniques, mechanical properties, physical and environmental factors affecting their performance and their applications as reinforcements in concrete.

Glass fibres are more popular in the construction sector than carbon and aramid fibres. This is due to the fact that they are easier to obtain and the least expensive. GFRP rebars are usually composed of glass fibres bound together with a thermosetting resin, and manufactured using a pultrusion process.

There are no standard bar sizes or surface profiles of FRPs yet due to the fact that each supplier has its own method of producing a bar. There are several companies producing FRP bars commercially in the UK (Fibreforce), USA, Japan, Canada, France, Germany and Holland. In this research, work has been focused upon using GFRP rebars (KODIAK-72% glass fibres+28% polyester resin) in concrete beams.

Embedded steel is generally very durable and it is protected from corrosion by the alkaline environment of concrete. However, in highly aggressive environments the protection offered by concrete to steel can be insufficient and necessitate expensive

work of concrete repair in service. In the case of FRP, the durability is a function of both resin and the fibre composition. The amount and the type of fibre in the composite directly influence the mechanical properties of FRP materials. One must note that glass fibres and some resins are degraded by the high alkalinity of concrete. So far, the works have been concentrated on alkali resistant glass (AR glass) or the use of carbons or aramids but little attention has been given to the resin[176].

The main advantage of FRP over steel is its corrosion free feature. High tensile strength, high fatigue performance, high energy absorption, low density, low conductivity and electrical interference, lower concrete cover in concrete applications such as in cladding panels and low maintenance cost are the potential advantages of FRPs over steel. However, there are also disadvantages present for FRPs compared with steel i.e. high cost, low elastic modulus, glass fibre deterioration by alkaline attack (although this may be couterbalanced by using alkali resistant glass and polyester and vinylester resins), FRP prestressing tendons need to be anchored with care, long term strength of FRP can be lower than short term strength.

Bond between reinforcing bars and concrete should be adequate for satisfactory performance of reinforced concrete sructures. In order to make the bond strength high, one has to consider the influential parameters such as concrete strength, embedment length, concrete cover, type of rebar and rebar spacing. Many people have studied the bond of steel. It is well known that steel bars having a ribbed surface texture have better bond than smooth rebars (plain rebars). The bigger the ribs are the higher the magnitude of the bond strength of steel rebars. Typical values for bond strength of reinforcement obtained from pull-out tests on concrete blocks are 2.22MPa (plain steel) and 3.34MPa(ribbed steel) for a concrete strength of 30MPa, 3.83MPa(plain steel) and 5.19MPa(ribbed steel) for a concrete strength of 77MPa. This suggests that the higher the concrete strength the higher the bond strength. When silica fume is used in the concrete, the bond strength is enhanced significantly. Having said that the number of methods available for determining the bond strength of steel reinforcement varies and hence the values for bond strength too. The bond of epoxy coated ribbed steel rebars is between 6% and 35% less than the bond strength

of uncoated ribbed steel bars. This could be due to the differences in rib geometry between rebars.

There are no available design guidelines for bond behaviour of FRP rebars in concrete. However, tests conducted for the bond of FRP rebars have so far used the current methods available for steel rebars. The bond strength of ribbed GFRP rebars obtained from pull-out tests is higher than smooth and sand coated GFRP rebars. The bond strength of GFRP is aproximately 10% lesser than steel rebars.

The development and the field applications of FRPs have been increasing since 1970s. Potential applications of FRP reinforced concrete structures are namely, structures subjected to de-icing salt, multistorey parking facilities, pavement slabs, concrete bridge decks, retaining walls, water treatment plants, chemical factories, paper mills, liquid gas and oil reservoirs, pipelines, chimneys and nuclear plants, foundation slabs etc. Wrapping FRP straps around the existing columns to increase their ductility and shear capacity is another alternative application for FRP composites.

In the whole life cost of analysis and comparison, one should consider not only the initial cost of material but the other expenses in relation to durability, maintenance, transportation and handling on site. FRPs' initial cost is high compared with steel but when the other factors are considered then the cost of using FRP in concrete will be less.

The external strengthening with steel plates on the concrete is a technique used for repairing concrete, increasing ductility, reducing crack width, increasing ultimate load capacity and increasing fatigue strength. Nevertheless, the weakness of steel against corrosion, which causes debonding, is still apparent. Hence, using FRP plates for external strenghtening (which is relatively new) eliminates the likelihood of bond failure as a result of corrosion. However, the selection of the adhesive plays an important role in FRP case. Before actually using the adhesive for bonding, it is important to find out its suitability through testing.

So far, there is very little information on the use of 3-D fibre fabric in structural concrete. However, the comparison made between FRP grid(cage) reinforced beams and steel cage reinforced beam shows a reduction in the number of flexural cracks less but wider than steel reinforced ones. In terms of load capacity 3D FRP reinforced beams perform better than steel cage reinforced beams for a similar amount of rebar.

FRP bars and cables are perfect candidates for prestressing due to the fact that the loss of prestress caused by creep, shrinkage, elastic strain and temperature changes in concrete are expected to be small because of the low modulus of elasticity of FRP compared to steel. The available anchorage systems used in prestressing steel cannot be applied on FRPs since their transverse strength is approximately 75% less than steel. Different types of achoring systems for FRP rebars were proposed by several researchers but the most common one used in the laboraory tests is embedding the ends of the rebar into steel/copper tubes which contain epoxy resin. This method is adopted for this study due to its reasonably fast production and good accuracy in the test results.

Steel reinforced concrete elements have been studied for many years and as a result of this the design methodology has been long established and in general, providing safe structures. Flexural behaviour of FRP reinforced unstressed beams has been looked at by several researchers, but still remains an ongoing process. The existing conventional (steel based) design formulae are used to predict how FRP reinforced beams may behave compared to steel reinforced ones. The question is to decide whether the existing codes and equation can be used for FRP reinforced elements or not. Up until now, flexural behaviour of FRP reinforced beams under two point loading can be summarised as follows.

Crack widths have traditionally been limited because it was thought that they influenced the corrosion of the steel reinforcement. It is now generally accepted that crack widths have little or no significant influence on the long term durability of reinforced concrete structures[177]. Therefore, the main reason for controlling crack widths appears to be the aesthetic view of the structures and perhaps also their

watertightness. In FRP elements cracks seem deeper and fewer compared to steel reinforced beams.

Deflections are likely to be higher than for equvalent steel-reinforced elements. For an uncracked section the deflection will be a function of the gross concrete cross section only and therefore not influenced so much by the type of reinforcement. In general, the actual deflection will depend on the distribution of cracks, which will be influenced by the bond between the reinforcement and concrete.

Shear and rupture of FRP rebars are typically observed failure modes with or without, stirrups used in the beams. Some reduction factors have already been suggested for FRP's ultimate strength to minimize the risk of failure due to breaking of FRP rebars which is more brittle than that due to crushing of concrete alone. Up to present, most research suggests using existing design equations helps to predict the behaviour of FRP reinforced beams.

The idea of using GFRP in this research is that glass is less expensive than corrosion resistant steel, less rebar cover is needed, hence reduced handling weight and the possibility of using a lower concrete grade to reduce cost.

Despite FRP's recogniseable properties and durability, it is unlikely that the FRP reinforcement will fully replace steel in future. Previous work so far has shown that FRP reinforcement is a viable and cost effective alternative to steel in special circumstances i.e. as an alternative to stainless steel[110]. Also, it has been accepted so far that the use of FRP in applications where the consequences of failure are not too severe should be considered. There are several significant aspects that need to be addressed for use of FRP such as suitable reinforcement shapes with a consistent quality in terms of their properties, better understanding of the behaviour of the concrete elements reinforced with FRP under different load and environmental conditions, an orthodox development of design for structures reinforced with FRP. The need for Codes and Standards for FRP reinforced concrete elements is essential. There are so far design guidelines reported by the ACI[178] and the Institution of Structural Engineers[179]. More research and development work is required on different

FRP materials embedded in different type of concrete elements before fibre composites can be widely accepted. In this way general design rules can be based upon different configurations and dimensions of rebars for the best value solutions. Following on from the last point, the application of FRP reinforced concrete beams for use in precast concrete elements such as lintels and short span wall units, where deflection is not likely to be a critical consideration but exposure is would be particularly appropriate. Precast lintels are very common and used widely throughout the construction and building industry and there is much commercial scope for replacing steel rebar with FRP especially for small beam cross sections; where cover is necessarily limited. The market potential could be considerable; encompassing units up to 4.5m in length[180] and with typical commercial section of rectangular 100mm wide 200mm deep up to 200mm by 200mm[181].

However, one has to decide whether[154] to adopt existing design methods or devise a completely new set of design rules, which although technically correct but might not justify the time and effort involved for the economic return gained. Therefore, it would be more expedient, at least in the first instance, to opt for following the former course i.e. use existing standards and codes as a basis and tailor them to suit the particular properties and behaviour of the new material.

Resumé of objective targets for Research Programme

The properties, behaviour, existing and possible applications of FRP materials have been comprehensively discussed in this chapter. Therefore, in summary the Author considers that the proposed programme should incorporate a further consideration and investigation of the following aspects and points stated below:

- the practicalities of the specimen size in respect of an experimental programme
- a simple performance comparison within the context of the adopted design envelope
- the context of the current design codes such as BS8110
- areas of practical application
- the efficient use of the materials
- serviceability constraints
- the influence of different grades and types of materials
- novel approaches to design element geometry

2.9 REFERENCES

[1] Weidmann G et al, Structural Materials, ISBN 0408 04658 9, 1990.

[2] Gupta P K, Glass Fibres for Composite Materials, Composite Materials Series, V2, 1988, pp19-71.

[3] Savage G, Carbon-Carbon Composites, ISBN 0412 36150 7, 1993.

[4] Fitzer E & Heine M, Carbon Fibre Manufacture and Surface Treatment, Composite Materials Series, V2, 1988, pp73-148.

[5] Yang H H, Kevlar Aramid Fibre,ISBN 0 471 93765 7, 1992.

[6] Yang H H, Aramid Fibres, Composite Materials Series, V2, pp249-329, 1988.

[7] Chapman C B, Fibres, ISBN 0408 70575 2, 1974.

[8] Vodran G L, Applications of Steel Fibre Reinforced Concrete, Concrete International,November 1991, pp44-49.

[9] Soroushian P & Bayasi Z, Fibre-type Effects on the Performance of Steel Fibre Reinforced Concrete, ACI Materials Journal, March-April 1991, pp129-134.

[10] ACI Committee 506, State -of-the-Art Report on Fibre Reinforced Shotcrete, Concrete Internatinal, Dec. 1984, pp15-27.

[11] Abdul-Wahab, H M S, Strength of Vertical Joints with Steel Fibre Reinforced Concrete in Large Panel Structures, ACI Structural Journal, July-August 1992, pp367-374.

[12] Ogorkiewicz R M, Thermoplastics, , ISBN 0 47165306 3, 1974.

[13] Miesseler H J and Preis L, High Performance Glass Fiber Composite Bars as Reinforcement in Concrete and Foundation Structures, Strabag Bau-Ag, Bayer, pp1-26.

[14] Shields J, Adhesives Handbook, ISBN 0408 70064 5, 1970.

[15] Benmokrane, Chaallal & Masmoudi, Glass Fibre Reinforced Plastic(GFRP) Rebars for Concrete Structures, Construction and Building Materials, 1995, V9, No 6, pp353-364.

[16] Taylor G D, Materials in Construction, ISBN 0 582 21431 9, 1994.

[17] C Ballinger, Structural FRP Composites, Civil Engineering, 1990, V60, PT7, pp63-65.

[18] Ellyin F et al, Material Processing and Manufacturing Technology, Advanced Composite Materials with Applications to Bridges, pp126-178.

[19] Vangiduram R et al, Effects of Process variables on the Ultrasonic and Vibration Response of Pultruded Glass/Epoxy Composites, Materials FO4 Noise and Vibration Control ASME, V80, 1994, pp17-25.

[20] Lackey E & Vaughan J G, Effect of Pultrusion Process Parameters on Flexural Strength, 38th International SAMPE Symposium, V1, May 1993, pp461-470.

[21] Lackey E et al, A Comparison of Properties and Processing of Epoxy Resins Used in Pultrusion, 49thAnual Conference, The Society of Plastics Industry, Feb. 1994, pp1-6.

[22] Lackey E & Vaughan J G, An Analysis of Factors Affecting Pull Force for the Pultrusion of Graphite/Epoxy Composites, Journal of Reinforced Plastics and Composites, V13, March 1994, pp188-198.

[23] Vangipuram R & Raju M P, Effect of Process Variables on the Ultrosonic and Vabriation Resaponse of Pultruded Glass/Epoxy Composites, Materials for Noise and Vibration Control, 1994, V18/DE V80, pp17-25.

[24] Ehsani M R, Alternative Materials and the Reinforcement and Prestressing of Concrete, ISBN 0 75 14000 76, 1993, pp34-54.

[25] Erki M A & Rizkalla S H, FRP Reinforcement for Concrete Structures, Concrete International, June 1993, pp48-53.

[26] Saadatmanesh H, Fibre Composites for New and Existing Structures, ACI Journal, May-June 1994, pp346-354.

[27] Johansen G E & Roll F A, Prestressed Kevlar/FRP Structural System, Proceedings of 1st Materials Engineering Congress, ASCE, 1990, pp640-648.

[28] Bedard C, Composite Reinforcing Bars: Assessing Their Use in Construction, Concrete International, Jan 1992, pp55-59.

[29] Tamuzs V & Tepfers R, Ductility of Non-metallic Hybrid Fibre Composite Reinforcement for Concrete, Proceedings of the Second International RILEM Symposium, FRPRCS-2, 1995, pp18-25.

[30] Neale K W & Labossiere P, Material Properties of Fibre Reinforced Plastics, Chapter 2, Advanced Composite Materials with Application to Bridges.

[31] Warring R H, The New Glass Fibre Book, Model & Allied Publications, 1976, pp1-123.

[32] Clarke J L & Waldron P, The Reinforcement of concrete Structures with Advanced Composites, Journal of the Institution of Structural Engineers, September 1996, V74, No 17/3, pp283-288.

[33] Dervaux G & Tousseyn L, Pultruded Glass Fibre reinforced Plastic Profiles, pp617-622.

[34] Ueda T et al, Failure Criteria for FRP Rods Subjected to a Combination of Tensile and Shear Forces, Proceedings of the Second International RILEM Symposium, 1995, pp26-33.

[35] McCrum N G, A Review of the Science of Fibre Reinforced Plastics Book, September 1970.

[36] Agbim C C, Concrete Reinforced with Glass Fibres, Magazine of Concrete Research, V16, No 49, Dec 1964, pp195-202.

[37] Bruce R, Fiber Reinforced Plastic Bridges in Chogqing, pp581-586.

[38] Wu W P, Thermomechanical Properties of Fibre Reinforced Plastic (FRP) Bars, PhD thesis, West Virginia University, 1991.

[39] Petrina P & White R N, Laminated Composite Reinforcemen for Cvoncrete Structures, Proceedings of the Second International RILEM Symposium, FRPRCS-2, 1995, pp10-17.

[40] Chaallal O & Benmokrane B, Pullout and Bond of Glass-fibre Rods Embedded in Concrete and Cement Grout, Materials and Structures, No26, 1993, pp167-175.

[41] Benmokrane B et al, Glass Fibre Reinforced Plastic (GFRP) Rebars for Concrete Structures, Construction and Building Materials, V9, N6, 1995, pp353-364.

[42] Bank L C, Shear Properties of Pultruded Glass FRP Materials, Journal of Materials in Civil Enginering, ASCE, May1990, V2, No 2, pp118-122.

[43] Masmoudi R et al, An Experimental Investigation of the Flexural Behaviour of Concrete Beams Reinforced with GFRP Rebars, Corrosion and Corrosion Protection of Steel in Concrete, July 1994, pp1340-1351.

[44] Kodiak FRP bars Data Sheet, International Gratings Ltd, 1995.

[45] Iosipescu N, New Accurate Procedure for Single Shear Testing of Metals, Journal of Materials, V2, No 3, Sept 1967, pp537-566.

[46] Walrath D E & Adams D F, The Iosipescu Shear Test as Applied to Composite Materials, Experimental Mechanics, V23, No1, 1983, pp105-110.

[47] ASTM, D-2344-76, Short Beam Method for Determining Shear Strength.

[48] Jones R, Mechanics of Composite Materials, ISBN 0 07 032790 4, 1975.

[49] Weinberg M, Shear Testing of Neat Thermolastic Resins and Their Unidirectional Graphite Composites, Composites, V18, No 5, 1987, pp386-392.

[50] Rahman A H et al, Behaviour of FRP Grid Reinforcement for Concrete Under Sustained Load, Proceedings of the Second International RILEM Symposium, FRPRCS-2, 1995, pp90-99.

[51] Benmokrane B et al, Bond Strength and Load Distribution of Composite GFRP Reinforcing Bars in Concrete, ACI Materials Journal, May-June 1996, V93, No3, pp246-253.

[52] Mandell J F et al, Tensile Fatigue Performance of Glass Fibre Dominated Composites, The Society of the Plastic Industry Inc., Feb 1981, Section-A pp1-5.

[53] Gerritse A & Den Uijl J A, Long-term Behaviour of Arapree, Proceedings of the Second International RILEM Symposium, FRPRCS-2, 1995, pp57-66.

[54] Uomoto T et al, Static and Fatigue Strength of FRP Rods for Concrete Reinforcement, Proceedings of the Second International RILEM Symposium, FRPRCS-2, 1995, pp100-107.

[55] Aslonova L G & Resnyansky O A, The Principal Operational Properties of New Types of Non-Metallic Reinforcement for Structures, Proceedings of the Second International RILEM Symposium, FRPRCS-2, 1995, pp3-9.

[56] Katsuki F & Uomoto T, Prediction of Deterioration of FRP Rods due to Alkali Attack, Proceedings of the Second International RILEM Symposium, FRPRCS-2, 1995, pp82-89.

[57] Zayed A M, Deterioration Assesment of Fiber-Glass Plastic Rebars in Different Environments, NACE Annual Conference, March 1991, p130.

[58] Tannous F E & Saadatmanesh H, Environmental Effects on the Mechanical Properties of E-Glass FRP Rebars, ACI Materials Journal, March/April 1998, pp.87-100.

[59] Abdalla H A & Elbadry M M, Temperature Effects on Concrete Members Reinforced with FRP Reinforcement, Annual Conference of the Canadian Society for Civil Engineering, May 27-30, 1997, pp171-180.

[60] Page C L & Anchor R D, Stress Corrosion Cracking of Stainless Steels in Swimming Pools, Structural Engineers, Dec 1988, p416.

[61] Stichel W, Corrosion of Stainless Steel Structural Components in Swimming Pools Atmospheres, Amts-und Mitteilungsblatt der Bundesanstalt fur Materialprufung (BAM), V16, No 4, 1986, pp511-515.

[62] Tanano H et al, Fire Resistance of Continious Fibre Reinforced Concrete, Proceedings of the Second International RILEM Symposium, FRPRCS-2, 1995, pp368-375.

[63] Doran D K, Construction Materials Pocket Book, ISBN 0 7506 1666 0, 1994.

[64] Fujisaki T et al, Research and Development of Grid Shaped FRP Reinforcement, ACI International Symposium, SP-138, 1993, pp177-192.

[65] Okamoto T et al, Practical Application and Performance of PPC Beam Reinforced with Braided FRP Bars, ACI International Symposium, SP-138, 1993, pp875-894.

[66] Kong F K & Evans R H, Reinforced and Prestressed Concrete, 1994, ISBN 0 412 37760 8, pp220-224.

[67] Darwin D & Graham E K, Effect of Deformation Height and Spacing on Bond Strength of Reinforcing Bars, ACI Structural Journal, Nov-Dec 1993, pp646-657.

[68] BS8110, Structural Use of Concrete, 1985.

[69] Chana P S, A Test Method to Establish Realistic Bond Stresses, Magazine of Concrete Research, June 1990, V42, No151, pp83-90.

[70] BS4449, Carbon Steel Bars for the Reinforcement of Concrete, BSI, London, 1988.

[71] RILEM, Bond Test on Reinforcing Steel, Pull-out Test, 1983.

[72] BS5400, Steel, Concrete and Composite Bridges, 1984.

[73] Azizinamini A et al, Bond Performance of Reinforcing Bars Embedded in High-Strength Concrete, ACI Structural Journal, Sept-Oct 1993, pp554-561.

[74] Abrams D A, Tests of Bond Between Concrete and Steel, Bulletin71, Engineering Experimental Station, University of Illinious, 1913.

[75] Menzel C A, Some Factors Influencing Results of Pullout Bond Test, ACI Journal, Proceedings, V35, No6, June 1939, pp517-544.

[76] http://www.ce.luth.se/~groth/paperd/utdrag.html, Single Fibre Pullout Test.

[77] Mohamed A Z & Clark L A, Bond Behaviour of Low- Strength Concrete, Magazine of Concrete Research, Sept. 1992,V44, No160, pp195-203.

[78] Clarke J L & Birjandi F K, Bond Strength Tests for Ribbed Bars in Lighweight Aggregate Concrete, Magazine of Concrete research, V45, No163, 1993, pp79-87.

[79] Hwang S J et al, Tensile Bond Strengths of Deformed Bars of High Strength Concrete, ACI Structural Journal, Jan-Feb 1996, pp11-20.

[80] Al-Shawi F A, Mangat P S and Halabi W, A simplified Approach to Corbels made with High Strength Conrete, Materials and Structures, V 32, October 1999, pp579-583.

[81] Larrard F et al, Effect of Bar Diameter on the Bond Strength of Passive Reinforcement in High-Performance Concrete, ACI Materials Journal, July-Aug. 1993, pp333-339.

[82] Goldman A & Bentur A, Bond Effects in High-Strength Silica Fume Concretes, ACI Materials Journal, Sept-Oct 1989, pp440-447.

[83] Gjorv O E et al, Effect of Condensed Silica Fume on the Steel Concrete Bond, ACI Materials Journal, Nov-Dec 1990, pp573-580.

[84] Soroushian P et al, Bond of Deformed Bars to Concrete: Effects of Confinement and Strength of Concrete, ACI Materilas Journal, May-June 1991, pp227-232.

[85] Treece R A & Jirsa J O, Bond Strength of Epoxy-Coated Reinforcing Bars, ACI Materials Journal, March-April 1989, pp167-174.

[86] Cairns J & Abdullah R, Bond Strength of Black and Epoxy-Coated Reinforcement-A Theoretical Approach, ACI Materials Journal, July-Aug 1996, pp362-369.

[87] Cairns J & Abdullah R, Fundamental Tests on the Effect of an Epoxy Coating on Bond Strength, ACI Materials Journal, July-August 1994, pp331-338.

[88] Clearly D B & Ramirez J A, Bond Strength of Epoxy-Coated Reinforcement, ACI Materials Journal, March-April 1991, pp146-149.

[89] Ghaffari H H et al, Bond of Epoxy-coated Reinforcement: Cover, Casting Position, Slump and Consolidation, ACI Structural Journal, Jan-Feb 1994, pp59-68.

[90] Swamy R N & Koyama S, Epoxy Coated Rebars, Proceedings, UK Corrosion'88 Conference, Brighton, Oct.1988, pp197-209.

[91] Ehsani M R et al, Design Recommendations for Bond of GFRP Rebars to Concrete, Journal of Structural Engineering, March 1996, pp247-254.

[92] Nanni A et al, Bond of FRP Reinforcement to Concrete- Experimental Results, Proceedings of the Second International RILEM Symposium, 1995, pp135-145.

[93] Hattori A et al, A Study on Bond Creep Behaviour of FRP Rebars Embedded in Concrete, Proceedings of the Second International RILEM Symposium, 1995, pp172-179.

[94] Cosenza E et al, Analytical Modelling of Bond Between FRP Reinforcing Bars and Concrete, Proceedings of the Second International RILEM Symposium, 1995, pp164-171.

[95] Taerwe L & Palleman I, Force Transfer of AFRP Bars in Concrete Prisms, Proceedings of the Second International RILEM Symposium, 1995, pp154-163.

[96] Jerrett C V & Ahmad S H, Bond Tests of Carbon Fibre Reinforced Plastic (CFRP) Rods, Proceedings of the Second International RILEM Symposium, 1995, pp180-191.

[97] Pleimann L, Strength, Modulus of Elasticity and Bond of Deformed FRP Rods, Advanced Composite Materials in Civil Engineering Structures ASCE, 1991, pp99-110.

[98] Granga Rao H V S et al, Designing Concrete Beams with FRP Beams, Proceedings of the International Conference, Concrete 2000 University of Dundee, 7-9 Sept. 1993, V2, pp1847-1856.

[99] RILEM/CEB/FIB, Test of the Bond Strength of Reinforcement of Concrete: Test by Bending, Recommendation RC.5, 1978.

[100] Daniali S, Development Length for Fibre Renforced Plastic Bars, Advanced Composite Materials in Bridges and Structures Canadian Society of Civil Engineers, 1992, pp179-188.

[101] Benmokrane B et al, Bond Strength of Fiber Reinforced Plastic (FRP) Bars Embedded in Concrete Beams, Annual Conference of the Canadian Society for Civil Engineering, May 27-30, 1997, pp111-120.

[102] Ehsani et al, Bond of GFRP Rebars to Ordinary Strength Concrete, International Symposium on Fibre Reinforced Plastic Reinbursement for Concrete, 1993, pp333-345.

[103] Khalifa M A, Bridges Constructed Using Fibre Reinforced Plastics, Concrete International, June 1993, pp43-47.

[104] Rizkalla S H & Tadros G, A Smart Highway Bridge in Canada, Concrete International, June 1994, pp42-44.

[105] Hirai T, Use of Continious Fibres for Reinforcing, Concrete International, Dec. 1992, pp58-60.

[106] Chaalal O et al, Use of a New Glass-Fibre Rod as Reinforcement for Concrete Structures, ACI International Concrence, SP128, V1, 1991, pp515-528.

[107] Meier U, Case Histories, Chapter 9, Advanced Composite Materials with Application to Bridges.

[108] Santoh N et al, Report on the Use of CFCC in Prestressed Concrete Bridges in Japan, ACI International Symposium, SP-138, 1993, pp895-911.

[109] Shaw G et al, Design, Construction and Instrumentation of Prestressed Masonry Box Girder Footbridges, Proceedings of the Second International RILEM Symposium, FRPRCS-2, 1995, pp672-679.

[110] Clarke J, Steeling Concrete with Fibre Reinforced Plastics, Materials World, Feb. 1998, pp78-80.

[111] Norikate K et al, Practical Applications of Aramid FRP Rods to Prestressed Concrete Structures, ACI International Symposium, SP-138, 1993, pp853-873.

[112] Iyer S L, Advanced Composite Bridge Deck, ACI International Symposium, SP-138, 1993, pp831-852.

[113] Wolff R & Miesseler H J, Glass-fibre Prestressing System, Alternative Materials or the Reinforcement and Prestressing of Concrete, ISBN 0 75 14000 76, 1993, pp127-152.

[114] Grant L et al, Toward Development of Bridges in the Next Century, Proceedings of the Second International RILEM Symposium, FRPRCS-2, 1995, pp654-662.

[115] Hemanth K et al, FRP Reinforcement in Bridge Decks, Concrete International, June 1998, pp47-50.

[116] Rizkalla S et al, The New Generation, Concrete International, June 1998, pp35-38.

[117] Meier U and Winistorfer A, Retrofitting of Structures through External Bonding of CFRP Sheets, Proceedings of the Second International RILEM Symposium, FRPRCS-2, 1995, pp465-472.

[118] Ehsani M R, Strengthening of Earthquake-Damaged Masonry Structures with Composite Materials, Proceedings of the Second International RILEM Symposium, FRPRCS-2, 1995, pp680-687.

[119] Kobayashi A et al, Repair and Reinforcement of Concrete Structure with Carbon Fibre Tow Sheet, Proceedings of the Second International RILEM Symposium, FRPRCS-2, 1995, pp688-695.

[120] Neale K W & Labossiere P, Fibre Composite Sheets in Cold Climate Rehab, Concrete International, June 1998, pp22-24.

[121] Shehata E et al, Roof Retrofit, Concrete International, June 1998, pp44-46.

[122] Saadatmanesh H, Wrapping with Composite Materials, Proceedings of the Second International RILEM Symposium, FRPRCS-2, 1995, pp593-600.

[123] Jungwirth D & Windisch A, Tendons made of Non-metallic Materials, Requirenments and Economic Application, Proceedings of the Second International RILEM Symposium, FRPRCS-2, 1995, pp34-40.

[124] Larralde J et al, Fibreglass Reinforced Plastic Rebars in Lieu of Steel Rebars, ASCE 7th Annual Structures Congress, California, May 1989, pp1-9.

[125] Saadatmanesh H & Ehsani M R, Fibre Composite Bar for Reinforced Concrete Construction, Journal of Composite Materials, V25, No2, Feb. 1991, pp117-222.

[126] MacDonald M D & Calder A J, Bonded Steel Plating for Strengthening Concrete Structures, International Journal of Adhesion and Adhesives, V2, No2, April 1982, pp119-127.

[127] Jones R et al, Composite Behaviour of Composite Beams with Epoxy Bonded External Reinforcement, International Journal of Cement Composites and Lightweight Concrete, V2, No2, May 1980, pp91-107.

[128] Clarke J L, Strenthening Concrete Structures with Fibre Composites, Concrete Communication Conference 2000, 2000, p280.

[129] Clarke J L, Strenthening Concrete Structures with Fibre Composites, Concrete Communication Conference 2000, 2000, p283.

[130] Saadatmanesh H & Ehsani M R, Fiber Composite Plates can Strengthen Beams, Concrete International, March 1990, pp65-71.

[131] Ritchie P A et al, External Reinforcement of Concrete Beams using Fibre Reinforced Plastics, ACI Structural Journal, July-August 1991, pp490-500.

[132] Erki M A & Heffernan P J, Reinforced Concrete Slabs Externally Strengthened with Fibre-Reinforced Plastic Materials, Proceedings of the Second International RILEM Symposium, FRPRCS-2, 1995, pp509-516.

[133] Alfarabi S et al, Strengthening of Initially Loaded Reinforced Concrete Beams Using FRP Plates, ACI Structural Journal, V91, No2, March-April 1994, pp???.

[134] An W et al, RC Beams Strengthened with FRP Plates II:Analysis and Parametric Study, Journal of Structural Engineering, Nov. 1991, V117, P11, pp3434-3455.

[135] Swamy R N & Mukhopadhyaya P, Role and Effectiveness of Non-metallic Plates in Strengthening and Upgrading Concrete Structures, Proceedings of the Second International RILEM Symposium, FRPRCS-2, 1995, pp473-482.

[136] Arduini M et al, Fracture Mechanisms of Concrete Beams Bonded with Composite Plates, Proceedings of the Second International RILEM Symposium, FRPRCS-2, 1995, pp483-491.

[137] Wight et al, Post-Strengthening Concrete Beams with Prestressed FRP Sheets, Proceedings of the Second International RILEM Symposium, FRPRCS-2, 1995, pp568-575.

[138] Green M, Soudki K A & Johnson M M, Freeze-Thaw Beahviour of Reinforced Concrete Beams Strengthened by Fibre Reinforced Plastic Sheets, Annual Conference of the Canadian Society for Civil Engineers, May 27-30, 1997, pp31-39.

[139] Fujisaki T, New Material for Reinforced Concrete in Place of Reinforcing Steel Bars, IABSE Symposium in Paris Versailles, September 1987, pp413-418.

[140] Sekijima K & Hiraga H, FRP Grid Reinforcement for Concrete Structures.

[141] Zia P et al, Flexural and Shear Behaviour of Concrete Beams Reinforced with 3-D Continuous Carbon Fiber Fabric, Concrete International, December 1992, pp48-52.

[142] Bank L C & Xi Z, Punching Shear Behaviour of Pultruded FRP Grating Reinforced Concrete Slabs, Proceedings of the Second International RILEM Symposium, FRPRCS-2, 1995, pp360-367.

[143] Ahmad S H et al, Punching Shear Tests of Slabs reinforced with 3-D Carbon Fiber Fabric, Concrete International, June 1994, pp36-41.

[144] Bank L C et al, Three-Dimensional Fibre-Reinforced Plastic Grating Cages for Concrete Beams: A Pilot Study, ACI Structural Journal, V94, No6, Nov-Dec 1997, pp643-652.

[145] Rubinsky I et al, A Preliminary Investigation of the Use of Fibre-glass for Prestressed Concrete, Magazine of Concrete Research, September 1954, V6, No17, pp71-78.

[146] Sekijima K et al, Study on Prestressed Concrete with FRP Grid Tendon, Transaction of the Japan Concrete Institute, December 1988, V10, pp425-432.

[147] Kajfasz I S, Some Tests on Beams Prestressed by Fibre-glass Cords, Magazine of Concrete Research, V35, 1960, pp91-98.

[148] Prestressing, Glass Fibre Composite Prestressing, Concrete, Dec. 1987, p15.

[149] Somes N F, Resin-Bonded Glass-fibre Tendons for Prestressed Concrete, Magazine of Concrete research, 1963, V15, No45, pp151-158.

[150] Iwaki R et al, Flexural Behaviour of Prestressed Concrete beams Reinforced with Aramid Fiber reinforced Plastic Flat Bars, Proceedings ACI International Conference, Hong Kong, 1991, SP 128, V2, pp909-925.

[151] Mutsuyoshi H et al, Behaviour of Prestressed Concrete Beams using FRP as External Cable, Transactions of the Japan Concrete Institute, V13, 1991, pp247-252.

[152] Currier J et al, Deflection Control of Fibre Reinforced Plastic Pretensioned Concrete Beams, Proceedings of the Second International RILEM Symposium, FRPRCS-2, 1995, pp413-420.

[153] Faza S S & Gangarao H V S, Pre-and Post-Cracking Deflection Behaviour of Concrete Beams Reinforced With Fibre- Reinforced Plastic Rebars, Advanced

Composite Materials in Bridges and Structures, Canadian Society for Civil Engineers, 1992, pp151-160.

[154] Clarke J, Steeling Concrete with Fibre Reinforced Plastics, Materials World, February 1998, pp78-80.

[155] Nawy E G & Neuwerth, Behaviour of Fiber Glass Reinforced Concerete Beams, Journal of the Structural Division, ASCE, September 1971, pp2203-2215.

[156] ACI318 Building Code Requirenments.

[157] Benmokrane, O et al, Flexural Response of Concrete Beams Reinforced with FRP Reinforcing Bars, ACI Structural Journal, V93, No1, Jan-Feb 1996, pp46-55.

[158] Satoh K, Kodama K & Ohki H, A Study on the Bending Behaviour of Repaired reinforced Concrete Beams using FRP and Polymer Mortars, Proceedings ACI International Conference Hong Kong, 1991, V2, SP128, pp1017-1031.

[159] Okamura H et al, Design Concept for Concrete Members Using Continious Fibre Reinforcing Materials, ACI International Symposium, SP138, 1993, pp549-559.

[160] Al-Sayed S H et al, Flexural Behaviour of Concrete Elements Reinforced by GFRP Bars, Proceedings of the Second International RILEM Symposium, FRPRCS-2, 1995, pp219-226.

[161] Mikami H et al, Fatigue Characteristics of Concrete Beams Reinforced with Braided AFRP Rods, Transactions of the Japan Concrete Institute, V12, 1990, pp223-230.

[162] Standard Specification of Design and Construction of Concrete Structures, Part 1 (Design), JSCE, 1987, mainly pp15-33, pp74-88.

[163] Ozawa K, Sekijima K et al, Flexural Fatigue Behaviour of Concrete Beam with FRP Reinforcement, Transactions of the Japan Concrete Institute, 1987, V9, pp289-296.

[164] Ngo D & Scordelis A C, Finite Element Analysis of Reinforced Concrete Beams, ACI Journal 1967, pp152-163.

[165] Alsayed S H & Al-Salloum Y A, Optimization of Flexure Environment of Concrete Beams Reinforced with Fibre-reinforced Plastic Rebars, Magazine of Concrete Research, March 1996, V48, No174, pp27-36.

[166] Kakizawa T et al, Flexural Behaviour and Energy Absorption of Carbon FRP Reinforced Concrete Structures, SP138, ACI, 1993, pp585-598.

[167] Faza S S & GangaRao H V S, Theoretical and Experimental Correlation of Behaviour of Concrete Beams Reinforced with Fibre Reinforced Plastic Rebars, SP138, ACI, 1993, pp599-614.

[168] Nanni A, Flexural Behaviour and Design of RC Members using FRP Reinforcement, Journal of Structural Engineers ASCE, November 1993, V119, No111, pp3344-339.

[169] Kobayashi K & Fujisaki T, Compressive Behaviour of FRP Reinforcement in Non-Prestressed Concrete Members, Proceedings of the Second International RILEM Symposium, FRPRCS-2, 1995, pp267-274.

[170] Faza S S & GangaRao H V S, Bending Response of Beams Reinforced with FRP Rebars for varying Concrete Strengths, advanced Composite Materials, ASCE, 1991, pp262-270.

[171] ACI Committee 435, Deflections of Reinforced Concrete Flexural Members, ACI Journal Proceedings, 1966, V63, PT6, pp637-674.

[172] Alsayed S H, Flexural Behaviour of Concrete Beams Reinforced with GFRP Bars, Cement and Concrete Composites, V20, 1998, pp1-11

[173] Nawy E G & Neuwerth A M, Fibreglass Reinforced Concrete Slabs and Beams, Journal of the Structural Division, February 1977, pp421-440.

[174] Masmoudi R, Neutral Axis Position in Concrete Beams Reinforced with FRP Rebars, Annual Conference of the Canadian Society for Civil Engineering, May 27-30, 1997, pp161-170.

[175] Theriault M et al, Theoretical and Experimental Investigation on Crack Width, Deflection and Deformability of Concrete Beams Reinforced with FRP Rebars, Annual Conference of the Canadian Society for Civil Engineering, May 27-30, 1997, pp151-160.

[176] Clarke J L, FIbre-Reinforced Plastic Reinforcement for Concrete, Current Practice Sheet No 114, Concrete, January 1999, pp15-16.

[177] Clarke J L, Non-Ferrous Reinforcement for Structural Concrete, Proceedings of International Conference, Concrete 2000, University of Dundee, 1993, V1, pp229-238.

[178] ACI Committee 440, State of the Art Report on Fiber Reinforced Plastic (FRP) Reinforcement for Concrete Structures, January 1996.

[179] The Institution of Structural Engineers, Interim Guidance on the Design of Reinforced Concrete Structures using Fibre Composite Reinforcement, August 1999.

[180] BS5077-2:1983, Lintels-Part2:Specification for Prefabricated Lintels.

[181] ReadingRock Concrete Masonry Units, http://www.radingrock.com/concrete_lintels.htm

[182] Buyle-Bodin F & Benhouna M, Flexural Behaviour of JITEC FRP Reinforced Beams, Proceedings of the Second International RILEM Symposium, FRPRCS-2, 1995, p235-241.

[183] Srinivasa, L I et al, Testing and Evaluating Fibreglass, Graphite and Steel Prestressing Cables for Pretensionad Beams, Advanced Composite Materials in Civil Engineering Structures, Jan-Feb 1991, p44-56.

[184] Mashima M & Iwamoto K, Bond Characteristics of FRP Rod and Concrete after Freezing and Thawing Deterioration, ACI International Symposium-SP 138, 1993, p51-69.

[185] Sueoka K et al, Mechanical Properties of Composite Beams by FRP, ACI International Symposium-SP 138, 1993, p133-148.

[186] Maruyama T et al, Experimental Study on Tensile Strength of Bent Portion of FRP Rods, ACI International Symposium-SP 138, 1993, p163-176.

[187] Tamura T et al, Absorbing Capacity of Cushion System Using Concrete Slab Reinforced with AFRP Rods, ACI International Symposium-SP 138, 1993, p301-313.

[188] Holte L E et al, Epoxy Socketed Anchors for Non-Metallic Prestressing Tendons, ACI International Symposium-SP 138, 1993, p381-400.

[189] Iwamoto K et al, Flexural Fatigue Behaviour of Prestressed Concrete Beams Using Aramid-Fibre Tendons, ACI International Symposium-SP 138, 1993, p509-523.

[190] Yonekura A et al, Flexural and Shear Behaviour of Prestressed Concrete Beams Using FRP Rods as Prestressing Tendons, ACI International Symposium-SP 138, 1993, p525-548.

[191] Tottori S et al, Shear Capacity of RC and PC Beams Using FRP Reinfrocement, ACI International Symposium-SP 138, 1993, p615-632.

[192] Nakano K et al, Flexural Performance of Concrete Beams Reinforced with Continious Fibre Bars, ACI International Symposium-SP 138, 1993, p743-766.

[193] Kanakuba T et al, Bond Performance of Concrete Members Reinforced with FRP Bars, ACI International Symposium-SP 138, 1993, p767-788.

[194] Kage T et al, Long Term Deflection of Continious Fibre Reinforced Concrete Beams, Proceedings of the Second International RILEM Symposium, FRPRCS-2, 1995, p251-258.

[195] Kobayashi K & Fujisaki T, Compressive Behaviour of FRP Reinforcement in Non-Prestressed Concrete Members, Proceedings of the Second International RILEM Symposium, FRPRCS-2, 1995, p267-274.

[196] Mathhys S & Taerwe L, Loading Tests on Concrete Slabs Reinforced with FRP Grids, Proceedings of the Second International RILEM Symposium, FRPRCS-2, 1995, p287-297.

[197] Zhao W et al, Shear Behaviour of Concrete Beams Reinforced by FRP Rods as Longitidunal and Shear Reinforcement, Proceedings of the Second International RILEM Symposium, FRPRCS-2, 1995, p352-359.

[198] Okamoto T et al, Long Term Loading Tests on PPC Beams Using Braided FRP Rods, Proceedings of IV. International Symposium, July 1992, p1000-1014.

[199] Scheibe M & Rostasy F S, Stress-Rupture of AFRP Subjected to Alkaline Solutions and Elevated Temperature-Experiments, Proceedings of the Second International RILEM Symposium, FRPRCS-2, 1995, pp67-73.

[200] Xu H et al, Bond Strength of Fibre Reinforced Plastic (FRP) Cement Grouted Anchor Bolts, Proceedings of the Second International RILEM Symposium, 1995, pp209-216.

[201] Mochizuki S & Udagawa T, On Bond and Anchorage of Two Dimensional Grid Type FRP, Proceedings of the Second International RILEM Symposium, 1995, pp200-208.

[202] Kakizawa T et al, Magnetic Characteristics of the 3-Dimensional FRP Reinforcement used for Non-Magnetic Chamber, Proceedings of the Second International RILEM Symposium, FRPRCS-2, 1995, pp124-131.

CHAPTER 3

3. EXPERIMENTAL WORK

3.1 Test Programme & Methodology

The two-point loading test programme was split into four parts and contained 59 concrete beam tests in total. The purpose of the first part was to investigate the performance of different grade of concrete beams reinforced with conventional steel and the state-of-the-art material GFRP rebars. In the second part, the same grade of concrete beams tested having different profiles of GFRP rebars. The third part contained beams having the same GFRP rebar profiles but with different types of concrete. In the final part, the same grade of concrete beams contained steel and GFRP main rebars and mild steel/GFRP stirrups. A test rig of 300kN load capacity free standing frame was used for the tests. The test mode was in deflection control in order to eliminate sudden catastrophic failure and also to monitor the behaviour of the beams at each load increment safely. Applied load was monitored by the control panel and load deflection response by the plotter. Concrete and rebar strains as well as the crack patterns were observed and readings saved on the computer during the test. A video camera was used to film the behaviour of each beam. The overview of the testing apparatus used for two point loading can be seen in *Photo 3.1* (also play *control panel.mpeg* video clip on the compact disk). All beams in Part 1, 2, 3, 4 were simply supported on a span of 2440mm and were subjected to two equal concentrated loads 900mm apart and symmetrically placed at the mid-span. The shear span of the beams was a constant value of 770mm throughout the experimental work. Bottom and the top covers to the reinforcement were 25mm. Two concrete cylinders and six cube specimens corresponding to each beam were tested under compression using a 3000kN maximum load capacity Avery Denison machine.

Photo 3.1 An overview of the test apparatus used during two-point loading.

(1. control panel, 2. plotter, 3. deflection display, 4. computer data store, 5. printer, 6. test beam, 7. the frame, 8. LVDT)

Also, tensile tests were carried out on the reinforcing bars. The test programme is outlined as follows:

3.1.1 Part 1 - FRP & Steel Reinforced Normal, Medium and High Strength Concrete Beams

Beam specimens were split into two groups. One group containing concrete beams reinforced with two ribbed high tensile steel and the other group containing two GFRP reinforcing bars. The beams were reinforced in the tension zone (see *Figure 3.1*, (a), (b), (c) and (d)). A range of different concrete grades (C20, C40, C60) and different bar sizes, 8mm 12mm 16mm steel and 8.77mm 13.19mm 16.44mm GFRP were used (see *Photo 3.2).*

Photo 3.2 The size of the steel and GFRP rebars used in this study

The primary purpose of this part of the test programme was to make a comparison between the beams reinforced with steel and GFRP bars in terms of their structural performance and efficiency. A total number of twenty beams were tested at 42/43 days. In addition, two beams containing dispersed glass fibre added to the concrete mix were tested at 28 days. A number of tests was repeated bringing the total number of specimens in Part 1 to thirty.

The physical properties of the beams are summarized in *Table 3.1.* To comply with laboratory facilities and availability, the first eight beams were tested at 42/43 days. It was decided to test the next beams at the same age in order to maintain consistency throughout the investigation. The beams in further parts were tested at 28/29 days. Concrete generally increases its strength with age. This characteristic increase is fast up to 28 days and becomes more gradual thereafter1. Therefore, it should be noted that the difference in the cube strengths for 42/43 days and 28/29 days was not large for a given concrete grade.

Figure 3.1 Typical loading arrangement and rebar configurations used in Part 1

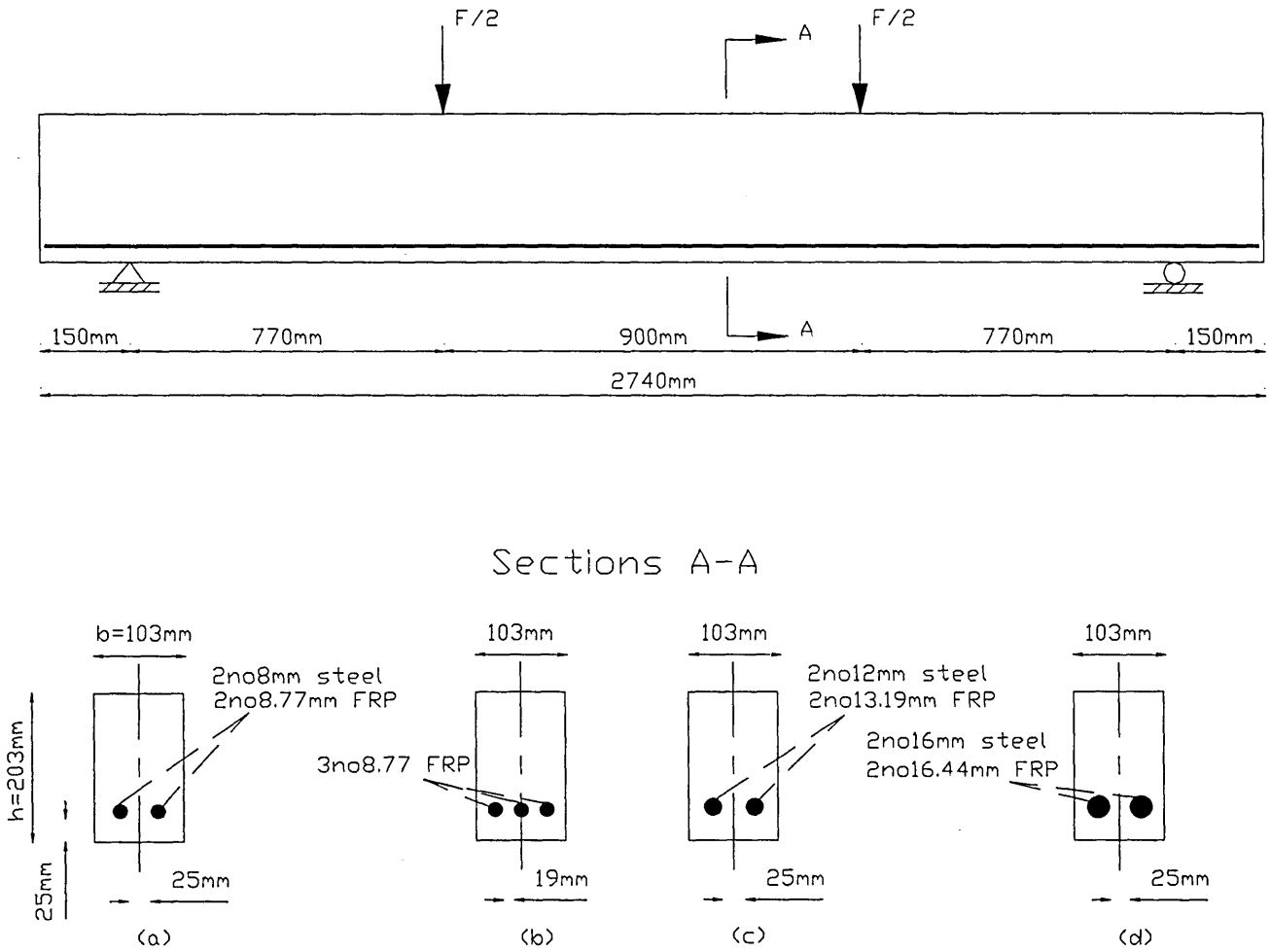

Table 3.1 The physical properties of Part 1

		CONCRETE								REINFORCEMENT		
No	Beam Code	Grade	Age (days)	Slump (mm)	Density (kg/m^3) Air/Water	f_c Strength (MPa) Air/Water	E_c MOE (GPa) Air	No-Dia/ Type	E_{st}/E_{FRP} MOE (GPa)	$f_{st/gfrp}$ Yield/ Ultimate Stress (MPa)	A_r Area (mm^2)	%Tension Rebar (A_r/bxh)x100
1[1*]	TB15	C20	42	45	2340/2420	41/41	33	2-08S	186	523.5	101	0.48
2[1]*	*RTB15*	*C20*	*42*	*40*	*2390/2426*	*50/50*	*35*	*2-08S*	*186*	*524*	*101*	*0.48*
3[1*]	TB13	C20	42	43	2310/2410	40/41	30	2-12S	189	497	226	1.08
4[1]*	*RTB13*	*C20*	*42*	*45*	*2345/2423*	*50/52*	*34*	*2-12S*	*189*	*497*	*226*	*1.08*
5[1*]	TB17	C20	42	50	2440/2370	43/47	30	2-16S	200	467	402	1.92
6[1*]	TB16	C20	43	45	2340/2400	41/42	33	2-08.77F	46	601	121	0.58
7[1]*	*RTB16*	*C20*	*43*	*45*	*2410/2430*	*49/52*	*36*	*2-08.77F*	*46*	*601*	*121*	*0.58*
8[1]*	*RRTB16*	*C20*	*43*	*55*	*2403/2406*	*47/49*	*29*	*2-08.77F*	*46*	*601*	*121*	*0.58*
9[1*]	TB14	C20	43	45	2345/2400	40/41	34	2-13.19F	39	471	273	1.31
10[1*]	TB18	C20	43	40	2370/2430	39/42	33	2-16.44F	33	544	425	2.03
11[1]*	*RTB18*	*C20*	*43*	*35*	*2400/2430*	*45/52*	*31*	*2-16.44F*	*33*	*544*	*425*	*2.03*
12[1*]	TB5	C40	42	45	2400/2430	61/63	34	2-08S	186	524	101	0.48
13[1*]	TB1	C40	42	50	2370/2400	55/60	33	2-12S	189	497	226.2	1.08
14[1]*	*RTB1*	*C40*	*43*	*45*	*2395/2440*	*61/64*	*34*	*2-12S*	*189*	*497*	*226*	*1.08*
15[1*]	TB9	C40	42	45	2390/2450	61/65	35	2-16S	200	467	402.1	1.92
16[1*]	TB6	C40	43	55	2420/2430	69/63	34	2-08.77F	46	601	120.8	0.58
17[2**]	TTB16	C40 FB	28	N/A	2386/2416	59/62	34	2-08.77F	46	601	120.8	0.57
18[1]*	*RTB6*	*C40*	*43*	*45*	*2410/2440*	*65/68*	*40*	*2-08.77F*	*46*	*601*	*121*	*0.58*
19[1*]	TB2	C40	43	50	2370/2400	57/62	34	2-13.19F	39	471	273.28	1.31
20[1]*	*RTB2*	*C40*	*43*	*55*	*2420/2420*	*63/70*	*38*	*2-13.19F*	*39*	*471*	*273*	*1.31*
21[2**]	TTB21	C40 FB	28	N/A	2396/2363	54/57	32	2-13.19F	39	471	273	1.28
22[1*]	TB10	C40	43	50	2340/2420	51/63	33	2-16.44F	33	544	424.54	2.03
23[1*]	TB7	C60	42	55	2420/2420	73/81	33	2-08S	186	524	100.5	0.48
24[1*]	TB3	C60	42	50	2400/2470	72/74	35	2-12S	189	497	226.2	1.08
25[1*]	TB11	C60	42	50	2420/2470	75/79	37	2-16S	200	467	402.1	1.92
26[1*]	TB8	C60	43	45	2420/2470	72/78	35	2-08.77F	46	601	120.8	0.58
27[1]*	*RTB8*	*C60*	*43*	*50*	*2430/2450*	*70/74*	*36*	*2-08.77F*	*46*	*601*	*121*	*0.58*
28[1]*	*RRTB8*	*C60*	*43*	*55*	*2453/2490*	*78/82*	*35*	*2-08.77F*	*46*	*601*	*121*	*0.58*
29[1*]	TB4	C60	43	50	2440/2470	79/80	38	2-13.19F	39	471	273.28	1.31
30[1*]	TB12	C60	43	50	2400/2460	76/75	36	2-16.44F	33	544	424.54	2.03

S (Steel) TB: Test Beam RTB: First Repeat of TB RRTB: Second Repeat of TB FB: Glass fibres added concrete

F (FRP) TTB: New Test Beam includes new geometry of rebars and concrete strengths and types MOE: Modulus of Elasticity

[1*] 103mm wide(b) x 203mm deep(h) x 2740mm long (2440mm long span) [2**] 104mm wide(b) x 205mm deep(h) x 2740mm long (2440mm long span)

3.1.2 Part 2 - High Strength Concrete Beams Reinforced with GFRP Reinforcing Bars Using Straight & Curved Geometric Configurations

The Part 2 tests were based upon the results obtained from the Part1 and was concerned with applying different configurations i.e. curved or straight profiles (*Figure 3.2* a, band *Figure 3.3* a, b, c) of 8.77mm FRP bars for the same concrete grade (C60) with different reinforcement areas (121mm^2, 181.5mm^2, 242mm^2 and 546.56mm^2) in order to assess the structural performance of the beams with more conventional configuration.

The majority of the GFRP reinforced beams in Part 1 failed in shear and in some cases resulted in rebars snapping in the shear region. It was felt that if the profile of the GFRP rebars were modified, this could reduce or eliminate the propensity for shear failure and enhance the performance of the beams. Therefore, Part 2 contained beams reinforced with, 'straight only', 'curved only' and the combined 'straight and curved' profiles. A total of eleven beams were tested in this part of the investigation at 28/29 days. The physical properties of the beams are summarized in *Table 3.2*. TB8 (T:Test, B:Beam, 8:number of the beam) and the repeats from Part1 here also included in this part of the programme.

Figure 3.2 Typical loading arrangement and rebar configurations used in Part 2

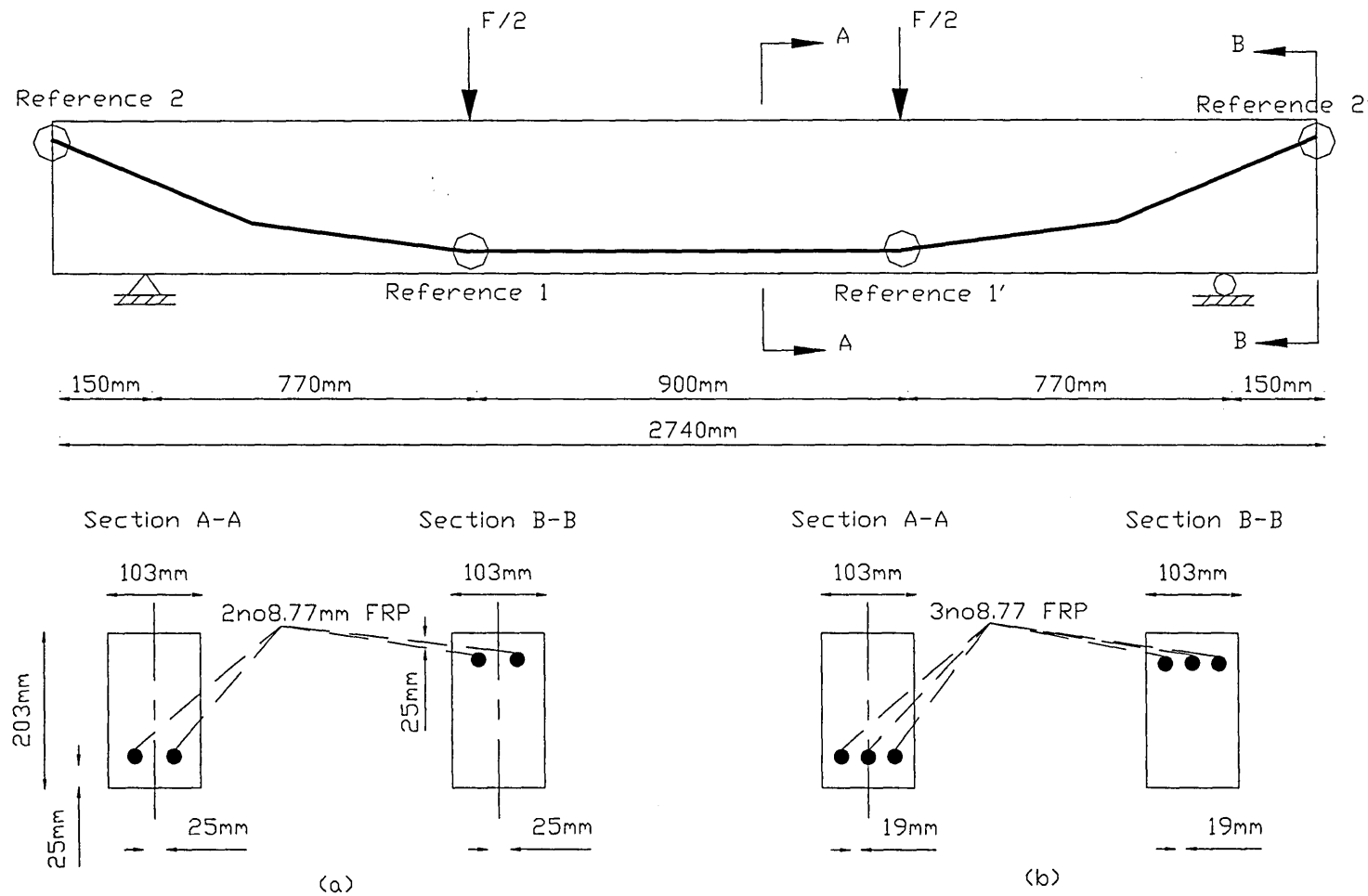

3.1.2.1 Procedure for Rebar Fixing

End plates of steel/wood 104mm width x 204mm height were manufactured and drilled with the necessary numbers of holes and they were fixed at both ends of the beam moulds before the rebars were put through. Two symmetrical reference numbers which are shown in *Figure 3.2,* were selected prior to bending of rebars. The rebars were put through Reference2-2' first, then fixed at Reference 1-1' in order to be bent (see also *Photo 3.3).* Top and bottom cover to the main reinforcement was maintained at 25mm for all beams.

Photo 3.3 Two curved and two straight profile GFRP rebars fixed in a mould prior to manufacturing

Table 3.2 The Physical Properties of Part 2 Beams

		CONCRETE						REINFORCEMENT					
No	**Beam Code**	**Grade**	**Age (days)**	**Slump (mm)**	**Density (kg/m^3) Air/Water**	**f_c Strength (MPa) Air/Water**	**E_c MOE (GPa) Air**	**No-Dia/ Type**	**Profile**	**E_{st}/E_{FRP} MOE (GPa)**	**$f_{st/gfrp}$ Yield/ Ultimate Stress (MPa)**	**A_r Area (mm^2)**	**%Tension Rebar (A_r/bxh)x10**
1[1*]	TB8	C60	43	45	2420/2470	72/78	35.00	2-08.77F	straight	45.98	601	121.00	0.58
2[1*]	RTB8	C60	43	50	2430/2450	70/74	36.00	2-08.77F	straight	45.98	601	121.00	0.58
3[1*]	RRTB8	C60	43	55	2453/2490	78/82	35.00	2-08.77F	straight	45.98	601	121.00	0.58
4[2*]	TTB3	C60	28	60	2442/2400	77/79	38.00	2-08.77F	curved	45.98	601	121.00	0.57
5[2*]	TRIAL	C60	28	50	2440/2400	77/77	38.00	3-08.77F	curved	45.98	601	181.50	0.86
6[2*]	RTRIAL	C60	28	50	2450/2470	73/80	33.00	3-08.77F	curved	45.98	601	181.50	0.86
7[2*]	TTB4	C60	28	50	2440/2460	77/78	39.50	3-08.77F	straight	45.98	601	181.50	0.86
8[2*]	TTB1	C60	28	47	2446/2455	78/77	41.00	3-08.77F	straight + curved	45.98	601	181.50	0.86
9[2*]	TTB2	C60	29	60	2440/2486	80/75	39.00	4-08.77F	straight + curved	45.98	601	242.00	1.14
10[2*]	RTTB2	C60	28	55	2470/2486	73/74	33.00	4-08.77F	straight + curved	45.98	601	242.00	1.14
11[2*]	TTB7	C60	28	45	2443/2460	70/71	38.00	4-13.19F	straight + curved	38.75	470.7	546.56	2.58

TB: Test Beam RTB: First Repeat of TB RRTB: Second Repeat of TB TRIAL: The very first of TTBs RTRIAL: First Repeat of TRIAL

TTB: New Test Beam includes new geometry of rebars and concrete strengths and types

[1*]103mm wide(b) x 203mm deep(h) x 2740mm long (2440mm long span)

[2**]104mm wide(b) x 204mm deep(h) x 2740mm long (2440mm long span)

3.1.3 Part 3 - Various Concrete Types of Beams Reinforced with Optimum GFRP Rebar Configurations

From the results of Part 2, it was decided to carry out the tests for Part 3 based on the beams with the best performance for a given area of reinforcement (242mm^2 and 546.56mm^2) having a novel geometry, using two straight and two curved profiles of GFRP rebars (see *Figure 3.3* (b), (c)). It was decided to compare the performance of beams with the model geometry of the GFRP rebars before ultimately comparing them with conventional shear reinforcement in the final part of the programme. Partly due to problems with delivery of GFRP shear reinforcements.

The beams were reinforced with four 8.77mm, and four 13.19mm FRP and were tested at 28/29 days. The tests were set up for 15 beams including one repeat. The concrete grades and types used were C20 and C40 normal weight, C20 normal weight with microsilica, C20 and C50 lightweight, C20 lightweight with microsilica and C40 normal weight and with dispersed glass fibres. The physical properties of the beams are summarized in *Table 3.3*. Note that all the rebar profiles involve the combinations of straight and curved for GFRP only.

Figure 3.3 Typical loading arrangement and rebar configurations used in Part 3

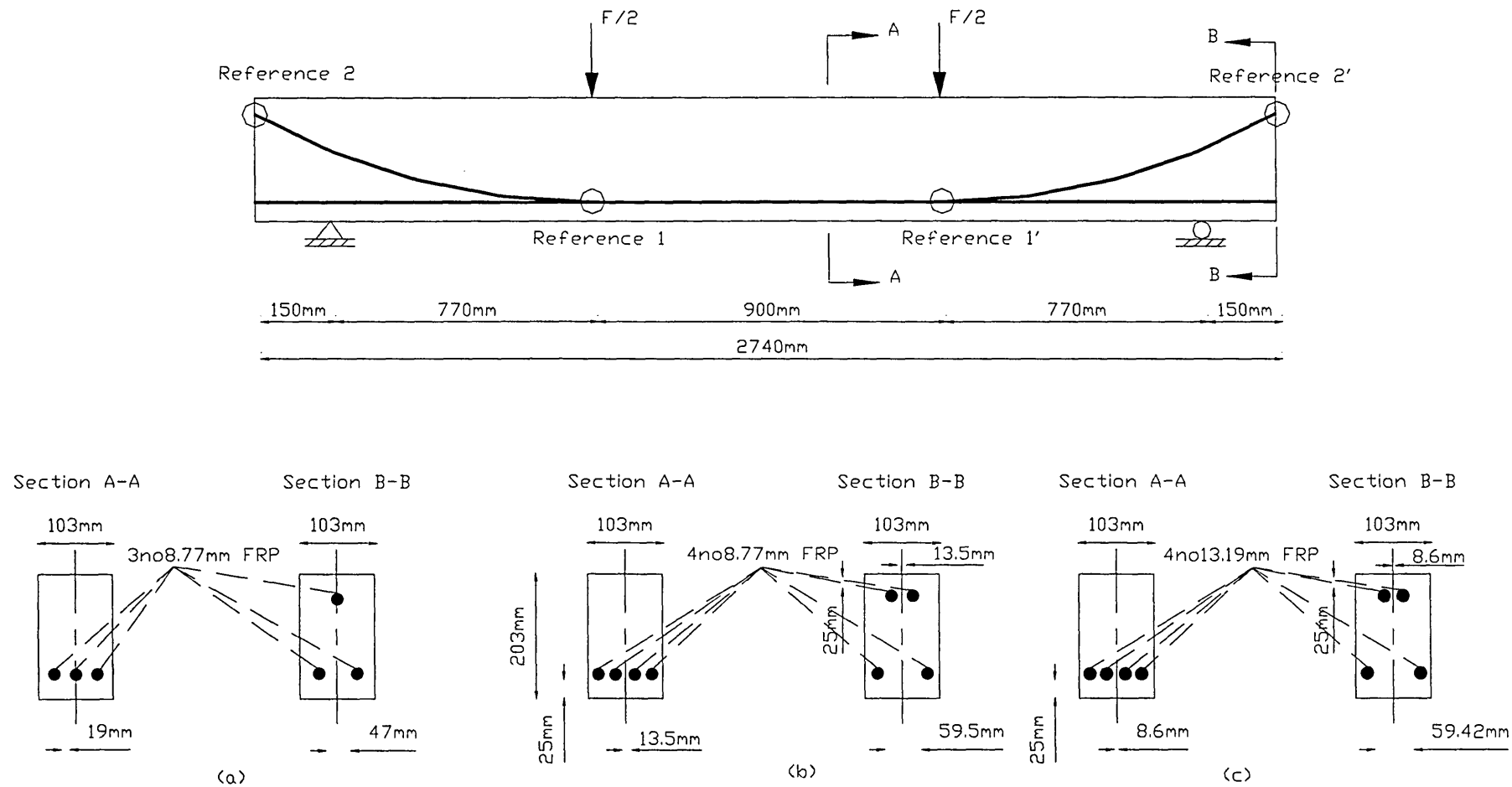

Table 3.3 The Physical Properties of Part 3 Beams

CONCRETE								REINFORCEMENT				
No	**Beam Code**	**Grade**	**Age (days)**	**Slump (mm)**	**Density (kg/m^3) Air/Water**	**f_c Strength (MPa) Air/Water**	**E_c MOE (GPa) Air**	**No-Dia/ Type**	**E_{st}/E_{FRP} MOE (GPa)**	**$f_{st/gfrp}$ Yield/ Ultimate Stress (MPa)**	**A_r Area (mm^2)**	**%Tension Rebar (A_r/bxh)x100**
1[1*]	TTB5	C20	28	60	2413/2436	43/44	34	4-08.77F	45.98	601.00	242.00	1.14
2[1*]	RTTB5	C20	28	75	2413/2416	44/44	30	4-08.77F	45.98	601.00	242.00	1.14
3[1*]	TTB6	C20	28	70	2410/2440	43/45	31	4-13.19F	38.75	470.70	546.56	2.58
4[1*]	TTB8	C20 LT	29	85	1983/2033	45/45	21	4-8.77F	45.98	601.00	242.00	1.14
5[1*]	TTB9	C20 LT	28	55	1973/2013	48/47	22	4-13.19F	38.75	470.70	546.56	2.58
6[1*]	TTB10	C20 SIL	28	55	2416/2406	59/64	34	4-08.77F	45.98	601.00	242.00	1.14
7[1*]	TTB11	C20 SIL	28	55	2340/2438	51/66	32	4-13.19F	38.75	470.70	546.56	2.58
8[1*]	TTB12	C20 LT SIL	28	30	1960/2010	63/64	24	4-08.77F	45.98	601.00	242.00	1.14
9[1*]	TTB13	C20 LT SIL	28	30	1993/2026	61/66	24	4-13.19F	38.75	470.70	546.56	2.58
10[1*]	TTB20	C40	28	85	2420/2440	61/64	34	4-08.77F	45.98	601.00	242.00	1.14
11[1*]	TTB17	C40 FB	28	N/A	2376/2403	56/52	35	4-08.77F	45.98	601.00	242.00	1.14
12[1*]	TTB19	C40	28	65	2416/2443	59/61	34	4-13.19F	38.75	470.70	545.56	2.57
13[1*]	TTB18	C40 FB	28	N/A	2390/2390	59/59	33	4-13.19F	38.75	470.70	546.56	2.58
14[1*]	TTB14	C50 LT	29	35	1993/2023	69/69	25	4-08.77F	45.98	601.00	242.00	1.14
15[1*]	TTB15	C50 LT	28	85	1973/2000	62/63	23	4-13.19F	38.75	470.70	546.56	2.58

TTB: New Test Beam includes new geometry of rebars and concrete strengths and types

RTTB: Second Repeat of TTB

LT (Lightweight concrete)

SIL (Silica added concrete)

FB (Glass fibre added concrete)

[1*]104mm wide(b) x 204mm deep(h) x 2740mm long (2440mm long span)

3.1.4 Part 4 - Normal Weight (C20) Concrete Beams Reinforced with GFRP and High Tensile Steel Rebars combined with GFRP and Steel Stirrups

Six beams were cast using C20 grade of concrete mix throughout Part 4 tests, which were split into three groups. The first group of beam specimens contained two 8mm and two 12mm diameter high tensile steel rebars respectively along with twenty-four 6mm mild steel stirrups. Two 8.77mm and two 13.19mm diameter GFRP rebars were used instead of steel rebars as the main reinforcements in the second group. The beams in the third group consisted of the same diameter of main reinforcement as in the second group along with twenty-four 6.9mm GFRP stirrups. All the beams contained two 6mm mild steel rebars in the compression zone i.e. top rebars. This was for the stirrups to be held perpendicular to the top and the bottom rebars. The reason for the selection of nominal C20 grade concrete in this part was due to; firstly, the average strength of concrete suggested the use of nominally lower grade of concrete for GFRP beams not significantly prejudice their performance in terms of both load capacity and durability. The physical properties of the beams are summarized *in Table 3.4*. The loading arrangement and beam details are shown in *Figure 3.4*.

Figure 3.4 Typical loading arrangement and rebar configurations used in Part 4

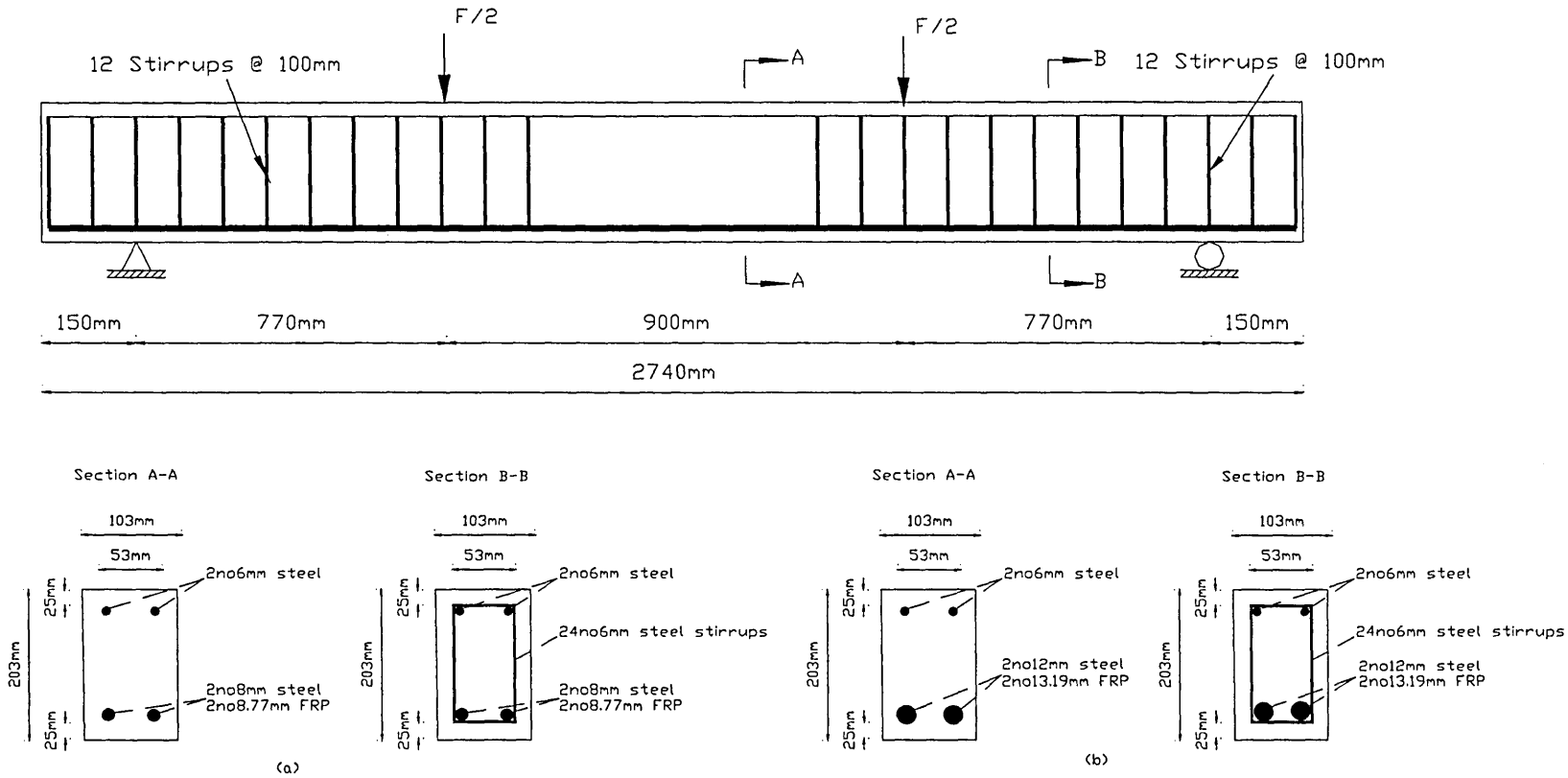

Table 34 The Physical Properties of Part 4 Beams

3.2 MATERIALS

3.2.1 Reinforcement

3.2.1.1 Steel rebars

Three different diameters of nominal size, 8mm, 12mm and 16mm of hot rolled deformed high tensile steel reinforcing bars were used as tension reinforcement and 6mm mild steel reinforcing bars were used as top bars in the compression zone and as stirrups within the shear zones in the concrete beams. The steel was supplied by Derim Steels Ltd., Chesterfield, Derbyshire. Tensile tests were carried out on reinforcing bars using 300kN capacity ESH machine located in the laboratory in accordance with BS/EN 10002-1:1990 2 (see *Photo 3.4).*

Photo 3.4 ESH Tensile testing apparatus : 1. plotter, 2. control panel, 3. bottom jaw, 4. top jaw, 5. rebar sample

The tensile properties obtained from the tests are given in *Table 3.6.* Stress-strain graphs for all four diameters of steel rebars are shown in *Figure 3.5.* All high tensile steel reinforcing bars exhibited less necking than the mild steel reinforcing bars

before failure occurred. Linear elastic behaviour was exhibited by all steel rebars. The applied load became constant at the yield point with increase in strain without increase in load. All four diameter rebars exhibited linear elastic behavior up to the yield point. The standard deviation of the modulus of elasticity was calculated for each bar diameter. The values of modulus of elasticity for all rebars fell within ± 5% of the mean value for the group (see *Table 3.6*). The percentage range in the table is expressed as the ratio of mean modulus of elasticity to the standard deviation. The chemical composition of the steel reinforcements is given in *Table 3.5*.

Table 3.5 Chemical composition of the steel rebars provided by the manufacturer[3]

	Diameter (mm) [type]			
Chemical Composition (%)	**6 [mild]**	**8 [high tensile]**	**12 [high tensile]**	**16 [high tensile]**
C	0.100	0.170	0.170	0.200
Mn	0.600	0.620	0.770	0.760
Si	0.120	0.200	0.160	0.200
S	0.027	0.019	0.022	0.016
P	0.018	0.023	0.014	0.016
Cr	-	0.110	0.070	0.090
Ni	-	0.230	0.270	0.130
Mo	-	0.070	0.070	0.050
N	-	0.009	0.010	0.009
Cu	-	0.520	0.430	0.320
Ceq	-	0.359	0.372	0.384

Table 3.6 Tensile Properties of Steel Rebars

Diameter (mm)	**6**	**8**	**12**	**16**
(Type)	**(mild)**	**(high tensile)**	**(high tensile)**	**(high tensile)**
Density (kg/m^3)	7920	7730	7690	7880
Grip Pressure (MPa)	2.76	2.76	2.76	2.76
Rebar Surface Texture	smooth	ribbed	ribbed	ribbed
No. of Test Samples	3	6	6	6
Yield Load (kN)	8.60	26.31	56.15	93.88
***Yield Stress (N/mm^2)**	304	523.5	497	467
****Yield Stress (N/mm^2)**	382	581.6	580	558.3
Strain at Yield	0.0015	0.0028	0.0026	0.0023
Ultimate Load (kN)	10.90	28.67	67.96	118.9
Ultimate Stress (N/mm^2)	386	571	601	592
Elastic Modulus (GPa)	195	186	189	200
Standard Deviation (GPa)	6.512	3.002	4.216	16.597
(Range -%)	(3)	(2)	(2)	(8)
Failure Mode	ductile	ductile	ductile	ductile

* Based on nominal area of cross-section
** Results given by the manufacturer based on six specimens for each diameter

Figure 3.5 Stress versus Strain Graphs of steel rebars obtained during the tensile test.

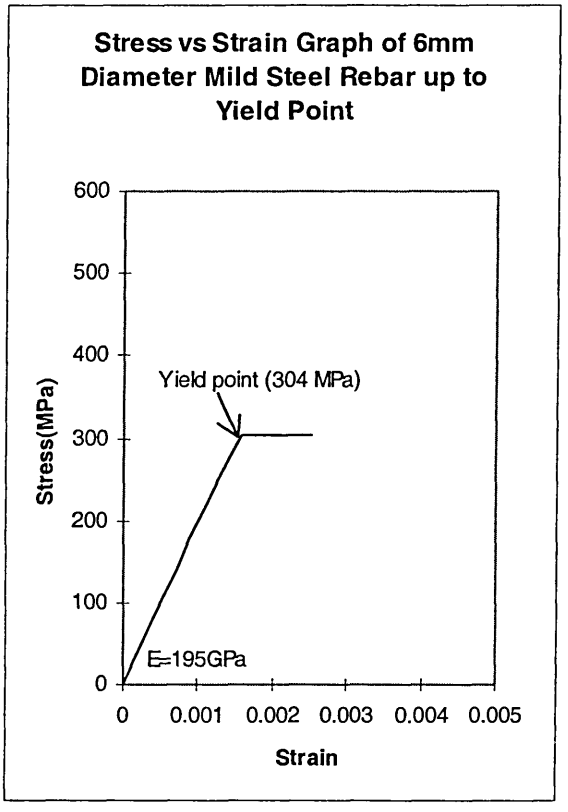

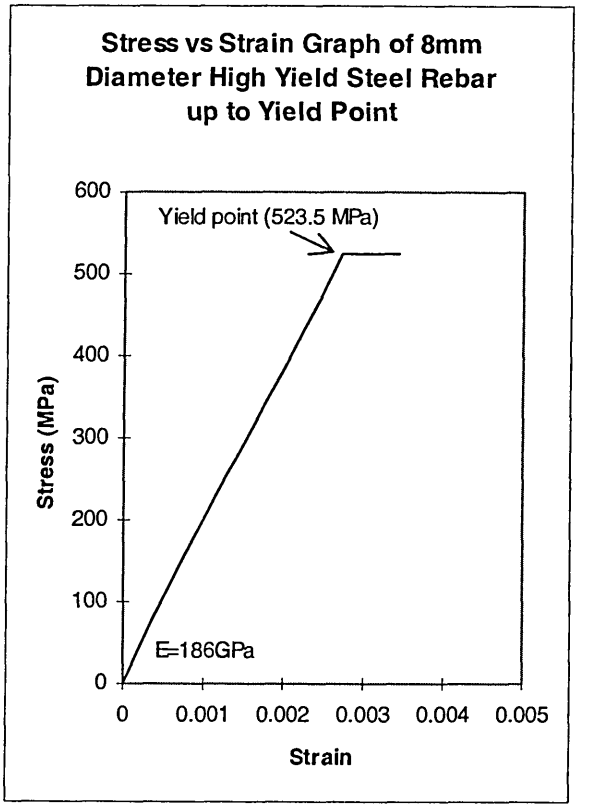

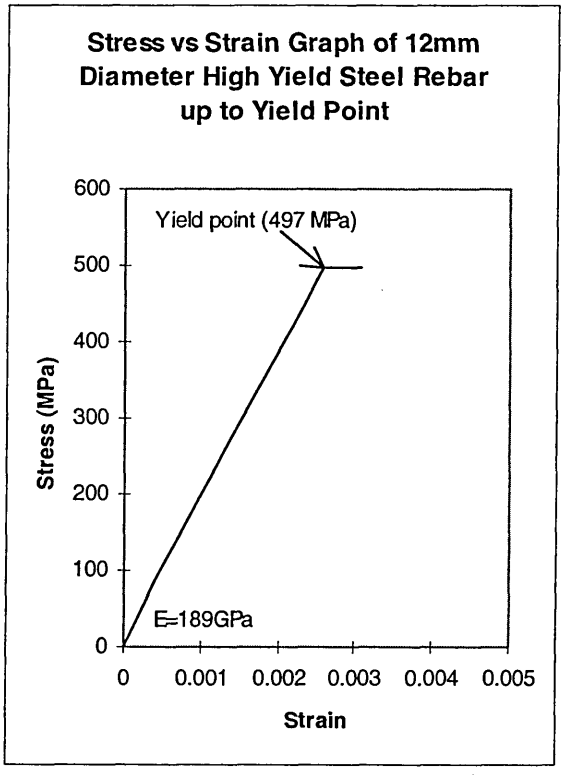

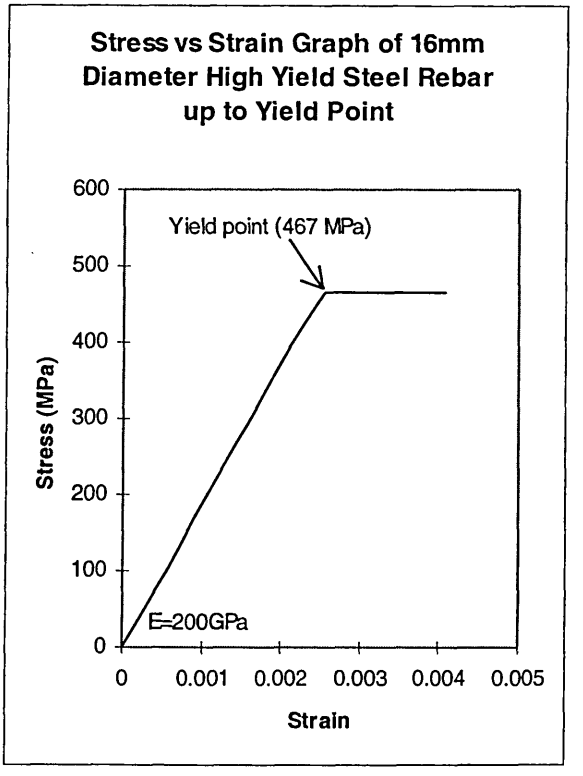

3.2.1.2 GFRP rebar

The Kodiak rebars are manufactured by an American company, International Grating Inc. and are made of E-glass fibres. These fibres are impregnated in a thermosetting polyester resin of 72% by volume and includes a small quantity of fibres which are wrapped around the longitudinal fibres in a helical pattern to induce deformation on the surface of the rebar so that, enhanced bond behaviour with concrete can be achieved. The mechanical properties of the Kodiak GFRP rebars were provided by the manufacturer as shown in *Table 3.7.* Note that the figures in the table are the typical values and not specified for any diameter (size) of GFRP rebars.

Table 3.7 Typical mechanical properties of GFRP specified by the manufacturer[4]

Ultimate Tensile Strength (MPa)	695
Modulus of Elasticity (GPa)	50.04
Compressive Strength (MPa)	417
Bond Strength (MPa)	8.34
Shear Strength (MPa)	59.07
Yield Strength (MPa)	N/A
Water Absorption (%)	0.25 max.
Specific Gravity	2

The diameters of reinforcing bars and their area of cross sections used in the concrete beams are given in *Table 3.8.* The equivalent diameter of GFRP rebars determined through the method for determination of density of hardened concrete in BS1881:Part114[5].

Table 3.8 GFRP and Steel rebar diameters and the areas of the cross section.

Rebar Type	**Diameter (mm) [Area (mm^2)]**			
GFRP	6.9 [37.39]	8.77 [60.50]	13.19 [136.50]	16.44 [212.50]
Steel	6 [28.27]	8 [50.50)	12 [113.00]	16 [201.00]

3.2.1.3 Test Methods & Properties

The tensile specimens were selected from different batches and cut into 500mm lengths. Load versus extension graphs were obtained directly from a 100mm gauge length extensometer which was attached to the specimen at the middle. Static tensile tests were carried out for all four diameters of GFRP reinforcing bars as well as the steel reinforcing bars. All reinforcing bars were subjected to uniaxial tension. The main concern for GFRP rebar was the gripping mechanism of the ends since they are weak in shear. For this reason, the ends of each specimen were protected by casting into tubes thus alleviating the stress concentration resulting from the very deep indentations on the actual rebar caused by the jaws of the testing machine. The grip pressures used and the test results obtained from all the tests are included in *Table 3.9*. The speed rate of the cross-head for the tensile test was chosen to be either 1mm/min. or 5mm/min following a survey of relevant standards (see *Table 3.10*). Note that ASTM D3916-84[6] is the only standard available for tensile testing of GFRP rebars which have a circular cross section.

Table 3.9 Comparison of tensile test results of GFRP rebars from three different methods of end-anchorage

	Diameter (mm)	Density (kg/m^3)	Rebar Surface Texture	Grip Pressure (MPa)	No of Tests	Yield Load (kN)	Yield Stress (MPa)	Ultimate Load (kN)	Ultimate Stress (MPa)	Calculated Ultimate Strain	Elastic Modulus (GPa)	Standard Deviation (GPa)	Failure Mode
plain ends	6.9	2150	deformed	0.69	2	N/A	N/A	22.53	604.00	0.01335	45.26	1.49	brittle
	8.77	2110	deformed	1.38	2	N/A	N/A	35.19	576.50	0.01153	50.00	8.30	brittle
	13.19	2070	deformed	1.38	2	N/A	N/A	45.72	334.50	0.00828	40.40	1.18	brittle
	16.44	2000	deformed	1.38	2	N/A	N/A	59.7	281.90	0.00853	33.05	0.00	brittle
copper ends	6.9	2080	deformed	2.76	3	N/A	N/A	21.71	581.00	0.0134	43.28	1.40	brittle
	8.77	2330	deformed	3.45	8 (7)	N/A	N/A	45.75	601.00	0.01300	45.98	3.34	brittle
	13.19	2030	deformed	1.38-4.13	9	N/A	N/A	71.75	470.70	0.01215	38.75	1.94	brittle
	16.44	1870	deformed	1.38	8	N/A	N/A	115.5	544.00	0.01638	33.21	2.31	brittle
steel ends	6.9	2050	deformed	5.52	4	N/A	N/A	21.67	579.50	0.01383	41.89	3.71	brittle
	8.77	2080	deformed	2.76-5.52	5 *(4)	N/A	N/A	42.86	702.25	0.01427	49.20	5.95	brittle
	13.19	2020	deformed	5.52	5 *(3)	N/A	N/A	75.3	551.33	0.01342	41.07	2.92	brittle
	16.44	2030	deformed	5.52	4 *(2)	N/A	N/A	111.9	527.00	0.01552	33.95	1.80	brittle

( ) note that the first rebar specimen was accidentally compressed vertically by the jaws prior to testing and therefore the results of 7 specimens used in the results

*( ) the number of steel-end specimens not pulled out and therefore used in the experimental results

Note: The 'plain end' appear to give superior values of elastic modulus except for largest diameters and similarly for the ultimate tensile stress for the small diameter bars although the effect of protected ends gives very pronounced enhancement of ultimate tensile stress for larger diameter rebars

The mechanical properties of FRP rebars differ from one manufacturer to another. Most manufacturers specify the tensile strength of the rebars based on the gross area of the rebar[7]. It is also pointed out that the resin matrix does not contribute significantly to the overall tensile capacity of the tendon and hence it can be ignored in strength calculations. In the majority of papers published, the reported strength of the tendons is lower than the strength of an individual fibre that composes the fibre. *Dolan's*[7] paper states that when the probability of failure of an individual fibre and the redundancy of a multiple fibre bundle considered, the total tendon strength is reduced by 35% to account for the matrix volume fraction of the cross section.

Table 3.10 Standards available for tensile test speed

Name of the Standard	**Form of Tensile Specimen**	**Test Speed (mm/min)**
BS 2782: Part 10: 1977[8]	plastic coupon	2
ISO/R527:1966 (E)[9]	plastic coupon	1
JIS (Japanese) K 7054:1987[10]	GFRP coupon	1
JIS (Japanese) K 7073:1988[11]	CFRP coupon	1-2-3 or 5
ASTM D 3916-84[6]	GFRP rod	5

The methods used for tensile testing are outlined below:-

3.2.1.3.1 Method 1 - GFRP rebars having plain ends

In this approach all GFRP rebars were tested under tension in a plain form. That is to say, the ends of the rebars were not protected. Two specimens from each diameter were tested using ASTM D 3916-84[6] standard which specifies the speed of the test (rate of separation of the grips of the test machine) as 5mm/min. Only 6.9mm GFRP rebar failed in a satisfactory manner i.e. the failure took place along the free length of the specimen. The remaining of the rebars failed close to the jaws and their ends disintegrated. It was noted for all the rebars that the helical fibres ruptured before complete failure occurred. It can be seen in *Figure 3.6* that there is a big difference in failure stress for each diameter. It seems that the larger diameter GFRP rebas are more susceptible to the grip pressure of the jaws and hence the larger the diameter the less is the apparent strength. This is due to the rebars being severed by the jaws before the full tensile capacity of the rebars can be fully utilized. The absence of yield of GFRP can also be noted in *Figure 3.6* even though the failures were not satisfactory. It can be concluded that some sort of protection needs to be applied on the ends of the rebars to enable the tensile strength to be accurately determined.

Figure 3.6 Stress versus Strain Graphs of plain-end GFRP rebars obtained during the tensile test

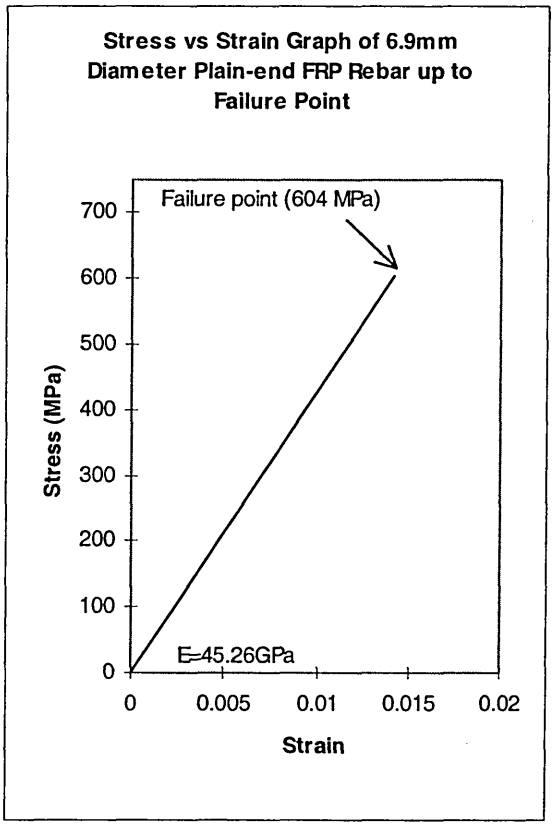

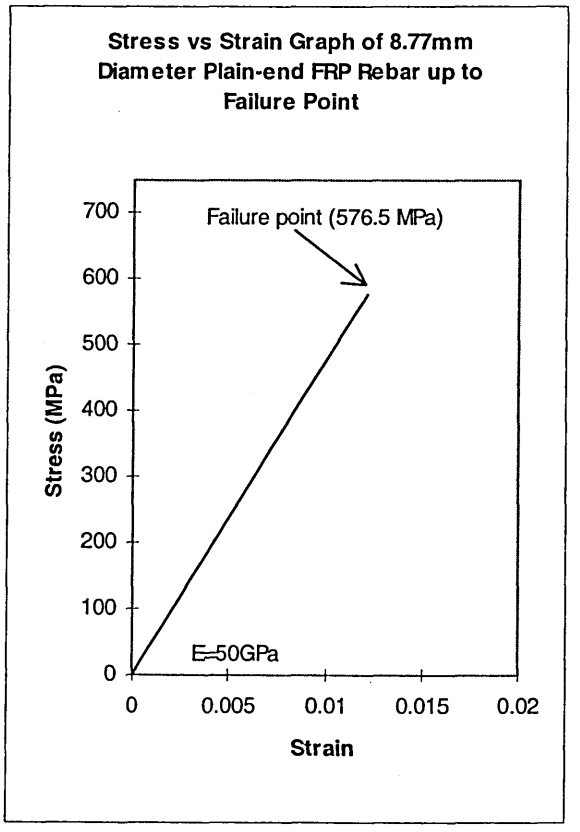

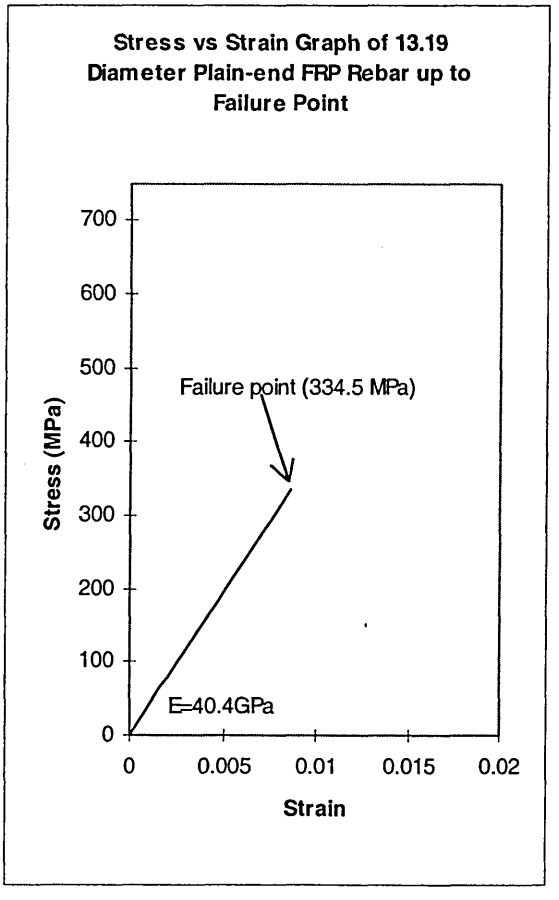

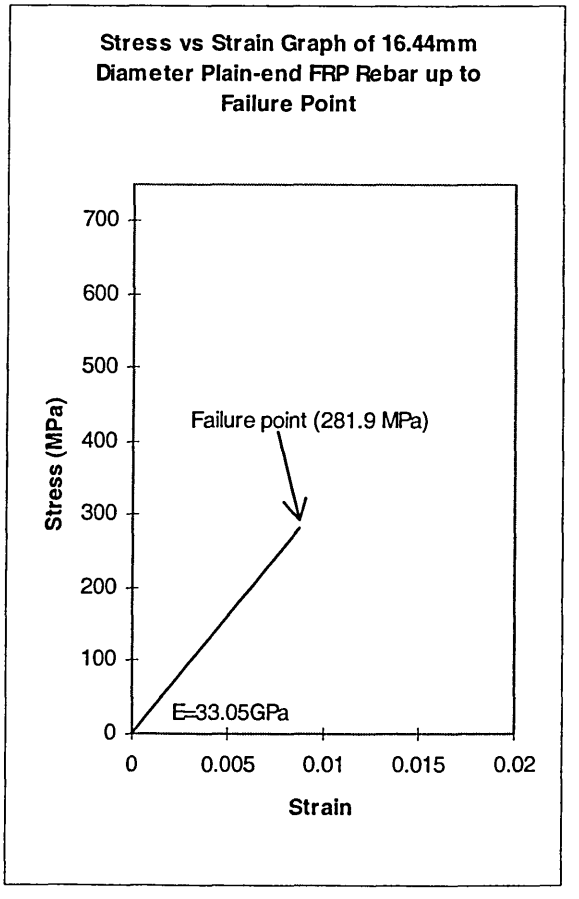

3.2.1.3.2 Method 2 - GFRP rebars having cast ends

In this method the ends of the tensile specimens were cast into 100mm length copper and steel tubes having a thickness of 1.5mm and 2.5mm respectively. The inside of each tube was sand blasted in order to give a clean surface to ensure a good bond between the resin and the tubes. Sand blasting also creates a fine striated area where resin can flow in and bond to the tube adequately. Five specimens were prepared for each diameter of rebar. To enable systematic and accurate assembly of the specimens a stand apparatus has been designed by the Author in order to cast the rebars into tubes (see *Photo 3.5).*

Photo 3.5 Vertical Stand Apparatus (VSA) for casting the ends of the GFRP rebars

Steel/Copper Tube

Six rebars can be cast one end at a time using the stand. The tubes are then fastened to the bottom of the stand. Their bottom ends, resting on a flat surface, were covered with an adhesive tape in order to prevent the leakage of the epoxy resin which was injected inside the tubes. The rebars were placed inside the tubes before the resin was poured. In order to cast the ends in line the other six tubes were secured at the top of the stand. The other end of the rebars was then cast into tubes after twenty-four

hours. It was important to decide on the appropriate epoxy to be suitable for this application in terms of its compatibility with the resin type used in the rebar and for its viscosity to be sufficiently low for ease of the injection. The type of epoxy used for casting was suggested by the rebar manufacturer. The epoxy, Sikadur 32 is a two component resin and it is mainly used to permanently bond freshly mixed mortar or concrete, to hardened concrete, glazed bricks, tiles, steel or other structural materials[12]. *Table 3.11* contains the technical data of the epoxy. 2/3 of part A and 1/3 of part B of Sikadur 32 were mixed in a glass container using a speed controllable stirrer before the injection. The rebars were tested after the epoxy was fully cured for seven days in the laboratory where the temperature is kept between 20-23°C.

Table 3.11 Technical data of Sikadur 32[12]

Colour	Grey
Density(mixed)	1.4kg/litre (approx.)
Cure rates at	5°C 10°C 20°C 30°C
Full cure	13 days 10 days 7 days 5 days
Tensile strength	22 N/mm^2
Flexural strength	35 N/mm^2
Compressive strength	70 N/mm^2
Application range	min 5°C - max 30°C
Adhesion strengths	to concrete typical 3 N/mm^2 (concrete failure) to steel typical 20N/mm^2 (epoxy failure)

ASTM D 3916-84[6] standard was used to conduct the tensile tests on GFRP rebars. A cross head speed rate of 1mm/min which is in the Japanese standards[10], was also used in order to find out the effect of test speed on the tensile properties of the rebars. Five 8.77mm diameter rebars with copper ends were tested at both test speeds, 5mm/min and 1mm/min. It can be seen in *Table 3.12* that the influence of test speed is not significant in terms of the tensile properties of the rebars.

Table 3.12 Comparison on the tensile properties of GFRP rebars using two different test speed extracted from Japanese and American Standards

	[Test Speed] mm/min	
	[1] JIS K 7054 1987[10]	[5] ASTM D3916-84[6]
Diameter (mm)	8.77	8.77
Grip pressure (MPa)	3.45	3.45
No of Test Samples	5	*5
Ultimate Load (kN)	28.33	29.49
Ultimate Stress (MPa)	464.20	483.13
Ultimate strain (calc.)	0.01085	0.01071
Elastic Modulus (GPa)	42.76	45.09
Standard deviation (GPa)	2.576	3.669

*First sample was initial compressed vertically by the jaws and hence the average results of 4 samples were used in here.

The results of tensile tests on glass FRP reinforcing bars with three methods of cast-ends are given in *Table 3.9*. Note that these results are based on the test speed of 5mm/min. The numbers in the brackets indicate the results obtained from rebars which did not pull out. Apart from the pulled out specimens, the rest of the rebars cast in both copper and steel ends failed in a satisfactory manner i.e. failure took place within the free length of the specimen (see *Photo 3.6*). The failure for all the rebars took place with the prior snapping of helical fibres before the ultimate rupture of the rebar.

Some of the rebars, which were cast into steel tubes, were debonded i.e. the resin and the rebar together were pulled out from the tube (see *Photo 3.6* and *Photo 3.7*). The test results of those were not included in the Table. *Figure 3.7* and *Figure 3.8* are the stress versus strain diagrams of the GFRP specimens with steel and copper ends respectively.

Photo 3.6 Thefailed GFRP specimens with steel/copper ends.

Figure 3.7 Stress versus Strain Graphs of steel-end GFRP rebars obtained during the tensile test

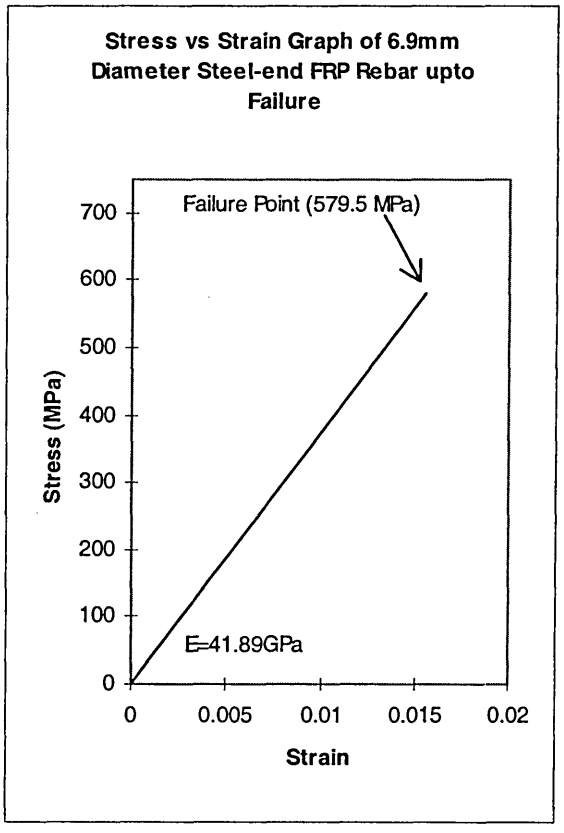

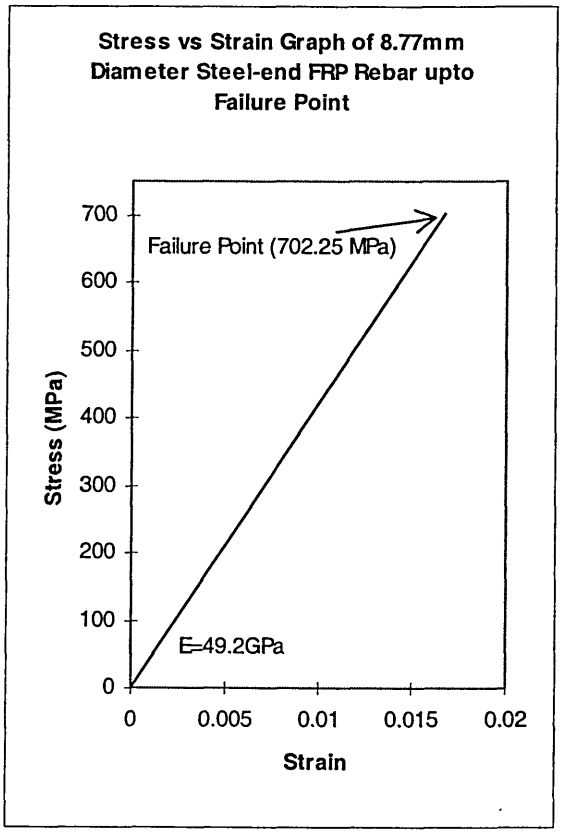

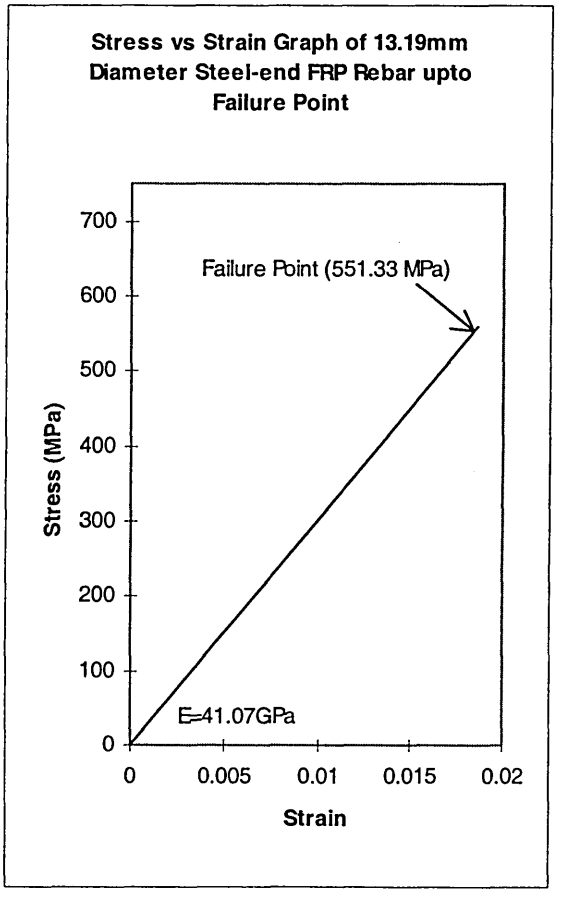

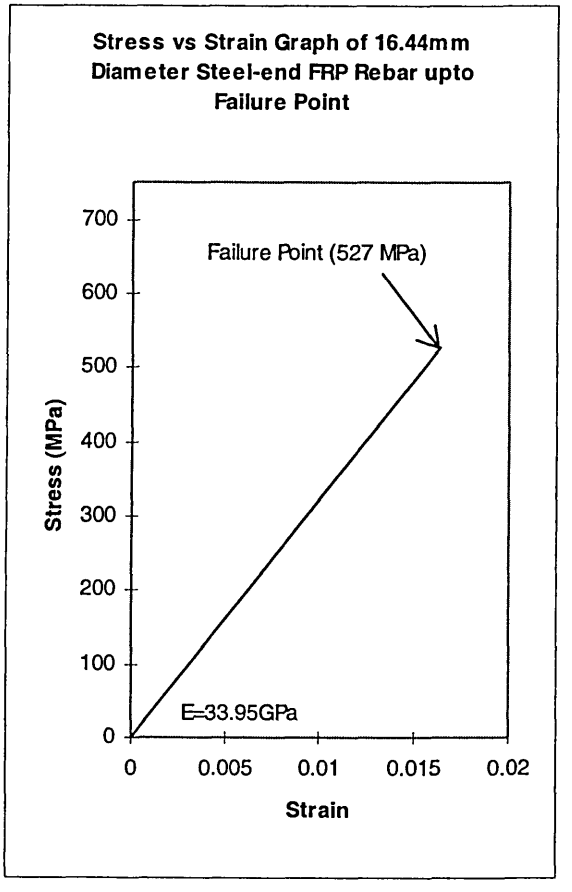

Figure 3.8 Stress versus Strain Graphs of copper-end GFRP rebars obtained during the tensile test

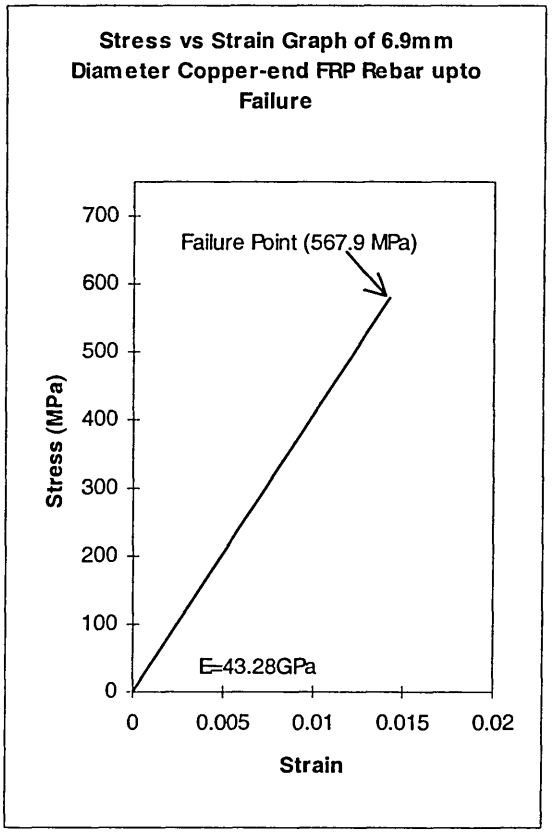

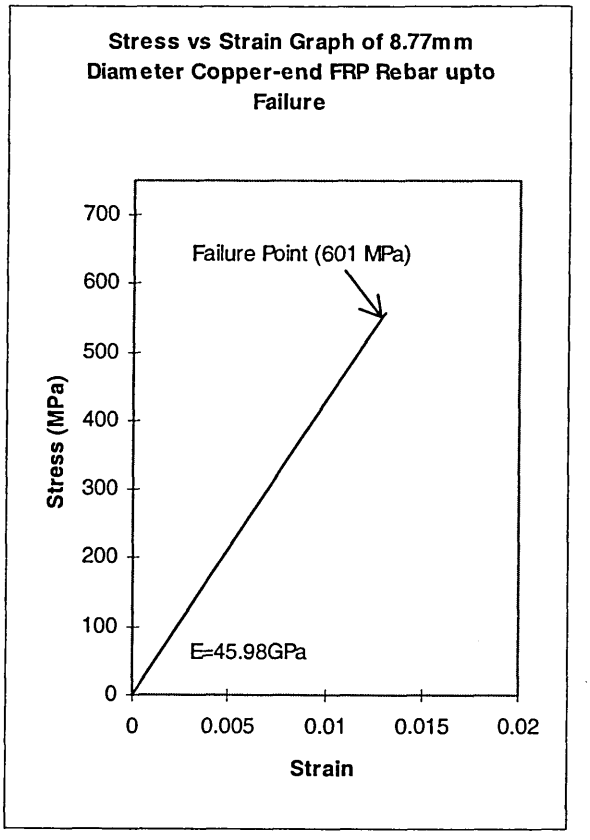

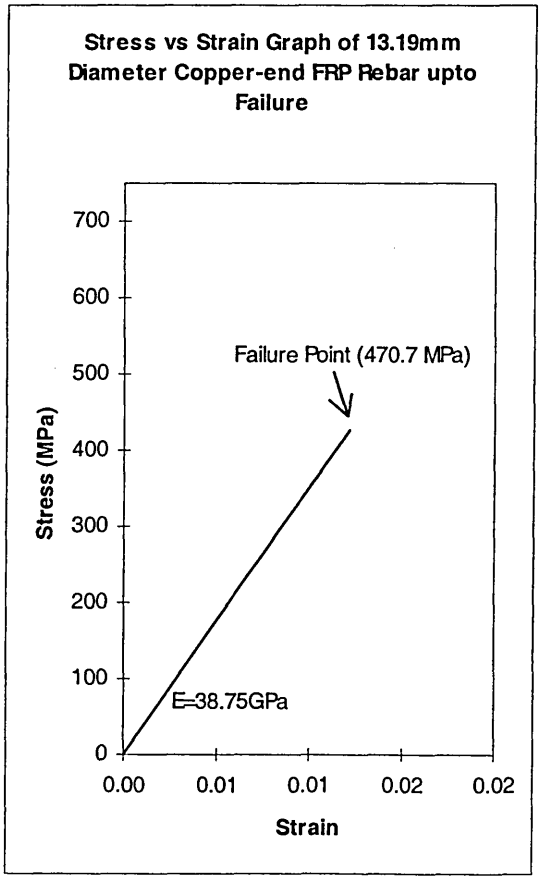

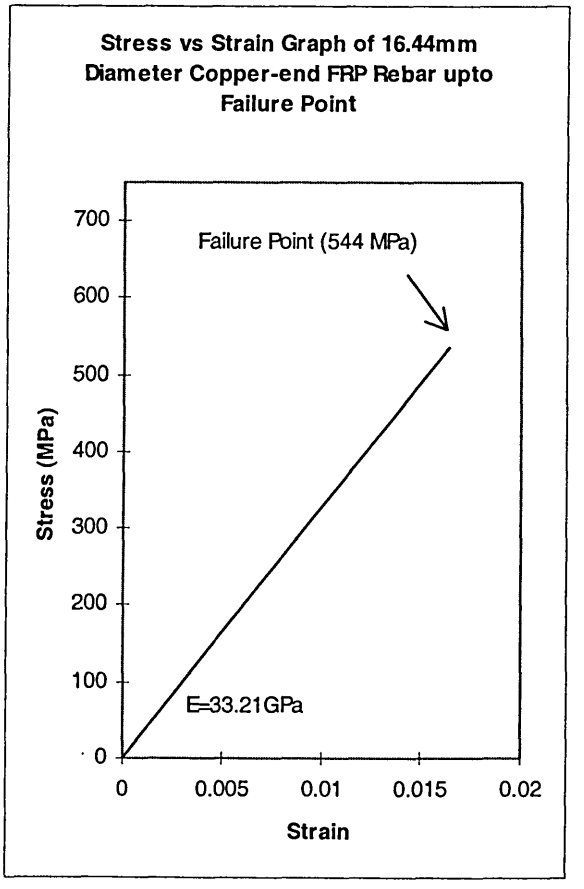

It can be seen in the stress versus strain diagrams of GFRP rebars that the magnitude of 'failure stress' for particularly Ø13.19 and Ø16.44 rebars are more influenced by having their ends cast in steel/copper tubes. These tubes play an important role against the 'bite-in' action of the jaws and hence better results can be achieved. Some complex fibre-matrix and specimen- grip interactions rather than being dominated purely by the fibre properties could influence the tensile failure results for each method of end casting. It also seems that the tensile properties of these rebars are dependent on specimen diameter. Generally, the steel-end rebars give higher stress values at failure for a given diameter, than the copper-end rebars. However, it should be noted that the results for the steel-end rebars are based on a smaller number of specimens than the copper-end ones (see *Table 3.9*). The tensile strengths were based on the copper-end specimens throughout the investigation due to the fact that a more satisfactory failure was achieved. Also, none of the copper tubes pulled out during the tensile test.

Figure 3.9 shows the typical recovery of Ø8.77, Ø13.19 and Ø16.44 GFRP rebars under tension. The tension was applied to the rebars up to 70% of its ultimate load capacity then the tension load was reduced to zero and finally the load applied again up to failure. The figure shows that the elastic recovery of the material is influenced by the rebar diameter.

It was decided to monitor the tensile strains simultaneously for a GFRP rebar (Ø16.44) using an extensometer and a strain gauge attached to the rebar. This was to whether there is a big difference between the reading from two different instruments. *Figure 3.10* confirms the consistency of the readings obtained.

Figure 3.9 A representative graphs for the recovery of GFRP rebars under tension

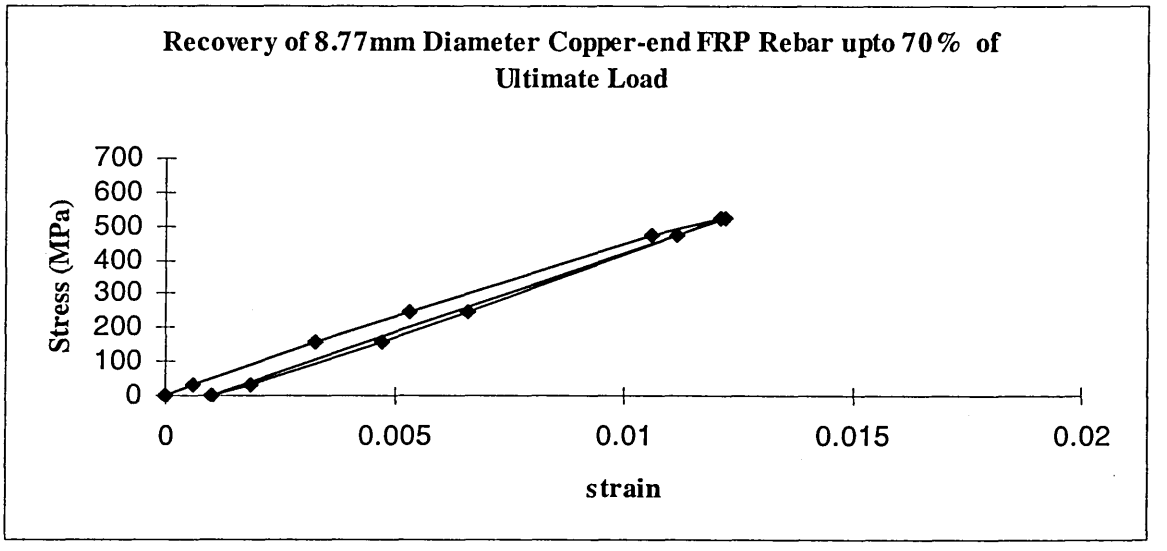

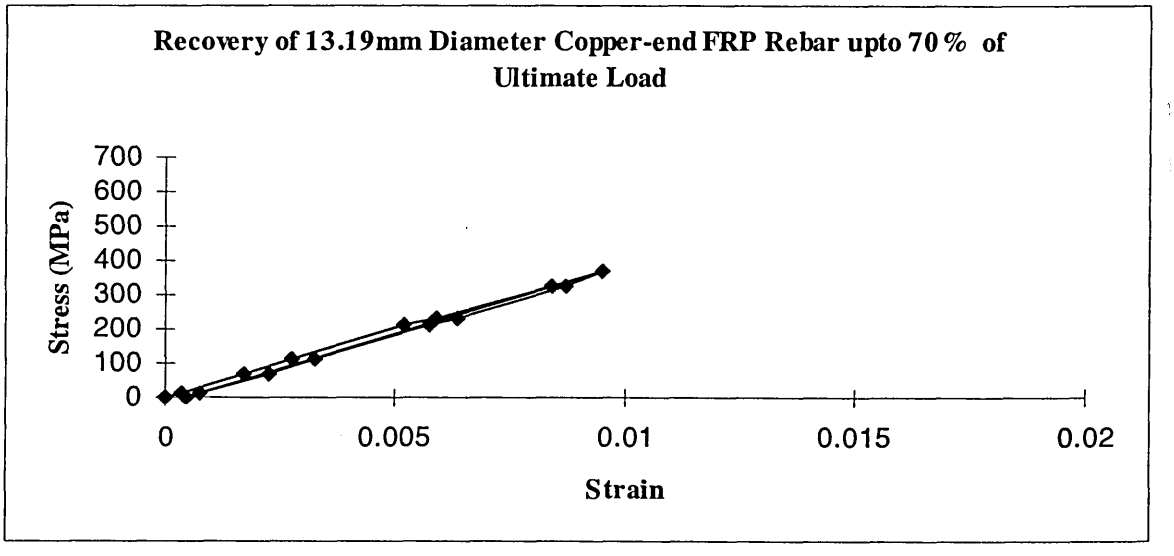

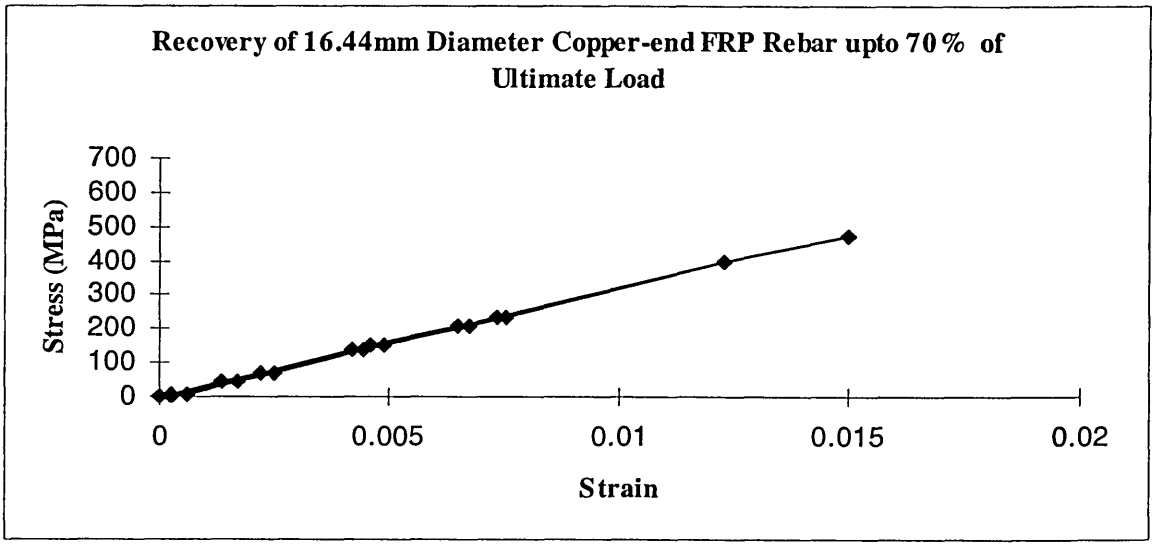

Figure 3.10 A representative tensile stress versus strain graph of GFRP rebar measured by an extensometer and a strain gauge

(BJI/V) SS3JIS

The results of tensile tests (see *Table 3.13*) carried out by Malvar[13] on four different types of, Type A, Type B (look very similar to Kodiak rebars used in the investigation), Type C and Type D 19mm diameter glass FRP rods having a fibre fraction of 45% or more embedded in a vinlyester or polyester resin. The author also used ASTM D 3916-84 standard for conducting the tests. The results of tensile tests carried out by the Author for the reinforcing bars used in this investigation are given in *Table 3.14*.

Table 3.13 The tensile test results reported by Malvar

Bar type	**No of tests**	**Modulus of elasticity (GPa)**	**Ultimate Stress (MPa)**	**Ultimate strain**
A	5	45.5	598	0.0014
B	5	28.29	449.19	0.0017
C	5	47.4	562	0.0012
D	5	39.8	561	0.0018

Table 3.14 Tensile test results of steel and GFRP rebars used in this study

Rebar Type	Nominal Rebar Diameter (mm)	Density (kg/m^3)	Rebar Surface Texture	Grip Pressure (MPa)	No of Tests	Yield Load (kN)	Yield Stress (MPa)	Ultimate Load (kN)	Ultimate Stress (MPa)	Calculated Ultimate (Yield) Strain	Elastic Modulus (GPa)	Standard Deviation (GPa)	Failure Mode
High Tensile/ *Mild* Steel	*6*	*7920*	*smooth*	*2.76*	*3*	*8.60*	*304*	*10.90*	*386*	*(0.0015)*	*195*	*6.512*	*ductile*
	8	7730	deformed	2.76	6	26.31	523.50	28.67	571.00	(0.0028)	186	3.002	ductile
	12	7690	deformed	2.76	6	56.15	497.00	67.96	601.00	(0.0026)	189	4.216	ductile
	16	7880	deformed	2.76	6	93.88	467.00	118.9	592.00	(0.0023)	200	16.597	ductile
copper anchorage GFRP	6.9	2080	deformed	2.76	3	N/A	N/A	21.71	581.00	0.0134	43.28	1.40	brittle
	8.77	2330	deformed	3.45	8 *(7)	N/A	N/A	45.75	601.00	0.01300	45.98	3.34	brittle
	13.19	2030	deformed	1.38-4.13	9	N/A	N/A	71.75	470.70	0.01215	38.75	1.94	brittle
	16.44	1870	deformed	1.38	8	N/A	N/A	115.5	544.00	0.01638	33.21	2.31	brittle

*( ) the actual number of the specimens of which the results obtained

3.2.2 Cementitious Materials

3.2.2.1 Cement

Portland Cement (OPC-42.5) having a range of particle size of 5μm to 30μm was provided by Castle Cement Ltd. Their product was used throughout the investigation. Cement from the manufacturer was delivered several times over a period of four years throughout the programme. Chemical composition and the physical characteristics of Portland Cement (PC) and are given in *Table 3.15.*

3.2.2.2 Microsilica

EMSAC 500 S microsilica was provided by the manufacturer, ELKEM in Buckinghamshire with an average particle size of 0.15μm product was used in some of the beams in Part 3. The microsilica content, which is recommended in the technical data sheet[14], was 10% of the original cement content added to the mixes. Chemical composition and the physical characteristics of microsilica are given in *Table 3.15.* The purpose of using microsilica for the beam testing programme was to achieve higher strength concrete and bond *[see Chapter 2, ref. 81]* through the improvement in cohesion of mix constituents. It can be seen in *Table 3.15* that one kilogram of microsilica covers 40-50 times bigger area than OPC. In other words, fine particulated microsilica is able to fill the micro gaps in the concrete reducing bleeding and therefore, it was felt that this would provide an enhancement in bond between GFRP reinforcing bars and the concrete.

Table 3.15 Physical & Chemical Data Comparison between Microsilica(Elkem) and Portland Cement

	SiO_2 (%)	Al_2O_3 (%)	Fe_2O_3 (%)	Cl (%)	Na_2O (%)	K_2O (%)	MgO (%)	SO_3 (%)	CaO (%)	Surface Area (m^2/kg)	Bulk Density (kg/m^3)	Specific Gravity
OPC	21	5	3	0.03	0.13	0.67	1.1	3.1	64.5	380	1444	3.12
Microsilica	92	1	1	1.5	0.3	0.8	0.6	0.3	0.3	15000-20000	200-300	2.20

3.2.2.3 Chopped Glass Fibre Strands

CEM-FIL 60/2, 24mm long chopped fibres were supplied by the manufacturer in Merseyside, Liverpool. These fibres were used in some of the beams in Part 3 (see *Photo 3.8)*. The tensile strength, modulus of elasticity and the density of the fibres are 1700 MPa, 72 GPa and 2680kg/m3(specific gravity 2.68) respectively. Glass fibre strands were added to the mix by sprinkling shortly after water was added to the dry mix of cement, coarse and fine aggregate. In this way better and more even distribution of fibres within the mix could be achieved. It was felt that the use of chopped fibres in the beams might be able to contribute to the resistance in shear and improve bond condition around the rebar *[see Chapter 2, ref. 155]*.

Photo 3.8 A sample of chopped glassfibre strands used in concrete mixes

CEM-FIL fibres exhibit a high degree of general, acid and alkali, chemical resistance but were specifically developed to resist the very high alkalinity produced by the hydration of cement. They are corrosion resistant and incombustible with good heat resistance13.

3.2.3 Aggregates

3.2.3.1 Coarse aggregates

3.2.3.1.1 Normal weight

5-20mm graded quartzitic coarse aggregates supplied by Tarmac Roadstone Ltd. (Nottingham) used throughout except for some lightweight aggregate beams in Part 3 (see *Photo 3.9*). This size of aggregates is commonly used in reinforced concrete structures. The grading curve of the aggregates is given in *Appendix 3*. This was determined in accordance with BS 812[16].

3.2.3.1.2 Lightweight

6-12mm graded Lightweight aggregates (see *Photo 3.10*) were used in some of the beams in Part 3. The product is available from Boral Lytag manufacturer in Eggborough. Lytag is specifically designed for reducing concrete self-weight[17] improving its specific performance in respect of strength and stiffness. The basic material is pelletised pulverised fuel ash (the waste product from the generation of electricity at coal burning power stations) which is suitable to produce lightweight aggregates. The grading curve of the aggregate is given in *Appendix 3*.

3.2.3.2 Fine Aggregate

The fine aggregate consisted of a medium grade sand ('M' sand) used in all the beams. The grading curve was determined in accordance with BS 812[16] is given in *Appendix 3*.

Photo 3.9 A sample of 5-20mm coarse aggregate used in concrete mixes

Photo 3.10 A sample of 6-12mm lightweight aggregate used in concrete mixes

3.2.4 Admixtures

CORMIX SP4 type super plasticiser was used in only two micro silica added lightweight concrete beams, which are in Part3. The mix for those beams appeared to be too dry resulting in reduction of workability of the mix i.e. slump being outside the range (30mm-60mm). Therefore, the addition of super plasticiser compensated for this. The specified slump was achieved for the trial mixes of normal weight concrete containing microsilica, without any addition of superplasticiser.

3.2.5 Concrete Mixes

3.2.5.1 Properties & Mix Proportions

3.2.5.1.1 Normal, Medium and High Strength Concrete

C20, C40 and C60 normal weight concrete mixes were designed according to the design process given in Building Research Establishment Report[18] "Design of normal concrete mixes". Concrete mix proportions and properties are given in *Table 3.16*. The mean density and the mean strength of concrete were obtained from six cube specimens. The designation 'wet condition' for strength in *Table 3.16* is represented by three specimens which were cured in water tanks in accordance with BS 1881[19]. The designation 'dry condition' is for the other three specimens which were wrapped in plastic sheet and kept in the laboratory conditions similar to those of the beam specimens.

It should be pointed out that there is an apparent discrepancy between nominal grades and the actual strengths produced. In order to satisfy the workability criteria without either having unacceptably high workability or excessive fine aggregate content in fully compacted concrete, average mix strengths are generally higher than would normally be associated with the nominal grade. However the, mix design was consistent with the procedure given in the design of normal concrete mixes.

Table 3.16 OPC-Normalweight Concrete Properties & Mix Proportions

CONCRETE GRADE (Nominal)	MEAN SLUMP (mm)	MEAN DENSITY Condition DRY (kg/m^3)	MEAN DENSITY Condition WET (kg/m^3)	MEAN STRENGTH Condition DRY (MPa)	MEAN STRENGTH Condition WET (MPa)	MIX PROPORTIONS (kg/m^3) W/C	Water	Cement	FA	CA
C20	50	2384	2418	43	45	0.56	180	321	570	1329
C40	54	2396	2428	60	64	0.42	180	429	787	1254
C60	56	2435	2459	75	77	0.30	180	600	405	1215

3.2.5.1.1.1 Mixing Process

In order to obtain the design free water content, moisture condition of fine aggregate was determined before batching the concrete. This was carried out using the 'Speedy Moisture Tester' in the laboratory. Cement, coarse and fine aggregates were mixed for 30 to 40 seconds and then the required amount of water was added to the concrete for a further 1.5 minutes mixing. The 'Slump' workability test was carried out in accordance with BS 1881:Part 102[20].

3.2.5.1.2 Microsilica Added Concrete

The original C20 mix design was used for concrete containing microsilica. Microsilica added to the mix was 10% of total cement content which is recommended by the manufacturer, ELKEM[14]. Concrete mix proportions and properties are shown in *Table 3.17*. There was no need to use superplasticiser in the mixes since the 'Slump Test' was giving values within the range of required slump target range (30mm to 60mm).

Table 3.17 OPC-Microsilica Concrete Properties & Mix Proportions

CONCRETE GRADE (Nominal)	MEAN SLUMP (mm)	MEANDENSITY Condition DRY (kg/m^3)	MEANDENSITY Condition WET (kg/m^3)	MEAN STRENGTH Condition DRY (MPa)	MEAN STRENGTH Condition WET (MPa)	MIX PROPORTIONS (kg/m^3) W/(C+S)	Water	Cement	SILICA	FA	CA
C20	55	2378	2422	55	65	0.51	180	321	32.10	570	1329

3.2.5.1.2.1 Mixing Process

Mixing procedure of microsilica concrete was followed as recommended[14]. The Fine Aggregate(FA) and Coarse Aggregate(CA) were mixed at the beginning for 30 to 40 seconds. In order to achieve the required standard consistency in concrete, microsilica slurry (i.e. water mixed with microsilica) were poured into the mix and mixed for another 40 seconds. The cement was then added to the mix and further mixing was carried out for 1.5 minutes. The determination of moisture condition of fine aggregate and carrying out 'Slump Test' were as previously described.

3.2.5.1.3 Glassfibre Concrete Mix

The mix proportions of C40 concrete having chopped strand glass fibres are given in Table 3.18. Adding glassfibres into the mix tends to reduce workability of the concrete and hence both the workability of normal and glass fibre concrete must be measured so that some adjustments are made to improve it. For this reason, the slump of the original mix (C40) was designed to be greater, 50 to 100mm. Although the 'Slump Test' does not reflect the whole workability of the concrete, it is useful in detecting the uniformity of the fresh concrete for given proportions. The slump of the glass fibre concrete is in the range of 0-25mm, and the slump test cannot detect its uniformity since in this case the concrete is very dry. Therefore, the 'Vebe Test' in accordance with BS 1881:Part 104[21] was used to measure the workability. This test is very suitable for the dry concrete and the treatment during the test is close to its use in practice. After several trial mixes, the proportions were adjusted to incorporate glass fibres of 0.5% of the total volume of the mix. Concrete mix proportions and properties are shown in *Table 3.18.*

Table 3.18 Cement-Glassfibre Concrete Properties & Mix Proportions

		MEAN DENSITY		MEAN STRENGTH							
CONCRETE	MEAN	Condition		Condition		MIX PROPORTIONS (kg/m^3)					
GRADE (Nominal)	SLUMP (mm)	DRY (kg/m^3)	WET (kg/m^3)	DRY (MPa)	WET (MPa)	W/C	Water	Cement	FIBRES	FA	CA
C40	N/A	2387	2393	57	60	0.42	195	464	13	711	1159

3.2.5.1.3.1 Mixing Process

The procedure was similar to that for the cement concrete mix except that the glassfibres were sprinkled into the mix at the final stage of mixing and mixed for 1.5 minutes after adding fibres. This mixing process was kept to a minimal time whilst ensuring good fibre dispersion. The typical Vebe time recorded for the glass fibre mix was 9.7 seconds and this is within the range of normal mix (8-10seconds) for a given equivalent slump.

3.2.5.1.4 Lightweight Concrete

For lightweight concrete, Lytag manufacturer's C20 and C50 lightweight concrete mix designs were used. Concrete mix proportions and properties are shown in *Table 3.19.* Microsilica added to the C20 mix was 10% of total cement content.

Table 3.19 Cement-Microsilica-Lightweight Concrete

		MEAN DENSITY		MEAN STRENGTH								
CONCRETE	MEAN	Condition		Condition		MIX PROPORTIONS (kg/m^3)						
GRADE (Nominal)	SLUMP (mm)	DRY (kg/m^3)	WET (kg/m^3)	DRY (MPa)	WET (MPa)	W/C *W/(C+S)*	Plasticiser	Water	Cement	SILICA	FA	LA
C20	70	1978	2023	47	46	0.5	-	180	360	-	600	796
C20	30	1977	2018	62	65	*0.45*	1.00	180	360	36	600	796
C50	60	1983	2012	66	66	0.3	-	180	600	-	345	802

3.2.5.1.4.1 Mixing Process

Mixing procedure for lightweight concrete was followed as recommended by the Boral Lytag manufacturer. Moisture condition in sand and Lytag aggregates determined before mixing. Typical percentage of moisture content determined in the lightweight aggregate (7% to 10%) was more than the fine aggregate (1% to 3%). Lytag aggregate particles were crushed then the moisture content was measured. The original water content was then adjusted. Approximately 50% of total water content was poured in the bowl of the mixer. Lytag aggregates, fine aggregate, cement and the remaining water were then added to the mix in sequence. The mixing time spent on the sequence of constituents was 1 minute, (40-90) seconds, (30 -40) seconds and 90seconds respectively. Approximately 3.5 minutes mixing time was considered sufficient to distribute the materials uniformly.

The trial mixes of C20 lightweight concrete containing microsilica was proved to be very dry and gave 'slumps' outside the required range (30mm to 60mm). Thus, CORMIX SP4 superplasticiser was added. Two slurries were prepared. The first one contained water and microsilica and the second one contained water and the superplasticiser. The second slurry was added to the mix at the final stage of mixing. The same sequence was carried out as previously with a slightly longer time of mixing.

3.3 Manufacturing and Curing of Concrete Specimens

The steel moulds in which the specimens cast were oiled lightly before the casting began. The concrete was mixed in an horizontal pan type mixer. One batch containing 187kg of total constituents was sufficient to manufacture a beam and the control specimens (cubes and cylinders). A slump test was carried out for each mix according to BS1881 Part102:1983[20] (see *Photo 3.11*). The concrete was placed and compacted in 50mm layers for all specimens. The compaction applied was by a vibrating poker for the beams and vibrating table for the control specimens. 6 number of 100mm side test cubes along with 2 number of 100mm diameter 200mm high cylinders were manufactured from each mix (see *Photo 3.12*). 3 number of cubes and 2 number of cylinders were cured adjacent to the test beam in the laboratory and wrapped with plastic sheet as the beam. The other 3 number of cubes were retained in the water tank after they stayed in the 90% humidity mist curing room for 24 hours. The cylinders were capped with a 3:1 mortar of high alumina cement and sieved (300μm) fine sand and were retained in the high humidity room 24 hours before the flexure test was conducted for beams. The concrete strength and the elastic modulus for each beam were obtained from the cubes and the cylinders respectively by conducting compression tests according to BS1881 Part116:1983[22] and BS1881 Part121:1983[23].

Photo 3.11 Slump test carried out in the laboratoiy

Photo 3.12 The control specimens cast in the laboratory during the manufacturing of the beams

3.4 Instrumentation

3.4.1 Electrical Resistance Strain Gauges

The strain in the reinforcing bars was measured by using electric resistance polyester (PS-20-11) and foil (FLA6) backed strain gauges attached to the reinforcements. These gauges were supplied by Techni Measure Ltd., Warwickshire. The details of the gauges are given in *Table 3.20.*

Table 3.20 Details of the two types of strain gauges[24].

Type	Polyester/PS-20-11	Foil/FLA-6
Gauge Length (mm)	20	6
Gauge width (mm)	1	2.2
Base (mm)	30x2	12.5x4.3
Nominal Resistance (Ω)	120 ± 0.3	120 ± 0.3
Gauge Factor	2.14	2.12
Strain Limit (%)	2	3
Compatible Adhesives	[P-2, CN, RP-2, NP-50, PS], EA-2	[P-2, CN, NP-50], EA-2
Operational Temperature (°C)	[-30 ~ +80], -196 ~ +80	[-30 ~ +80], -196 ~ +80

PS-20-11 gauges were used in the first twelve beams. Initially, it was thought that the advantage of using this type of gauge is its long gauge length (20mm) which would give a good average of strain values and thin gauge width (1mm) which was convenient particularly for 8mm steel and 8.77mm FRP reinforcing bars. The surface of the location of the strain gauge was filed down. A flat surface was necessary for this type of strain gauge to be attached to the rebar since they are insufficiently supple to stick to a round surface. It was realized that the amount of these gauges available in stock was not enough to use throughout the investigation. It was also not possible to acquire more gauges from the manufacturer since they stopped making them in 1991.

It was therefore decided to use foil FLA-6 strain gauges throughout the investigation. The surface to which the gauge sticks was filed circumferentially. Foil gauges are more supple than polyester gauges so that they can easily be seated on a round location. The gauge installation was carried out before the rebars were assembled in the moulds. A full description of the installation procedure is given below[25,26].

Summary of gauge fixing procedure

i. The location of the gauges on the rebars/stirrups was marked and any unevenness on the surface of the rebars was removed with a smooth file. 180 grit emery paper was then used for the final finish.

ii. The gauge area was cleaned using a solvent with cotton tipped applicators and a degreaser.

iii. The gauge to be installed was placed on a clean glass surface together with solder tab (terminal) leaving a space of approximately 1.5mm between the gauge backing and the terminal. Cellophane tape was tacked to the glass behind the gauge and wiped forward firmly over the gauge and the terminal. The tape was then carefully lifted at a shallow angle (approximately 45 degrees to the glass surface) bringing the gauge and the terminal with it.

iv. The gauge/tape assembly was positioned so that the alignment marks on the gauge were over the layout lines. After the correct alignment was made, one end of the tape was firmly fixed down.

v. The free end of the tape was then lifted at a shallow angle until the gauge and the terminal were free of the surface. The gauge area along with the back of the gauge and the terminal were then coated with P2 (Polyester) or CN (Cyanoacrylate) adhesive.

vi. The gauge/tape assembly was then wiped over the adhesive in a single stroke bringing the gauge back down on the alignment marks on the rebar. It was important to let as much adhesive as possible squeeze out during the wiping of the gauge/tape assembly.

A silicone gum pad was placed over the gauge and clamping pressures of between $0.54N/mm^2$ and $0.28N/mm^2$ were applied for twenty four hours for PS-20-11 and FLA-6 gauges respectively. However, this stage of the

installation process was quicker when CN adhesive was used for FLA-6 gauges, as its curing time is only one minute. The appropriate clamping pressure of could be achieved by pressing the thumb over the attached gauge for one minute. The details of the adhesives used in the installation process are given in *Table 3.21*.

Table 3.21 Adhesives used in Strain Gauge Installation[25]

Adhesive Type	P-2	CN
Base	Polyester	Cyanoacrylate
Curing Time	2~3 hours	1 min
Cure Pressure	0.20~0.30 N/mm^2	0.98 N/mm^2
Specimen Material Compatibility	All except some plastics	All except some plastics and concrete
Strain Limit	3 %	20 %

viii. A stress relief loop was placed between the gauge and the terminal. The lead wires were then soldered to the gauge and the terminal and the resistance of the gauge monitored to ensure full connection. A protective coating using P-2 adhesive was applied to the overall gauge area in two layers. In the second layer, sand coating was applied to the installation area soon after the adhesive reached the gel form.

3.4.1.1 Determination of a Suitable Location for the Strain Gauges

One of the concerns regarding strain gauge installation was to decide on gauge location on the FRP rebar and the amount of material needing to be removed during filing. The average distance between the spiral bindings (pitch length) measured from 3m long FRP rebars for four different diameters are given in *Table 3.22*.

Table 3.22 Average pitch length of FRP rebars

Diameter (mm)	6.9	8.77	13.19	16.44
No of rebars	5	5	5	5
Overall Length (mm)	3000	3000	3000	3000
Avarage pitch length (mm)	11	12	15	32
(FLA-3 strain gauge) Backing length (mm)	8.8	8.8	8.8	8.8
(FLA-6 strain gauge) Backing length (mm)	12.5	12.5	12.5	12.5

Tensile tests were carried out for 2∅13.19 rebars up to failure. A total of four locations was selected. Two strain gauges, one through the binding (G1) and another one on the binding (G2) were attached on the first rebar. On the second rebar, both two gauges, G3 and G4, were attached within the pitch length owing to the cases of removing of an amount of material. All these are sketched in *Figure 3.11.* It can be seen from *Table 3.22* that the 13.19mm and 16.44mm diameter rebars have the most suitable pitch length for FLA-6 strain gauge to be installed between the bindings for this observation. Therefore, these gauges were applied on 13.19mm diameter rebars only, since this diameter of rebars used mostly together with 8.77mm diameter GFRP rebars throughout the investigation. Also, note that the spiral binding on ∅16.44 rebars had hardly any resin on them and hence the surface texture was not suitable for strain gauge installation.

Figure 3.11 Sketch of strain gauge locations

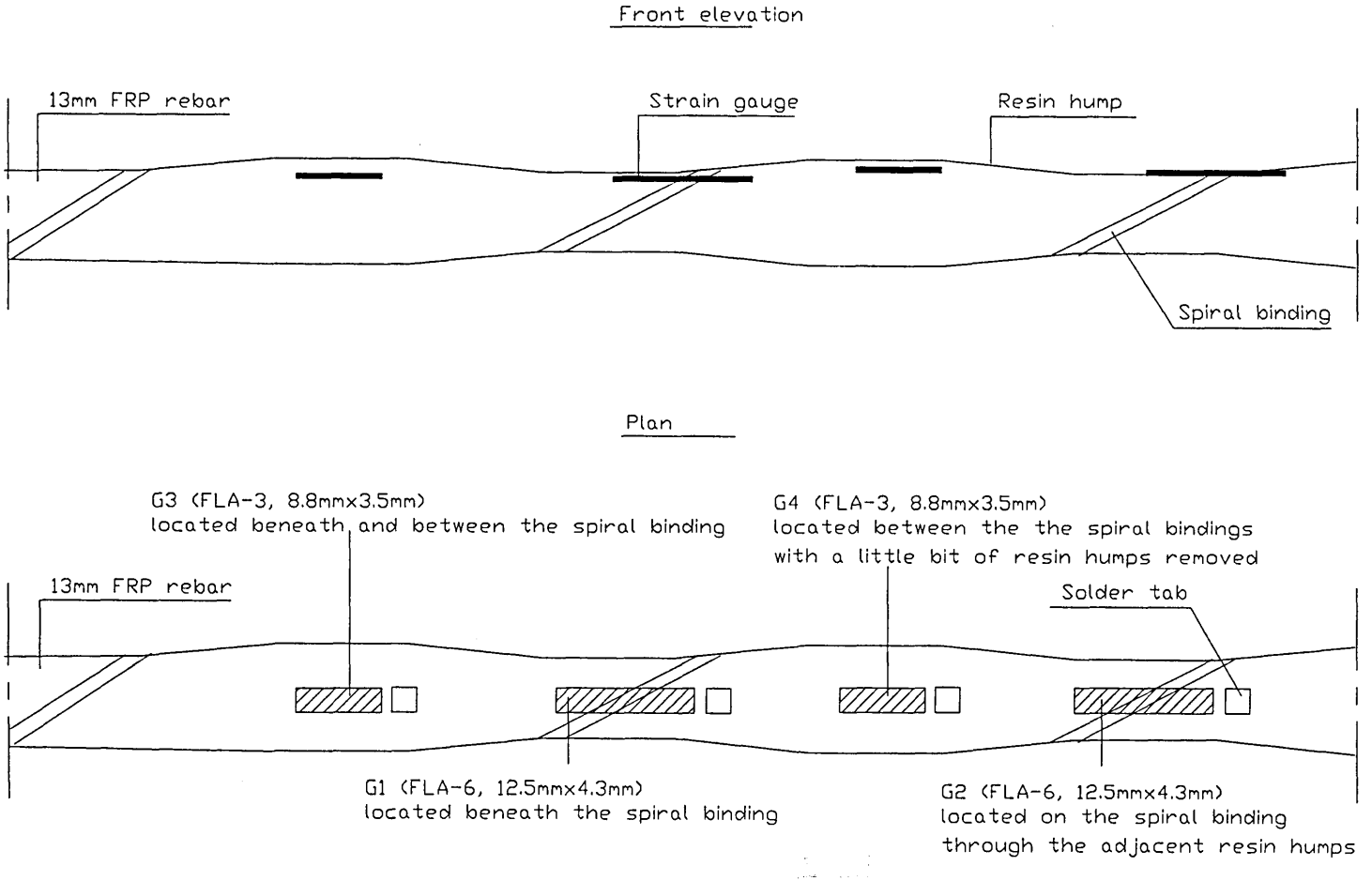

It can also be seen in *Figure 3.12* that the strain gauges installed either on or beneath the spiral bindings follow the same trend as the extensometers suggesting that the location on the spiral binding with a small amount of resin removed is suitable for accurate strain measurements. The strain gauge (G4) installed between the spiral bindings with a smaller amount of resin removed also followed the same trend as strain gauges (G1, G2) and the extensometers. However, both strain gauges (G1, G3) beneath the level of spiral bindings debonded before the failure of the rebars. This consideration for strain gauge installation on GFRP rebars, could suggest that it is better to avoid removing excess material and hence reducing the cross sectional area of the rebar. The location of strain gauge (G4) has been adopted for the majority of the test programme.

Figure 3.12 Example of strain gauge readings monitored from different locations on GFRP rebar.

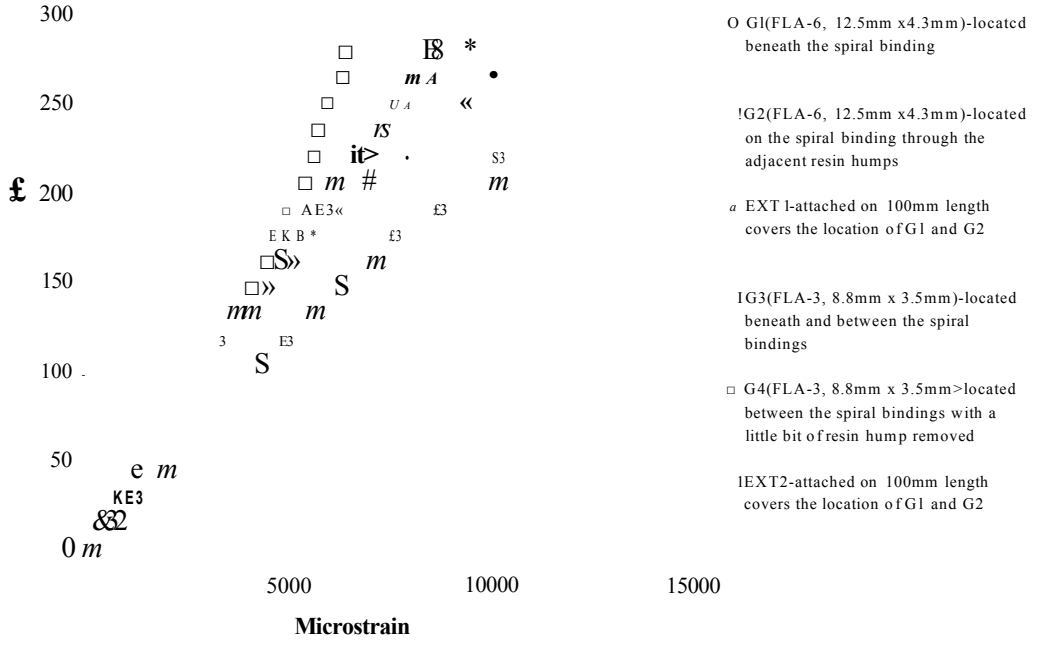

3.4.2 Extensometer gauges

On the concrete beams, the strain for the maximum moment and shear region was measured with a gauge length of 900 mm and 200mm manual extensometer using mechanical Demec disks located on the beams. Prior to testing, the pins were positioned and stuck on both sides of the beam using chemical metal adhesive (plastic padding) together with 900mm and 200mm long setting bars. The position and the location of the electrical resistance strain gauges on the bars and the DEMECs on the beams are shown in *Figure 3.13*. Demec disks were also fixed to both sides of the cylinder specimens in order to measure the strain over a gauge length of 100mm using an appropriate extensometer.

3.4.3 Linear Variable Differential Transformer (LVDT)

In order to facilitate the crack marking, whitewash was applied to the overall length of the beam before commencement of the test. The beams were instrumented with a linear variable differential transformer (LVDT) and a central deflection dial gauge at mid-span to monitor deflection. A modified LVDT was used on its own for further tests in order to monitor the deflection up to failure of the beams. Avery Schenk beam rig was set up for two point loading in stroke control mode (Servo Control Hydraulic Actuator). An automatic data logger system was used to monitor loadings, mid-span deflection and deformations in the reinforcement and of the concrete.

Figure 3.13 Locations of DEMECs and strain gauges

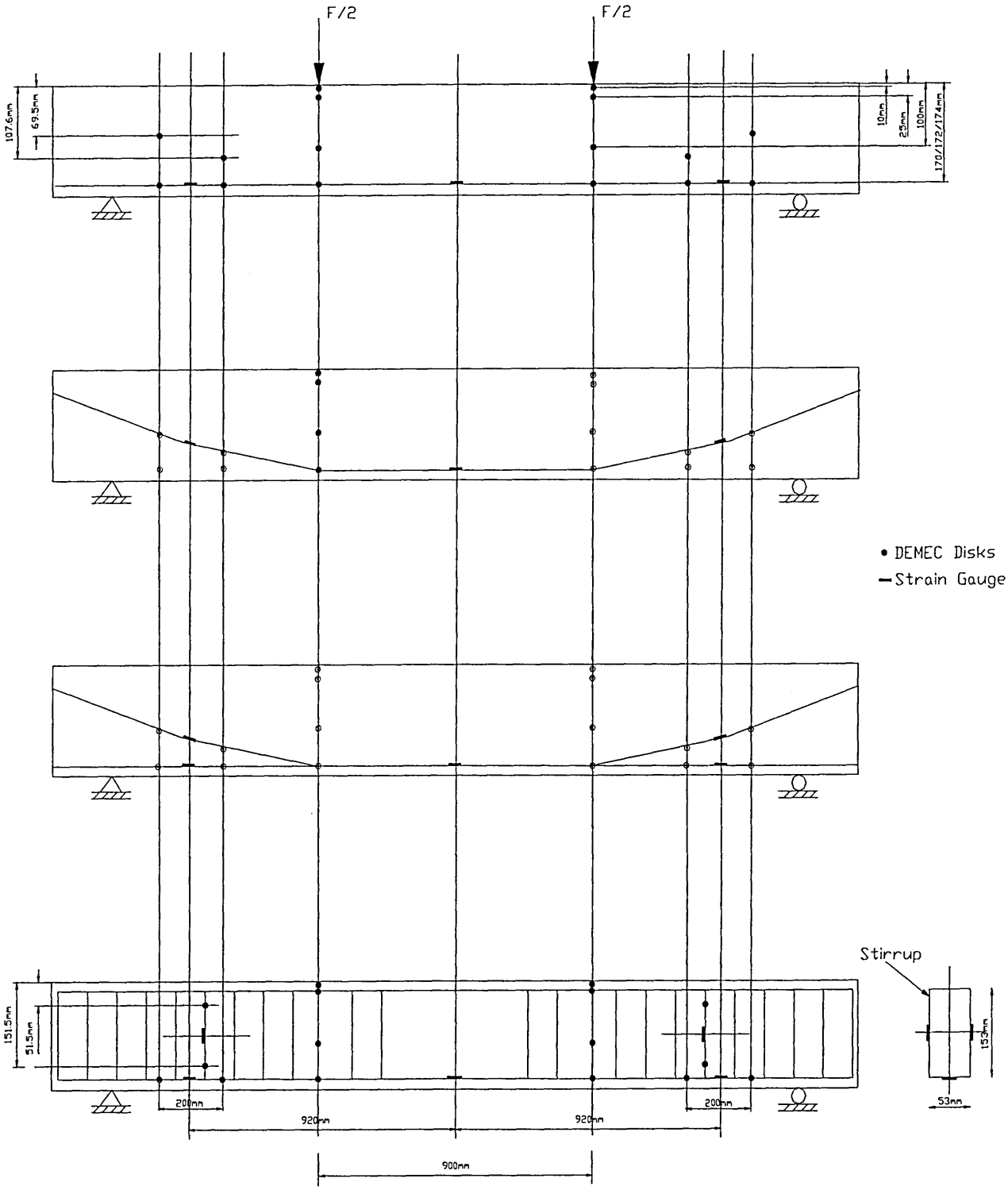

3.4.4 Health and Safety Risk Assessment on Structural Testing of Concrete Beams

It was experienced from Part 1 tests that the failure of both steel and FRP reinforced concrete beams could be catastrophic and explosive without warning. Therefore, it was necessary for the beam testing procedure to be risk assessed in terms of the likely hazards and the mode of their occurrence taking into account the need to be close to the test specimen during the experiment in order to monitor surface cracks and deformation.

Although, the machine operator's experience must be relied upon during such tests as his or her feeling for the beam's response will be critical, it was decided that the 'hands on ' working had to cease either at the 2/3 of expected maximum load or when it is not practicable to obtain two sets of DEMEC readings. It was also decided that the apparatus such as dial gauges and displacement transducers were to be removed at this stage. Therefore, the displacement transducer was modified in a way that the readings could be monitored up to the failure load by applying thorough cover protection (see *Photo 3.13* and play *LVDT.mov* file on the compact disk). This new transducer can monitor deflections up to 150mm. This was necessary due to the high flexibility of GFRP reinforced beams and their large elastic range.

Photo 3.13 The LVDT with cover protection used to monitor deflection during the test

3.5 Test Procedure

All of the beams were tested over a 2440mm span and loaded symmetrically at two points to give a 900mm long zone of uniform bending. The load was applied through 103mm side square steel plates and was applied to the beam in increments of 2kN by means of one 300kN hydraulic actuator and was measured with a load cell. At each load, the cracks were marked on both sides and the deflection, strain from both reinforcements and concrete were recorded. The test was continued until failure either in flexure or shear occurred. The overall behaviour of reinforced concrete beams, in terms of crack patterns, load-deflection hysterises, failure mode together with load carrying capacities were filmed and photographed. Each test on average took approximately 4 hours. Filming each test was particularly useful for further observations and retrospective appraisal and analysis. Examples of the video clips for some of the tests and testing apparatuses are compressed in a compact disk and included in the thesis (see the disk pocket attached at the end). It is believed to be useful and valuable contribution to the method of monitoring experiments. These video clips can be viewed with QuickTime software programme, which runs on Windows 95,98, NT and 2000. It requires an Intel Pentium or compatible processor, 32MB of RAM, SoundBlaster or compatible sound card and speakers.

Small specimen testing

Control specimens, cubes (for compressive strength) and cylinders (for elastic modulus) were tested in a 3000kN capacity Avery-Denison compression test machine in accordance with BS1881 Part 116 and 121[22 23]. The average concrete strength of each beam was obtained from the cubes, which gave a normal failure mode. For each beam, specimens strains were measured up to 1/3 of the corresponding maximum concrete strength from the two cylinders. The linear elastic line was plotted within the stress versus strain graph. The modulus of elasticity of concrete was computed from the graphs and was taken as the average of the two cylinders (see *Appendix 4*).

3.6 Conclusions

3.6.1 Materials

1. Glass Fibre Reinforced Plastics can be manufactured in the form of longitudinal bars with circular cross section.
2. The helical strands applied to the GFRP rebars provide a nonuniform surface texture and therefore could improve the bond between the rebars and the concrete.
3. Tensile tests can be conducted on GFRP rebars as for the steel by providing an appropriate anchorage at both ends of the material. The research showed that the copper/steel tubes at the ends of test specimens could be employed to achieve good anchorage.
4. GFRP rebars exhibited linear elastic behaviour up to failure under tension, whereas steel rebars had a post yielding plateau.
5. The study confirmed that the concrete beams could be manufactured with different types and strengths of concrete using both GFRP and steel reinforcements.

3.6.2 Equipment

1. 300kN-load cell capacity displacement control beam test rig was used successfully to assess the behaviour of the concrete beams under two-point loading. The control panel had the facility for monitoring the load and displacement response of the beams.
2. A 150mm gauge length of a new LVDT has been used for the experiments. The apparatus has been put in a protective box, which could function as a shield to prevent its breakage under catastrophic failure

3. 600kN-load cell capacity multi-mode control universal test machine was used successfully to obtain tensile properties of both steel and GFRP rebars.
4. A 'stand apparatus' can be used for casting the ends of the GFRP rebars into copper/steel tubes. An attention needs to be paid to the alignment of the rebars whilst injecting the epoxy (Sikadur 32) inside the anchorage tubes.
5. 1000kN-load cell capacity of compression test machine was used successfully to test concrete cube and cylinder specimens and to obtain the concrete properties.

3.6.3 Method of Monitoring Test

1. It is advisable to carry out a formal Health and Safety risk assessment for the two point loading test in the laboratory prior to experimental programme of study. This could then provide data for the 'test conductor' to be aware of the precautions and to carry out tests safely.
2. Video filming and photographing were successfully adopted for monitoring the behaviour of the concrete beams. Particularly, the inclusion of the video clips on a compact disk is believed to provide an original way for introducing the test equipment and presenting the results.

3.7 REFERENCES

[1] BS8110, Part 1, Structural Use of Concrete, 1985.

[2] BS/EN 10002-1, Part 1-4, Tensile Testing of Metallic Materials, 1990.

[3] Derim Steels Ltd product sheet, Chesterfield, Derbyshire, UK.

[4] KODIAK Fiberglass-Reinforced Plastic Rebar product brochure, International Grating Inc.

[5] BS 1881, Part 114, Methods for determination of density of hardened concrete, 1983.

[6] ASTM D3916-84, Tensile Properties of Pultruded Glass-Fibre Reinforced Plastic Rod.

[7] Dolan C W, FRP Prestressing in the USA, Concrete International, V21, No10, October 1999, pp21-24.

[8] BS 2782, Part 10, Method 1003, Plastics, Determination of Tensile Properties, 1977.

[9] ISO Recommendation R 527, Plastics, Determination of Tensile Properties, 1966.

[10] JIS K 7054, Japenese Industrial Standard, Testing Method for Tensile Properties of Glass Fibre Reinforced Plastics, 1987.

[11] JIS K 7073, Japanese Industrial Standard, Testing Method for Tensile Properties of Carbon Fibre Reinforced Plastics, 1988.

[12] Sikadur 32 Technical Data Sheet.

[13] Malvar L J , Tensile and Bond Properties of GFRP Reinforcing Bars, ACI Materials Journal, May-June 1995, pp276-285.

[14] ELKEM, EMSAC 500 S Data Sheet.

[15] CEM-FIL Fibres Product Details, CEM-FIL International Ltd.

[16] BS 812, Part1, Method for sampling and testing of mineral aggregates, sands and fillers, 1975.

[17] Boral Lytag Data Brochure, Boral Lytag Ltd.

[18] Building Research Establishment (BRE) Report, Design of normal concrete mixes, 1992.

[19] BS 1881, Part111, Method of normal curing of test specimens, 1983.

[20] BS 1881, Part 102, Method for determination of slump, 1983.

[21] BS 1881, Part 104, Method for determination of vebe time, 1983.

[22] BS1881, Part116, Method for determination of compressive strength of concrete cubes, 1983.

[23] BS1881, Part121:1983"Method for determination of static modulus of elasticity in compression, 1983.

[24] Strain Gauges Technical Data Book, Techni Measure Ltd.

[25] Student Manual for Strain Gauge Technology, Measurement Group, Education Division, Bulletin 309.

[26] O'Flaherty F, Long Term Performance of Concrete Repair in Highway Structures, PhD Thesis, March 1998.

CHAPTER 4

4. Part1: GFRP & Steel Reinforced Normal, Medium and High Strength Concrete Beams

4.1 Section Design and Detailing

4.1.1 Concrete Beam Sizing

BS 8110[1] was used for checking the beam dimensions and detailing based on cover to the reinforcement, breadth (b), effective depth (d) and overall depth (h). The same overall beam dimensions were used for all parts of the investigation.

4.2 Experimental and Theoretical Results

4.2.1 Behaviour up to Failure

Bending tests were conducted on thirty concrete beams having three different concrete grades, mainly C20, C40 and C60 including some of the repeats (see *Table 4.1*). The chopped strand glass fibres added C40 grade concrete beams were also included in this Part. The main purpose was to investigate and compare the behaviour and performance of concrete beams reinforced with FRP rebars whether perform in a similar manner with those reinforced with high strength steel rebars.

The simply supported rectangular beams with the details shown in *Figure 3.1* from Chapter 3, were tested under two point loading condition. In order to take advantage of the high tensile strengths of the FRP rebars, it was anticipated that using higher strength concrete could maximize the bending resistance of the beams in certain cases.

Table 4.1 The physical properties and the test results used in the analysis of Part 1

		CONCRETE								REINFORCEMENT			OBSERVATIONS		
No	Beam Code	Grade	Age (days)	Slump (mm)	Density (kg/m^3)	f_c Strength (MPa)	E_c MOE (GPa)	No-Dia/ Type	E_{st}/E_{FRP} MOE (GPa)	f_y/Ffrp Yield/ Ultimate Stress (MPa)	A_r Area (mm^2)	%Tension Rebar (A_r/bxh)x100	Failure Mode	Initial Crack Load (kN)	Failure Load (kN)
1[1*]	TB15	C20	42	45	2340	41	33	2-08S	186	523.5	101	0.48	Flexure	6.00	23.00
2[1]*	*RTB15*	*C20*	*42*	*40*	*2390*	*50*	*35*	*2-08S*	*186*	*523.5*	*101*	*0.48*	*Flexure*	*6.00*	*25.10*
3[1*]	TB13	C20	42	43	2310	40	30	2-12S	189	497	226	1.08	Shear-Bond	4.00	42.00
4[1]*	*RTB13*	*C20*	*42*	*45*	*2345*	*50*	*34*	*2-12S*	*189*	*497*	*226*	*1.08*	*Shear*	*4.00*	*38.70*
5[1*]	TB17	C20	42	50	2440	43	30	2-16S	200	467	402	1.92	Shear-Bond	6.00	56.30
6[1*]	TB16	C20	43	45	2340	41	33	2-08.77F	45.98	601	121	0.58	Flexure	4.00	28.00
7[1]*	*RTB16*	*C20*	*43*	*45*	*2410*	*49*	*36*	*2-08.77F*	*45.98*	*601*	*121*	*0.58*	*Shear*	*4.00*	*24.00*
8[1]*	*RRTB16*	*C20*	*43*	*55*	*2403*	*47*	*29*	*2-08.77F*	*45.98*	*601*	*121*	*0.58*	*Shear*	*4.00*	*26.00*
9[1*]	TB14	C20	43	45	2345	40	34	2-13.19F	38.75	470.7	273	1.31	Shear-Bond	4.00	31.50
10[1*]	TB18	C20	43	40	2370	39	33	2-16.44F	33.21	544	425	2.03	Shear-Bond	4.60	30.00
11[1]*	*RTB18*	*C20*	*43*	*35*	*2400*	*45*	*31*	*2-16.44F*	*33.21*	*544*	*425*	*2.03*	*Shear*	*4.00*	*26.60*
12[1*]	TB5	C40	42	45	2400	61	34	2-08S	186	523.5	101	0.48	Flexure	6.00	24.00
13[1*]	TB1	C40	42	50	2370	55	33	2-12S	189	497	226	1.08	Flexure	8.00	50.00
14[1]*	*RTB1*	*C40*	*43*	*45*	*2395*	*61*	*34*	*2-12S*	*189*	*497*	*226*	*1.08*	*Flexure*	*6.00*	*51.00*
15[1*]	TB9	C40	42	45	2390	61	35	2-16S	200	467	402	1.92	Shear-Bond	12.00	68.00
16[1*]	TB6	C40	43	55	2420	69	34	2-08.77F	45.98	601	121	0.58	Shear	6.80	20.00
17[2**]	TTB16	C40 FB	28	N/A	2386	58	34	2-08.77F	45.98	601	121	0.57	Shear	6.00	33.60
18[1]*	*RTB6*	*C40*	*43*	*45*	*2410*	*64*	*40*	*2-08.77F*	*45.98*	*601*	*121*	*0.58*	*Shear*	*4.00*	*22.00*
19[1*]	TB2	C40	43	50	2370	57	34	2-13.19F	38.75	470.7	273	1.31	Shear-Bond	4.90	34.00
20[1]*	*RTB2*	*C40*	*43*	*55*	*2420*	*63*	*38*	*2-13.19F*	*38.75*	*470.7*	*273*	*1.31*	*Shear*	*5.00*	*31.60*
21[2**]	TTB21	C40 FB	28	N/A	2396	54	32	2-13.19F	38.75	470.7	273	1.28	Shear	6.00	36.00
22[1*]	TB10	C40	43	50	2340	51	33	2-16.44F	33.21	544	425	2.03	Shear-Bond	5.00	29.00
23[1*]	TB7	C60	42	55	2420	73	33	2-08S	186	523.5	101	0.48	Flexure	6.00	24.00
24[1*]	TB3	C60	42	50	2400	72	35	2-12S	189	497	226	1.08	Flexure	8.00	48.00
25[1*]	TB11	C60	42	50	2420	75	37	2-16S	200	467	402	1.92	Shear-Bond	9.00	58.00
26[1*]	TB8	C60	43	45	2420	72	35	2-08.77F	45.98	601	121	0.58	Flexure	6.00	26.00
27[1]*	*RTB8*	*C60*	*43*	*50*	*2430*	*70*	*36*	*2-08.77F*	*45.98*	*601*	*121*	*0.58*	*Shear*	*4.00*	*26.40*
28[1]*	*RRTB8*	*C60*	*43*	*55*	*2453*	*78*	*35*	*2-08.77F*	*45.98*	*601*	*121*	*0.58*	*Shear*	*6.00*	*30.00*
29[1*]	TB4	C60	43	50	2440	79	38	2-13.19F	38.75	470.7	273	1.31	Shear-Bond	6.00	38.00
30[1*]	TB12	C60	43	50	2400	76	36	2-16.44F	33.21	544	425	2.03	Shear-Bond	5.80	28.00

S (Steel) TB: Test Beam RTB: First Repeat of TB RRTB: Second Repeat of TB FB: Glass fibres added concrete

F (FRP) TTB: New Test Beam includes new geometry of rebars and concrete strengths and types MOE: Modulus of Elasticity

[1*] 103mm wide(b) x 203mm deep(h) x 2740mm long (2440mm long span)

[2**] 104mm wide(b) x 205mm deep(h) x 2740mm long (2440mm long span)

4.2.2 Reinforcement Strains in the Maximum Bending Moment Region

The strain gauges were mounted on the reinforcing bars to measure the strains in the maximum bending moment region of all the beams. The locations of the strain gauges are shown in *Figure 4.1.*

Figure 4.1 The location of the strain gauges in both shear and maximum bending moment regions

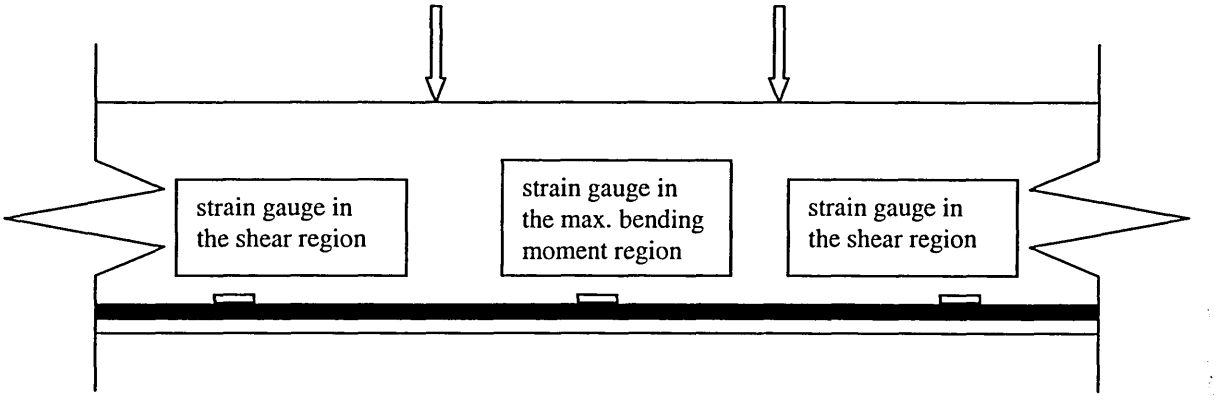

It can be seen in *Figure 4.2* the strain curves up to the initial crack load are straight lines for both steel and GFRP reinforced beams. The slope of the curve gets smaller beyond this but still continues on a straight line up to failure. The strains obtained from GFRP reinforcing bars are greater than those in the steel reinforcing bars at equal loads. This is due to the fact that the lower elastic modulus of GFRP makes the rebar bend more, resulting in a higher magnitude of strain. This is very similar to the load vs concrete strain relationship in *Figure 4.3.* This indicates that the average (bottom) reinforcement strains agreed quite well with average surface strains at the level of reinforcement. One can conclude from this that taking multiple mechanical surface strain measurements on the tension zone of a reinforced concrete member not only gives an accurate indication of crack width but also allows a fairly accurate estimate of average reinforcement strains or beam curvature, provided slippage between concrete and reinforcement is minor[2]. For the two GFRP reinforced beams the dotted lines in the Figures designate the strains at failure extrapolated from the regression line on the spreadsheet. This was necessary in cases where unbonding of the strain gauges occurred before the failure of the beam. However, the strain readings from

both the strain gauge and the dial gauge are dependent upon the proximity of the cracks to the instruments and the variable properties of the concrete.

In this investigation, term *'uncracked section'* designates that there are no visible cracks observed but concrete may be considered to resist a small amount of tension. Similarly, the term *'cracked section'* designates concrete no longer resisting tension and visible cracks observed along the length of the beam.

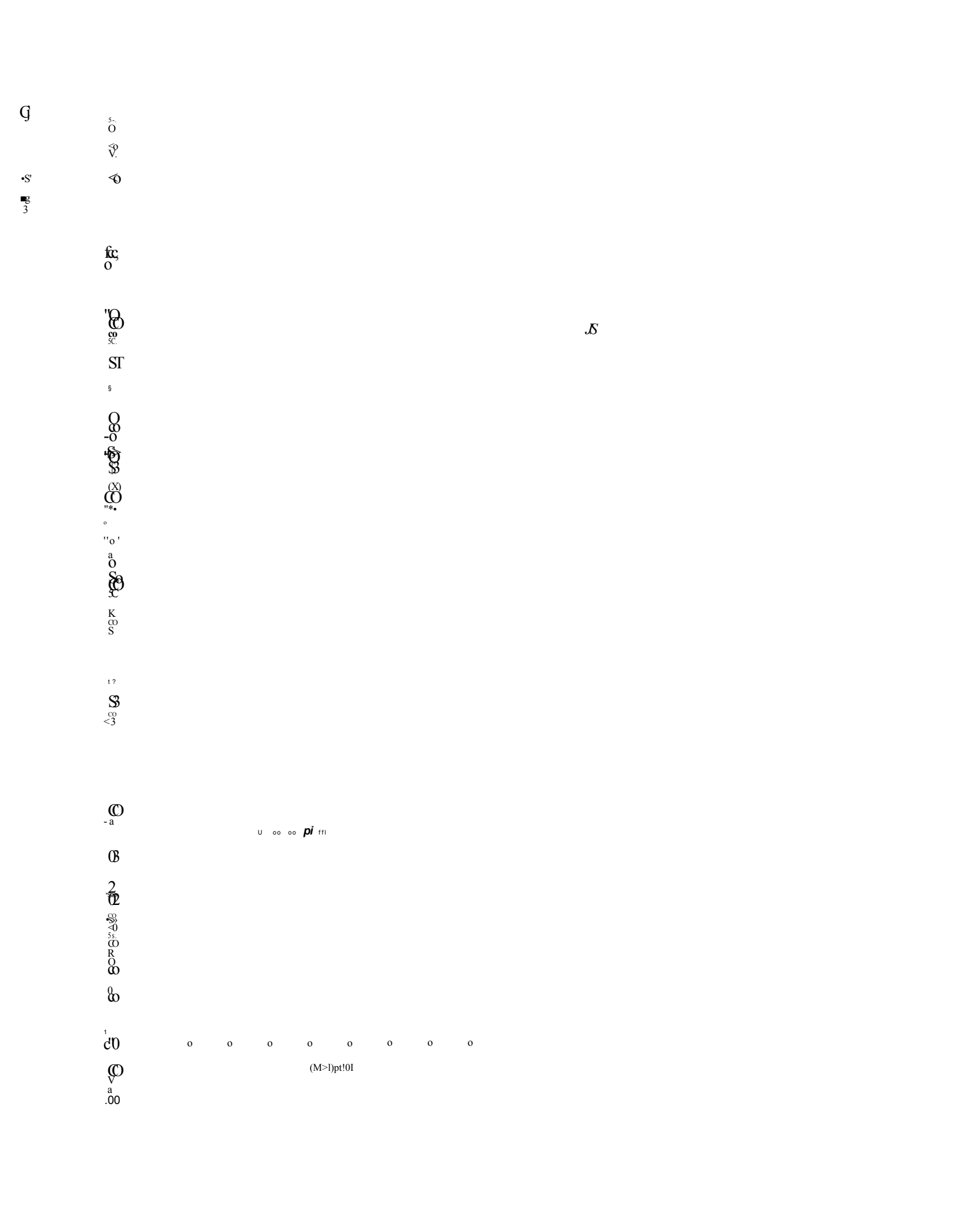

The stresses and strains in the reinforcing bars were calculated based upon the theory of bending at the cracked section. The formulae used for this purpose are given below. The sample calculations are included in *Appendix 5*.

Determination of stress & strain in the reinforcements

cracked section:

$$\sigma_{st/gfrp\,actual_{cr}} = \alpha_e \frac{M_{actual\,cr}}{I_{actual\,cr}}(d - \chi_{actual\,cr}) \qquad \varepsilon_{st/gfrp\,actual\,cr} = \frac{\sigma_{st/gfrp\,actual_{cr}}}{E_{st/gfrp}}$$

Table 4.2 contains the comparison of stresses in the rebars from the tensile (see Chapter 3) and bending tests. The maximum values obtained from the bending test (column 6) are based on using BS8110 equation at the cracked section and designate the experimental results used in the equation.

The comparison of data in Table 4.2

It can be seen that the maximum stresses (column 5 & 6) in the steel rebars reach almost their full tension capacity whereas this is not quite the same with GFRP rebars except the ϕ8.77 rebars. This could suggest that the rebar stresses are under the influence of failure modes i.e. the stresses in the rebars are more likely be close to the ultimate tensile capacity when the beam fails in flexure.

Table 4.2 The comparison of tensile stresses in steel and GFRP rebars from the tensile test and BS8110 equation

1	2	3	4	5	6
Beam	Concrete	Rebar	Failure	**Maximum Tensile Stresses in the Rebars (MPa)**	
Code	grade	No. Dia/Type	Mode	**Tensile Test Measured**	**Bending Test *Calculated**
TB15	C20	2-08S	Flexure	523.5	505.6
RTB15	*C20*	*2-08S*	*Flexure*	*523.5*	*650.43*
TB13	C20	2-12S	Shear-Bond	497	240.91
RTB13	*C20*	*2-12S*	*Shear*	*497*	*411.81*
TB17	C20	2-16S	Shear-Bond	467	335.67
TB16	C20	2-08.77F	Flexure	601	508.84
RTB16	*C20*	*2-08.77F*	*Shear*	*601*	*542.66*
RRTB16	*C20*	*2-08.77F*	*Shear*	*601*	*545.86*
TB14	C20	2-13.19F	Shear-Bond	470.7	314.95
TB18	C20	2-16.44F	Shear-Bond	544	194.03
RTB18	*C20*	*2-16.44F*	*Shear*	*544*	*186.64*
TB5	C40	2-08S	Flexure	523.5	605.94
TB1	C40	2-12S	Flexure	497	580.28
RTB1	*C40*	*2-12S*	*Flexure*	*497*	*605.02*
TB9	C40	2-16S	Shear-Bond	467	496.98
TB6	C40	2-08.77F	Shear	601	452.47
TTB16	C40 FB	2-08.77F	Shear	601	678.73
RTB6	*C40*	*2-08.77F*	*Shear*	*601*	*512.39*
TB2	C40	2-13.19F	Shear-Bond	470.7	340.54
RTB2	*C40*	*2-13.19F*	*Shear*	*470.7*	*329.23*
TTB21	C40 FB	2-13.19F	Shear	470.7	345.99
TB10	C40	2-16.44F	Shear-Bond	544	193.60
TB7	C60	2-08S	Flexure	523.5	645.63
TB3	C60	2-12S	Flexure	497	599.68
TB11	C60	2-16S	Shear-Bond	467	431.72
TB8	C60	2-08.77F	Flexure	601	583.85
RTB8	*C60*	*2-08.77F*	*Shear*	*601*	*607.11*
RRTB8	*C60*	*2-08.77F*	*Shear*	*601*	*642.03*
TB4	C60	2-13.19F	Shear-Bond	470.7	402.98
TB12	C60	2-16.44F	Shear-Bond	544	192.46

*based on BS8110 equation for cracked section using actual bending moment and neutral axis depth

The comparison of data in Table 4.3

The tensile strains in steel and GFRP rebars obtained from 'direct tensile test' and 'beam bending test' are compared in *Table 4.3*. The calculated strains in column 7 were determined based upon substituting 'actual' bending moment, neutral axis depth and the second moment of area of the beams into the formula given previously (see also *Appendix 5* for sample calculation). Generally, the agreement between the 'measured' and 'calculated' strains based on the bending test is good (see column 6 &7). The results indicated that the maximum tensile strains in the steel rebars reach almost their full tensile strain capacity whereas this is not quite the same with GFRP rebars except the ϕ8.77 rebars (see column 5 & 6).

Table 4.3 The comparison of tensile strains in steel and GFRP rebars obtained from the 'tensile' and 'bending' tests at failure load

1	2	3	4	5	6	7
Beam	Concrete	Rebar		**Maximum Tensile Strains in the Rebars (MPa)**		
Code	grade	No. Dia/Type	Failure Mode	Tensile test Measured	Bending test Measured	Bending test Calculated
TB15	C20	2-08S	Flexure	0.0028	0.00299	0.00270
RTB15	*C20*	*2-08S*	*Flexure*	*0.0028*	*0.00575*	*0.00350*
TB13	C20	2-12S	Shear-Bond	0.0026	0.00289	0.00127
RTB13	*C20*	*2-12S*	*Shear*	*0.0026*	*0.00221*	*0.00218*
TB17	C20	2-16S	Shear-Bond	0.0023	0.00200	0.00168
TB16	C20	2-08.77F	Flexure	0.0130	0.01392	0.01120
RTB16	*C20*	*2-08.77F*	*Shear*	*0.0130*	*0.02111*	*0.01203*
RRTB16	*C20*	*2-08.77F*	*Shear*	*0.0130*	*0.00935*	*0.01211*
TB14	C20	2-13.19F	Shear-Bond	0.0120	0.00515	0.00815
TB18	C20	2-16.44F	Shear-Bond	0.0164	0.00168	0.00543
RTB18	*C20*	*2-16.44F*	*Shear*	*0.0164*	*0.00566*	*0.00522*
TB5	C40	2-08S	Flexure	0.0028	0.00288	0.00326
TB1	C40	2-12S	Flexure	0.0026	0.00338	0.00307
RTB1	*C40*	*2-12S*	*Flexure*	*0.0026*	*0.00252*	*0.00320*
TB9	C40	2-16S	Shear-Bond	0.0023	0.00197	0.00248
TB6	C40	2-08.77F	Shear	0.0130	0.01333	0.01005
TTB16	C40 FB	2-08.77F	Shear	0.0130	0.01285	0.01508
RTB6	*C40*	*2-08.77F*	*Shear*	*0.0130*	*0.01385*	*0.01139*
TB2	C40	2-13.19F	Shear-Bond	0.0120	0.00441	0.00873
RTB2	*C40*	*2-13.19F*	*Shear*	*0.0120*	*0.00587*	*0.00844*
TTB21	C40 FB	2-13.19F	Shear	0.0120	0.00629	0.00887
TB10	C40	2-16.44F	Shear-Bond	0.0164	0.00531	0.00538
TB7	C60	2-08S	Flexure	0.0028	0.00356	0.00347
TB3	C60	2-12S	Flexure	0.0026	0.00238	0.00317
TB11	C60	2-16S	Shear-Bond	0.0023	0.00235	0.00216
TB8	C60	2-08.77F	Flexure	0.0134	0.02667	0.01297
RTB8	*C60*	*2-08.77F*	*Shear*	*0.0134*	*0.01195*	*0.01349*
RRTB8	*C60*	*2-08.77F*	*Shear*	*0.0134*	*0.01132*	*0.01427*
TB4	C60	2-13.19F	Shear-Bond	0.0120	0.01019	0.01033
TB12	C60	2-16.44F	Shear-Bond	0.0164	0.00318	0.00535

4.2.3 Reinforcement Strains in the Shear Region

After the completion of Part 1, as most of the GFRP reinforced beams failed in shear (some of them were catastrophic), for the repeats in Part 1 and for further tests it was decided to measure reinforcement strains in the shear zone. It was felt that this way, one could also predict the likehood failure mode of the beam (mainly shear) and its location; whether on the left hand side or the right hand side of the beam (if it is a shear failure) and prevent the risk of injury due to catastrophic failure.

The load vs shear strains in the reinforcements from the repeat tests can be seen in *Figure 4.4* and *Figure 4.5*. It can be seen that the average strains in GFRP rebars are greater than the steel rebars. This could indicate that the GFRP reinforced beams may be more susceptible to shear type of failure. The relationship between load and the strain is linear elastic up until the appearance of invisible cracks in the shear region for both steel and GFRP reinforced beams. The strains in the left and in the right hand side of all types of beams are very close in magnitude but the location of a large increase in strain indicates whether the beam will fail in shear on the left or the right hand side. The strains of ϕ8.77 GFRP rebars are greater for all concrete grades compared to steel reinforced beams. This could be due to the crack widths being larger than for the steel reinforced beams. It can be seen in *Figure 4.5* that C40 chopped strand glass fibre reinforced beams (TTB16 and TTB21) reinforced with ϕ8.77 GFRP and ϕ13.19 GFRP rebars give higher stiffness in the shear region compared to C40 beams reinforced with the same size of GFRP rebars. This could indicate that the chopped fibres used in the concrete contribute to higher shear capacity.

(RTB18) Left hand-side 2-16.44 GFRP straight profile Shear failure — O — (RTB18) Right hand-side 2-16.44 GFRP straight profile Shear failure

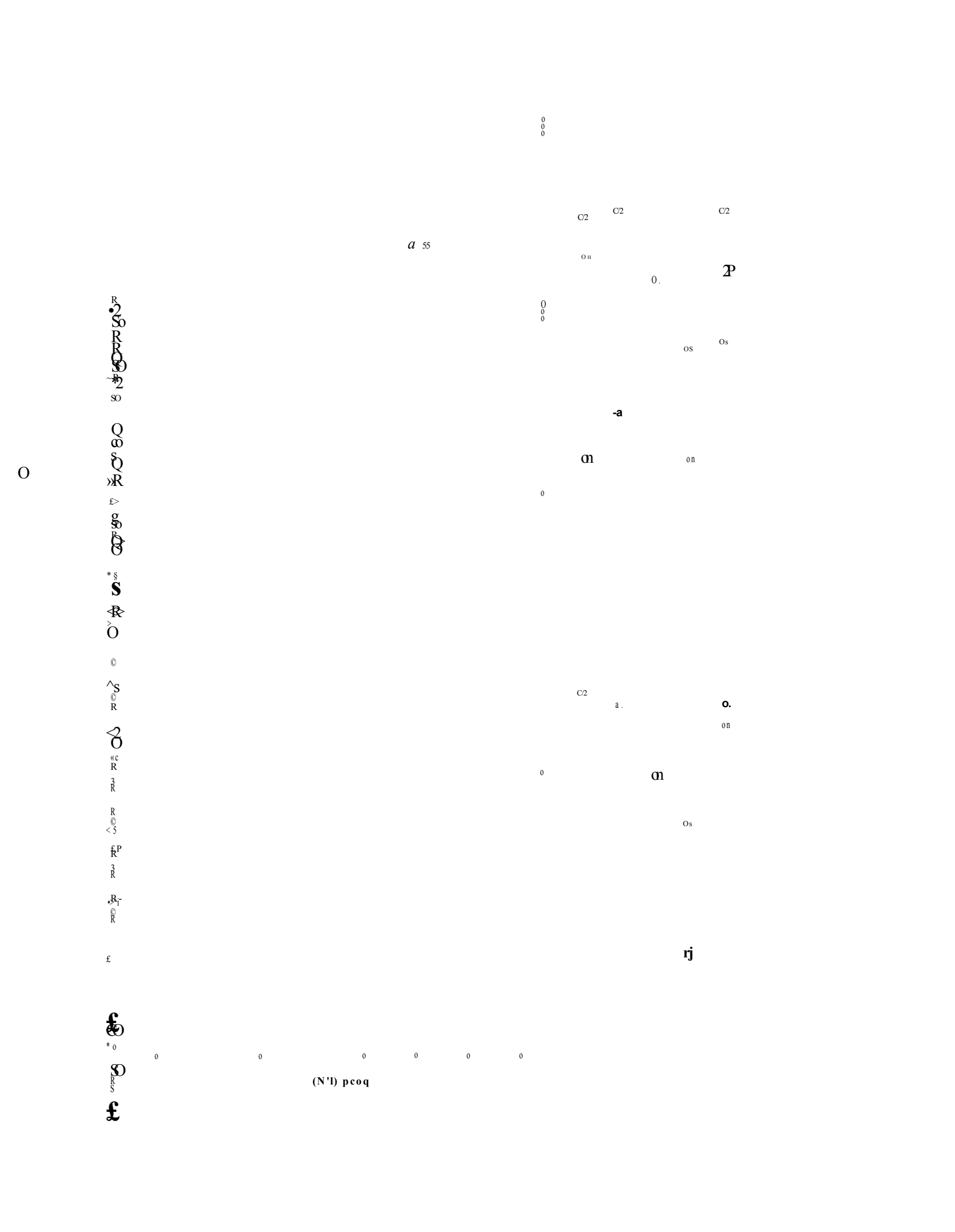
(N'l) pcoq

4.2.3.1 Concrete Strains in the Maximum Bending Moment Region

Concrete strains were measured (see *Figure 4.6*) through the depth of the beams using a DEMEC gauge over a 900mm gauge length. This data enabled the neutral axis depth and strain distribution to be examined. The measurements were taken after 2kN each load increment until concrete spalling caused the dial gauge to become loose or to extend up to its limit. This behaviour was consistent for all the beams, indicating that the failure of the beam was imminent.

Figure 4.6 The location of the concrete strains measured at the maximum bending moment region of the beams

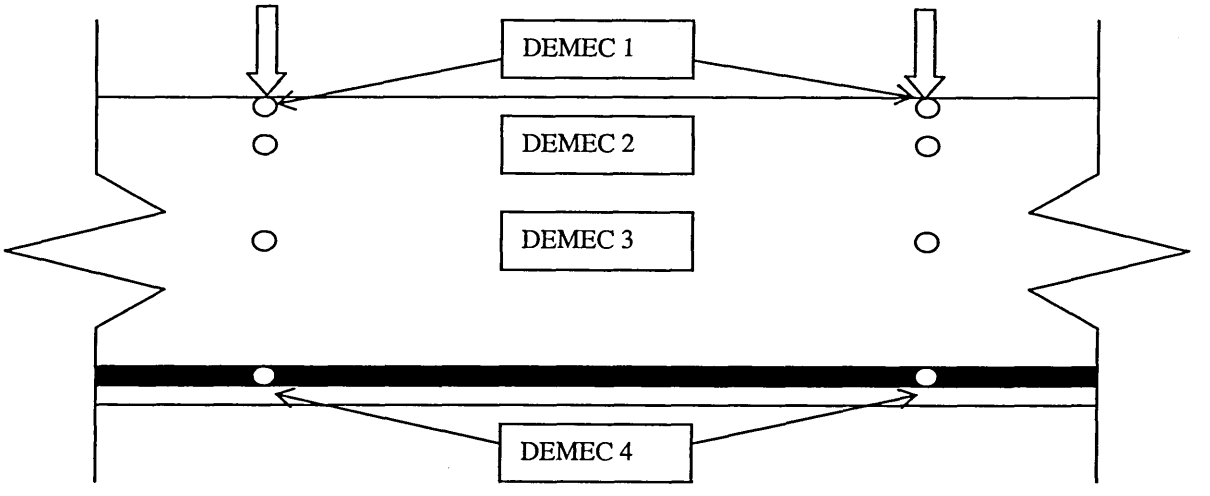

An example load vs concrete strain curves are shown in *Figure 4.7*, *Figure 4.8* and *Figure 4.9* for beams reinforced with steel and GFRP rebars, failing in either flexure or shear. The flexural failure mode designates that either rebars (steel) yield followed by the concrete crushing at the top or the rebars rupture simultaneously with concrete splitting in the maximum bending moment region. The shear failure mode is designated by the diagonal cracks in the shear region developing rapidly when the beam approaches its ultimate capacity, followed by the flexural cracks within the maximum moment region and ultimately a large diagonal crack opens up to cause the beam to fail in shear.

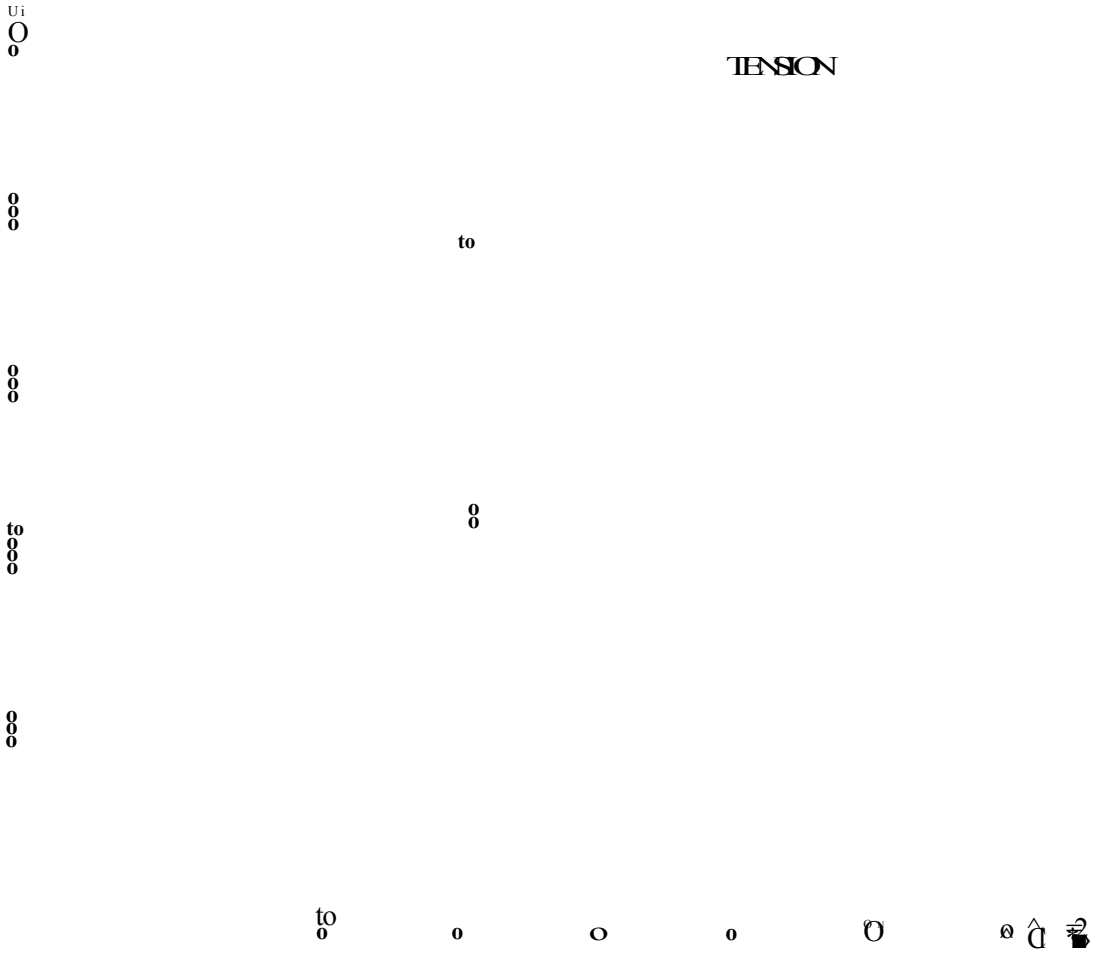

— (TB5) 2-08(101mm2) Steel straight profile C40(61MPa) Flexural failure

(TB6) 2-08.77(12 lmm2) GFRP straight profile C40(69MPa) Shear failure

(RTB6) 208.77(121mm2) GFRP straight profile C40(65MPa) Shear failure

(TTB16) 2-08.77(121mm2) GFRP straight profile C40FB(59MPa) Shear failure

Figure4.8 An example of the concrete strains measured at the maximum bending moment region of C40 concrete beams reinforced with 12mm/13.19mm diameter steel/GFRP rebars

TENSION

Microstrain

-A— (TB1) 2-12(226mm2) Steel straight profile C40(55MPa) Flexural failure

(RTB1) 2-12(226mm2) Steel straight profile C40(61MPa) Flexural failure

(TB2) 2-13.19(273mm2) GFRP straight profile C40(57MPa) Shear-bond failure

(RTB2) 2-13.19(273mm2) GFRP straight profile C40(63MPa) Shear failure

(TTB21)2-13.19(273mm2) GFRP straight profile C40FB(54MPa) Shear failure

COMPRESSION

Figure4.9 An example of the concrete strains measured at the maximum bending moment region of C40 concrete beams reinforced with 16mm/16.44mm diameter steel/GFRP rebars

TENSION

41— (TB9) 2-16(402mm2) Steel straight profile C40(61MPa)
Shear-bond failure

—* — (TB10) 2-16.44(425mm2) GFRP straight profile
C40(51MPa) Shear-bond failure

COMPRESSION

Microstrain

Figure 4.7, *Figure 4.8* and *Figure 4.9* show that regardless of size or type of reinforcing bars and concrete grade, the load vs strain curves are linear up to around load of 4kN (first visible crack appearance). Above this which the concrete strains above the neutral axis increase rapidly (more distinguishable in flexural failure and GFRP reinforced beams) with increasing load. This indicates that the concrete is in its non-elastic phase. As soon as the concrete reaches this phase, the neutral axis depth starts to decrease (*see* *Figure 4.10*, *Figure 4.11* and *Figure 4.12*). The neutral axis depth of the beams was measured from the top of the concrete beam section. The rate of increase in strain with load and decrease in neutral axis depth are both greater for GFRP reinforced beams compared to steel reinforced beams. However, this phenomenon is more obvious for both steel and GFRP concrete for all concrete grades C20, C40, C60 beams reinforced with small diameter (ϕ8 steel and ϕ8.77 GFRP) reinforcing bars. It seems that the strain distribution for all the beams is linear both above and below the neutral axis (see *Figure 4.13*, *Figure 4.14*). However, one must remember that once the concrete is cracked the dial gauge reading is not the true strain, but is an average 'strain' which depends on the position of the cracks. Therefore, the strain distribution may not be linear below the neutral axis for this reason.

Figure 4.10 An example of the experimental Neutral Axis (N.A.) Depth for C20 concrete beams reinforced with 8mm/8.77mm diameter steel/GFRP rebars

Figure 4.11 An example of the experimental Neutral Axis (N.A.) Depth for C20 concrete beams reinforced with 12mm/13.19mm diameter steel/GFRP rebars

Figure 4.12 An example of the experimental Neutral Axis (N.A.) Depth for C20 concrete beams reinforced with 16mm/16.44mm diameter steel/GFRP rebars

8
8
8
8
0
0
0

Figure 4.13 An example strain distribution of C20 concrete beam reinforced with 12mm diameter steel rebars

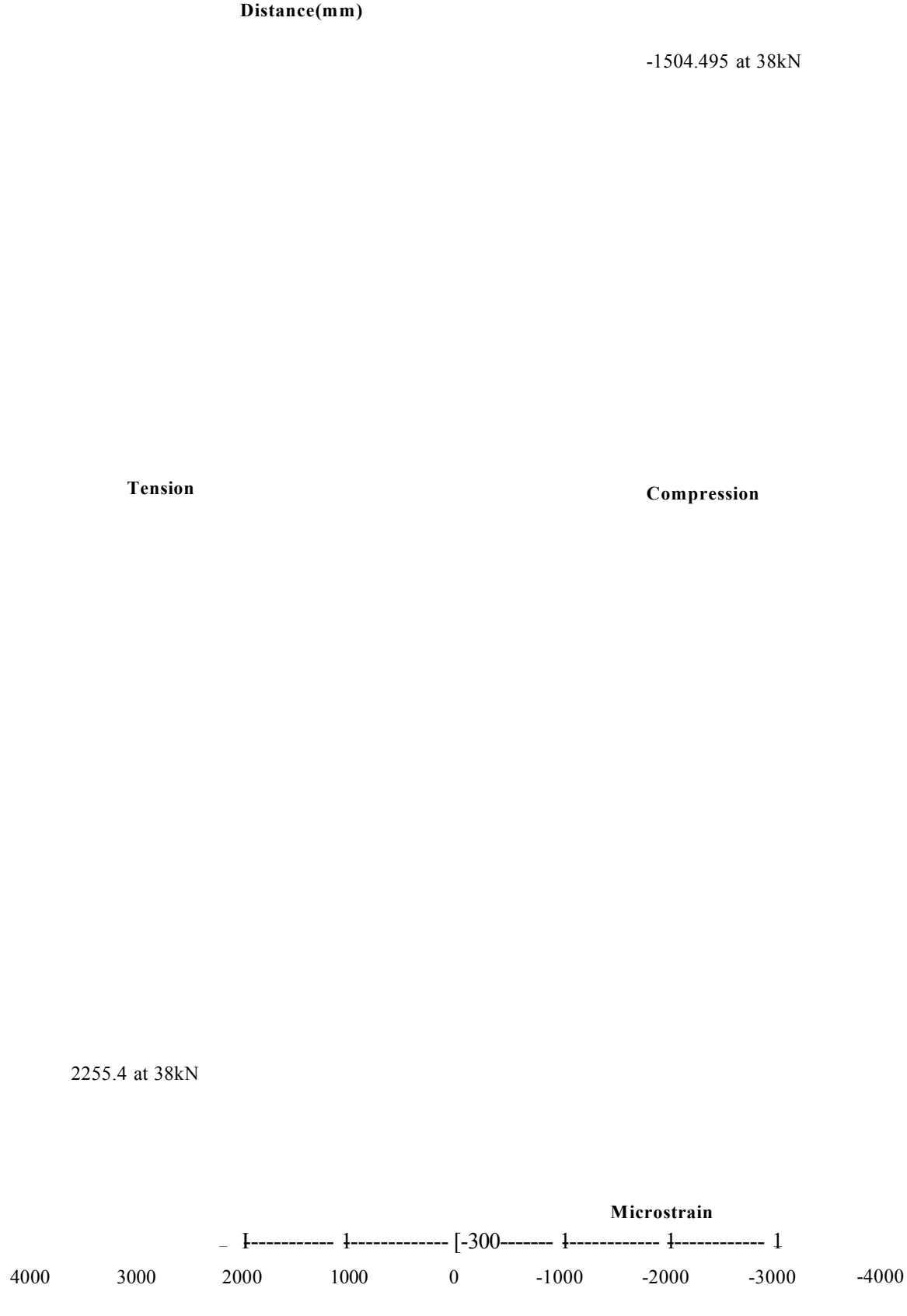

Figure 4.14 An example strain distribution of C20 concrete beam reinforced with 13.19mm diameter GFRP rebars

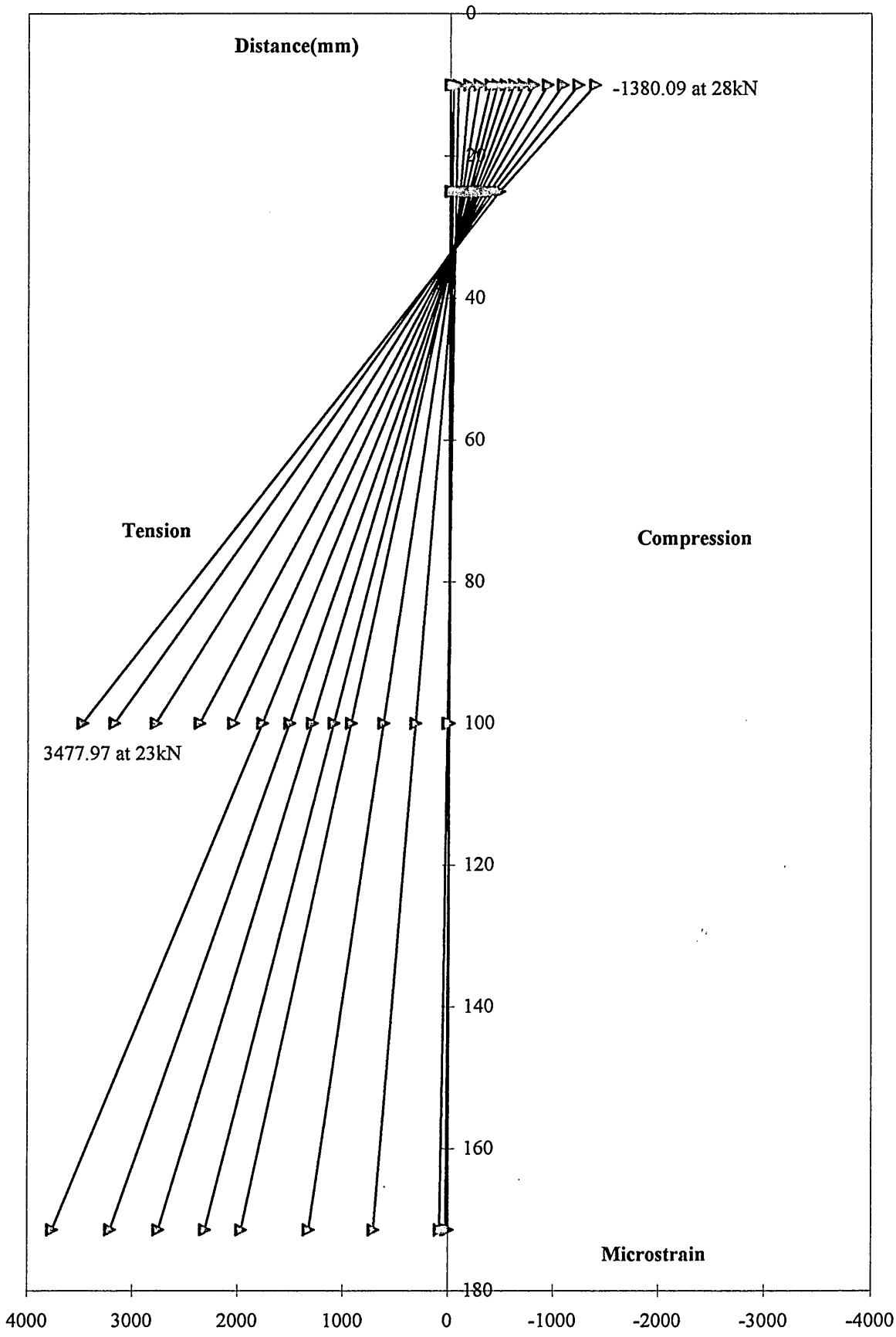

4.2.3.2 Maximum Concrete Compressive Strain

The typical concrete strain distribution across the section is shown in *Figure 4.15*. This can be used for determining the actual neutral axis depth and the maximum concrete compressive strain.

Figure 4.15 Determination of neutral axis depth and the maximum concrete compressive strain using measured concrete strains

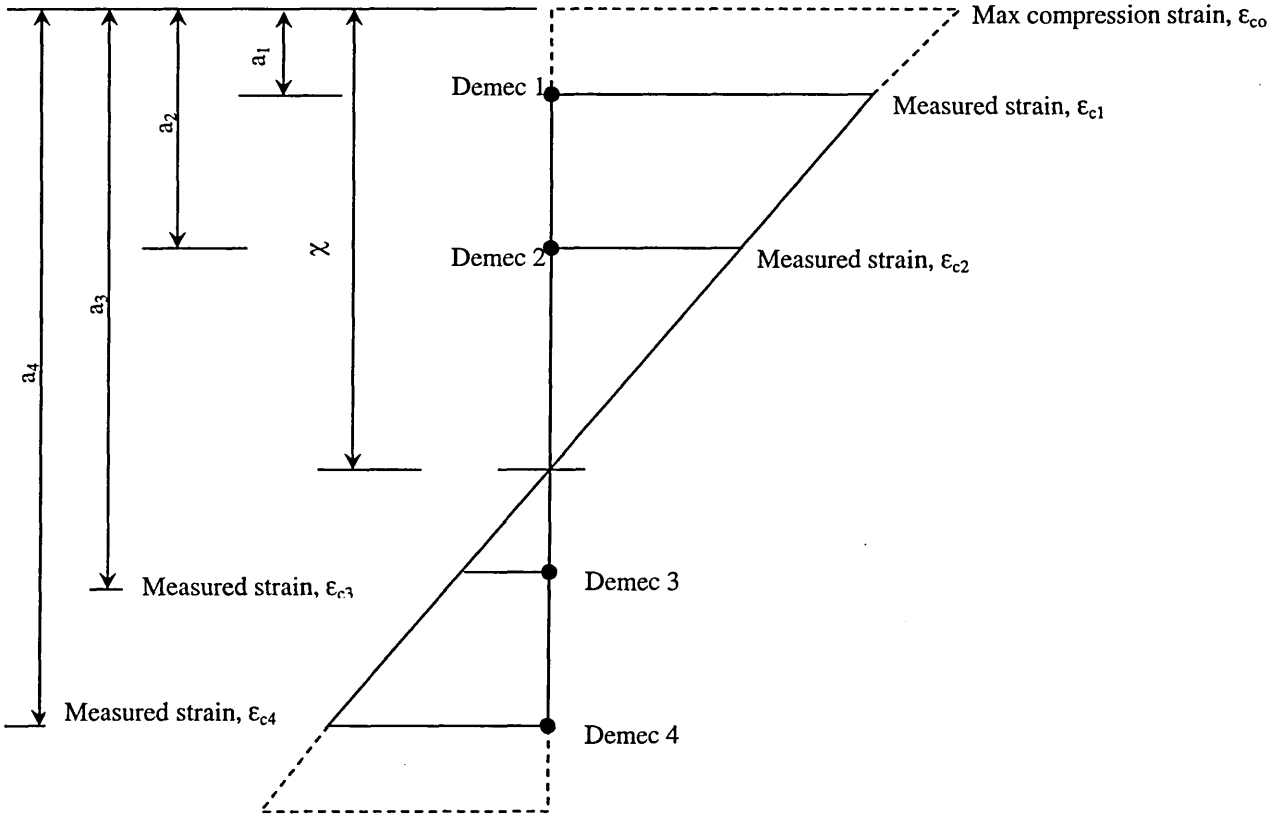

The derived formula (using similar triangles) below used to calculate the maximum concrete compressive strain. The sample calculations are included in *Appendix 5*.

maximun concrete compressive strength :

$$\frac{\varepsilon_{c1}}{\varepsilon_{co}} = \frac{(x-a_1)}{x} \Rightarrow (\text{max.compressive strain})\varepsilon_{co} = \frac{\varepsilon_{c1} x}{(x-a_1)}$$

Table 4.4 Extrapolated maximum concrete compressive strains in the beams

1 Beam Code	2 Concrete grade	3 Rebar No. Dia/Type	4 Failure Load (kN)	5 Maximum Concrete Compressive Strain
TB15	C20	2-08S	23.00	0.00109
RTB15	C20	2-08S	25.10	0.00268
TB13	C20	2-12S	42.00	0.00181
RTB13	C20	2-12S	38.70	0.00124
TB17	C20	2-16S	56.30	0.00185
TB16	C20	2-08.77F	28.00	0.00310
RTB16	C20	2-08.77F	24.00	0.00205
RRTB16	C20	2-08.77F	26.00	0.00206
TB14	C20	2-13.19F	31.50	0.00230
TB18	C20	2-16.44F	30.00	0.00212
RTB18	C20	2-16.44F	26.60	0.00124
TB5	C40	2-08S	24.00	0.00102
TB1	C40	2-12S	50.00	0.00173
RTB1	C40	2-12S	51.00	0.00129
TB9	C40	2-16S	68.00	0.00178
TB6	C40	2-08.77F	20.00	0.00152
TTB16	C40 FB	2-08.77F	33.60	0.00256
RTB6	C40	2-08.77F	22.00	0.00154
TB2	C40	2-13.19F	34.00	0.00236
RTB2	C40	2-13.19F	31.60	0.00181
TTB21	C40 FB	2-13.19F	36.00	0.00198
TB10	C40	2-16.44F	29.00	0.00170
TB7	C60	2-08S	24.00	0.00090
TB3	C60	2-12S	48.00	0.00142
TB11	C60	2-16S	58.00	0.00129
TB8	C60	2-08.77F	26.00	0.00222
RTB8	C60	2-08.77F	26.40	0.00186
RRTB8	C60	2-08.77F	30.00	0.00214
TB4	C60	2-13.19F	38.00	0.00199
TB12	C60	2-16.44F	28.00	0.00153

The comparison of data in Table 4.4

- The average compressive strains extrapolated (see *Figure 4.15*) from measured strains on top of the beam at failure were 0.0017 for C20 steel reinforced beams, 0.0015 for C40 steel reinforced beams and 0.0012 for C60 steel reinforced beams. This suggests that the concrete could take more load in the compression zone since the design ultimate compressive strain of concrete, 0.0035, has not been reached.
- The average maximum concrete compressive strains extrapolated from the measured values were 0.0021 for C20 GFRP reinforced beams, 0.0019 for C40 and C60 GFRP reinforced beams. Although most GFRP beams failed in shear (except TB16 and TB8) it seems that the max compressive strains for GFRP reinforced beams are higher than the steel reinforced beams due to the fact that the number of cracks in GFRP beams less but deeper than for the steel beams (see *Appendix 6* to *Appendix 8*) leaving the maximum bending region of the beam under more stress.
- The concrete compressive strains in the steel and GFRP reinforced beams seem to be slightly influenced by the rebar diameter and the concrete grade. There is some evidence for both GFRP and steel reinforced beams that the maximum compressive strains are less for beams of higher concrete grades with bigger diameter bars than the lower grade of concrete beams reinforced with small diameter bars (see column 5 in *Table 4.4*). This is due to the fact that the higher grade concrete with bigger bars will resist bending more than the lower grade concrete with smaller bars.

4.2.3.3 Neutral axis Depth at the uncracked and the cracked sections

Figure 4.15 can be adopted for determining the neutral axis depth for both steel and GFRP reinforced beams as well as the equations which are available in the BS 8110 design code. A sample calculation is included in *Appendix 5*.

direct measurement of the neutral axis depth at the uncracked and cracked sections :

$$\frac{\varepsilon_{c2}}{\varepsilon_{c1}} = \frac{(x-a_2)}{(x-a_1)} \text{ (similar triangles)}$$

$$\varepsilon_{c1}x - \varepsilon_{c2}x = \varepsilon_{c1}a_2 - \varepsilon_{c2}a_1 \Rightarrow x = \frac{(\varepsilon_{c1}a_2 - \varepsilon_{c2}a_1)}{(\varepsilon_{c1} - \varepsilon_{c2})}$$

theoretical equations of the neutral axis depth at the uncracked and cracked sections

uncracked:

$$\frac{\chi_{theo\,uncr}}{d} = \frac{\alpha_e\rho + \frac{1}{2}\left(\frac{h}{d}\right)^2}{\alpha_e\rho + \left(\frac{h}{d}\right)}$$

cracked:

$$\frac{\chi_{theo\,cr}}{d} = \sqrt{\alpha_e\rho(2+\alpha_e\rho)} - \alpha_e\rho$$

<u>The comparison of data in Table 4.5</u>

Table 4.5 contains the theoretical and the experimental neutral axis depth of the beams.

- The theoretical neutral axis depth of both steel and GFRP reinforced beams is in good agreement with the experimental values at the cracked section regardless of the modes of failure (see column 5 and 6).
- For all beams it was observed that the neutral axis depth decreases as the load increases and it becomes almost a constant value towards the failure (see *Figure 4.10*, *Figure 4.11* and *Figure 4.12*).
- The neutral axis depth of GFRP reinforced beams at failure is far less than the steel reinforced ones due to the lower modulus of elasticity of the GFRP rebars.

- The concrete grade does not seem to have an influence on the neutral axis depth. However, the rebar diameter seems to affect the depth of neutral axis i.e. the bigger the diameter of rebar the less the upward movement of the depth of the neutral axis. This is more obvious with steel reinforced beams.
- Note that the measured depths of neutral axis at the cracked section is based on the last DEMEC reading at a load nearer to the failure. It can be seen in the *Figure 4.10*, *Figure 4.11* and *Figure 4.12* that once the section cracks neutral axis depths eventually become straight line towards the failure.

Table 4.5 The experimental and the theoretical neutral axis depths of the beams at the uncracked and cracked sections

1	2	3	4	5	6
Beam Code	Concrete grade	Rebar No. Dia/Type	**Neutral axis depth (mm)** Theory Uncracked	Theory$_{max}$ Cracked	Measured$_{max}$ Cracked
TB15	C20	2-08S	103.15	36.14	48.60
RTB15	C20	2-08S	103.06	35.21	43.70
TB13	C20	2-12S	105.35	52.83	92.10
RTB13	C20	2-12S	104.92	50.18	66.00
TB17	C20	2-16S	108.14	67.00	84.90
TB16	C20	2-08.77F	101.98	20.50	29.40
RTB16	C20	2-08.77F	101.94	19.68	22.50
RRTB16	C20	2-08.77F	102.06	21.96	30.20
TB14	C20	2-13.19F	102.37	27.09	32.80
TB18	C20	2-16.44F	102.73	32.09	39.60
RTB18	C20	2-16.44F	102.81	33.00	33.90
TB5	C40	2-08S	103.11	35.67	46.00
TB1	C40	2-12S	105.02	50.82	61.50
RTB1	C40	2-12S	104.92	50.18	59.40
TB9	C40	2-16S	107.27	63.18	68.80
TB6	C40	2-08.77F	101.97	20.18	23.90
TTB16	C40 FB	2-08.77F	102.97	20.23	29.20
RTB6	C40	2-08.77F	101.90	18.71	18.00
TB2	C40	2-13.19F	102.37	27.22	32.60
RTB2	C40	2-13.19F	102.28	25.86	27.70
TTB21	C40 FB	2-13.19F	103.42	28.05	35.60
TB10	C40	2-16.44F	102.74	32.17	37.50
TB7	C60	2-08S	103.15	36.06	42.50
TB3	C60	2-12S	104.83	49.60	54.90
TB11	C60	2-16S	106.99	61.83	66.00
TB8	C60	2-08.77F	101.96	19.91	23.30
RTB8	C60	2-08.77F	101.94	19.66	20.20
RRTB8	C60	2-08.77F	101.96	19.93	26.40
TB4	C60	2-13.19F	102.28	25.87	24.40
TB12	C60	2-16.44F	102.64	30.94	33.60

Note: The measured neutral axis depths at the uncracked section are omitted due to the fact that once the beam is loaded, the section starts to crack. Therefore, the actual values cannot be compared easily with the theoretical ones.

4.2.4 Elastic & Ultimate Load/Moment Capacities

In *Table 4.6* the theoretical and measured (actual) bending moment capacities of each beam were calculated using BS8110 formulae below (see also *Appendix 5*). Note that the actual moment capacity of the beams was calculated by substituting the experimental load into the formulae whereas the theoretical bending moments were calculated using the theoretical neutral axis depth.

Actual and theoretical bending moments :
uncracked/cracked section :

$$M_{actual} = \frac{\frac{F}{2}(L_s - e)}{2} + \frac{wL_s^{\,2}}{8}$$

uncracked section :

$$M_{theo_{uncr}} = f_{st/gfrp} A_{s/gfrp} \left(d - \frac{\chi_{theo_{uncr}}}{3} \right) \text{ based on steel}$$

cracked section :

$$M_{theo_{cr}} = f_{st/gfrp} A_{st/gfrp} \left(d - \frac{\chi_{theo_{cr}}}{3} \right) \text{ based on steel}$$

The comparison of data in Table 4.6

- It can be seen in column 6 that the initial capacity (initial crack load) of the steel and GFRP reinforced beams are more or less the same. It also seems that the initial capacity of steel and GFRP beams is slightly increased with medium and high strength concrete.
- In columns 10 and 11 that the agreement between actual and theoretical maximum moment capacities of steel reinforced beams for all three diameters can be considered fair. When applied to GFRP reinforced beams, theory overestimates the ultimate moment capacity except the beams reinforced with ϕ8.77 GFRP rebars. It is believed that this difference may have originated from possible material variations (e.g. slightly larger average area, or lower modulus of elasticity of the GFRP rebar). In addition to this, it may have resulted from the GFRP

beams exhibiting very large deformations before reaching the ultimate flexural capacity so that, the simplifying assumptions made in the analysis caused larger errors than in conventional steel beams that reached their maximum moment at a considerably smaller curvature. However, it should be noticed that the values for ϕ8.77 GFRP reinforced beams are well within the range of theoretical values. This is particularly so with high strength concrete.

- Failure loads suggest that the steel reinforced beams are more sensitive to rebar area and less sensitive to concrete grade than those reinforced with GFRP, however cognisance must be taken of failure mode in this respect. It was also interesting to note that the smaller diameter, ϕ8.77 GFRP reinforced beams showed similar ultimate load capacity to steel, ϕ8 reinforced beams even though most of GFRP beams failed in shear.

Table 4.6 Elastic & ultimate load/moment capacity of Part 1 beams obtained from theory and experiment

1	2	3	4	5	6	7	8	9	10	11
Beam Code	Concrete grade	Rebar No. Dia/Type	Rebar Area (mm^2)	Tension Rebar %	Initial Crack Load kN	Failure Load kN	**Bending Moment (kNm)** Theory Uncracked	Measured Uncracked	$Theory_{max}$ Cracked	$Measured_{max}$ Cracked
TB15	C20	2-08S	101	0.48	6	23	1.68	2.67	8.56	9.21
RTB15	C20	2-08S	101	0.48	6	25.1	1.68	2.67	8.58	10.03
TB13	C20	2-12S	226	1.08	4	42	1.09	1.89	17.34	16.52
RTB13	C20	2-12S	226	1.08	4	38.7	1.10	1.90	17.44	15.26
TB17	C20	2-16S	402	1.92	6	56.3	1.61	2.68	27.72	22.05
TB16	C20	2-08.77F	121	0.58	4	28	1.11	1.90	12.13	11.14
RTB16	C20	2-08.77F	121	0.58	4	24	1.11	1.91	12.15	9.61
RRTB16	C20	2-08.77F	121	0.58	4	26	1.11	1.91	12.09	10.38
TB14	C20	2-13.19F	273	1.31	4	31.5	1.10	1.90	20.87	12.49
TB18	C20	2-16.44F	425	2.03	4.6	30	1.25	2.13	36.78	11.91
RTB18	C20	2-16.44F	425	2.03	4	26.6	1.25	1.91	36.71	10.61
TB5	C40	2-08S	101	0.48	6	24	1.68	2.68	8.57	9.61
TB1	C40	2-12S	226.2	1.08	8	50	2.19	3.44	17.43	19.61
RTB1	C40	2-12S	226	1.08	6	51	1.64	2.68	17.44	20.00
TB9	C40	2-16S	402.1	1.92	12	68	3.22	4.98	27.97	26.54
TB6	C40	2-08.77F	120.8	0.58	6.8	20	1.88	2.99	12.12	8.07
TTB16	C40 FB	2-08.77F	120.8	0.57	6	33.6	1.68	2.68	12.26	13.31
RTB6	C40	2-08.77F	121	0.58	4	22	1.11	1.91	12.17	8.84
TB2	C40	2-13.19F	273.3	1.31	4.9	34	1.35	2.25	20.88	13.45
RTB2	C40	2-13.19F	273	1.31	5	31.6	1.37	2.29	20.92	12.54
TTB21	C40 FB	2-13.19F	273	1.28	6	36	1.67	2.68	21.08	14.23
TB10	C40	2-16.44F	424.5	2.03	5	29	1.35	2.28	36.73	11.52
TB7	C60	2-08S	100.5	0.48	6	24	1.68	2.68	8.52	9.61
TB3	C60	2-12S	226.2	1.08	8	48	2.19	3.45	17.48	18.85
TB11	C60	2-16S	402.1	1.92	9	58	2.42	3.83	28.05	22.70
TB8	C60	2-08.77F	120.8	0.58	6	26	1.66	2.68	12.12	10.38
RTB8	C60	2-08.77F	121	0.58	4	26.4	1.11	1.91	12.15	10.53
RRTB8	C60	2-08.77F	121	0.58	6	30	1.66	2.68	12.14	11.92
TB4	C60	2-13.19F	273.3	1.31	6	38	1.65	2.68	20.94	15.00
TB12	C60	2-16.44F	424.5	2.03	5.8	28	1.57	2.60	36.83	11.15

4.2.5 Ultimate Shear Capacity

In *Table 4.7* the theoretical and actual (measured based on the ultimate failure load) shear capacities of each beam calculated using the formulae below (see also *Appendix 5*).

Actual & theoretical shear strength of the beams

$$v_{s_{actual}} = \frac{1000(F + \text{Beam self weight})}{2bh}$$

$$v_{\max_{theo}} = k_1 k_2 0.79 \left(\frac{100 A_{st/gfrp}}{bd}\right)^{1/3} \left(\frac{400}{d}\right)^{1/4} \quad \text{where } k_1 = 1 \text{ and } k_2 = \left(\frac{f_c}{25}\right)^{1/3}$$

where f_c is not to be taken as greater than $40MPa$

The comparison of data in Table 4.7

- The comparison between the theoretical and measured values indicates that the theory overestimates the shear capacity of both steel and GFRP reinforced beams.
- Generally, the shear resistance of the steel reinforced beams is higher than the GFRP reinforced ones. The results in the steel reinforced beams show that the shear resistance increases with increase in rebar area.
- C40 concrete beam (TTB16) mixed with glass fibre chopped strands give higher shear resistance (measured) for the section containing the same rebar area in GFRP reinforced beams (TB6 and RTB6).

Table 4.7 Ultimate shear capacity of Part1 Beams

1	2	3	4	5	6	7	8	9
Beam Code	Concrete grade	Rebar No. Dia/Type	Rebar Area (mm^2)	Tension Rebar %	Shear span/ effective depth	Failure Mode	**Shear Resistance (MPa)** $Theory_{max}$ Cracked	$Measured_{max}$ Cracked
TB15	C20	2-08S	101	0.48	4.43	Flexure	0.94	0.58
RTB15	*C20*	*2-08S*	*101*	*0.48*	*4.43*	*Flexure*	*0.94*	*0.63*
TB13	C20	2-12S	226	1.08	4.48	Shear-Bond	1.24	1.04
RTB13	*C20*	*2-12S*	*226*	*1.08*	*4.48*	*Shear*	*1.24*	*0.96*
TB17	C20	2-16S	402	1.92	4.53	Shear-Bond	1.51	1.38
TB16	C20	2-08.77F	121	0.58	4.43	Flexure	1.00	0.70
RTB16	*C20*	*2-08.77F*	*121*	*0.58*	*4.43*	*Shear*	*1.00*	*0.61*
RRTB16	*C20*	*2-08.77F*	*121*	*0.58*	*4.43*	*Shear*	*1.00*	*0.65*
TB14	C20	2-13.19F	273	1.31	4.49	Shear-Bond	1.32	0.78
TB18	C20	2-16.44F	425	2.03	4.54	Shear-Bond	1.54	0.75
RTB18	*C20*	*2-16.44F*	*425*	*2.03*	*4.54*	*Shear*	*1.54*	*0.67*
TB5	C40	2-08S	101	0.48	4.43	Flexure	0.94	0.61
TB1	C40	2-12S	226	1.08	4.48	Flexure	1.24	1.23
RTB1	*C40*	*2-12S*	*226*	*1.08*	*4.48*	*Flexure*	*1.24*	*1.25*
TB9	C40	2-16S	402	1.92	4.53	Shear-Bond	1.51	1.66
TB6	C40	2-08.77F	121	0.58	4.43	Shear	1.00	0.51
TTB16	C40 FB	2-08.77F	121	0.57	4.38	Shear	0.99	0.82
RTB6	*C40*	*2-08.77F*	*121*	*0.58*	*4.43*	*Shear*	*1.00*	*0.56*
TB2	C40	2-13.19F	273	1.31	4.49	Shear-Bond	1.32	0.84
RTB2	*C40*	*2-13.19F*	*273*	*1.31*	*4.49*	*Shear*	*1.32*	*0.79*
TTB21	C40 FB	2-13.19F	273	1.28	4.44	Shear	1.31	0.88
TB10	C40	2-16.44F	425	2.03	4.54	Shear-Bond	1.54	0.72
TB7	C60	2-08S	101	0.48	4.43	Flexure	0.94	0.61
TB3	C60	2-12S	226	1.08	4.48	Flexure	1.24	1.18
TB11	C60	2-16S	402	1.92	4.53	Shear-Bond	1.51	1.42
TB8	C60	2-08.77F	121	0.58	4.43	Flexure	1.00	0.65
RTB8	*C60*	*2-08.77F*	*121*	*0.58*	*4.43*	*Shear*	*1.00*	*0.66*
RRTB8	*C60*	*2-08.77F*	*121*	*0.58*	*4.43*	*Shear*	*1.00*	*0.75*
TB4	C60	2-13.19F	273	1.31	4.49	Shear-Bond	1.32	0.94
TB12	C60	2-16.44F	425	2.03	4.54	Shear-Bond	1.54	0.70

4.2.6 Deflection

The deflection behaviour of steel reinforced beams that failed in flexure showed yield line of steel reinforcing bars before the concrete crushed at the top of the beam (see *Figure 4.16*, *Figure 4.17* and *Figure 4.18*). This was not the case with steel beams failed in shear. In the case of GFRP reinforced beams regardless of their modes of failure, all the beams behaved in a similar manner. The load vs deflection graphs are similar in shape for all concrete grades. In the pre-cracking stage the slope of first segment is steep i.e. small increase in deflection when load increases. The second segment is linear leading to beam failure. The slope of this portion is relatively smaller than the initial portion. This shows that once the concrete had cracked, the beam deflected at a faster rate when load continued to increase. When flexural cracking develops, the contribution of concrete in the tension region is considered negligible. This is also reflected by the results in that concrete grade is not the main factor that affects the deflection at a failure. It is apparent from the graphs that as well as elastic modulus of each material, the area of reinforcement also contributes to the deflection behaviour of the beams i.e. at the same load for a given beam the larger the area of rebar the smaller the deflection and the larger the load capacity.

CL r s

8N

& 1

Gt ^

♦ f \ +

Figure 4.17 Deflection of C40 grade concrete beams reinforced with GFRP/steel rebars

Figure 4.18 Deflection of C60 grade concrete beams reinforced with GFRP/steel rebars

The midspan deflection values in *Table 4.8*, columns 10 & 12 were calculated using the formulae below (see also *Appendix 5*) corresponding to the initial crack and failure loads of the beams. The measured values were obtained directly from the test.

The second moment of area of transformed section

uncracked

$$\frac{I_{uncr}}{bd^3} = \frac{1}{12}\left(\frac{h}{d}\right)^3 + \frac{h}{d}\left(\frac{\chi_{uncr}}{d} - \frac{h}{2d}\right)^2 + \alpha_e\rho\left(1 - \frac{\chi_{uncr}}{d}\right)^2$$

cracked

$$\frac{I_{cr}}{bd^3} = \frac{1}{3}\left(\frac{\chi_{cr}}{d}\right)^3 + \alpha_e\rho\left(1 - \frac{\chi_{cr}}{d}\right)^2$$

Moment curvature relationship & deflection :

uncracked section

$$\left(\frac{1}{r_b}\right)_{theo_{uncr}} = \frac{M_{theo\,uncr}}{E_c I_{uncr}}$$

$$\Delta_{theo_{uncr}} = KL^2 \frac{1}{r_{b_{theo_{uncr}}}}$$

cracked section

$$\left(\frac{1}{r_b}\right)_{theo_{cr}} = \frac{M_{theo\,cr} - \frac{bd^2}{3}\frac{\left(\frac{h}{d} - \frac{\chi_{cr}}{d}\right)^3}{\left(1 - \frac{\chi_{cr}}{d}\right)}}{EI_{cr}}$$

$$\Delta_{theo_{cr}} = KL^2 \frac{1}{r_{b_{theo_{cr}}}}$$

The comparison of data in Table 4.8

- Generally, the calculated deflections of all the beams within the elastic limit (first segment of the curve) are smaller than the measured ones.
- The measured midspan deflections of GFRP reinforced beams at the uncracked section, are generally higher than the steel reinforced ones for a given initial crack load.
- The maximum calculated deflections of the steel and GFRP reinforced beams are very close to the measured deflections at the cracked section.
- The measured deflections of GFRP reinforced beams are bigger than the steel reinforced beams for a given load at failure at the cracked section.
- The 'calculated' deflections verified that the BS8110 equation can be used for predicting the deflection of the beams reinforced with either GFRP or steel.

Table 4.8 Deflections of C20, C40 and C60 beams reinforced with GFRP/steel rebars

1	2	3	4	5	6	7	8	9	10	11	12	13
Beam Code	Concrete grade	Rebar No. Dia/Type	Rebar Area (mm^2)	Tension Rebar %	**Second Moment Area (mm^4)**		**Curvature (1/mm)**		**Deflection (mm)**			
					*Calculated Uncracked	*Calculated Cracked	*Calculated Uncracked	*Calculated Cracked	*Calculated Uncracked	**Measured Uncracked	*Calculated Cracked	**$Measured_{max}$ Cracked
TB15	C20	2-08S	101	0.48	9.01E+07	1.16E+07	8.97E-07	1.93E-05	0.58	0.67	12.41	13.70
RTB15	*C20*	*2-08S*	*101*	*0.48*	*7.47E+07*	*1.07E+07*	*1.02E-06*	*2.40E-05*	*0.66*	*0.86*	*15.42*	*14.31*
TB13	C20	2-12S	226	1.08	1.42E+08	3.45E+07	4.43E-07	1.54E-05	0.29	0.62	9.89	17.98
RTB13	*C20*	*2-12S*	*226*	*1.08*	*8.52E+07*	*2.18E+07*	*6.55E-07*	*1.94E-05*	*0.42*	*0.44*	*12.50*	*12.20*
TB17	C20	2-16S	402	1.92	1.31E+08	3.73E+07	6.85E-07	1.91E-05	0.44	0.42	12.30	15.17
TB16	C20	2-08.77F	121	0.58	1.80E+08	3.81E+06	3.20E-07	6.95E-05	0.21	2.29	44.69	70.04
RTB16	*C20*	*2-08.77F*	*121*	*0.58*	*7.43E+07*	*3.35E+06*	*7.13E-07*	*6.86E-05*	*0.46*	*0.41*	*44.09*	*65.25*
RRTB16	*C20*	*2-08.77F*	*121*	*0.58*	*1.22E+08*	*4.31E+06*	*5.50E-07*	*7.44E-05*	*0.35*	*0.97*	*47.81*	*48.38*
TB14	C20	2-13.19F	273	1.31	9.02E+07	6.24E+06	6.19E-07	5.31E-05	0.40	0.51	34.11	45.17
TB18	C20	2-16.44F	425	2.03	7.74E+07	8.66E+06	8.35E-07	3.77E-05	0.54	0.46	24.22	33.43
RTB18	*C20*	*2-16.44F*	*425*	*2.03*	*8.58E+07*	*8.91E+06*	*7.16E-07*	*3.40E-05*	*0.46*	*0.59*	*21.86*	*22.40*
TB5	C40	2-08S	101	0.48	8.67E+07	1.11E+07	9.08E-07	2.27E-05	0.58	0.87	14.60	13.94
TB1	C40	2-12S	226	1.08	8.92E+07	2.14E+07	1.17E-06	2.65E-05	0.75	1.18	17.06	25.70
RTB1	*C40*	*2-12S*	*226*	*1.08*	*9.14E+07*	*2.07E+07*	*8.61E-07*	*2.71E-05*	*0.55*	*0.60*	*17.45*	*17.75*
TB9	C40	2-16S	402	1.92	1.08E+08	3.09E+07	1.32E-06	2.38E-05	0.85	2.01	15.30	18.61
TB6	C40	2-08.77F	121	0.58	2.05E+08	3.53E+06	4.28E-07	5.62E-05	0.28	8.18	36.13	47.97
TTB16	C40 FB	2-08.77F	121	0.57	1.05E+08	3.80E+06	7.50E-07	9.31E-05	0.48	0.71	59.83	62.74
RTB6	*C40*	*2-08.77F*	*121*	*0.58*	*8.09E+07*	*3.02E+06*	*5.90E-07*	*6.16E-05*	*0.38*	*0.48*	*39.61*	*55.50*
TB2	C40	2-13.19F	273	1.31	1.07E+08	6.29E+06	6.19E-07	5.72E-05	0.40	1.76	36.77	49.32
RTB2	*C40*	*2-13.19F*	*273*	*1.31*	*1.08E+08*	*5.62E+06*	*5.59E-07*	*5.27E-05*	*0.36*	*0.39*	*33.89*	*42.47*
TTB21	C40 FB	2-13.19F	273	1.28	9.87E+07	6.91E+06	8.49E-07	5.88E-05	0.55	0.69	37.84	38.34
TB10	C40	2-16.44F	425	2.03	1.57E+08	8.59E+06	4.41E-07	3.65E-05	0.28	0.41	23.47	33.23
TB7	C60	2-08S	101	0.48	1.29E+08	1.10E+07	6.30E-07	2.34E-05	0.40	0.65	15.07	13.67
TB3	C60	2-12S	226	1.08	7.83E+07	1.99E+07	1.26E-06	2.57E-05	0.81	1.16	16.54	18.79
TB11	C60	2-16S	402	1.92	8.72E+07	2.96E+07	1.19E-06	2.00E-05	0.76	0.94	12.85	13.20
TB8	C60	2-08.77F	121	0.58	1.96E+08	3.44E+06	3.91E-07	7.53E-05	0.25	2.80	48.41	64.51
RTB8	*C60*	*2-08.77F*	*121*	*0.58*	*8.21E+07*	*3.33E+06*	*6.46E-07*	*7.65E-05*	*0.42*	*0.41*	*49.21*	*57.16*
RRTB8	*C60*	*2-08.77F*	*121*	*0.58*	*1.40E+08*	*3.52E+06*	*5.48E-07*	*8.65E-05*	*0.35*	*1.71*	*55.60*	*56.55*
TB4	C60	2-13.19F	273	1.31	1.42E+08	5.62E+06	4.98E-07	6.41E-05	0.32	1.22	41.19	56.72
TB12	C60	2-16.44F	425	2.03	1.33E+08	7.89E+06	5.42E-07	3.49E-05	0.35	1.91	22.47	31.23

* Column 6-7 using actual n.a depth * Column 8-9 using actual bending moment * Column 10-12 using actual curvature ** Column 11-13 experimental readings

4.2.7 Cracking Behaviour

It is well known that concrete has a low tensile strength compared to its compressive strength. When the principal tensile stress from external and internal forces exceeds the tensile strength of concrete, cracks occur. The tensile strength of concrete will initially depend on the type of concrete mix, the compaction and the curing conditions. These cracks may reduce the durability of steel reinforcement significantly and it is necessary to limit the size and the distribution of them. Controlling the cracks is an advantage especially in aggressive environments where steel reinforcement requires large concrete covers.

Formation of cracks can happen soon after casting due to settlement of the plastic concrete. Also, during curing process of concrete the heat produced by the hydration will create temperature differences between internal and external parts that could give rise to cracks. All in all cracks can be formed both in a random manner or be influenced by structural characteristics of the external and internal forces, and material composition.

Excessive cracking is undesirable because it reduces stiffness and causes the possibility of deterioration of especially steel reinforced concrete with undesirable appearance. The crack control limits have been laid out in BS8110 Part2 Section 3.

ϕ8 Steel and ϕ8.77 GFRP Reinforced C20 C40 C60 Concrete Beams

First hairline cracks became visible at the maximum bending moment region under 6kN total load for steel reinforced beams and subsequently grew more prominent and numerous as the load increased (see *Appendix 6*). The cracks developed in C40, C60 grade concrete beams have more branches compared to C20 grade concrete beams. The length of crushing in the compression zone of C60 beam was longer than C20 and C40 beams. As would be expected for GFRP having a low modulus of elasticity, most GFRP reinforced beams started to exhibit visible cracks under relatively low loads, 4kN, and cracks grew rather large when load increased. *Table 4.9* contains the average number of cracks at failure of the beams.

Table 4.9 Average number of cracks in 8mm diameter steel and 8.77mm diameter GFRP reinforced beams at failure

	No. of cracks at failure			**First crack load (kN)**		
	C20	C40	C60	C20	C40	C60
∅8 Steel	18	23	18	6	6	6
∅8.77 GFRP	9	9	9	4	4	4
∅8.77 GFRP (fibre mix)		12				

ϕ12 Steel and ϕ13.19 GFRP Reinforced C20 C40 C60 Concrete Beams

The first hairline cracks became visible within the maximum bending moment region under a 4kN total load for C20 and 8kN for C40 (except RTB1 which was 6kN) and C60 steel reinforced beams and subsequently grew more prominent and numerous as the load increased (see *Appendix 7*). The crack patterns resemble those reinforced with ϕ8 steel reinforced beams for all grades of concrete in this category. The C20, GFRP reinforced beams developed visible cracks under relatively low load 4kN compared to C40-average of 5kN and C60 at 6kN load GFRP reinforced beams. Afterwards, the cracks grew much large when load increased. In this category, it seems that the number of cracks increases with an increased load capacity in high strength and fibre mix concrete. The comparison between ϕ12 steel and ϕ13.19 GFRP reinforced beams showed that the number of cracks developed in ϕ13.19 GFRP is approximately 50-80% less than that of steel beams at failure. *Table 4.10* contains the average number of cracks at failure of the beams.

Table 4.10 Average number of cracks in 12mm diameter steel and 13.19mm diameter GFRP reinforced beams at failure

	No. of cracks at failure			**First crack load (kN)**		
	C20	C40	C60	C20	C40	C60
∅12 Steel	25	25	30	4	8(6)	6
∅13.19 GFRP	13	13 to 16	19	4	5	6
∅13.19 GFRP (fibre mix)		18				

ϕ16 Steel and ϕ16.44 GFRP Reinforced C20 C40 C60 Concrete Beams

Initial cracking of the steel reinforced beams was observed under 6kN in C20, 12kN in C40 and 9kN in C60 concrete. The crack spaces in these beams are closer to each other compared to ϕ8 small and ϕ12 medium steel reinforced beams (see *Appendix 8*). This is probably due to the fact that the load capacity of these beams is higher than the small and medium size steel reinforced beams. This means that more cracks are developing to resist the beam in bending. *Table 4.11* contains the average number of cracks at failure of the beams.

Cracking started in GFRP reinforced beams at a total load of 4kN to 4.6kN in C20, 5kN in C40 and 5.8kN in C60 subsequently followed a pattern similar to that of beams reinforced with ϕ8.77 GFRP with similar load capacities (except the cracks have more branches in this category). The number of cracks developed at failure again similar to the beams reinforced with ϕ8.77 GFRP beams. The comparison between ϕ16 steel and ϕ16.44 GFRP reinforced beams showed that the number of cracks developed in ϕ16.44 GFRP is approximately 60-80% less than that of steel beams at failure.

Table 4.11 Average number of cracks in 16mm diameter steel and 16.44mm diameter GFRP reinforced beams at failure

	No. of cracks at failure			**First crack load (kN)**		
	C20	C40	C60	C20	C40	C60
Ø16 Steel	27	29	39	6	12	9
Ø16.44 GFRP	10	9	8	4/4.6	5	5.8

4.2.7.1 Modes of Failure

The typical failure modes of the beams are shown in *Photo 4.1* and *Photo 4.2*. The test carried out on GFRP and steel reinforced beams can be viewed on the representative video clips from the compact disk (play *FRP_beamtest_flat.mov*, *FRP_beamtest1.mov* and *Steel_tb17_1 &2.mov*). Initially, vertical cracks emanating from the bottom surface within the middle section preceded failure in all cases. In some cases, these were followed by inclined cracks towards the supports. At the

ultimate condition, the beams in Part 1 failed either in flexure or in shear. The flexure failures comprised two types; meaning that the beams either failed gradually resulting in rebar yielding followed by concrete crushing in the compression zone or catastrophically in which rebars snapped followed by concrete broken at the midspan. The failure mode for GFRP reinforced beams was predominately shear failure. The shear failure was of two types. Type I resulted from simple diagonal shear between load point and support and Type II by shear-bond failure; along a line emanating from a loading point and passing diagonally across the section then horizontally along the rebar-concrete interface between one loading point and a support.

Development of crack pattern leading to Flexure Failure

The tensile stresses in the concrete are transferred to the reinforcing bar through bond forces developed between concrete and reinforcing bar. At the cracked section, tensile stress in concrete is relieved and becomes zero across the crack. As a result, the reinforcing bar must carry the tensile forces at that cracked section. The neutral axis then shoots upward at the cracked section in order to maintain equilibrium of the forces at that section. More cracks will appear between the 'old cracks' and this will continue at different locations until the concrete strains exceed the limiting concrete tensile stress. Eventually the increase in crack number will stop due to either the excessive slip between the rebar and concrete or the limit on the distance between cracks to transfer sufficient stress to the concrete to maintain equilibrium. When this happens the branches of the cracks will propagate at the midspan (max. bending moment region) until the flexural failure of the beam.

Photo 4.1 A view offlexuralfailure of2(j)8 steel reinforced C20 grade concrete beam

Photo 4.2 A view ofshearfailure of2(/)8.77 GFRP reinforced C60 grade concrete beam

Development of crack pattern leading to Shear (Diagonal Tension) Failure

The mechanism of shear (diagonal tension) failure in reinforced concrete is not a simple phenomenon and despite the amount of experimental and theoretical research work, it is not fully understood. However, in all the principal reinforced concrete design texts, it is given that there are three main components in shear resistance of a beam without shear reinforcement. These are, with reference to concrete in the compression zone, dowelling action of tensile reinforcement and aggregate interlock across flexural cracks. The purpose of a beam is to transfer a load from its point of application to the support. This transfer creates tension cracks in the concrete which means that the load will rest on the longitudinal reinforcing bar (except in the case where the load is close to the support). If there is nothing in the beam to resist this load, then the reinforcing bar will be split apart from the concrete. It is emphasized in *Nielsen et al's*[3] paper that this failure type should be avoided for two reasons. Firstly, it may occur at a load which is much lower than the flexural capacity of the beam and secondly, it is a sudden failure which may cause severe collapse.

In summary, nearer the supports, the cracks are inclined towards the span due to the combination of flexure and shear. In this case, the principal compression stresses are inclined at a steeper angle, so that the tensile stresses are liable to cause diagonal cracking. Under further load increments, these diagonal cracks develop quickly to cause failure.

ϕ8 Steel and ϕ8.77 GFRP Reinforced C20 C40 C60 Concrete Beams

The morphology of beam failures is given in *Table 4.12*. As it can be seen in table that all steel reinforced beams were failed in flexure whereas GFRP reinforced beams were failed in shear with the exception of C20 TB16 and C60 TB8 beams. Shear failure occurred in two repeats of these two beams, RTB16, RRTB16, RTB8 and RRTB8.

Table 4.12 The modes of failure of ϕ8 Steel and ϕ8.77 GFRP Reinforced C20 C40 C60 Concrete Beams

Beam Code	Concrete Grade (Cube Strength-MPa)	Rebar No Dia/Type	Failure Morphology (Failure Load-kN)
TB15	C20(36)	2ϕ8 Steel	**Flexure(balanced)**-Catastrophic failure at the midspan, concrete broke in two parts, steel bars disintegrated in the same region (23)
RTB15	C20(50)	2ϕ8 Steel	**Flexure**-Steel yielded and concrete spalled in the compression zone (25.10)
TB5	C40(61)	2ϕ8 Steel	**Flexure**-Steel yielded and concrete spalled in the compression zone (24)
TB7	C60(73)	2ϕ8 Steel	**Flexure**-Steel yielded and concrete spalled in the compression zone (24)
TB16	C20(35)	2ϕ8.77 GFRP	**Flexure(balanced)**-Catastrophic failure at the midspan, concrete broke in two parts, GFRP bars disintegrated in the same region (28)
RTB16	C20(49)	2ϕ8.77 GFRP	**Shear**-Diagonal tension crack propagated across the section outside the maximum bending moment region (24)
RRTB16	C20(47)	2ϕ8.77 GFRP	**Shear**-Diagonal tension crack propagated across the section outside the maximum bending moment region (26)
TB6	C40(69)	2ϕ8.77 GFRP	**Shear**-Diagonal tension crack propagated across the section outside the maximum bending moment region (20)
RTB6	C40(65)	2ϕ8.77 GFRP	**Shear**-Diagonal tension crack propagated across the section outside the maximum bending moment region (22)
TTB16	C40FB(59)	2ϕ8.77 GFRP	**Shear**-Diagonal tension crack propagated across the section outside the maximum bending moment region (33.60)
TB8	C60(72)	2ϕ8.77 GFRP	**Flexure(balanced)**-Catastrophic failure at the midspan, concrete broke in two parts, GFRP bars disintegrated in the same region (26)
RTB8	C60(70)	2ϕ8.77 GFRP	**Shear**-Diagonal tension crack propagated across the section outside the maximum bending moment region (26.40)
RRTB8	C60(78)	2ϕ8.77 GFRP	**Shear**-Diagonal tension crack propagated across the section outside the maximum bending moment region (30)

ϕ12 Steel and ϕ13.19 GFRP Reinforced C20 C40 C60 Concrete Beams

The morphology of beam failures is given in *Table 4.13*. As it can be seen in the table that all steel reinforced beams failed in flexure with exception of C20 TB13 and its repeat which failed in shear. All GFRP reinforced beams failed in shear.

Table 4.13 The modes of failure of ϕ12 Steel and ϕ13.19 GFRP Reinforced C20 C40 C60 Concrete Beams

Beam Code	Concrete Grade (Cube Strength MPa)	Rebar No Dia/Type	Failure Morphology (Failure Load-kN)
TB13	C20(21)	2ϕ12 Steel	**Shear-bond**-Diagonal tension crack propagated across the section and along the rebar, outside the maximum bending moment region (42)
RTB13	C20(50)	2ϕ12 Steel	**Shear**-Diagonal tension crack propagated across the section outside the maximum bending moment region (38.70)
TB1	C40(55)	2ϕ12 Steel	**Flexure**-Steel yielded and concrete spalled in the compression zone (50)
RTB1	C40(61)	2ϕ12 Steel	**Flexure**-Steel yielded and concrete spalled in the compression zone (51)
TB3	C60(72)	2ϕ12 Steel	**Flexure**-Steel yielded and concrete spalled in the compression zone (48)
TB14	C20(39)	2ϕ13.19 GFRP	**Shear-bond**-Diagonal tension crack propagated across the section and along the rebar, outside the maximum bending moment region (31.50)
TB2	C40(57)	2ϕ13.19 GFRP	**Shear-bond**-Diagonal tension crack propagated across the section and along the rebar, outside the maximum bending moment region (34)
RTB2	C40(63)	2ϕ13.19 GFRP	**Shear**-Diagonal tension crack propagated across the section outside the maximum bending moment region (31.60)
TTB21	C40FB(54)	2ϕ13.19 GFRP	**Shear-bond**-Diagonal tension crack propagated across the section and along the rebar, outside the maximum bending moment region (36)
TB4	C60(79)	2ϕ13.19 GFRP	**Shear-bond**-Diagonal tension crack propagated across the section and along the rebar, outside the maximum bending moment region (38)

The morphology of beam failures is given in *Table 4.14*. As it can be seen in the table that both steel and GFRP reinforced beams failed in shear or shear-bond.

Table 4.14 The modes of failure of ϕ16 Steel and ϕ16.44 GFRP Reinforced C20 C40 C60 Concrete Beams

Beam Code	Concrete Grade (Cube Strength MPa)	Rebar No Dia/Type	Failure Morphology (Failure Load-kN)
TB17	C20(47)	2ϕ16 Steel	**Shear-bond**-Diagonal tension crack propagated across the section and along the rebar, outside the maximum bending moment region (56.30)
TB9	C40(61)	2ϕ16 Steel	**Shear-bond**-Diagonal tension crack propagated across the section and along the rebar, outside the maximum bending moment region (68)
TB11	C60(75)	2ϕ16 Steel	**Shear-bond**-Diagonal tension crack propagated across the section and along the rebar, outside the maximum bending moment region (58)
TB18	C20(42)	2ϕ16.44 GFRP	**Shear-bond**-Diagonal tension crack propagated across the section and along the rebar, outside the maximum bending moment region (30)
RTB18	C20(45)	2ϕ16.44 GFRP	**Shear**-Diagonal tension crack propagated across the section outside the maximum bending moment region (26.60)
TB10	C40(51)	2ϕ16.44 GFRP	**Shear-bond**-Diagonal tension crack propagated across the section and along the rebar, outside the maximum bending moment region (29)
TB12	C60(76)	2ϕ16.44 GFRP	**Shear-bond**-Diagonal tension crack propagated across the section and along the rebar, outside the maximum bending moment region (28)

4.2.7.2 Estimation of Flexural Crack Widths

Mogaham & Sentler[4] suggest that the reinforcement of GFRP can be placed close to the surface where it can be expected to be the most effective. *Nawy & Neuwerth*[5] measured the cracks on fourteen beams (127mmx305mmx3000mm) and compared them with ACI 318-71 code formulae. The reinforcement % varied from 0.65% to 2.88%. The results showed that the calculated crack widths seem less than the observed ones. This is probably due to the possibility that the concrete area in tension for fibreglass reinforced beams would have to be considered larger than stipulated by the code for steel reinforced beams. *Nawy & Neuwerth*[6] also emphasized that using

fibreglass as reinforcement should permit higher tolerable crack widths, since corrosion of FRP is no longer a major criterion for crack control.

Mosley & Bungey[7] gives an expression for maximum surface crack width based upon BS8110 as below (see also *Appendix 5*). The detail of the cross section used in the crack width estimation is shown in *Figure 4.19*.

$$w_{\max} = \frac{3a_{cr}\varepsilon_m}{1+2\left(\frac{a_{cr}-c_{\min}}{h-x_{cr}}\right)}$$

Figure 4.19 Detail of the cross section used in the crack width estimation

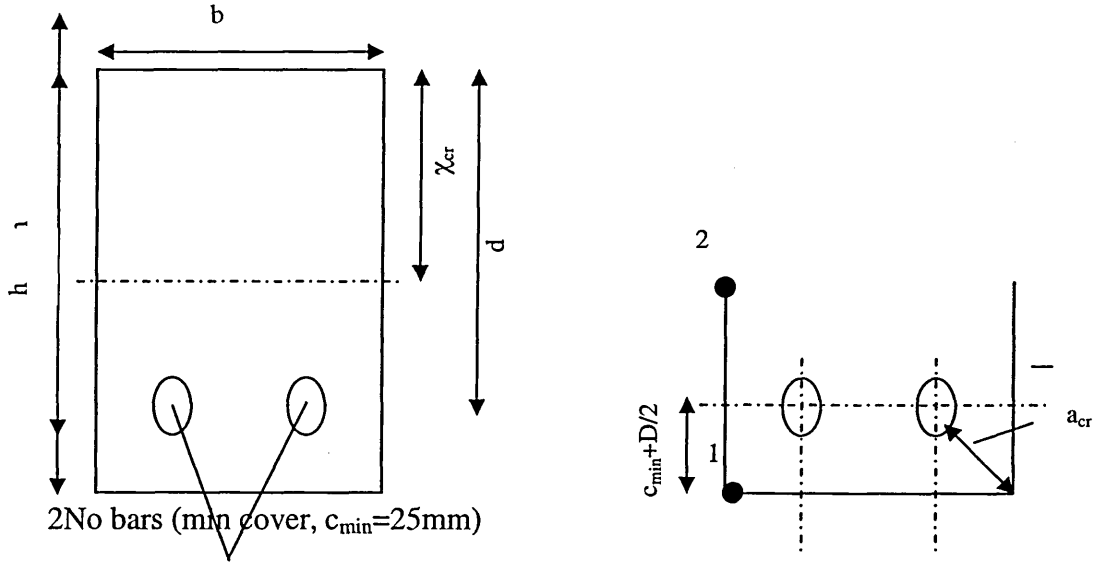

The estimated crack widths of Part 1 beams are given in Table 4.15.

The correlation between the theoretical and the experimental (using dial gauge method) crack widths for all steel reinforced beams is good. In the table, it can be seen that for steel reinforced beams, the values obtained from the equation are higher than the values obtained from the dial gauge method. Conversely, the values from the GFRP reinforced beams are higher than the values from the equation. Furthermore, the agreement between the two methods seem to be in a better agreement for higher strength concrete beams reinforced with GFRPs. The experimental values are generally higher than BS8110 for C20/C40 but lower for C60 concrete. Over all, the results show that using a dial gauge is not just useful to measure the strains in the concrete but also estimating the crack widths. The equation derived by the Author for estimating the crack widths using 900mm long dial gauge within the maximum bending moment region is given below (see also *Figure 4.20*).

Figure 4.20 Sketch of maximum bending moment portion of the beam showing the strains measured at two positions.

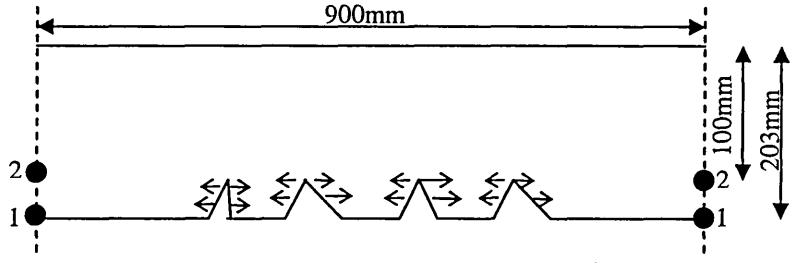

$$\varepsilon_{1,2} = \frac{\Delta_{L_{1,2}}}{GaugeLength(G.L.)} \Rightarrow \Delta_{L_1} = \varepsilon_1 \times G.L. \text{ and } \Delta_{L_2} = \varepsilon_2 \times G.L.$$

$$\Delta_{L_{average}} = \frac{\Delta_{L_1} - \Delta_{L_2}}{\text{no of cracks in max. bending moment region}}$$

Table 4.15 The estimated crack widths of Part1 beams

1	2	3	4	5	6
				Estimated crack widths (mm)	
Beam Code	Concrete grade	Rebar No. Dia/Type	*Number of Cracks	**BS8110	***Experiment
TB15	C20	2-08S	10	0.23	0.21
RTB15	C20	2-08S	10	0.77	0.72
TB13	C20	2-12S	14	0.14	0.10
RTB13	C20	2-12S	13	0.18	0.13
TB17	C20	2-16S	12	0.20	0.16
TB16	C20	2-08.77F	5	1.06	1.94
RTB16	C20	2-08.77F	5	0.90	1.64
RRTB16	C20	2-08.77F	8	0.65	0.75
TB14	C20	2-13.19F	7	0.79	1.03
TB18	C20	2-16.44F	7	0.53	0.69
RTB18	C20	2-16.44F	5	0.38	0.68
TB5	C40	2-08S	12	0.30	0.23
TB1	C40	2-12S	10	0.29	0.27
RTB1	C40	2-12S	12	0.17	0.13
TB9	C40	2-16S	13	0.26	0.19
TB6	C40	2-08.77F	4	0.69	1.58
TTB16	C40 FB	2-08.77F	5	0.90	1.66
RTB6	C40	2-08.77F	6	0.76	1.15
TB2	C40	2-13.19F	7	0.74	0.96
RTB2	C40	2-13.19F	7	0.64	0.83
TTB21	C40 FB	2-13.19F	8	0.59	0.68
TB10	C40	2-16.44F	5	0.48	0.87
TB7	C60	2-08S	10	0.22	0.20
TB3	C60	2-12S	14	0.27	0.18
TB11	C60	2-16S	15	0.19	0.12
TB8	C60	2-08.77F	11	0.89	0.74
RTB8	C60	2-08.77F	10	0.95	0.87
RRTB8	C60	2-08.77F	14	0.76	0.50
TB4	C60	2-13.19F	11	0.87	0.72
TB12	C60	2-16.44F	4	0.51	1.14

*in the maximum bending moment region **based upon the formula

***based upon the dial gauge measurements

4.3 Performance Quotient (Q_p)

This is a concept in which the efficiency of the structural unit or system is expressed in terms of the relationship between functional performance and the quantity and quality of material of which it is comprised. Using this principle the relative performance of different elements can be objectively measured and compared.

To assess the efficiency of the beam in resisting load it is useful to relate cost in real terms or energy equivalence to strength[8]. As an alternative to obviate the effect of capricious influences associated with market and manufacturing factors which vary from time to time, the Author proposes a quotient relating the load capacity with the load bearing potential based upon a measure of the strength of component materials and their average cross sectional area throughout the beam. This indicates also a measure of efficiency of utilisation of material for a given depth and span. It may be expressed as:

$$Q_p = \frac{1000(F + \text{Beam Self Weight})}{f_c(bh - A_{st,gfrp}) + f_{st,gfrp}A_{st,gfrp}} \quad 9$$

For flexural failure the Performance Quotient (Q_p) for steel and GFRP reinforced beams were comparable although not for the shear type failures (see *Table 4.16*). The high value of Q_p indicates that the ultimate load capacity of a beam is also high (see *Appendix 5* for sample calculations). In column 13, the numbers indicate that the steel reinforced concrete beams predominate in the ranking. The numbers formatted as 'bold' is to show the beams have a very similar performance value.

Table 4.16 Performance of Part 1 beams based upon performance quotient

1 Beam Code	2 Concrete grade	3 Rebar No. Dia/Type	4 Width b mm	5 Height h mm	6 Rebar Area (mm^2)	7 Beam Self Weight kN	8 Failure Mode	9 Failure Load kN	10 Yield/Ultimate Stress MPa	11 Cube Strength MPa	12 Perform. Quotient Actual	13 Ranking	Span/ Depth	Shear Span/ Depth
TB15	C20	2-08S	103	203	101	1.32	Flexure	23	523.50	41	0.0268	13	12.0	3.79
RTB15	*C20*	*2-08S*	*103*	*203*	*101*	*1.34*	*Flexure*	*25.1*	*523.50*	*50*	*0.0241*	*15*	12.0	3.79
TB13	C20	2-12S	103	203	226	1.30	Shear-Bond	42	497.00	40	0.0461	3	12.0	3.79
RTB13	*C20*	*2-12S*	*103*	*203*	*226*	*1.32*	*Shear*	*38.7*	*497.00*	*50*	*0.0346*	*6*	12.0	3.79
TB17	C20	2-16S	103	203	402	1.37	Shear-Bond	56.3	467.00	43	0.0539	1	12.0	3.79
TB16	C20	2-08.77F	103	203	121	1.32	Flexure	28	601.00	41	0.0317	8	12.0	3.79
RTB16	*C20*	*2-08.77F*	*103*	*203*	*121*	*1.35*	*Shear*	*24*	*601.00*	*41*	*0.0274*	*12*	12.0	3.79
RRTB16	*C20*	*2-08.77F*	*103*	*203*	*121*	*1.35*	*Shear*	*26*	*601.00*	*47*	*0.0263*	*14*	12.0	3.79
TB14	C20	2-13.19F	103	203	273	1.32	Shear-Bond	31.5	470.70	40	0.0344	7	12.0	3.79
TB18	C20	2-16.44F	103	203	425	1.33	Shear-Bond	30	544.00	39	0.0304	10	12.0	3.79
RTB18	*C20*	*2-16.44F*	*103*	*203*	*425*	*1.35*	*Shear*	*26.6*	*544.00*	*45*	*0.0242*	*15*	12.0	3.79
TB5	C40	2-08S	103	203	101	1.35	Flexure	24	523.50	61	0.0191	19	12.0	3.79
TB1	C40	2-12S	103	203	226	1.33	Flexure	50	497.00	55	0.0414	4	12.0	3.79
RTB1	*C40*	*2-12S*	*103*	*203*	*226*	*1.35*	*Flexure*	*51*	*497.00*	*61*	*0.0379*	*5*	12.0	3.79
TB9	C40	2-16S	103	203	402	1.34	Shear-Bond	68	467.00	61	0.0483	2	12.0	3.79
TB6	C40	2-08.77F	103	203	121	1.36	Shear	20	601.00	69	0.0143	26	12.0	3.79
TTB16	C40 FB	2-08.77F	104	205	121	1.37	Shear	33.6	601.00	58	0.0269	13	11.9	3.76
RTB6	*C40*	*2-08.77F*	*103*	*203*	*121*	*1.35*	*Shear*	*22*	*601.00*	*64*	*0.0166*	*23*	12.0	3.79
TB2	C40	2-13.19F	103	203	273	1.33	Shear-Bond	34	470.70	57	0.0270	13	12.0	3.79
RTB2	*C40*	*2-13.19F*	*103*	*203*	*273*	*1.36*	*Shear*	*31.6*	*470.70*	*63*	*0.0231*	*17*	12.0	3.79
TTB21	C40 FB	2-13.19F	104	205	273	1.37	Shear	36	470.70	54	0.0295	11	11.9	3.76
TB10	C40	2-16.44F	103	203	425	1.32	Shear-Bond	29	544.00	51	0.0238	16	12.0	3.79
TB7	C60	2-08S	103	203	101	1.36	Flexure	24	523.50	73	0.0161	25	12.0	3.79
TB3	C60	2-12S	103	203	226	1.35	Flexure	48	497.00	72	0.0307	9	12.0	3.79
TB11	C60	2-16S	103	203	402	1.36	Shear-Bond	58	467.00	75	0.0343	7	12.0	3.79
TB8	C60	2-08.77F	103	203	121	1.36	Flexure	26	601.00	72	0.0173	22	12.0	3.79
RTB8	*C60*	*2-08.77F*	*103*	*203*	*121*	*1.37*	*Shear*	*26.4*	*601.00*	*70*	*0.0182*	*21*	12.0	3.79
RRTB8	*C60*	*2-08.77F*	*103*	*203*	*121*	*1.38*	*Shear*	*30*	*601.00*	*78*	*0.0185*	*20*	12.0	3.79
TB4	C60	2-13.19F	103	203	273	1.37	Shear-Bond	38	470.70	79	0.0224	18	12.0	3.79
TB12	C60	2-16.44F	103	203	425	1.35	Shear-Bond	28	544.00	76	0.0164	24	12.0	3.79

4.4 Conclusions

C20, C40 and C60 grade concrete beams reinforced with smaller (ϕ8.77 and ϕ8), medium (ϕ13.19 and ϕ12) and larger (ϕ16.44 and ϕ16) diameter GFRP and steel reinforcing bars tested under two point loading and the test results compared with theory (BS8110) based upon the aspects below:

- Stress and strain in the reinforcements and concrete at the maximum bending moment and shear regions (where obtainable)
- The depth of neutral axis
- The elastic and ultimate load/moment capacities
- The ultimate shear capacities
- The deflection
- The cracking behaviour and the estimation of crack widths
- The modes of failures and performance quotient

The stresses in the rebars at the cracked sections, can be calculated by substituting the actual (measured) bending moment, second moment of area and depth neutral axis in BS8110 equations (see *Appendix 5*). The results indicated that the maximum tensile stresses and strains in the steel rebars reach almost their full tensile capacity whereas this is not quite the same with GFRP rebars except the ϕ8.77 rebars (see *Table 4.2* and *Table 4.3*).

The rebar and concrete strains can also be monitored in the shear zone of the concrete beams. In this way, it is possible to predict the most likely failure mode of the beam.

The results showed that the neutral axis depth of both the steel and GFRP beams, decreases as the load increases. It seems that the concrete grade has no influence on the neutral axis depth. However, when larger reinforcing bars are used, the depth of neutral axis shoots up less and this is more pronounced with steel reinforced beams. The agreement between the theoretical and measured (experimental) values of the

depth of neutral axis of all types of beams at the cracked section is very good (see *Table 4.5*).

The initial crack (visible) load of all the beams seems to be approximately 4kN minimum (see *Table 4.6*). However, it also seems that this value increases as the concrete grade gets higher only for the beams reinforced with larger diameter rebars.

The ultimate load capacities of the beams seem to be influenced by the area of rebars for all the beams except the ones reinforced with ϕ16.44 GFRP (see also *Table 4.6*, column 7).

Theoretical bending moment capacity of all the beams is less than the measured ones at the uncracked section (see *Table 4.6*). Theoretical values of moment capacity of the steel beams compare well with the experimental data at the cracked section, whereas the theory overestimates the moment capacity of GFRP reinforced beams. However, the moment capacity of the smaller 8.77 GFRP reinforced beams at the cracked section (especially with high strength concrete) agrees with theory fairly well.

The maximum theoretical shear capacity of all the beams is higher than the measured ones (see *Table 4.7*). The shear capacity of steel and GFRP reinforced beams increases with increase in rebar area and the concrete strength. The contribution of chopped fibres in concrete to the shear capacity of the beams is also noticeable.

Generally, the calculated deflections of all the beams within the elastic limit are smaller than the measured ones (see *Table 4.8*). The measured deflections of GFRP reinforced beams are bigger than the steel reinforced beams for a given load at failure. The deflection of GFRP reinforced beams is larger than the steel reinforced beams due to lower modulus of elasticity of GFRP.

The crack development and the patterns of all the beams are generally the same. However, in comparison with steel reinforced beams, the cracks in GFRP reinforced beams are deeper and larger gaps between the adjacent cracks (see *Appendix 6).*

The theory for predicting the maximum crack widths in the beams is adequate for both steel and GFRP reinforced beams (see *Table 4.15*). Expectedly, cracks were wider in GFRP reinforced beams than the steel reinforced beams.

The mode of failure appears to be influenced by rebar type and area for all the beams (see *Table 4.12*, *Table 4.13* and *Table 4.14*). For flexural failure GFRP beams display a greater capacity to absorb energy as indicated by the area under the load deflection curve than steel for similar ultimate load capacity, although they exhibit reduced stiffness.

Performance Quotient (Q_p) relating load capacity to section potential for similar beam span dimensions and load configuration may be a useful efficiency comparator (see *Table 4.16*). The high value of Q_p indicates that the ultimate load capacity of a beam is also high. The results indicated that the steel reinforced concrete beams predominate using this method of ranking.

4.5 REFERENCES

[1] BS8110, Part 1, Structural Use of Concrete, 1985.

[2] Geymayer H G, Static Tests of Reinforced Concrete Beams, Technical Report No 6-818, March 1968, p36.

[3] Nielsen M P et al, Rational Analysis of Shear in Reinforced Concrete Beams, IABSE Proceedings P-15/78, May 1978, p2.

[4] Mogaham M & Sentler L, GFRP as Crack Control Reinforcement, Proceedings of the Second International RILEM Symposium, FRPRCS-2, 1995,pp243-250.

[5] Nawy E G and Neuwerth A M, Fibreglass Reinforced Concrete Slabs and Beams, Journal of the Strutural Division, February 1977, pp421-440.

[6] Nawy E G and Neuwerth A M, Fibreglass Reinforced Concrete Slabs and Beams, Journal of the Strutural Division, February 1977, pp421-440.

[7] Mosley W H & Bungey J H, Reinforced Concrete Design, ISBN 0 333 53718 1, p137.

[8] British Cement Association (BCA), UK Cement Manufacture and the Environment, p13.

[9] Ellis C & Ulas E, A Preliminary Investigation into the Comparative Performance of FRP and Steel Reinforcement in Medium and High Strength Concrete, Proceedings of the International Conference, Concrete In the Service of Mankind, Dundee, Scotland1996, pp463-472.

CHAPTER 5

5 PART2: HIGH STRENGTH CONCRETE BEAMS WITH GFRP REBARS USING CURVED & STRAIGHT GEOMETRIC CONFIGURATION

5.1 Experimental and Theoretical Results

5.1.1 Behaviour up to Failure

This section covers the second part of the experimental work and was conducted on C60 grade concrete beams using different configurations of 8.77mm diameter GFRP reinforcing bars. The behaviour of the beams in this Part was assessed and integrated similarly to that in Part 1 such as:

- Maximum failure load
- Deflection
- Rebar and concrete strains
- Performance quotient
- Type of failure e.g. flexural or shear
- Scope for improvement in capacity e.g. by changing mode of failure from shear to flexure and utilizing flexural capacity of GFRP rebars

The reinforcement configurations are set out in *Figure 5.1*, *Figure 5.2*, and *Figure 5.3*. The geometrical definition of the 'curved' rebars is expressed mathematically in *Appendix 11*. The physical properties and the summary of the test results are given in *Table 5.1*. It can be seen in *Figure 5.1* that the straight rebars were put straight in the tension zone of the concrete beams. *Figure 5.2* shows the beams reinforced with 2ϕ8.77 and 3ϕ8.77 curved profile GFRP bar only. *Figure 5.3* shows the beam reinforced with 3ϕ8.77 rebars (one rebar curved in the middle and the other two are straight) and 4ϕ8.77 (two rebars curved in the middle and two rebars straight). The results of TB8 from Part 1 and its two repeat tests, RTB8 and RRTB8 were also included in this part together with TTB7 beam which was the only beam reinforced

with 13.19mm diameter GFRP reinforcing bars (see *Table 5.1*). The beam, TRIAL, which contains three curved profile GFRP rebars was initially tested for risk assessment purposes to see what safety precautions would need to be considered for further tests. For this reason, the behaviour of the beam was not fully monitored apart from its load vs deflection response. However, the repeat test for TRIAL beam (RTRIAL) was conducted to obtain more data for its behaviour under bending. From the first part, it was found that the performance of steel and GFRP reinforced beams is comparable and in most cases the existing theory is applicable to both steel and GFRP reinforced beams to predict their structural behaviour under bending. It was also observed that the shear failure is the dominant mode in GFRP reinforced beams for all grades of concrete. The shear failure was sudden and catastrophic in high strength concrete beams reinforced with GFRP and steel reinforced beams and confirmed in *Imam et al's*[1] work. It is mentioned that this type of failure of high strength concrete is particularly relevant in structures which are subjected to earthquake, blast or suddenly applied loads. It is suggested by the author that the ideal solution for overcoming this disadvantage of high strength concrete is adding steel fibres into the mix and in this way also increase the ductility of the material. In Part 2 the work was mainly focused upon the GFRP reinforced beams. It was considered that in order to reduce the propensity to shear failure using different rebar profiles in high strength concrete beams with different geometry could be a solution. In this way it was considered that the ultimate load capacity of the beams could be enhanced together with a reduction in tendency to brittle failure. This chapter presents the results used to examine the behaviour of the beams reinforced with varying rebar profiles.

Table 5.1 The physical properties and test results used in the analysis of Part2

			CONCRETE						REINFORCEMENT					OBSERVATIONS		
No	**Beam Code**	**Rebar Profile**	**Grade**	**Age (days)**	**Slump (mm)**	**Density (kg/m^3) Air/Water**	**f_c Strength (MPa) Air/Water**	**E_c MOE (GPa) Air**	**No-Dia/ Type**	**E_{st}/E_{FRP} MOE (GPa)**	**$f_{st/gfrp}$ Yield/ Ultimate Stress (MPa)**	**A_r Area (mm^2)**	**%Tension Rebar (A_r/bxh)x100**	**Failure Mode**	**Initial Crack Load (kN)**	**Failure Load**
1[1*]	TB8	straight	C60	43	45	2420/2470	72/78	35.00	2-08.77F	45.98	601	120.80	0.58	Flexure	6	26.00
2[1]*	*RTB8*	*straight*	*C60*	*43*	*50*	*2430/2450*	*70/74*	*36.00*	*2-08.77F*	*45.98*	*601*	*121.00*	*0.58*	*Shear*	*4*	*26.40*
3[1]*	*RRTB8*	*straight*	*C60*	*43*	*55*	*2453/2490*	*78/82*	*35.00*	*2-08.77F*	*45.98*	*601*	*121.00*	*0.58*	*Shear*	*6*	*30.00*
4[2**]	TTB3	curved	C60	28	60	2442/2400	77/79	38.00	2-08.77F	45.98	601	121.00	0.57	Shear-Rupture	6	27.20
5[2**]	TRIAL	curved	C60	28	50	2440/2400	77/77	38.00	3-08.77F	45.98	601	181.50	0.86	Shear-Rupture	4	38.60
*6[2**]*	*RTRIAL*	*curved*	*C60*	*28*	*50*	*2450/2470*	*73/80*	*33.00*	*3-08.77F*	*45.98*	*601*	*181.50*	*0.86*	*Shear*	*6*	*38.00*
7[2**]	TTB4	straight	C60	28	50	2440/2460	77/78	39.50	3-08.77F	45.98	601	181.50	0.86	Shear	5.6	34.00
8[2**]	TTB1	straight & curved	C60	28	47	2446/2455	78/77	41.00	3-08.77F	45.98	601	181.50	0.86	Shear	6	35.20
9[2**]	TTB2	straight & curved	C60	29	60	2440/2486	80/75	39.00	4-08.77F	45.98	601	242.00	1.14	Compression	6	52.00
*10[2**]*	*RTTB2*	*straight & curved*	*C60*	*28*	*55*	*2470/2486*	*73/74*	*33.00*	*4-08.77F*	*45.98*	*601*	*242.00*	*1.14*	*Shear*	*4*	*50.00*
11[2**]	TTB7	straight & curved	C60	28	45	2443/2460	70/71	38.00	4-13.19F	38.75	470.7	546.56	2.58	Shear	4	54.00

TB: Test Beam RTB: First Repeat of TB RRTB: Second Repeat of TB TRIAL: The very first of TTBs RTRIAL: First Repeat of TRIAL

TTB: New Test Beam includes new geometry of rebars and concrete strengths and types

[1*]103mm wide(b) x 203mm deep(h) x 2740mm long (2440mm long span)

[2**]104mm wide(b) x 204mm deep(h) x 2740mm long (2440mm long span)

Figure 5.1 Details of the beam reinforced with 2 & 3straight profile GFRP rebars

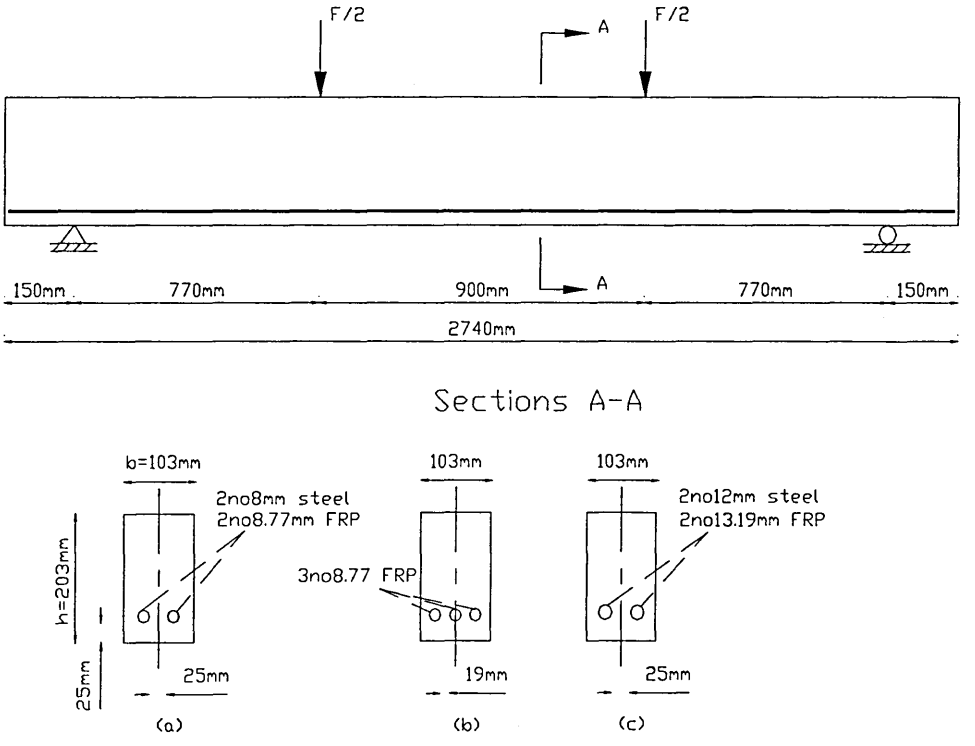

Figure 5.2 Details of the beam reinforced with 2 & 3curved profile GFRP rebars

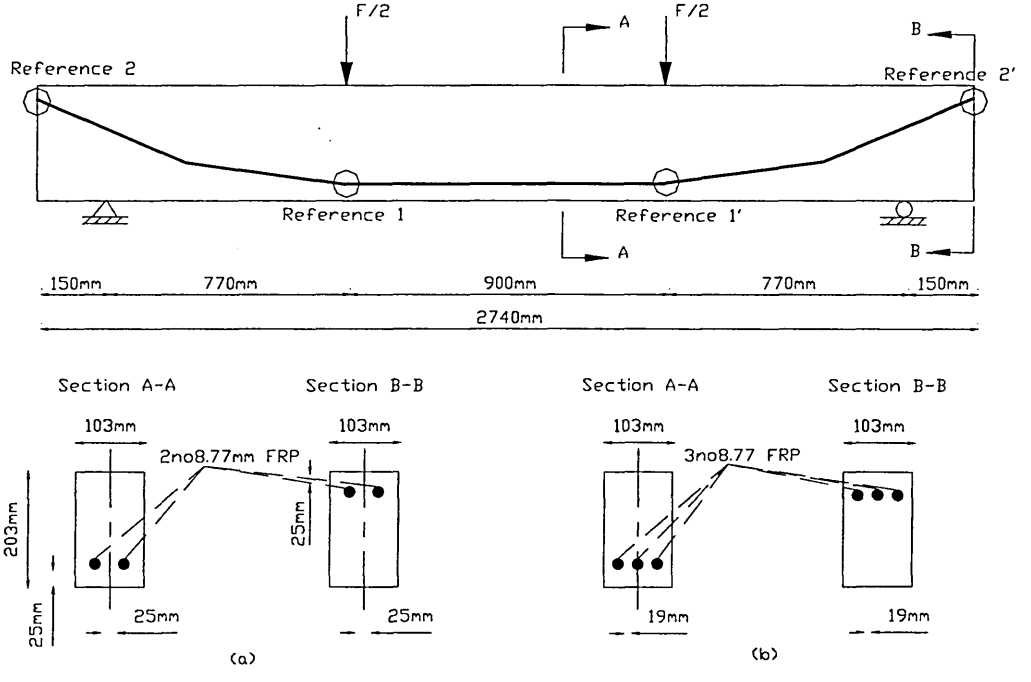

Figure 5.3 Details of the beam reinforced with 3 & 4 straight & curved profile GFRP rebars

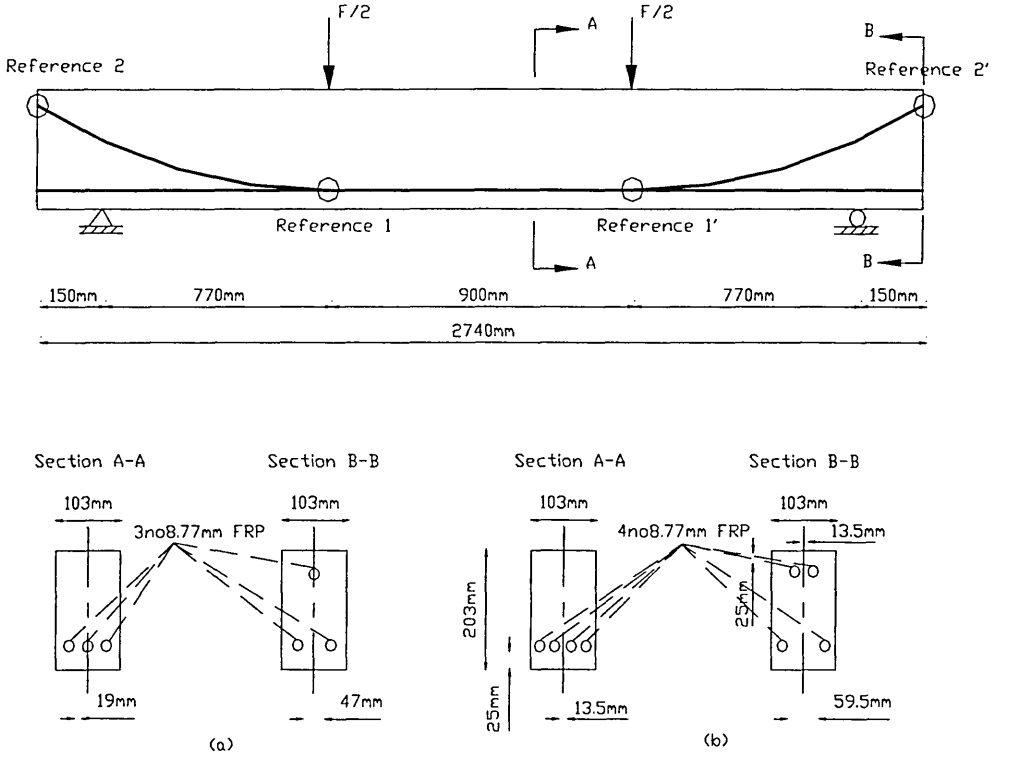

The current design code (BS8110) has a limit for spacing between the horizontal rebars i.e. space between the bars should not be less than maximum size of coarse aggregate (h_{agg})+5 in mm for allowing the concrete to pass between the rebars easily. For this work, the limit for the space between the rebars should be 20+5=25mm. However, it can be noted that this is not the case for the beams reinforced with more than two rebars within 900mm maximum moment region. However, this did not cause a problem for concrete distribution and compaction due to the rebar configuration in the shear zone. The rebar spacing was maintained in the shear zone and subsequent investigation showed that the concrete flowed and compacted satisfactorily around the reinforcing bars.

5.1.2 Reinforcement Stresses and Strains in the Maximum Bending Moment Region

The strain gauges were mounted on the reinforcing bars to measure the strains in the maximum bending moment and shear regions of all the beams. The locations of the strain gauges are shown in *Figure 5.4*.

Figure 5.4 The location of the strain gauges in both shear and maximum bending

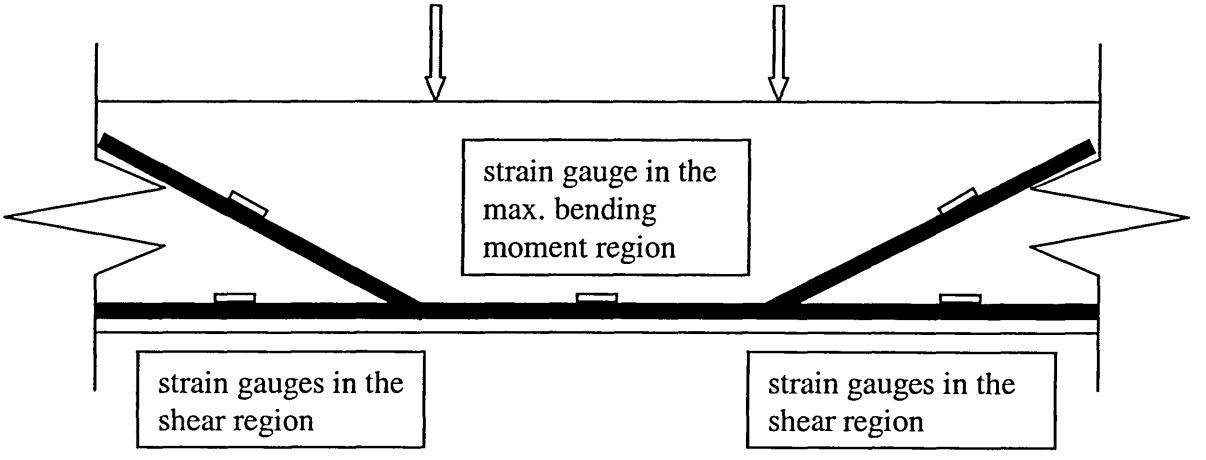

The strains measured from the rebars in each beam in the maximum bending moment region are shown in *Figure 5.5*. The dotted lines in the graph represent the best-fit line up to failure. The Figure shows that the strains up to the initial crack load are linear (elastic limit) for the beams. The gradient of the line then decreases beyond the elastic limit but still continues approximately in a straight line up to failure. It can also be observed that the rebar strains decrease with increasing rebar area at each load increment beyond the elastic portion of the curve. Note that the slope of the curve after the elastic limit is steeper for the beams containing larger rebar area.

(NH) PB° I

Stresses and strains in the reinforcing bars were calculated based on the bending theory at the cracked section (see *Table 5.2*). In the Table, 'calculated' values are based upon substituting the actual (measured) bending moment, second moment of area and the depth of the neutral axis in the theoretical equations (see column 7). The 'measured' values were obtained directly from the experiments (see columns 6, 8 and 9).

The comparison of data in Table 5.2

The tensile stresses and strains in GFRP rebars obtained from 'direct tensile test' and 'beam bending test' are compared in the Table. The stress in the GFRP rebars obtained from the 'tensile' and 'bending' tests are in reasonably good agreement. Also, the agreement between the 'measured' and 'calculated' strains based on the bending test is reasonably good (see column 9 & 10). The results indicated that the maximum tensile stress and strains in the GFRP rebars reach almost their full tensile strain capacity whereas this is not quite the same with ϕ13.19 GFRP rebars (see column 8, 9 & 10). This could be due to the fact that the concrete failed in shear before the rebars reached their maximum tensile capacity. This could also suggest that the bigger that rebar diameter the less the deformation.

Table 5.2 The comparison of tensile stresses and strains in GFRP rebars from the tensile and bending test (using BS8110 equation)

1	2	3	4	5	6	7	8	9	10
				Failure	**Maximum Tensile Stresses in the Rebars (MPa)**		**Maximum Tensile Strains in the Rebars**		
Beam Code	Concrete grade	Rebar No. Dia/Type	Rebar Profile	Mode	**Tensile Test** Measured	**Bending Test** *Calculated	**Tensile Test** Measured	**Bending Test** Measured	**Calculated
TB8	C60	2-08.77F	straight	Flexure	601.00	583.85	0.01300	0.02667	0.01273
RTB8	*C60*	*2-08.77F*	*straight*	*Shear*	*601.00*	*607.11*	*0.01300*	*0.01195*	*0.01323*
RRTB8	*C60*	*2-08.77F*	*straight*	*Shear*	*601.00*	*642.03*	*0.01300*	*0.01132*	*0.01402*
TTB3	C60	2-08.77F	curved	Shear-Rupture	601.00	628.45	0.01300	0.01325	0.01367
RTRIAL	*C60*	*3-08.77F*	*curved*	*Shear*	*601.00*	*554.28*	*0.01300*	*0.01524*	*0.01205*
TTB4	C60	3-08.77F	straight	Shear	601.00	516.14	0.01300	0.01474	0.01123
TTB1	C60	3-08.77F	straight & curved	Shear	601.00	532.67	0.01300	0.01446	0.01158
TTB2	C60	4-08.77F	straight & curved	Compression	601.00	588.52	0.01300	0.01528	0.01280
RTTB2	*C60*	*4-08.77F*	*straight & curved*	*Shear*	*601.00*	*551.34*	*0.01300*	*0.01128*	*0.01199*
TTB7	C60	4-13.19F	straight & curved	Shear	470.70	271.21	0.01200	0.00786	0.00700

*based on BS8110 equation for cracked section using actual bending moment and neutral axis depth

** strains calculated using the calculated stresses

5.1.3 Reinforcement Strains in the Shear Region

The reinforcement strains were measured for all beams in the shear region using strain gauges. In *Figure 5.6*, it can be seen that the strains from the left and the right hand side of the beams follow a similar pattern in that they exhibit linear elastic behaviour up to the point where the crack openings are wide. From this point onwards there is a large proportioned increase in strains until the gauges lose their bond with the rebar. This usually indicates that the failure is more likely be 'shear'.

The purpose of the Figure is to show the 'quantitative' and 'qualitative' difference between 'curved' and 'straight' rebars as well as between each side of the beam. Although, the 'curved' rebars exhibit reduced stiffness in the shear zone, it is also worth noticing that the 'curved' rebars in particular show a distinctive 'upward' trend in stiffness towards failure. The comparison between 2ϕ8.77 (RRTB8)/3ϕ8.77 'straight' (TTB4) and 2ϕ8.77 (TTB3)/3ϕ8.77 (RTRIAL) 'curved' profile rebars showed that the strains for a given load in the curved rebars are larger than the strains in the straight rebars. When comparison is made between 2ϕ8.77 (TTB3) curved and 3ϕ8.77 (RTRIAL) curved rebars, it is apparent that the increase in rebar area enhances the linear-elastic portion of the curve. This could indicate that the cracks are appearing in the shear region of the beam reinforced with 3ϕ8.77 GFRP rebars at a higher applied load compared to the beam reinforced with 2ϕ8.77 GFRP rebars.

(MJP10

5.1.4 Concrete Strains in the Maximum Bending Moment Region

Concrete strains were measured throughout the depth of the beams over a 900mm gauge length (see *Figure 5.7).*

The strain distributions in *Figure 5.8* and *Figure 5.9* show the linearity of the strains and the position of neutral axis across the depth of the beam at each load. It can also be seen in the Figures that the strain distributions of both beams reinforced with 3ϕ8.77 straight and curved profile GFRP rebars are very similar. The neutral axis depth of the beam reinforced with three curved profile rebars seems to be higher compared to the one reinforced with three straight profile rebars i.e. increase in stiffness (see also *Figure 5.7*). It can also be seen that the strains above (compression) the neutral axis are lower compared to the strains below (tension) the neutral axis for both beams.

Figure 5.7 An example of the concrete strains measured at the maximum bending moment region of C60 concrete beams reinforced with 3No. 8.77 straight and curvedprofde GFRP rebars

Figure 5.8 An example strain distribution of C60 grade concrete beam reinforced with 3No8.77 straight profile rebars

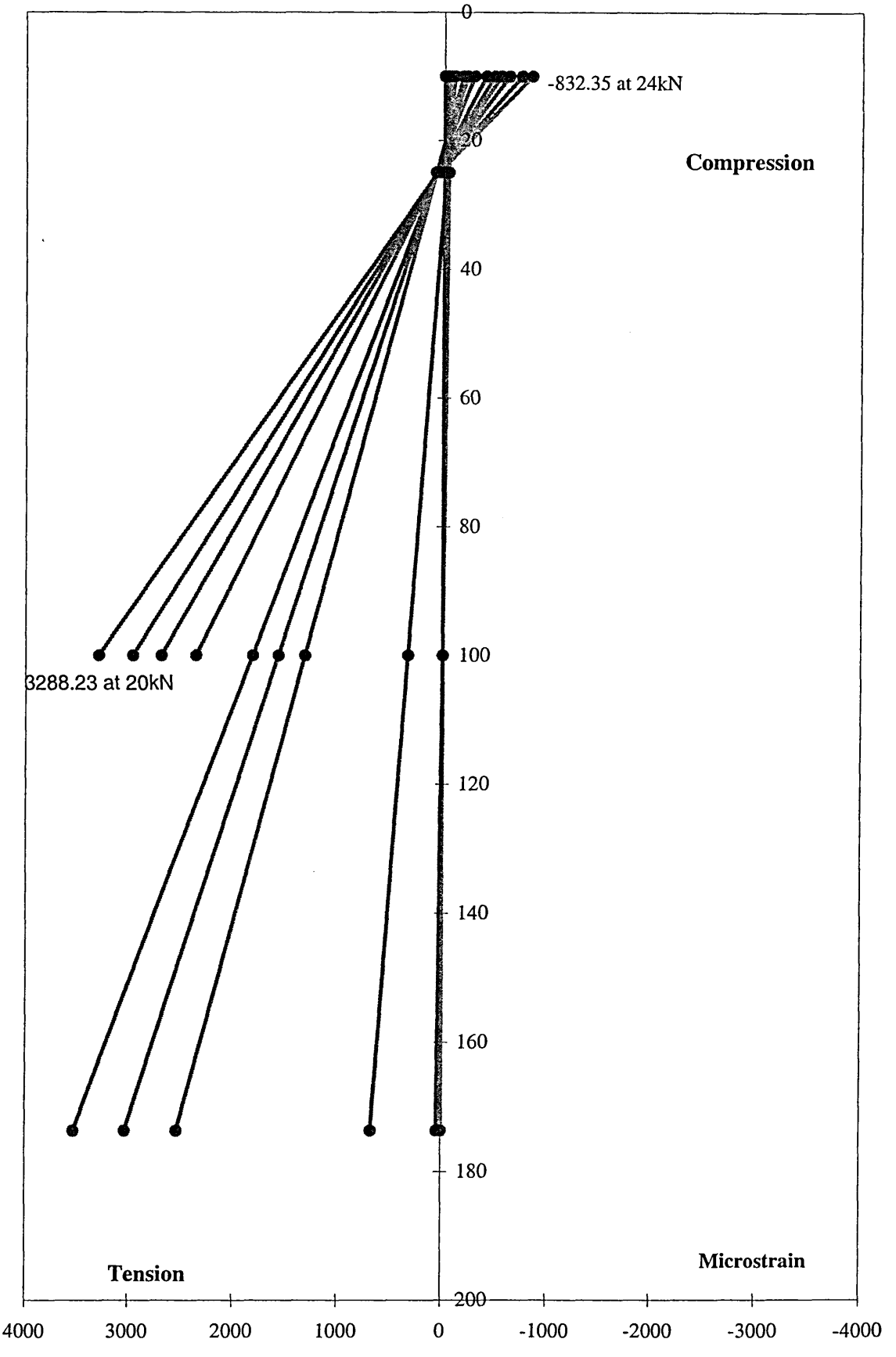

Figure 5.9 An example strain distribution of C60 grade concrete beam reinforced with 3No 8.77 curved profile rebars

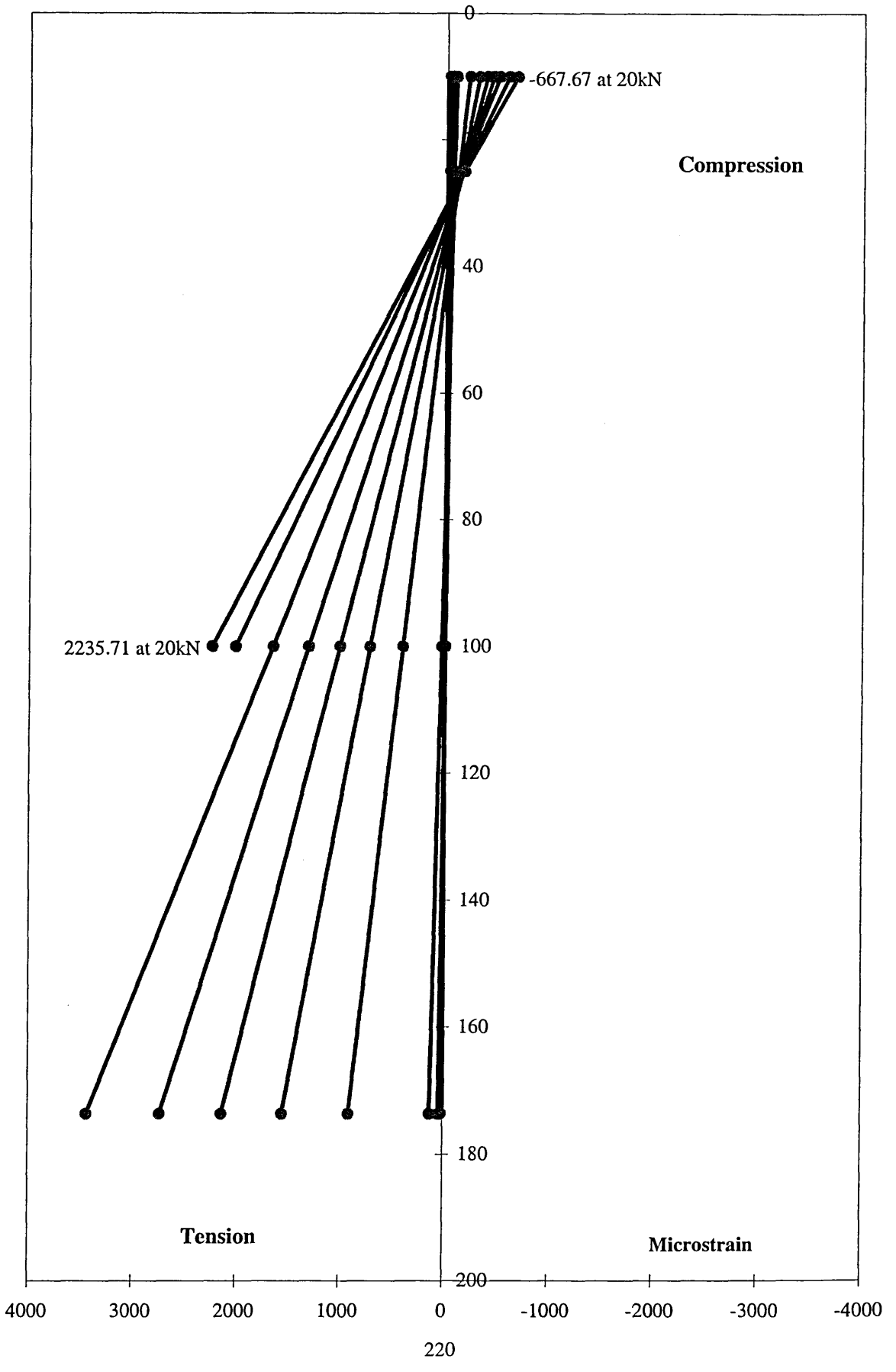

5.1.4.1 Maximum Concrete Compressive Strain

The maximum concrete compressive strain and the experimental neutral axis depth of the beams were determined using the linear line strain distributions (see *Figure 5.8* and *Figure 5.9*).

Table 5.3 Extrapolated maximum concrete compressive strains in the beams

1 Beam Code	2 Concrete grade	3 Rebar No. Dia/Type	4 Rebar Profile	5 Maximum Concrete Comp. Strain
*TB8	C60	2-08.77F	straight	0.0022
*RTB8	C60	2-08.77F	straight	0.0018
*RRTB8	C60	2-08.77F	straight	0.0021
TTB3	C60	2-08.77F	curved	0.0019
TRIAL	C60	3-08.77F	curved	-
RTRIAL	C60	3-08.77F	curved	0.0019
TTB4	C60	3-08.77F	straight	0.0021
TTB1	C60	3-08.77F	straight & curved	0.0019
TTB2	C60	4-08.77F	straight & curved	0.0024
RTTB2	C60	4-08.77F	straight & curved	0.0023
TTB7	C60	4-13.19F	straight & curved	0.0021

*beams tested in Part1 -the beam tested for the risk assessment and only its load vs deflection behavior monitored

The comparison of data in Table 5.3.

- The average compressive strains at failure extrapolated from measured strains on top of the beam are 0.0021. This is approximately 2/3 (approximately 67%) of the maximum design concrete compressive strain given in BS8110.
- The results suggest that the maximum concrete compressive strains of the beams reinforced with 'straight & curved' profile rebars give highervalue (average of 0.0023). The maximum concrete compressive strain of the beams containing curved profile rebars only seems to be slightly lower than the beams containing straight profile rebars for the same rebar area.

5.1.4.2 Neutral axis depth (N.A.) at the uncracked and the cracked sections

The calculation of the 'theoretical' and the 'measured' neutral axis depth of the beams was carried out using the formula given in *Appendix 9*.

Table 5.4 The experimental and the theoretical neutral axis depth of the beams at the uncracked and cracked sections

1	2	3	4	5	6	7
Beam Code	Concrete grade	Rebar No. Dia/Type	Rebar Profile	Neutral axis depth (mm)		
				Theory Uncracked	$Theory_{max}$ Cracked	$Measured_{max}$ Cracked
*TB8	C60	2-08.77F	straight	101.97	20.11	23.30
*RTB8	C60	2-08.77F	straight	101.95	19.87	20.20
*RRTB8	C60	2-08.77F	straight	101.97	20.13	26.40
TTB3	C60	2-08.77F	curved	102.43	19.34	17.70
TRIAL	C60	3-08.77F	curved	102.64	23.38	-
RTRIAL	C60	3-08.77F	curved	102.73	24.96	29.90
TTB4	C60	3-08.77F	straight	102.61	22.97	23.80
TTB1	C60	3-08.77F	straight & curved	102.59	22.57	23.60
TTB2	C60	4-08.77F	straight & curved	102.83	26.39	27.60
RTTB2	C60	4-08.77F	straight & curved	102.97	28.48	32.90
TTB7	C60	4-13.19F	straight & curved	103.53	35.25	40.50

*beams tested in Part1 -the beam tested for the risk assessment and only its load vs deflection behavior monitored

The comparison of data in Table 5.4

Table 5.4 contains the theoretical and the experimental neutral axis depth of the beams.

- As in the previous part, the theoretical neutral axis depth of the beams is in good agreement with the experimental values at the cracked section regardless of the modes of failure (see column 6 and 7).
- For all beams it was observed that the neutral axis depth decreases as the load increases and it becomes almost a constant value towards the failure (see *Figure 5.10*). Note that the neutral axis depths given in *Table 5.4* at the cracked section represent the values at failure.
- The rebar diameter seems to affect the depth of neutral axis i.e. the bigger the diameter of rebar the less the upward movement of the depth of the neutral axis.

- Note that the measured depths of neutral axis at the cracked section are based on the last DEMEC reading at a load close to the failure. It can be seen in that once the section cracks neutral axis depth tends towards a constant value until failure.
- The neutral axis depth of the beam reinforced with 2ϕ8.77curved profile GFRP rebars is less than the beams reinforced with 2ϕ8.77 straight profile beams. This was probably because of reduced average rebar depth over the length of beam. Another reason could be due to the fact that more bending of the beam was occurring with the curved rebars. However, this seems to be an opposite way round with 3ϕ8.77 reinforced beams. The results suggest that the increase in rebars area/diameter decreases the depth of neutral axis less i.e. increase in stiffness of the beam.

5.1.5 Concrete Strains in Shear Region

The concrete strains at the level of reinforcements were measured along a 200mm gauge length in the shear regions i.e. both the right and the left-hand side.

In *Figure 5.1f* it can be seen that the strains obtained from the location where the straight rebars were placed are greater than the strains at the location where the curved rebars were placed. This is probably due to the fact the cracks initiate from the bottom of the beam and increase in length as the load is applied. There is also evidence that when the area of rebar is increased the resistance of the beam in the shear regions also increases. The comparison between reinforcement strains and surface strains at the level of reinforcements *{Figure 5.6* and *Figure 5.11*) show quite good agreement up to the point where cracks are too wide to enable the dial gauge to be used. It seems that the concrete grade has no effect on the magnitude of strains together with the behaviour of the beam in the shear region. The strain gauges installed on the reinforcement give information regarding the shear behaviour of the beams.

Figure 5.11 The concrete strains obtained in the shear regions of the beams

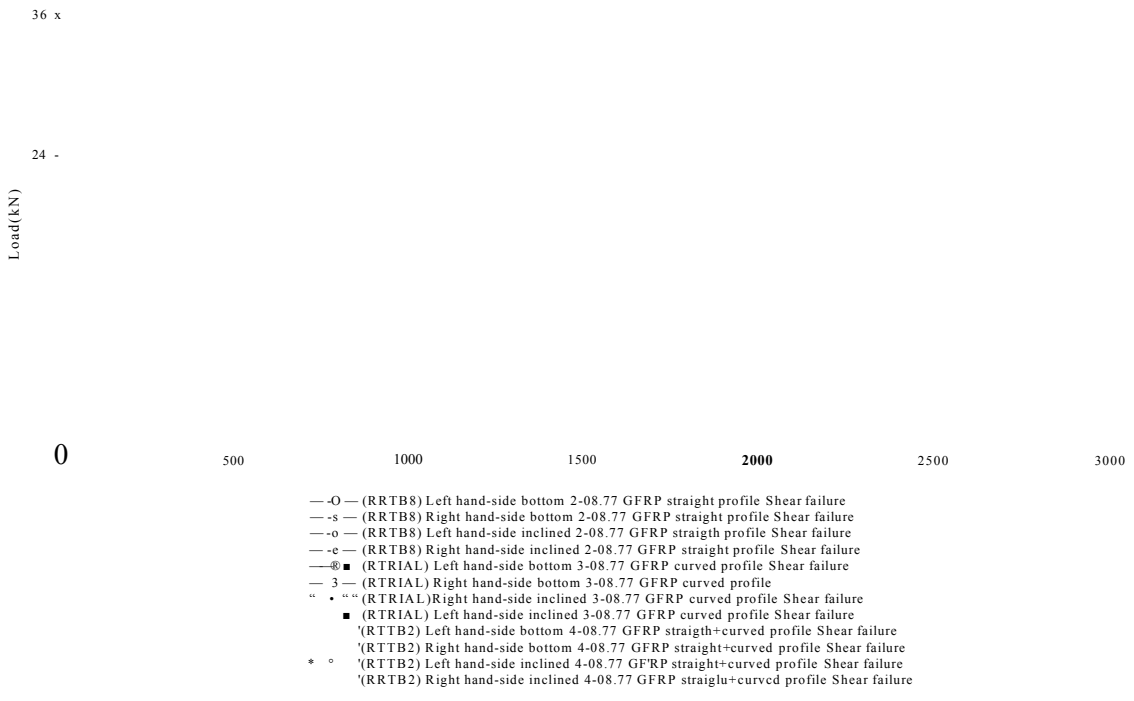

5.1.6 Elastic & Ultimate Load/Moment Capacities

In *Table 5.5*, the theoretical and measured (actual) bending moment capacities of each beam were calculated using the formulae in *Appendix 9*.

The comparison of data in Table 5.5

- In column 7, the initial crack capacity of the beams is more or less the same, 4kN to 6kN. This was also observed in the previous Part of the investigation.
- In columns 9 and 10, initial theoretical moment capacity of the beams reinforced with straight profile rebars seem to be less than the initial measured moment capacity. However, the theoretical and the measured values are in better agreement for the beams containing larger rebar area and curved profile bars.
- Column 8, 11& 12 shows that the difference in ultimate load/moment capacity of the beams reinforced with curved (TTB3) and straight profile (TB8 and its repeats) 2ϕ8.77 GFRP rebars is small. However, the ultimate load/moment capacity of the beams reinforced with curved (RTRIAL) 3ϕ8.77 GFRP rebars is generally higher than the straight (TTB4) profile 3ϕ8.77 GFRP reinforced beam.
- The beam (TTB1) containing 2 straight and 1 curved profile of ϕ8.77 GFRP rebars has an ultimate load/moment capacity less than the curved profile beams and higher than the straight profile beam.
- The results suggest that the ultimate load/moment capacity of the beams reinforced with the same geometry of rebars increases together with increase in rebar area for the same diameter rebars (e.g. compare TB8 with TTB4 or TTB1 with TTB2).
- Note that the ultimate load/moment capacity of the beam reinforced with 4ϕ13.19 is only slightly higher than the 4ϕ8.77 reinforced beams but has twice the rebar area.
- The theory overestimates the ultimate bending moment of the beams at the cracked section. The difference between the theoretical and the actual moment values becomes by between 11% and 26% for ϕ8.77 beams but by 49% for the ϕ13.19 beam.

Table 5.5 Elastic & ultimate load/moment capacity of Part 2 beams obtained from theory and experiment

1	2	3	4	5	6	7	8	9	10	11	12
Beam Code	Concrete grade	Rebar No. Dia/Type	Rebar Profile	Rebar Area (mm^2)	Tension Rebar %	Initial Crack Load kN	Failure Load kN	**Bending Moment (kNm)** Theory Uncracked	Measured Uncracked	$Theory_{max}$ Cracked	$Measured_{m}$ Cracked
*TB8	C60	2-08.77F	straight	121	0.68	6	26.00	1.66	2.68	12.12	10.38
RTB8	*C60*	*2-08.77F*	*straight*	*121*	*0.68*	*4*	*26.40*	*1.11*	*1.91*	*12.14*	*10.53*
RRTB8	*C60*	*2-08.77F*	*straight*	*121*	*0.68*	*6*	*30.00*	*1.66*	*2.68*	*12.14*	*11.92*
TTB3	C60	2-08.77F	curved	121	0.67	6	27.20	1.67	2.69	12.23	10.85
TRIAL	C60	3-08.77F	curved	181.5	1.00	4	38.60	1.67	1.92	18.20	15.24
RTRIAL	*C60*	*3-08.77F*	*curved*	*181.5*	*1.00*	*6*	*38.00*	*2.50*	*2.69*	*18.14*	*15.01*
TTB4	C60	3-08.77F	straight	181.5	1.00	5.6	34.00	2.34	2.53	18.21	13.47
TTB1	C60	3-08.77F	straight + curved	181.5	1.00	6	35.20	2.51	2.69	18.23	13.93
TTB2	C60	4-08.77F	straight + curved	242	1.33	6	52.00	3.34	2.69	24.12	20.40
RTTB2	*C60*	*4-08.77F*	*straight + curved*	*242*	*1.33*	*4*	*50.00*	*2.22*	*1.92*	*24.02*	*19.63*
TTB7	C60	4-13.19F	straight + curved	546.6	3.05	4	54.00	2.21	1.92	41.33	21.17

*beams tested in Part1 -the beam tested for the risk assessment and only its load vs deflection behavior monitored

5.1.7 Ultimate Shear Capacity

The theoretical and the measured shear capacity of the beams are given in *Table 5.6* (see also *Appendix 9* for the formulae used in the calculations).

The comparison of data in Table 5.6.

- The results showed that the shear capacity of the beams increases with increased percentage of reinforcement (see column 6, 9 and 10).
- The comparison between the measured and the theoretical shear capacities indicates that the theory generally overestimates the shear capacity of the beams reinforced with 2 and 3ϕ8.77 curved and straight profile rebars by between 17% and 35% (see column 9 and 10).
- The theoretical and the measured shear capacities of the beams reinforced with 4ϕ8.77 are in a good agreement. However, the theory overestimates the shear resistance of the beam reinforced with 4ϕ13.19 rebars by around 21%. The measured shear capacity of both 4ϕ8.77 and 4ϕ13.19 is comparable.

Table 5.6 Ultimate Shear Capacity of Part 2 Beams

1	2	3	4	5	6	7	8	9	10
Beam Code	Concrete grade	Rebar No. Dia/Type	Rebar Profile	Rebar Area (mm^2)	Tension Rebar %	Shear span/ effective depth	Failure Mode	**Shear Resistance (MPa)** Theory$_{max}$ Cracked	Measured$_{max}$ Cracked
*TB8	C60	2-08.77F	straight	121	0.68	4.43	Flexure	1.00	0.65
*RTB8	C60	2-08.77F	straight	121	0.68	4.43	Shear	1.00	0.66
*RRTB8	C60	2-08.77F	straight	121	0.68	4.43	Shear	1.00	0.75
TTB3	C60	2-08.77F	curved	121	0.67	4.41	Shear-Rupture	0.99	0.67
TRIAL	C60	3-08.77F	curved	181.5	1.00	4.41	Shear-Rupture	1.14	0.94
RTRIAL	C60	3-08.77F	curved	181.5	1.00	4.41	Shear	1.14	0.93
TTB4	C60	3-08.77F	straight	181.5	1.00	4.41	Shear	1.14	0.83
TTB1	C60	3-08.77F	straight & curved	181.5	1.00	4.41	Shear	1.14	0.86
TTB2	C60	4-08.77F	straight & curved	242	1.33	4.41	Compression	1.25	1.26
RTTB2	C60	4-08.77F	straight & curved	242	1.33	4.41	Shear	1.25	1.21
TTB7	C60	4-13.19F	straight & curved	546.56	3.05	4.47	Shear	1.65	1.31

*beams tested in Part1

5.1.8 Deflection

The load vs deflection response of the beams is similar for all configurations of rebars (see *Figure 5.12*) in that the precracked 'stiffness', as indicated by the ratio of load to deflection was considerably greater than the postcracked 'stiffness' (i.e. loads greater than 4kN-6kN).

None of the beams showed yielding plateau beyond the elastic stage i.e. the load vs deflection response was still curvilinear up to beam failure. The 'stiffness' of the beam increases with increase in rebar area; reflected by the small increase in deflection as the load increases for the beams reinforced with more rebar area. It can also be seen in *Figure 5.12* that the beams reinforced with 2ϕ8.77 'straight only' and 'curved only' profile rebars exhibit lower stiffness compared to the beams reinforced with 3ϕ8.77 'straight only' and 'curved only' profile. The beam reinforced with 4ϕ13.19 'curved and straight' profile rebars is stiffer than the beam reinforced with 4ϕ8.77 'curved and straight' profile rebars due to the bigger area of rebars.

u»d p«n

(M x)

The formulae for calculating the deflections of the beams are given in *Appendix 9*. In *Table 5.7* the calculated deflections are based upon the measured (actual) depth of neutral axis depth and the bending moments used in the theoretical formulae. The measured values were obtained directly from the test.

The comparison of data in Table 5.7

- Generally, the calculated deflections of the beams within the elastic limit (first segment of the curve) are smaller than the measured ones.
- The results suggest that the measured deflections at the uncracked section are smaller for the beams containing 4ϕ8.77 (RTTB2) and 4ϕ13.19 (TTB7) 'straight and curved' profile rebars than the rest of the beams. The theoretical deflections of these two beams agree well with the measured ones.
- The maximum calculated deflections of the beams are less than the measured deflections except for TTB2 & RTTB2 when the reverse is true.

Table 5.7 Theoretical and experimental deflections of Part2 beams

1	2	3	4	5	6	7	8	9	10	11	12	13	14
Beam Code	Concrete grade	Rebar No. Dia/Type	Rebar Profile	Rebar Area	Tension Rebar	**Second Moment Area (mm^4)**		**Curvature (1/mm)**		**Deflection (mm)**			
				mm^2	%	*Calculated Uncracked	*Calculated Cracked	*Calculated Uncracked	*Calculated Cracked	*Calculated Uncracked	**$Measured_{max}$ Uncracked	*Calculated Cracked	**$Measured_{max}$ Cracked
[1]*TB8	C60	2-08.77F	straight	120.8	0.58	1.96E+08	3.50E+06	3.91E-07	7.39E-05	0.25	2.80	47.51	64.51
[1] RTB8	*C60*	*2-08.77F*	*straight*	*121*	*0.58*	*8.22E+07*	*3.39E+06*	*6.46E-07*	*7.50E-05*	*0.42*	*0.41*	*48.24*	*57.16*
[1] RRTB8	*C60*	*2-08.77F*	*straight*	*121*	*0.58*	*1.40E+08*	*3.58E+06*	*5.48E-07*	*8.50E-05*	*0.35*	*1.71*	*54.63*	*56.55*
TTB3	C60	2-08.77F	curved	121	0.57	2.19E+08	3.28E+06	3.23E-07	7.56E-05	0.21	2.76	48.63	72.12
TRIAL	C60	3-08.77F	curved	181.5	0.86	-	-	-	-	-	2.85	-	71.42
[2] RTRIAL*	*C60*	*3-08.77F*	*curved*	*181.5*	*0.86*	*8.88E+07*	*5.46E+06*	*9.18E-07*	*7.63E-05*	*0.59*	*0.70*	*49.05*	*54.68*
TTB4	C60	3-08.77F	straight	181.5	0.86	1.89E+08	4.58E+06	3.39E-07	6.70E-05	0.22	2.58	43.08	62.45
TTB1	C60	3-08.77F	straight & curved	181.5	0.86	2.07E+08	4.43E+06	3.16E-07	6.93E-05	0.20	2.71	44.55	67.84
TTB2	C60	4-08.77F	straight & curved	242	1.14	1.94E+08	6.01E+06	3.55E-07	8.15E-05	0.23	1.57	52.43	48.27
RTTB2	*C60*	*4-08.77F*	*straight & curved*	*242*	*1.14*	*9.91E+07*	*7.03E+06*	*5.88E-07*	*7.93E-05*	*0.38*	*0.43*	*51.01*	*48.27*
TTB7	C60	4-13.19F	straight & curved	546.56	2.58	9.00E+07	1.05E+07	5.61E-07	5.02E-05	0.36	0.52	32.26	42.97

[1*] beams tested in Part1 [2*] the beam tested for the risk assessment and only its load vs deflection behavior monitored * Column 7-8 using actual n.a depth * Column 9-10 using actual bending moment

* Column 11-13 using actual curvature ** Column 12-14 experimental readings

5.1.9 Cracking Behaviour

The crack developments in the beams are discussed below and the summary of the average number of cracks for each beam is given in *Table 5.8.*

Table 5.8 The summary of average cracks in the beams

	Load at first crack (kN)			**Number of cracks at failure**		
	Straight	Curved	Straight & Curved	Straight	Curved	Straight & Curved
2 rebarsØ8.77	4/6	6	-	11	9	-
3 rebarsØ8.77	5.6	4/6	6	11	14	12
4 rebarsØ8.77	-	-	4/6	-	-	15
4 rebarsØ13.19	-	-	4	-	-	16

2ϕ8.77 'straight only' and 'curved only' profile GFRP rebars in C60 Concrete Beams

The crack patterns of the beams are shown in *Figure 5.13.* Typically, first hairline cracks appeared at the maximum bending moment region under 4kN/6kN total load in the beams and subsequently grew more prominent and numerous as the load increased. Flexural and diagonal cracks developed in both types of beams in a similar manner.

Figure 5.13 The cracks patterns of the beams reinforced with 2ϕ8.77 'straight only' and 'curved only' profile GFRP

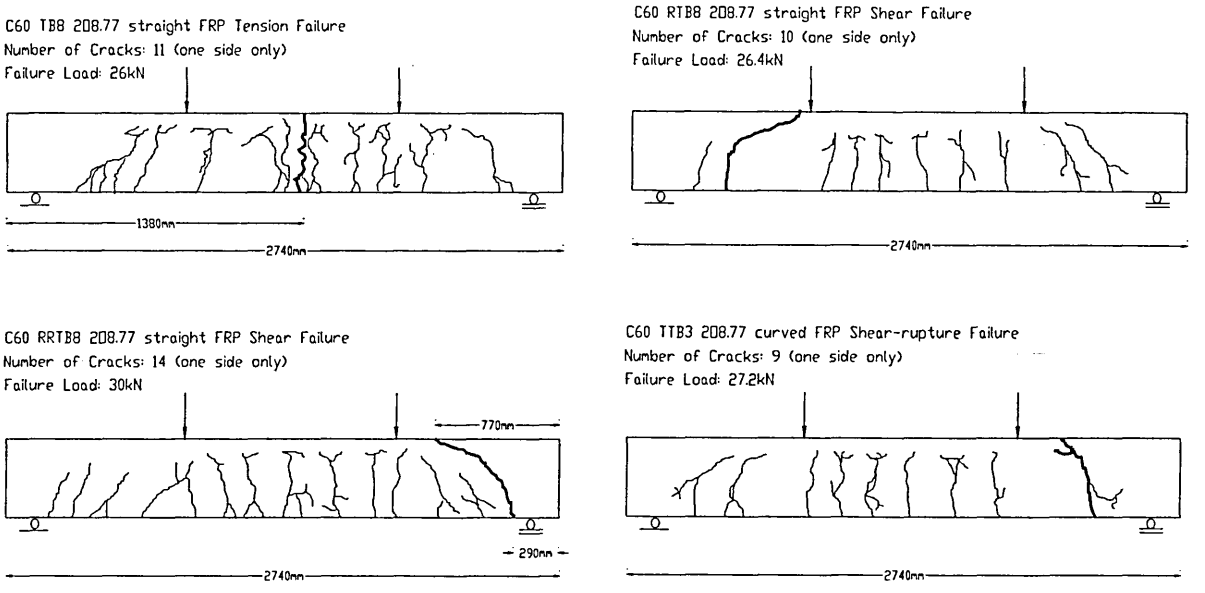

3ϕ8.77 'straight only' and 'curved only' and 'straight and curved' profile GFRP rebars in C60 Concrete Beams

The crack propagation in the pre and post cracking stages of the beams in this category is very similar to the previous category except the flexural cracks in this category are longer and closer to the top edge of the beams. Also more cracks were developed in the beams (see *Figure 5.14*). The average number of cracks in the beams reinforced with curved profile rebars is more than the straight profile beams. Note that the number of shear cracks is more in the curved profile beams compared with straight profile beams.

Figure 5.14 The cracks patterns of the beams reinforced with 3ϕ8.77 'straight only', 'curved only', 'straight and curved' profile GFRP

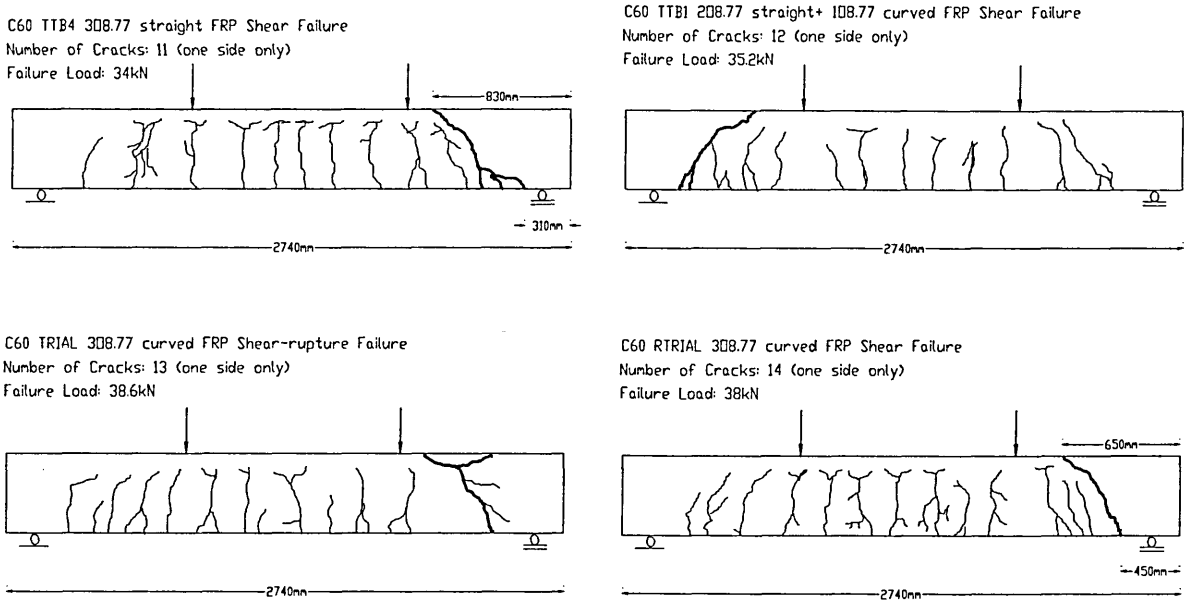

4ϕ8.77 combined with 'straight and curved' profile GFRP rebars in C60 Concrete Beams

The cracks that developed in these beams were similar to the previous ones except this time more branches appeared and the spacing between the cracks was closer (see *Figure 5.15*). The number of cracks observed in the beams was quite similar to the beams containing three curved GFRP rebars. In this category, the cracks were propagating with small increase in length at each load applied. This was started half way through to the load until the beams failed. This is probably due to the fact that these beams have higher load carrying capacities than the others.

Figure 5.15 The cracks patterns of the beams reinforced with 4ϕ8.77 'straight and curved' profile GFRP

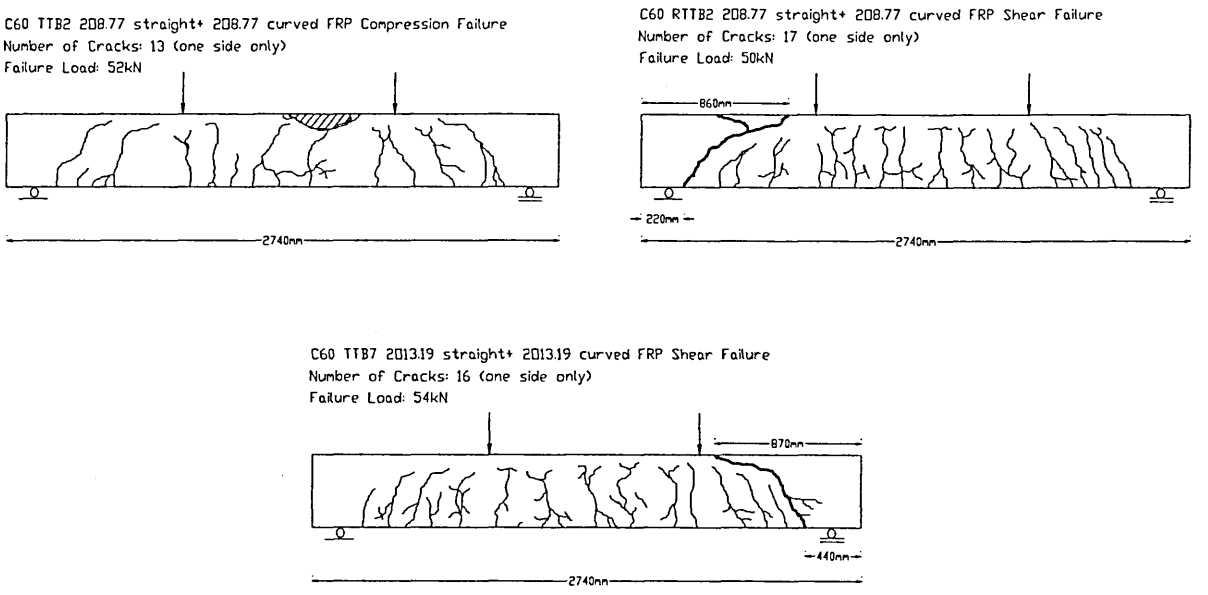

5.1.9.1 Modes of Failure

The typical shear-rupture and compression failures of the beams are shown in *Photo5.1* and *Photo 5.2*. The morphology of beam failures is given in *Table 5.9*. All beams except TB8 (reinforced with 2ϕ8.77 'straight only' profile rebars) and TTB2 (reinforced with 4ϕ8.77 'straight and curved' profile rebars) failed in shear at the ultimate condition. TB8 and TTB2 failed in flexure and compression respectively. Initially, vertical cracks developed from the bottom surface within the middle section and these were followed by diagonal cracks towards the supports in all cases.

The flexure failure occurred catastrophically in TB8 reinforced 2ϕ8.77 'straight only' profile rebars and the beam snapped at the midspan. Although, the repeats of TB8 i.e. RTB8 and RRTB8, failed in shear they both had a similar load capacity to TB8. The beams reinforced with 2ϕ8.77 and 3ϕ8.77 'curved only' profile rebars resulted in shear-rupture failure meaning that the beam was broken in the shear region and the rebars snapped. The rest of the beams exhibited shear failure as the diagonal crack widened between the load point and support. It should be noted that the failures in the beams containing curved profile rebars were more controlled in terms of the energy absorption and its dissipation within the beams even when the rebars were ruptured i.e. failed less suddenly.

Photo5.1 A view of 'shear-rupture' failure of 2<j)8.77 GFRP 'curved only' profile reinforced C60 grade concrete beam (code TTB3)

Photo 5.2 A view of 'compression' failure of 4<>8.77 GFRP 'straight and curved' profile

The beam reinforced with 4ϕ8.77 (code TTB2) straight and curved profile rebars failed in compression at the top of the beam between loading points [video clip of TTB2 can be viewed on *ttb2_part1, 2&3.mov* files from the compact disk]. On this occasion the failure scenario was different. The main diagonal cracks at both ends of the beam opened up wide and became dominant suggesting that the curved rebars were still intact and taking up more load together with the straight rebars in the tension zone. This gave more resistance to the beam against bending. More branches were developed on the flexural and shear cracks while the load was applied. The stress in the vertical flexural cracks due to the stress transfer from the shear regions and the bending was eventually released resulting in concrete being crushed at the top together with shear failures on both ends of the beam. The failure was remarkable since the GFRP rebars did not yield but the beam behaved like an over reinforced beam and everything failed together. This could be described as a 'balanced' failure.

The repeat test of TTB2, RTTB2 was performed in a similar manner except the beam had a main diagonal crack on both ends which resulted in shear failure. However, the repeat beam had a very close load carrying capacity to TTB2. It was noted that the number of cracks and the branches was more in the repeat test beam (RTTB2) than TTB2.

Table 5.9 The modes of failure of ϕ8.77 and ϕ13.19 'straight only', 'curved only' and 'straight and curved' profile GFRP Reinforced C60 Concrete Beams

Beam Code	Concrete Grade (Cube Strength MPa)	Rebar No Dia/Type (Profile)	Failure Morphology (Failure Load-kN)
TB8	C60(72)	2ϕ8.77 GFRP (straight)	**Flexure(balanced)**-Catastrophic failure at the midspan, concrete broke in two parts, GFRP bars disintegrated in the same region (26)
RTB8	C60(70)	2ϕ8.77 GFRP (straight)	**Shear**-Diagonal tension crack propagated across the section outside the maximum bending moment region (26.4)
RRTB8	C60(78)	2ϕ8.77 GFRP (straight)	**Shear**-Diagonal tension crack propagated across the section outside the maximum bending moment region (30)
TTB3	C60(77)	2ϕ8.77 GFRP (curved)	**Shear Rupture**-Diagonal tension crack propagated across the section outside the maximum bending moment region and the rebars snapped (27.2)
TRIAL	C60(77)	3ϕ8.77 GFRP (curved)	**Shear Rupture**-Diagonal tension crack propagated across the section outside the maximum bending moment region and the rebars snapped (38.6)
RTRIAL	C60(73)	3ϕ8.77 GFRP (curved)	**Shear**-Diagonal tension crack propagated across the section outside the maximum bending moment region (38)
TTB4	C60(77)	3ϕ8.77 GFRP (straight)	**Shear**-Diagonal tension crack propagated across the section outside the maximum bending moment region (34)
TTB1	C60(78)	3ϕ8.77 GFRP (straight & curved)	**Shear**-Diagonal tension crack propagated across the section outside the maximum bending moment region (35.2)
TTB2	C60(80)	4ϕ8.77 GFRP (straight & curved)	**Compression**- Double shear together with concrete crushed in the compression zone (52)
RTTB2	C60(73)	4ϕ8.77 GFRP (straight & curved)	**Shear**-Diagonal tension crack propagated across the section outside the maximum bending moment region on both ends, concrete at the top broken in the shear region with a wedge shape (50)
TTB7	C60(70)	4ϕ13.19 GFRP (straight & curved)	**Shear**-Diagonal tension crack propagated across the section outside the maximum bending moment region on both ends but, the failure occurred at weak end (54)

5.1.9.2 Estimation of Flexural Crack Widths

Theoretical and experimental estimations of the maximum crack widths are given in *Table 5.10.* The values were obtained from the equations which are given in *Appendix 9.*

Table 5.10 The estimated crack widths of Part 2 Beams

1	2	3	4	5	6	7
Beam Code	Concrete grade	Rebar No. Dia/Type	Rebar Profile	[1]*Number of Cracks	**Estimated crack widths (mm)** [2]**BS8110	[3]***Experiment
*TB8	C60	2-08.77F	straight	11	0.89	0.74
RTB8	*C60*	*2-08.77F*	*straight*	*10*	*0.95*	*0.87*
RRTB8	*C60*	*2-08.77F*	*straight*	*14*	*0.76*	*0.50*
TTB3	C60	2-08.77F	curved	9	1.26	1.27
TRIAL	C60	3-08.77F	curved	13	-	-
RTRIAL	*C60*	*3-08.77F*	*curved*	*15*	*0.62*	*0.38*
TTB4	C60	3-08.77F	straight	11	1.00	0.84
TTB1	C60	3-08.77F	straight & curved	12	0.85	0.65
TTB2	C60	4-08.77F	straight & curved	13	0.92	0.65
RTTB2	*C60*	*4-08.77F*	*straight & curved*	*16*	*0.74*	*0.43*
TTB7	C60	4-13.19F	straight & curved	16	0.53	0.31

*beams tested in Part1 -the beam tested for the risk assessment and only its load vs deflection behavior monitored

[1]*in the maximum bending moment region [2]**based upon the formulae [3]**based upon the dial gauge measurements

The values of max crack widths calculated using the equations in BS8110 are higher than the experimentally estimated values based on using dial gauge method (except for TTB3 where both values are very similar). As a general observation, it seems that when flexural and shear cracks have more branches, this could indicate a strong bond between the rebars and the concrete, thus reducing the maximum crack width in the maximum bending moment region i.e. the more the branches the less the width of maximum crack.

5.2 Performance Quotient (Q_p)

The performance quotient formula is given in *Appendix 9*. The performance quotients of the beams are given in *Table 5.11*. The Q_p of the beams showing similar load carrying capacities and reinforced with 2ϕ8.77 'straight only' and 'curved only' profile GFRP rebars is comparable.

However, the Q_p of the beams reinforced with 3ϕ8.77 'curved only' profile rebars probably due to their higher load carrying capacity and the geometry of the rebars is higher than the beam reinforced with 3ϕ8.77 'straight only' profile rebars.

It can be seen in the Table (column 13) that the Q_p of the beams having higher load capacity is also generally higher. This is possibly due to the fact that the increase in the number and profile change of rebars increases the stiffness of the beams. The 'concrete term' has disproportionate effect on the dominator term in the Q_p whereas the load capacity is more sensitive to rebar area. The combination of 'straight and curved' profile of rebars used in the beams (TTB2, RRTB2 and TTB7) give a highest Q_p. Also, when comparing the beams TTB2, RTTB2 reinforced with 4ϕ8.77 'straight and curved' profile rebars which TTB7 reinforced with 4ϕ13.19 'straight and curved' profile rebars, the Q_p of TTB7 is higher than both TTB2 and RTTB2 owing to the fact that the failure load of TTB7 is higher.

Table 5.11 Performance quotient of Part 2 Beams

1 Beam Code	2 Concrete grade	3 Rebar No. Dia/Type	4 Rebar Profile	5 Width b mm	6 Height h mm	7 Rebar Area (mm^2)	8 Beam Self Weight kN	9 Failure Mode	10 Failure Load kN	11 Yield/Ultimate Stress MPa	12 Cube Strength MPa	13 Perform. Quotient	14 Ranking
*TB8	C60	2-08.77F	straight	103	203	121	1.36	Flexure	26.00	601	72	0.0173	10
*RTB8	C60	2-08.77F	straight	103	203	121	1.37	Shear	26.40	601	70	0.0182	9
*RRTB8	C60	2-08.77F	straight	103	203	121	1.38	Shear	30.00	601	78	0.0185	8
TTB3	C60	2-08.77F	curved	104	204	121	1.39	Shear-Rupture	27.20	601	78	0.0166	11
TRIAL	C60	3-08.77F	curved	104	204	181.5	1.39	Shear-Rupture	38.60	601	76	0.0234	5
RTRIAL	C60	3-08.77F	curved	104	204	181.5	1.40	Shear	38.00	601	74	0.0236	4
TTB4	C60	3-08.77F	straight	104	204	181.5	1.39	Shear	34.00	601	77	0.0205	7
TTB1	C60	3-08.77F	straight & curved	104	204	181.5	1.39	Shear	35.20	601	78	0.0209	6
TTB2	C60	4-08.77F	straight & curved	104	204	242	1.39	Compression	52.00	601	78	0.0300	3
RTTB2	C60	4-08.77F	straight & curved	104	204	242	1.41	Shear	50.00	601	73	0.0307	2
TTB7	C60	4-13.19F	straight & curved	104	204	546.56	1.39	Shear	54.00	470.7	70	0.0325	1

*beams tested in Part1 -the beam tested for the risk assessment and only its load vs deflection behavior monitored

5.3 Conclusions

The performance of high strength concrete beams reinforced with GFRP rebars studied under two point loading. The rebars were put in the beams in three geometrical combinations ('straight only', 'curved only' and 'straight and curved' profiles) to identify the differences in their performances. The test results compared with theory (BS8110) based upon the same aspects as in Chapter 4.

The results indicated that the maximum tensile stresses and strains in the ϕ8.77 GFRP rebars reach almost their full tensile capacity whereas with ϕ13.19 GFRP this is approximately 58% of the tensile capacity (see *Table 5.2*). The maximum 'measured' strains in larger diameter (ϕ13.19) are less than the smaller diameter (ϕ8.77) rebars indicating that the bigger the rebar area the less the deformation.

Theoretical neutral axis depth of the beams is in good agreement with the experimental values at the cracked section regardless of the modes of failure. For all beams it was observed that the neutral axis depth decreases as the load increases and it becomes almost a constant value towards the failure (see *Figure 5.10*). The results suggest that the increase in rebars area/diameter increases the depth of neutral axis i.e. increase in stiffness of the beam.

The initial crack (visible) load of the beams is not affected either by the diameter of the rebars or the profile of the rebars and it is 4kN to 6kN on average (see *Table 5.5*).

The ultimate load carrying capacity of the beams is influenced by the rebar areas but also partly by the rebar configurations. The results showed that the ultimate load capacity of the beams is higher when the number of rebars/area is increased in the beams (see *Table 5.5*). The beams reinforced with 4ϕ8.77 and 4ϕ13.19 straight and curved profile rebars had the highest load carrying capacities of the group.

The theory overestimates the ultimate bending moment of the beams at the cracked section. The difference between the theoretical and the measured moment values becomes less when 4ϕ8.77 used in the beams. Overall, the ultimate loads/moments

suggest that the capacity of the beam increases with increase in rebar area and is enhanced by a curved profile (see ranking as evidence in *Table 5.11*).

Actual shear capacity of all beams increases with increase in rebar area (see *Table 5.6*). The experimental results of the beams reinforced with 3ϕ8.77 GFRP rebars indicated that the 'curved profile' contributes to the shear resistance of the beams (see also *Table 5.6*).

All the beams behaved in elasto-plastically up to first visible crack i.e. the slope of load vs deflection is steeper up to the initial crack load and beyond this point the slope decreases (see *Figure 5.12*). The slope in the elastoplastic stage is dominated by the rebar area i.e. the bigger the rebar area the steeper the slope. Overall, the calculated deflections where theoretical formula used are smaller than the measured ones at the uncracked section (see *Table 5.7*) except TTB2 and RTTB2 where reverse is true. Generally, the maximum calculated deflections of the beams are less than the measured deflections except TTB2 and RTTB2 where reverse is true. The rebar area and the configuration of the rebars seem to affect the deflection of the beams i.e. the greater the area of rebars the less the deflection. Furthermore, when straight and curved profile rebars are combined in the beam there is a reduction in deflection results.

The pattern of crack propagation in the beams is generally similar. However, beams reinforced with curved profile rebars seem to have more shear cracks compared to the beams reinforced with straight rebars. The beams reinforced with 4ϕ8.77/13.19 combined with straight and curved profile rebars developed more cracks and the gaps between them seem to be reduced (*Figure 5.15*).

The equation for predicting the crack widths can be employed for the beams reinforced with different configurations of GFRP rebars (*Table 5.10*). It seems that observing the number of shear cracks and the number of branches on the flexural and shear cracks could be very helpful to estimate the crack widths.

Overall, the mode of failure appears to be a shear type but rebar configuration seems to have an effect on behaviour of the beams approaching failure. The double shear occurrence is more common in the beams reinforced with 4ϕ8.77/13.19 'straight and curved' profile rebars.

Performance Quotient (Q_p) correlates well with the ultimate load carrying capacity of the beams and is also be influenced by the rebar area and the rebar geometry (see *Table 5.11*). However, this approach although fundamentally attractive gives a considerable weighting to concrete strength and is possibly disproportionate in terms of financial and environmental efficiency. The results suggest there is evidence that the optimum rebar configuration can enhance the performance of the concrete beams and that using a combination of 'straight and curved' profile GFRP rebars in the beams is a better solution for preventing a catastrophic type of failure as well for a better control in ultimate and the serviceability conditions. The next chapter is mainly focused upon this rebar geometry with different type/strength concrete beams

5.4 REFERENCES

[1] Imam M et al, Proportioning and Properties of very High Strength Concrete with and without Steel Fibres, Proceedings of the International Conference, Concrete 2000, September 1993, p1693-1705.

CHAPTER 6

6 PART3: BEAMS OF VARIOUS CONCRETE TYPES REINFORCED WITH OPTIMUM GFRP REBAR CONFIGURATIONS

6.1 Experimental and Theoretical Results

6.1.1 Behaviour up to Failure

This Part of the investigation was based upon the experimental results obtained from Part 2 (Chapter 5). Using the combination of 'straight and curved' (optimum) profile GFRP rebars in the high strength concrete beams suggested that higher load carrying capacity could be achieved. This rebar profile could also reduce the chance of the beam failing catastrophically. A total number of fifteen beams, eight beams reinforced with 4ϕ8.77 (two rebars curved in the middle and two rebars straight close to the edges) and seven beams reinforced with 4ϕ13.19 with the same rebar configurations, were tested under two point bending (see *Figure 6.1*). This Part contains beams manufactured from normal and lightweight concrete mixes. The cementitious material of microsilica (silicafume) and chopped glass fibres were added to the concrete mixes for some of the beams.

The performance of various types of concrete beams reinforced with optimum configuration of GFRP rebars was studied in this part of the programme. The physical properties used in the analysis of the beams are given in *Table 6.1*.

Table 6.1 The physical properties and test results used in the analysis of Part 3

		CONCRETE						REINFORCEMENT					OBSERVATIONS		
No	Beam Code	Grade	Age (days)	Slump (mm)	Density (kg/m^3) Air/Water	f_c Strength (MPa) Air/Water	E_c MOE (GPa) Air	No-Dia/ Type	E_{st}/E_{FRP} MOE (GPa)	$f_{st/gfrp}$ Yield/ Ultimate Stress (MPa)	A_r Area (mm^2)	% Tension Rebar (A_r/bxh)x100	Failure Mode	Initial Crack Load (kN)	Failure Load
1[1*]	TTB5	C20	28	60	2413/2436	43/44	34	4-08.77F	45.98	601.00	242.00	1.14	Shear/Shear	6	96
2[1*]	RTTB5	C20	28	75	2413/2416	44/44	30	4-08.77F	45.98	601.00	242.00	1.14	Shear	6	42.8
3[1*]	TTB6	C20	28	70	2410/2440	43/45	31	4-13.19F	38.75	470.70	546.56	2.58	Shear	4	37.2
4[1*]	TTB8	C20 LT	29	85	1983/2033	45/45	21	4-8.77F	45.98	601.00	242.00	1.14	Shear	4	34
5[1*]	TTB9	C20 LT	28	55	1973/2013	48/47	22	4-13.19F	38.75	470.70	546.56	2.58	Shear	4	39
6[1*]	TTB10	C20 SIL	28	55	2416/2406	59/64	34	4-08.77F	45.98	601.00	242.00	1.14	Shear	6	42
7[1*]	TTB11	C20 SIL	28	55	2340/2438	51/66	32	4-13.19F	38.75	470.70	546.56	2.58	Shear	6	42
8[1*]	TTB12	C20 LT SIL	28	30	1960/2010	63/64	24	4-08.77F	45.98	601.00	242.00	1.14	Shear/Shear	4	32
9[1*]	TTB13	C20 LT SIL	28	30	1993/2026	61/66	24	4-13.19F	38.75	470.70	546.56	2.58	Shear	4	36
10[1*]	TTB20	C40	28	85	2420/2440	61/64	34	4-08.77F	45.98	601.00	242.00	1.14	Shear	4	44
11[1*]	TTB17	C40 FB	28	N/A	2376/2403	56/52	35	4-08.77F	45.98	601.00	242.00	1.14	Shear	6	46.8
12[1*]	TTB19	C40	28	65	2416/2443	59/61	34	4-13.19F	38.75	470.70	545.56	2.57	Shear	4	50
13[1*]	TTB18	C40 FB	28	N/A	2390/2390	59/59	33	4-13.19F	38.75	470.70	546.56	2.58	Shear	6	51.4
14[1*]	TTB14	C50 LT	29	35	1993/2023	69/69	25	4-08.77F	45.98	601.00	242.00	1.14	Shear/Shear	6	30
15[1*]	TTB15	C50 LT	28	85	1973/2000	62/63	23	4-13.19F	38.75	470.70	546.56	2.58	Shear/Shear	6	37.7

TTB: New Test Beam includes new geometry of rebars and concrete strengths and types RTTB: Second Repeat of TTB [1*]104mm wide(b) x 204mm deep(h) x 2740mm long (2440mm long span)

LT (Lightweight concrete) SIL (Silica added concrete) FB (Glass fibre added concrete) *** note that all the rebar profiles are the combination of 'straight and curved'**

Figure 6.1 Details of the beam reinforced with optimum GFRP rebar configurations

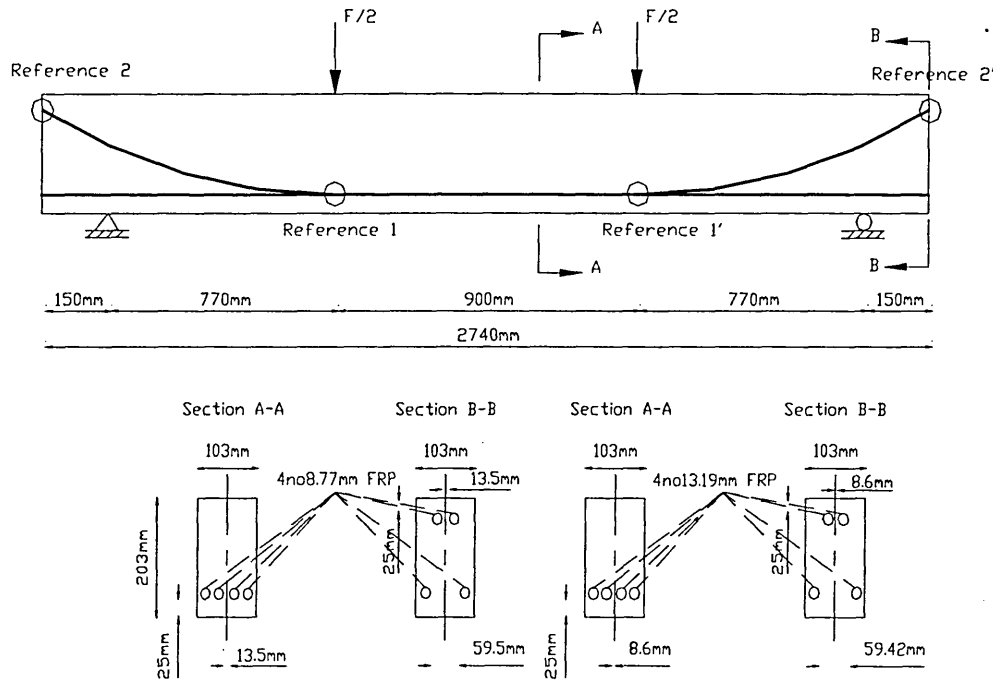

6.1.2 Reinforcement Stresses and Strains in the Maximum Bending Moment Region

The rebar strains were measured in three different locations as in Part 2 i.e. two shear regions and the maximum bending moment region. The rebar strains versus applied loads in the maximum bending moment region are shown in *Figure 6.2*. The strains exhibit linear elastic behaviour up to the initial crack load for all beams. Beyond this point the slope of the curve becomes less steep, however, strains still continue on a straight line up to failure. The results showed that the ϕ8.77 GFRP rebars are under the influence of higher stress during bending compared to stresses in ϕ13.19 GFRP rebars. This is presumably because of longer strains in ϕ8.77 rebars. The Figure also shows that the beams reinforced with the same diameter rebars fall into two separate groups with the ϕ8.77 rebars attaining lower loads and higher strains at failure than the ϕ13.19 rebars.

The rebar strains obtained from TTB5 followed the same trend up to 56kN (*see Figure 6.2*). However, beyond this point the strains started to reduce as the load applied was increased and rapidly followed a vertical straight line up to failure. This discontinuity in the relationship could be due to the strain gauges having lost their circuits or adhesion. This failure load was abnormally high compared with others in the group (the behavior of the is discussed in the 'deflection' section).

Stresses and strains in the reinforcing bars were calculated based on bending theory (see *Appendix 5),* at the cracked sections (see *Table 6.2*). In the Table, 'calculated' values are based upon substituting the actual (measured) bending moment, second moment of area and the depth of the neutral axis in the theoretical equations (see columns 6 and 9). The 'measured' values were obtained directly from the 'tensile' and 'bending' tests (see columns 5, 7 and 8).

The comparison of data in Table 6.2

- ϕ8.77 GFRP and ϕ13.19 rebars in the beams (except TTB5) reached approximately 67% and 46% respectively, of their ultimate tensile capacity on average
- Generally, the rebar strains measured from the bending test agreed well with the 'calculated' strains. The deformation in the small diameter (ϕ8.77) rebar strains was higher than the larger diameter (ϕ13.19) rebars at failure. Note that the rebar strains do not seem to be affected by the type of concrete.

Table 6.2 The comparison of tensile stresses and strains in GFRP rebars from the tensile and bending test (using BS8110 equation)

1	2	3	4	5	6	7	8	9
Beam Code	Concrete grade	Rebar No. Dia/Type	Failure Mode	**Maximum Tensile Stresses in the Rebars (MPa)**		**Maximum Tensile Strains in the Rebars**		
				Tensile Test	**Bending Test**	**Tensile Test**	**Bending Test**	
				Measured	*Calculated	Measured	Measured	**Calculated
TTB5	C20	4-08.77F	Shear/Shear	601.00	1104.22	0.01300	-	0.02402
RTTB5	*C20*	*4-08.77F*	*Shear*	*601.00*	*433.38*	*0.01300*	*0.00873*	*0.00943*
TTB6	C20	4-13.19F	Shear	470.70	200.87	0.01200	0.00555	0.00518
TTB8	C20 LT	4-8.77F	Shear	601.00	368.90	0.01300	0.00716	0.00802
TTB9	C20 LT	4-13.19F	Shear	470.70	190.84	0.01200	0.00500	0.00492
TTB10	C20 SIL	4-08.77F	Shear	601.00	414.49	0.01300	0.00801	0.00901
TTB11	C20 SIL	4-13.19F	Shear	470.70	218.51	0.01200	0.00529	0.00564
TTB12	C20 LT SIL	4-08.77F	Shear/Shear	601.00	354.49	0.01300	0.00621	0.00771
TTB13	C20 LT SIL	4-13.19F	Shear	470.70	182.56	0.01200	0.00392	0.00471
TTB20	C40	4-08.77F	Shear	601.00	419.75	0.01300	0.00968	0.00913
TTB17	C40 FB	4-08.77F	Shear	601.00	486.75	0.01300	0.01070	0.01059
TTB19	C40	4-13.19F	Shear	470.70	268.49	0.01200	0.00565	0.00693
TTB18	C40 FB	4-13.19F	Shear	470.70	253.27	0.01200	0.00809	0.00654
TTB14	C50 LT	4-08.77F	Shear/Shear	601.00	329.90	0.01300	0.00542	0.00717
TTB15	C50 LT	4-13.19F	Shear/Shear	470.70	188.20	0.01200	0.00442	0.00486

6.1.3 Reinforcement Strains in the Shear Region

The reinforcement strains measured for all beams in the shear region using strain gauges. It can be seen in *Figure 6.3* that the strains measured in the left and right hand-side of the beams followed a very similar pattern (particularly until the appearance of a crack in the shear region). This applies to both rebar profiles i.e. straight and curved. The 'blue' and the 'black' lines on the graph represent 'curved' and 'straight' profile rebars respectively. The results suggest that the deformation in large diameter rebars is less compared to the smaller diameter rebars in the shear regions. This could also indicate that the shear resistance of the beams increases with increased rebar area/diameter.

Figure 6.3 A typical GFRP rebar shear strains measured from the microsilica added lightweight concrete beams reinforced with 4(j).8.77 and 4(j)13.19

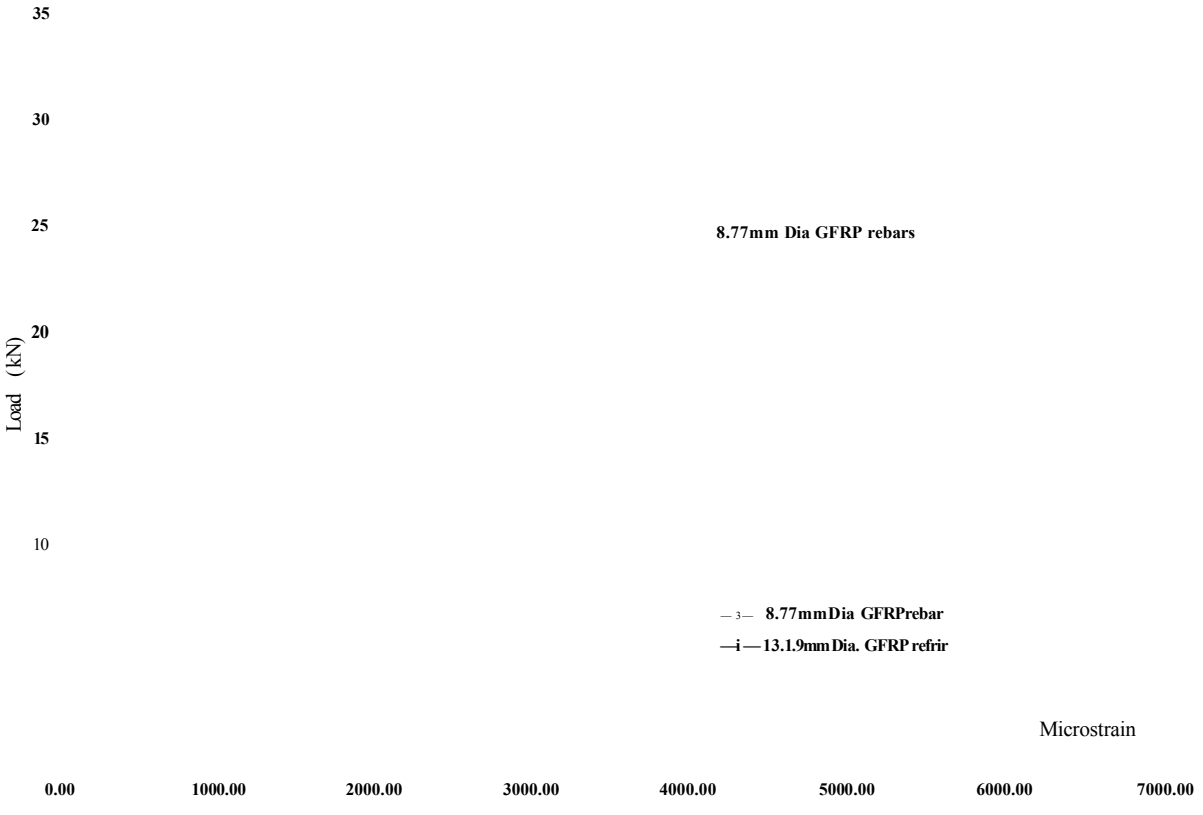

6.1.4 Concrete Strains in Maximum Bending Moment Region

The tensile strains were measured in the concrete throughout the depth of the beams over a 900mm gauge length. In *Figure 6.4* and *Figure 6.5*, it can be seen that the strains above (compression) the neutral axis are lower compared to the strains below (tension) the neutral axis for all beams, due to the fact that concrete is strong in compression and weak in tension. Strain distributions in *Figure 6.6* and *Figure 6.7* show the linearity of the strains and the changes in neutral axis across the depth of the lightweight concrete beams at each load. It can be seen that the neutral axis depth of the beam reinforced with smaller diameter (ϕ8.77) GFRP rebars is less than the one reinforced with larger (ϕ13.19) GFRP rebars.

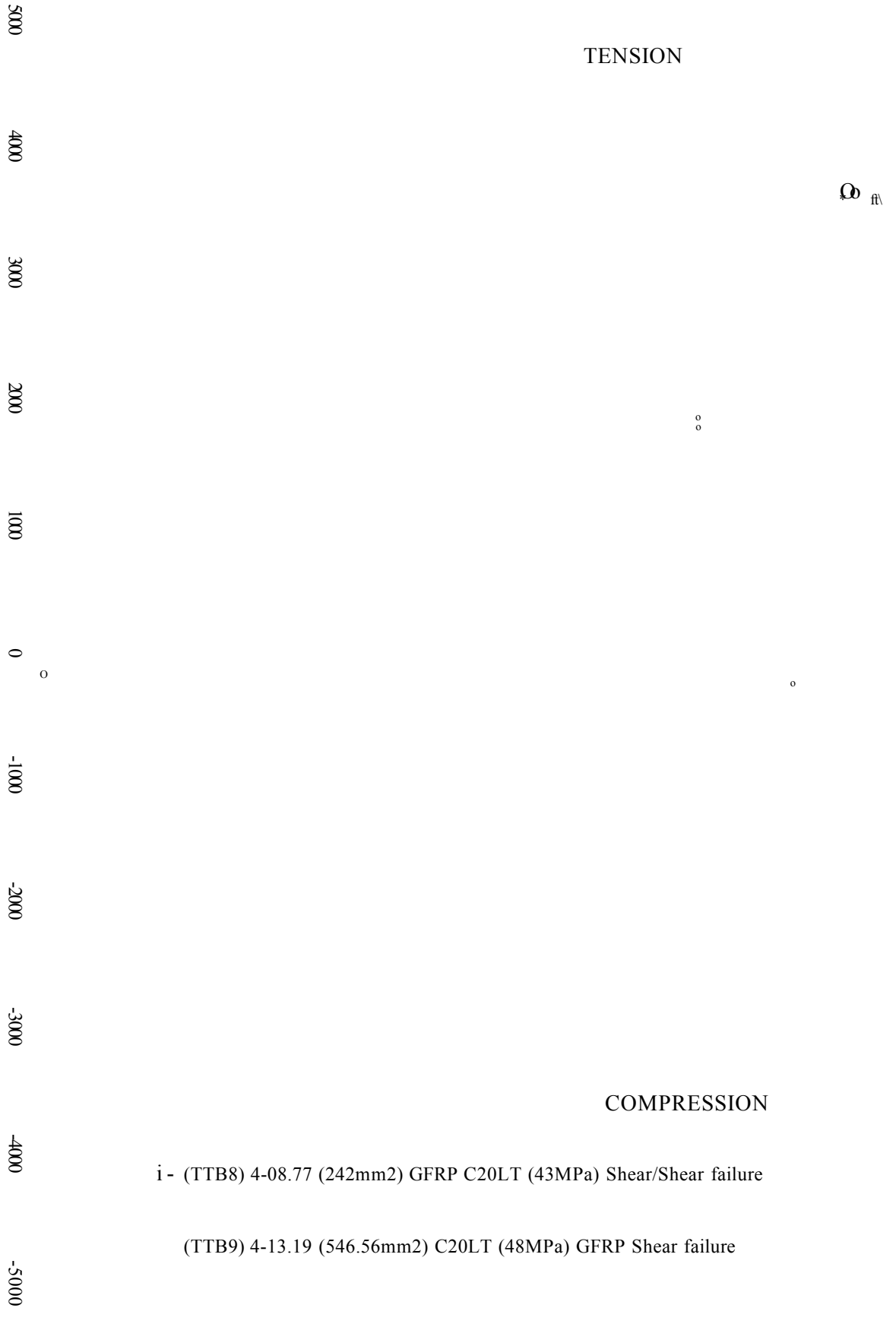
5000
4000
3000
2000
1000
0
-1000
-2000
-3000
-4000
-5000
TENSION
COMPRESSION
i - (TTB8) 4-08.77 (242mm2) GFRP C20LT (43MPa) Shear/Shear failure
(TTB9) 4-13.19 (546.56mm2) C20LT (48MPa) GFRP Shear failure

Figure 65 An example of the concrete strains measured at the maximum bending moment region C50 lightweight concrete beams

TENSION

5000 4000 3000 2000 1000 0 -1000 -2000 -3000 -4000 -5000

COMPRESSION

>- (TTB14) 4-08.77 (242mm2) GFRP C50LT (69MPa) Shear/Shear failure

(TTB15) 4-13.19 (546.56mm2) GFRP C50LT (62MPa) Shear/Shear failure

Figure 6.6 An example strain distribution of C20 grade lightweight aggregate concrete beam reinforced with 4No 8.77 'straight and curved' profile rebars

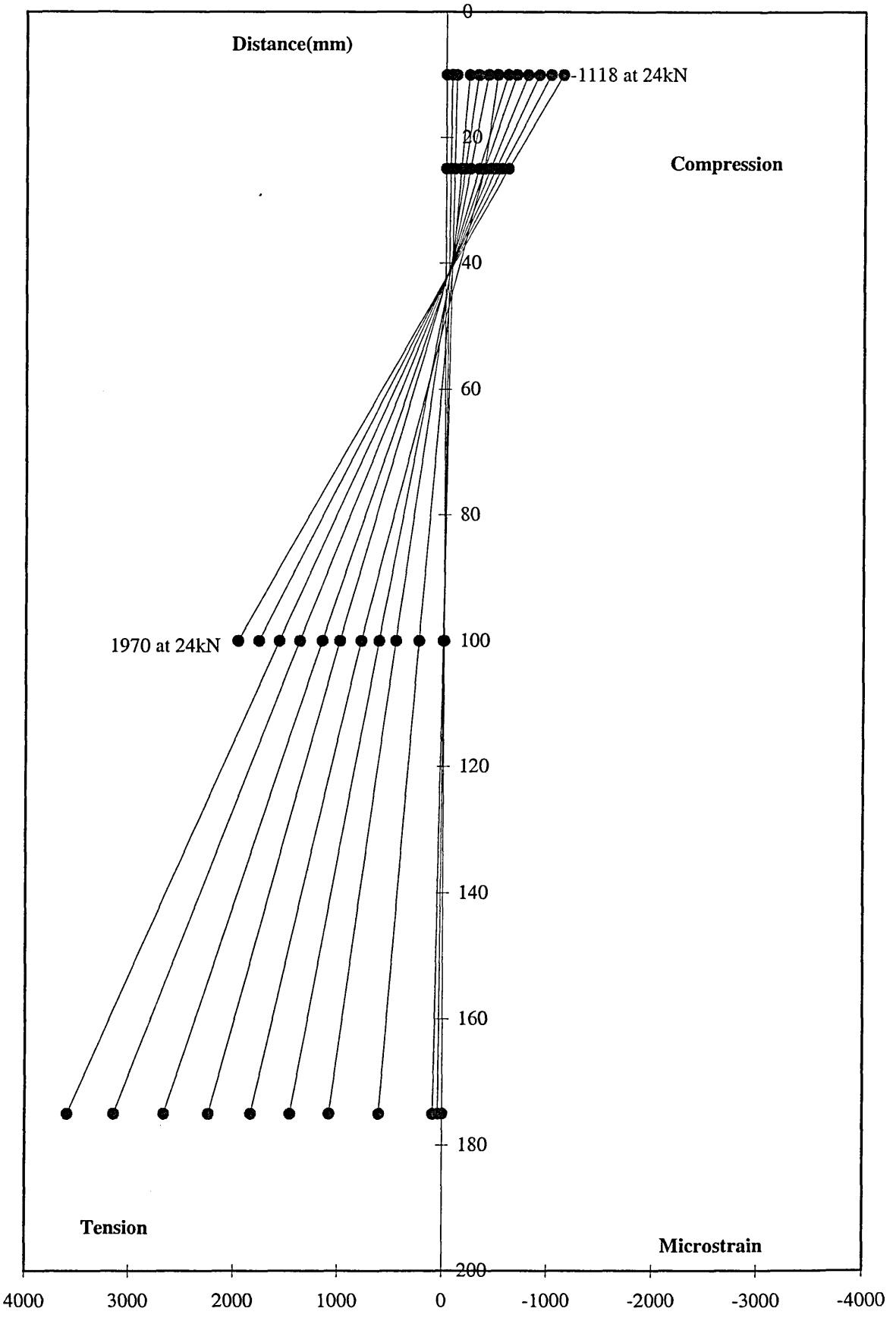

Figure 6.7 An example strain distribution of C20 grade lightweight aggregate concrete beam reinforced with 4No 13.19 'straight and curved' profile rebars

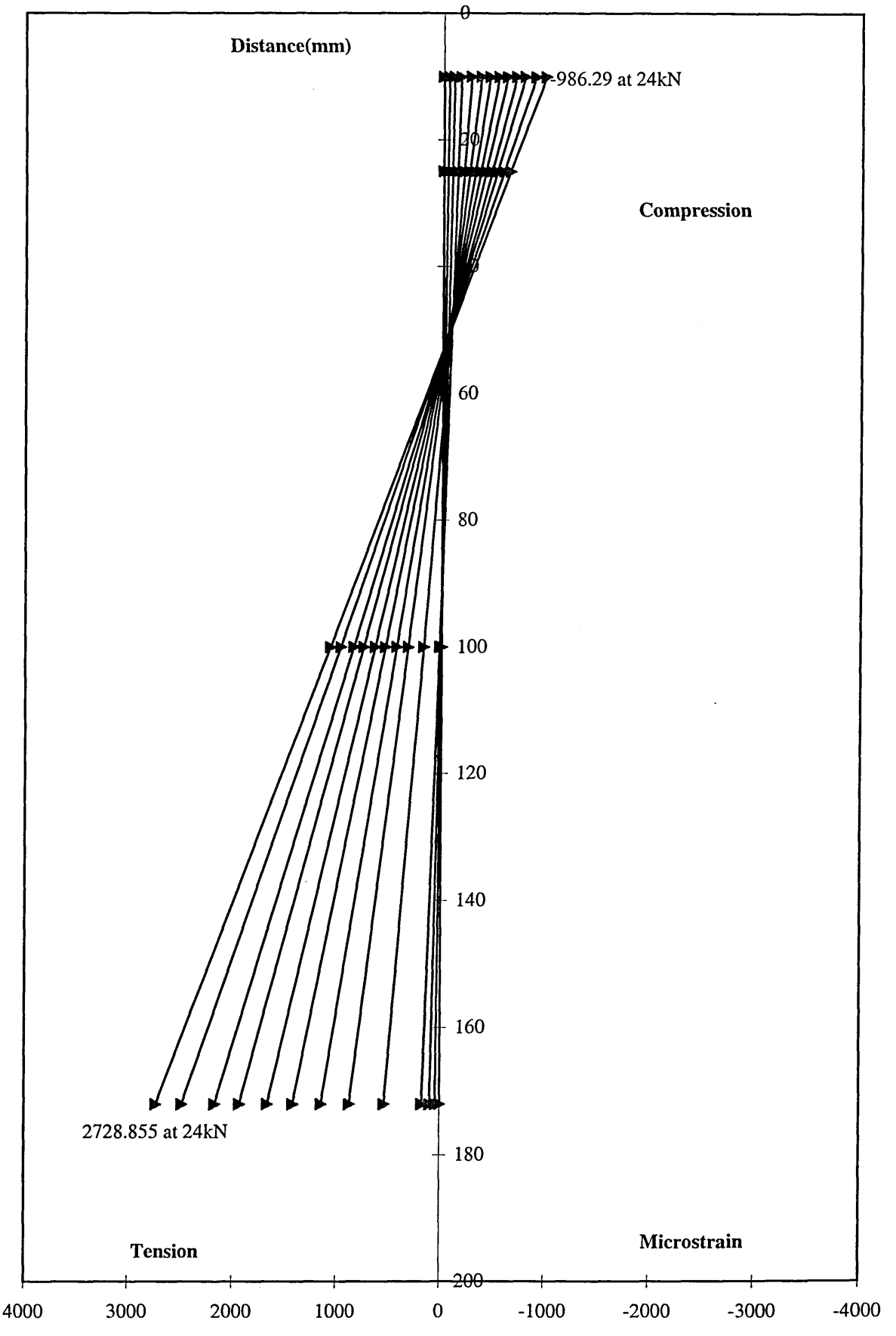

6.1.4.1 Maximum Concrete Compressive Strain

The maximum concrete compressive strain and the experimental neutral axis depth of the beams were determined from the strain distributions (see *Figure 6.6* and *Figure 6.7*). The maximum concrete strains are given in *Table 6.3*. The method followed for calculating the maximum compressive strains is given in *Appendix 5*.

Table 6.3 Extrapolated maximum concrete compressive strains in the beams

1 Beam Code	2 Concrete grade	3 Rebar No. Dia/Type	4 Max. Concrete Comp. strain
TTB5	C20	4-08.77F	-
RTTB5	C20	4-08.77F	0.0027
TTB6	C20	4-13.19F	0.0019
TTB8	C20 LT	4-8.77F	0.0022
TTB9	C20 LT	4-13.19F	0.0022
TTB10	C20 SIL	4-08.77F	0.0020
TTB11	C20 SIL	4-13.19F	0.0015
TTB12	C20 LT SIL	4-08.77F	0.0017
TTB13	C20 LT SIL	4-13.19F	0.0015
TTB20	C40	4-08.77F	0.0017
TTB17	C40 FB	4-08.77F	0.0024
TTB19	C40	4-13.19F	0.0023
TTB18	C40 FB	4-13.19F	0.0022
TTB14	C50 LT	4-08.77F	0.0016
TTB15	C50 LT	4-13.19F	0.0017

The comparison of data in Table 6.3

- The average maximum concrete compressive strain of 0.0027 obtained from C20 normal weight concrete beam reinforced with 4ϕ8.77 GFRP rebars. This is the highest value of all and is approximately 77% of the maximum design concrete compressive strain, 0.0035.
- Based upon the results, the maximum compressive strain of C20 silica added normal weight, C20 silica added lightweight and C50 lightweight concrete beams are less than the rest of the beams, approximately 0.0016 (this is approximately 46% of the maximum design concrete compressive strain of 0.0035).
- The results suggest that there is no dominant influential factor operating between different types of concrete beams for the maximum compressive strain.

6.1.4.2 Neutral axis Depth at the uncracked and the cracked sections

The theoretical and measured neutral axis depths of the beams are given in *Table 6.4*. The values for each beam were calculated using the formula given in *Appendix 5*. The results suggest similar findings as in Part1 and Part2 of the experimental study.

The comparison of data in Table 6.4

- The theoretical neutral axis depth (at ultimate) of all types of the beams is generally less than the corresponding measured ones at the cracked section except for the beams of TTB10 and TTB20 (see columns 5 and 6).

- It can also be observed that the neutral axis depth decreases once the beam cracks and it becomes almost a constant value towards the failure (see *Figure 6.8*).
- Generally, the neutral axis depth of the beams reinforced with 4ϕ8.77 GFRP rebars is only slightly less than the beams reinforced with 4ϕ13.19.

Table 6.4 The experimental and the theoretical neutral axis depth of the beams at the uncracked and cracked sections

1	2	3	4	5	6
Beam Code	Concrete grade	Rebar No. Dia/Type	**Neutral axis depth (mm)** Theory Uncracked	Theory$_{max}$ Cracked	Measured$_{max}$ Cracked
TTB5	C20	4-08.77F	102.95	28.16	25.00
RTTB5	C20	4-08.77F	103.08	29.81	40.20
TTB6	C20	4-13.19F	103.85	38.46	38.10
TTB8	C20 LT	4-8.77F	103.52	34.91	42.00
TTB9	C20 LT	4-13.19F	104.58	44.59	53.70
TTB10	C20 SIL	4-08.77F	102.95	28.10	39.80
TTB11	C20 SIL	4-13.19F	103.79	37.93	41.30
TTB12	C20 LT SIL	4-08.77F	103.33	32.89	38.10
TTB13	C20 LT SIL	4-13.19F	104.37	42.97	49.40
TTB20	C40	4-08.77F	102.95	28.10	41.40
TTB17	C40 FB	4-08.77F	102.93	27.79	36.10
TTB19	C40	4-13.19F	103.69	36.90	36.20
TTB18	C40 FB	4-13.19F	103.74	37.42	44.90
TTB14	C50 LT	4-08.77F	103.29	32.36	37.90
TTB15	C50 LT	4-13.19F	104.47	43.76	51.40

LT (Lightweight concrete) SIL (Silica added concrete)

FB (Glass fibre added concrete)

N.A.(mm)

6.1.5 Concrete Strains in the Shear Region

The concrete strains at the level of main 'straight' rebars and at the level of 'curved' rebars were measured along 200mm gauge length in the shear regions (see *Figure 6.9*). The concrete strains of all the beams exhibited similar trends as in *Figure 6.10.* It can be seen in the Figure that the strains obtained from the level of main rebars are greater than those obtained from the inclined plane as in Part I and Part II (see also *Table 6.5*). In the Table, strain in 'straight' rebars is approximately twice that in 'curved' rebars at higher loads. This partly explained by the curved rebars being much closest to the neutral axis. In the Table, the average ratio of strains at key points [20kN and 38kN] in cycle of Ø8.77:Ø13.19 is 2.25 compared with the ratio of rebar areas of 2.26 for Ø13.19:Ø8.77 respectively (see *Table 6.5*). This could be an evidence that when the area of rebar is increased the stiffness of the beam in the shear regions also increases. It can also be seen that the curved profile rebars contribute to the shear and flexural resistance and stiffness of the beams.

Figure 6.9 The location of DEMEC disks in the shear region

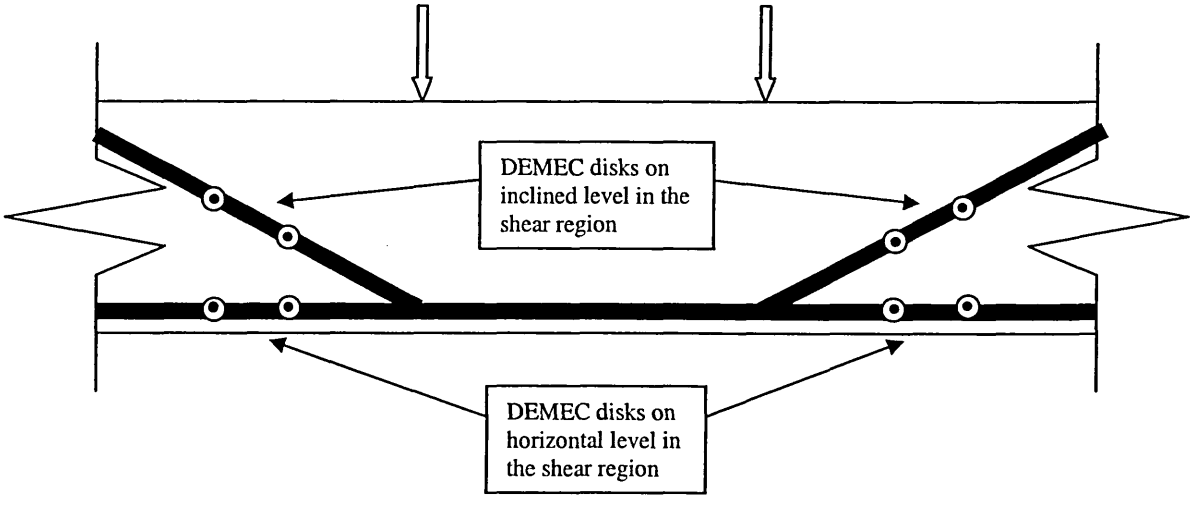

Table 6.5 A typical glassfibre added concrete strains measured from the shear regions of the beams reinforced with 4ϕ.8.77 and 4ϕ13.19 (microstrain)

	TTB17 4No. 8.77 GFRP C40 FB				**TTB18 4No 13.19 GFRP C40 FB**			
Position	*174.61mm*	*174.61mm*	*inclined*	*inclined*	*172.4mm*	*172.4mm*	*inclined*	*inclined*
Load (kN)	**Av. Straight concrete strain (Left)**	**Av. Straight concrete strain (Right)**	**Av. Curved concrete strain (Left)**	**Av. Curved concrete strain (Right)**	**Av. Straight concrete strain (Left)**	**Av. Straight concrete strain (Right)**	**Av. Curved concrete strain (Left)**	**Av. Curved concrete strain (Right)**
0	0	0	0	0	0	0	0	0
2	15	5	0	15	15	15	5	0
4	25	30	15	10	30	0	15	10
6	35	20	15	15	35	35	15	10
8	40	30	15	15	50	35	10	10
10	45	25	15	20	60	50	20	15
12	50	45	15	25	75	55	25	20
14	50	50	25	35	80	60	25	15
16	60	250	20	30	95	70	30	15
18	80	255	25	40	70	105	35	30
20	410	265	180	40	125	170	40	60
22	585	280	260	45	135	225	40	90
24	730	635	335	185	175	250	55	105
26	885	895	440	335	250	345	90	140
28	1065	1080	545	430	625	495	295	230
30	1245	1240	655	515	790	675	395	320
32	1430	1435	765	580	945	860	490	430
34	1630	1715	875	660	1075	1035	570	530
36	1895	2445	1040	790	1245	1230	675	645
38	2675	3775	1565	1925	1435	1475	780	775

(\P0PBOT

6.1.6 Elastic & Ultimate Load/Moment Capacities

Table 6.6 contains the theoretical and measured (actual) bending moment together with the initial crack and ultimate load capacities of the beams. Note that the initial crack load in the Table designates the first visible crack observed in the maximum bending moment region (see also *Appendix 5* for the formulae used in the calculations).

The comparison of data in Table 6.6

- Column 6 shows that the initial load capacity of the beams varies between 4kN and 6kN confirming the general trend in Part1 and Part2 test programmes. The rebar diameter/area and type of concrete have no significant effect on the initial load capacity.
- The highest ultimate load of 96kN was obtained for the beam (TTB5) reinforced with 4ϕ8.77 GFRP rebars (see column 7). This beam performed in a rather unusual manner compared to the rest of the beams included in Part1 and Part2. Its behaviour is discussed in the 'deflection' section.
- The lightweight aggregate concrete beams including those containing microsilica, failed at lower loads than the rest of the beams (see column 7). The average failure load obtained for these beams reinforced with 4ϕ8.77 and 4ϕ13.19 is 32kN and 38kN respectively. The results indicate that the concrete type seems to have an influence on the ultimate load/moment capacities.
- Generally, theory overestimates the bending moment capacity of the beams at the uncracked section compared to those measured (applied). The results suggest that the measured bending moment capacity of the beams reinforced with 4ϕ8.77 and 4ϕ13.19 is approximately 82 % that of the theoretical bending moment (see column 8 and 9).
- The theory also overestimates the bending moment capacity of the beams at the cracked (ultimate) section compared to those measured (applied). The difference between the theoretical and the measured values varies depending on the type of concrete i.e. the measured values are between 35% and 76% that of the theoretical values (see columns 10 and 11).

Table 6.6 Elastic & Ultimate Load/Moment Capacity of Part 3 Beams obtained from theory and experiment

1	2	3	4	5	6	7	8	9	10	11
Beam Code	Concrete grade	Rebar No. Dia/Type	Rebar Area (mm^2)	Tension Rebar %	Initial Crack Load kN	Failure Load kN	**Bending Moment (kNm)** Theory Uncracked	Measured Uncracked	$Theory_{max}$ Cracked	$Measured_{max}$ Cracked
TTB5	C20	4-08.77F	242	1.33	6	96	3.35	2.68	24.09	37.33
RTTB5	C20	4-08.77F	242	1.33	6	42.8	3.35	2.68	24.01	16.85
TTB6	C20	4-13.19F	546.6	3.06	4	37.2	2.20	1.91	40.95	14.70
TTB8	C20 LT	4-8.77F	242	1.33	4	34	2.22	1.85	23.70	13.40
TTB9	C20 LT	4-13.19F	546.6	3.06	4	39	2.19	1.85	40.43	15.32
TTB10	C20 SIL	4-08.77F	242	1.33	6	42	3.34	2.68	24.03	16.54
TTB11	C20 SIL	4-13.19F	546.6	3.06	6	42	3.30	2.67	41.00	16.53
TTB12	C20 LT SIL	4-08.77F	242	1.33	4	32	2.22	1.84	23.80	12.62
TTB13	C20 LT SIL	4-13.19F	546.6	3.06	4	36	2.20	1.85	40.56	14.17
TTB20	C40	4-08.77F	242	1.33	4	44	2.22	1.91	24.03	17.31
TTB17	C40 FB	4-08.77F	242	1.33	6	46.8	3.35	2.68	24.11	18.39
TTB19	C40	4-13.19F	545.6	3.05	4	50	2.20	1.91	41.01	19.62
TTB18	C40 FB	4-13.19F	546.6	3.06	6	51.4	3.30	2.68	41.04	20.16
TTB14	C50 LT	4-08.77F	242	1.33	6	30	3.34	2.62	23.88	11.86
TTB15	C50 LT	4-13.19F	546.6	3.06	6	37.7	3.29	2.62	40.50	14.82

6.1.7 Ultimate Shear Capacity

The theoretical and the measured (applied) shear capacity of the beams are given in *Table 6.7* (see also *Appendix 5* for the formulae used in the calculations).

The comparison of data in Table 6.7

- It can be seen in the Table that the theoretical shear resistances of all the beams (except TTB5) are higher than the measured ones (see columns 8 and 9). Note that the actual shear resistance values are based upon the ultimate failure loads of the beams.
- The results showed that, generally, the shear capacity of the beams increases with increased percentage of reinforcement together with the increase in concrete strength (compare TTB6 and TTB19, TTB17 and TTB18 in column 9).
- C40 grade glass fibre added concrete beams seem to give the highest values for the shear resistance (see column 9). This may indicate that the fibres make an extra contribution to aggregate interlock.
- The lightweight concrete (C20 and C50) and silica added lightweight beams seem to have less shear resistance compared to the rest of the beams. This could be due to LYTAG particles having lower crushing strength than the normal weight coarse aggregates.

Table 6.7 Ultimate Shear Capacity of Part 3 Beams

1	2	3	4	5	6	7	8	9
Beam Code	Concrete grade	Rebar No. Dia/Type	Rebar Area (mm^2)	Tension Rebar %	Shear span/ effective depth	Failure Mode	**Shear Resistance (MPa)** Theory$_{max}$ Cracked	Measured$_{max}$ Cracked
TTB5	C20	4-08.77F	242	1.33	4.40	Shear/Shear	1.25	2.29
RTTB5	C20	4-08.77F	242	1.33	4.40	Shear	1.25	1.04
TTB6	C20	4-13.19F	546.56	3.06	4.48	Shear	1.65	0.91
TTB8	C20 LT	4-8.77F	242	1.33	4.41	Shear	1.00	0.83
TTB9	C20 LT	4-13.19F	546.56	3.06	4.48	Shear	1.32	0.95
TTB10	C20 SIL	4-08.77F	242	1.33	4.41	Shear	1.25	1.02
TTB11	C20 SIL	4-13.19F	546.56	3.06	4.48	Shear	1.65	1.02
TTB12	C20 LT SIL	4-08.77F	242	1.33	4.41	Shear/Shear	1.00	0.78
TTB13	C20 LT SIL	4-13.19F	546.56	3.06	4.48	Shear	1.32	0.88
TTB20	C40	4-08.77F	242	1.33	4.41	Shear	1.25	1.07
TTB17	C40 FB	4-08.77F	242	1.33	4.40	Shear	1.25	1.13
TTB19	C40	4-13.19F	545.56	3.05	4.48	Shear	1.65	1.21
TTB18	C40 FB	4-13.19F	546.56	3.06	4.48	Shear	1.65	1.24
TTB14	C50 LT	4-08.77F	242	1.33	4.40	Shear/Shear	1.00	0.73
TTB15	C50 LT	4-13.19F	546.56	3.06	4.48	Shear/Shear	1.32	0.91

6.1.8 Deflection

The mid-span deflections of all the beams were measured using an LVDT during the test. The load vs deflection response of all the beams up to failure, can be seen in *Figure 6.11.*

The 'elastic stage' or the initial crack load ranged between 4kN or 6 kN. All of the beams displayed a small increase in deflection as the load increased up to the initial visible crack load. Subsequently, the slope of load vs deflection relationship of the beams reduced and followed an approximately linear form up to failure (elasto-plastic stage). The Figure also shows that the slope of the 'plastic stage' increases as the area of rebars increases i.e. the stiffness of the beam increases with increase in rebar area. Thus the beams reinforced with 4ϕ8.77 GFRP rebars exhibit lower stiffness compared to the beams reinforced with 4ϕ13.19 GFRP rebars.

TTB5, C20 beam reinforced with 4ϕ8.77 exhibited different type of stiffness (see *Figure 6.11*). The behaviour of this beam can also be reviewed on the compact disk (play *ttb5_part1, 2, 3, 4 &5 (96kN).mov* files). The value of the deflection increased rapidly from 34kN to 36kN with the difference being 11.62mm (approximately 20%). The deflection difference between 36kN and 38kN was only 2.63mm (approximately 4%). From this point onward, the slope of the load versus deflection curve increases steeply until failure at a load of 96kN. A solid shear crack line could be distinguished on one side of the beam at 36kN, however, it did not fail until the second shear crack appeared at the other end of the beam resulting in double shear failure. The mode of this anomalous behaviour and failure has not been explained but could be due to a secondary constraint arising from the unusual geometry of the rebars. The experiment was repeated (beam RTTB5) but the beam behaved in a more conventional manner but with a higher overall stiffness than TTB5.

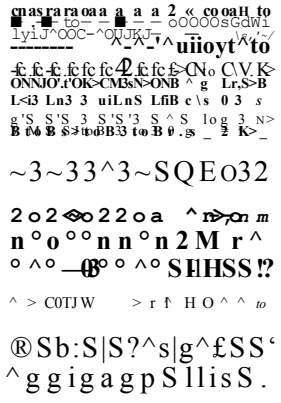

The comparison of data in Table 6.8

- Generally, 'measured' deflections at the uncracked section of the beams are greater than those calculated (see columns 10 and 11).
- The 'calculated' deflections of all the beams at the cracked section (except TTB5) are very similar to those 'measured' (see columns 12, 13).
- The experimental results showed that the deflections of the beams reinforced with 4ϕ8.77 are greater than the ones reinforced with 4ϕ13.19 rebars.
- Generally, the lightweight aggregate concrete beams seem to have larger deflection compared with the rest of the beams (except beam TTB5) for a given load and rebar area (see column 14 and its ranking).

Table 6.8 Theoretical and experimental deflections of Part3 beams

1	2	3	4	5	6	7	8	9	10	11	12	13	14	
Beam Code	Concrete grade	Rebar No. Dia/Type	Rebar Area mm^2	Tension Rebar %	Second Moment Area (mm^4)		Curvature (1/mm)		Deflection (mm)					
					*Calculated Uncracked	*Calculated Cracked	*Calculated Uncracked	*Calculated Cracked	*Calculated Uncracked	**$Measured_{max}$ Uncracked	*Calculated Cracked	**$Measured_{max}$ Cracked	#$Measured_{30kN}$ Cracked	Ranking
TTB5	C20	4-08.77F	242	1.33	1.35E+08	6.86E+06	5.86E-07	1.54E-04	0.38	2.03	99.29	71.78	39.70	7
RTTB5	C20	4-08.77F	242	1.33	1.53E+08	8.03E+06	5.84E-07	6.52E-05	0.38	1.10	41.94	45.85	28.26	4
TTB6	C20	4-13.19F	546.56	3.06	1.51E+08	1.22E+07	4.10E-07	3.56E-05	0.26	1.06	22.89	27.91	21.11	7
TTB8	C20 LT	4-8.77F	242	1.33	7.93E+07	1.05E+07	1.11E-06	5.55E-05	0.71	0.67	35.67	35.22	30.40	5
TTB9	C20 LT	4-13.19F	546.56	3.06	7.95E+07	1.67E+07	1.06E-06	3.89E-05	0.68	0.75	25.03	26.78	19.48	6
TTB10	C20 SIL	4-08.77F	242	1.33	8.86E+07	7.28E+06	8.91E-07	6.23E-05	0.57	0.70	40.03	42.15	26.25	3
TTB11	C20 SIL	4-13.19F	546.56	3.06	8.86E+07	1.20E+07	9.43E-07	4.02E-05	0.61	0.76	25.82	24.39	16.09	1
TTB12	C20 LT SIL	4-08.77F	242	1.33	7.67E+07	9.31E+06	1.00E-06	5.13E-05	0.64	0.54	32.98	35.78	32.36	6
TTB13	C20 LT SIL	4-13.19F	546.56	3.06	9.79E+07	1.54E+07	7.87E-07	3.56E-05	0.51	0.60	22.89	24.85	18.50	5
TTB20	C40	4-08.77F	242	1.33	1.06E+08	7.43E+06	5.30E-07	6.41E-05	0.34	0.57	41.21	44.25	25.76	2
TTB17	C40 FB	4-08.77F	242	1.33	8.99E+07	6.89E+06	8.51E-07	7.13E-05	0.55	0.73	45.86	44.80	24.96	1
TTB19	C40	4-13.19F	546.56	3.05	7.70E+07	1.13E+07	7.31E-07	4.79E-05	0.47	0.37	30.79	31.58	16.12	2
TTB18	C40 FB	4-13.19F	546.56	3.06	7.65E+07	1.19E+07	1.06E-06	4.86E-05	0.68	0.67	31.26	33.97	16.93	3
TTB14	C50 LT	4-08.77F	242	1.33	1.15E+08	9.06E+06	9.10E-07	4.72E-05	0.59	0.73	30.36	24.96	24.96	1
TTB15	C50 LT	4-13.19F	546.56	3.06	1.09E+08	1.60E+07	1.05E-06	3.75E-05	0.67	1.20	24.11	27.98	18.06	4

* Column 6-7 using actual n.a depth
* Column 8-9 using actual bending moment
* Column 10-12 using actual curvature
** Column 11-13 experimental readings
# deflections measured at 30kN

6.1.9 Cracking Behaviour

In this section, the crack developments in the beams are discussed. The summary of average cracks in all the beams is given in *Table 6.9*.

4φ8.77 'straight and curved' profile GFRP rebars in beams of various types of concrete

The crack patterns developed in the beams can be seen in *Figure 6.12*. In this category, the beams containing smaller diameter of GFRP rebars with different types of concrete beams are put together. The reason for this is to show if the crack patterns differ from one type of concrete to another one. As in the Part1 and Part2 of the beam tests, first hairline cracks appeared at the maximum bending moment region under 4kN or 6kN total load in the beams and subsequently grew to be more prominent and numerous as the load increased. The average numbers of cracks developed in the overall length of the C20 beams was 14 for TTB5 and 21 for RTTB5. In TTB5 beam, the flexural cracks propagated more deeply and very close to the top edge of the beam whereas in the repeat experiment, the flexural cracks in the beam have more extensions. The C20 grade concrete beam containing microsilica and the C40 grade normal weight concrete beam developed similar amounts of total cracks (19 and 18 respectively). Nevertheless, the flexural cracks in the maximum bending moment region of the silica added concrete beam have more branches and they are more closely spaced compared to the C40 grade concrete beam. The C40 glass fibre added concrete beam has the same amount of cracks as the C40 beam (total of 18) but, the number of branches in the fibre added concrete is greater compared to the C40 beam. When the C20 lightweight concrete beam is compared with the C50 lightweight beam, the total numbers of cracks in C50 beam are less than the C20 beam. The C20 lightweight silica added concrete has fewer cracks than the C20 lightweight concrete, however, the branches in the silica added beams are more numerous compared to the C20 lightweight beam. Taken as a whole, it seems that adding silica and glass fibres into the beams increases the amount of crack branching but reduces the size of the cracks within the beams (see column 7 in *Table 6.11*).

Figure 6.12 The crack patterns of the various types of concrete beams reinforced with 4ϕ 8.77 'straight and curved' profile GFRP

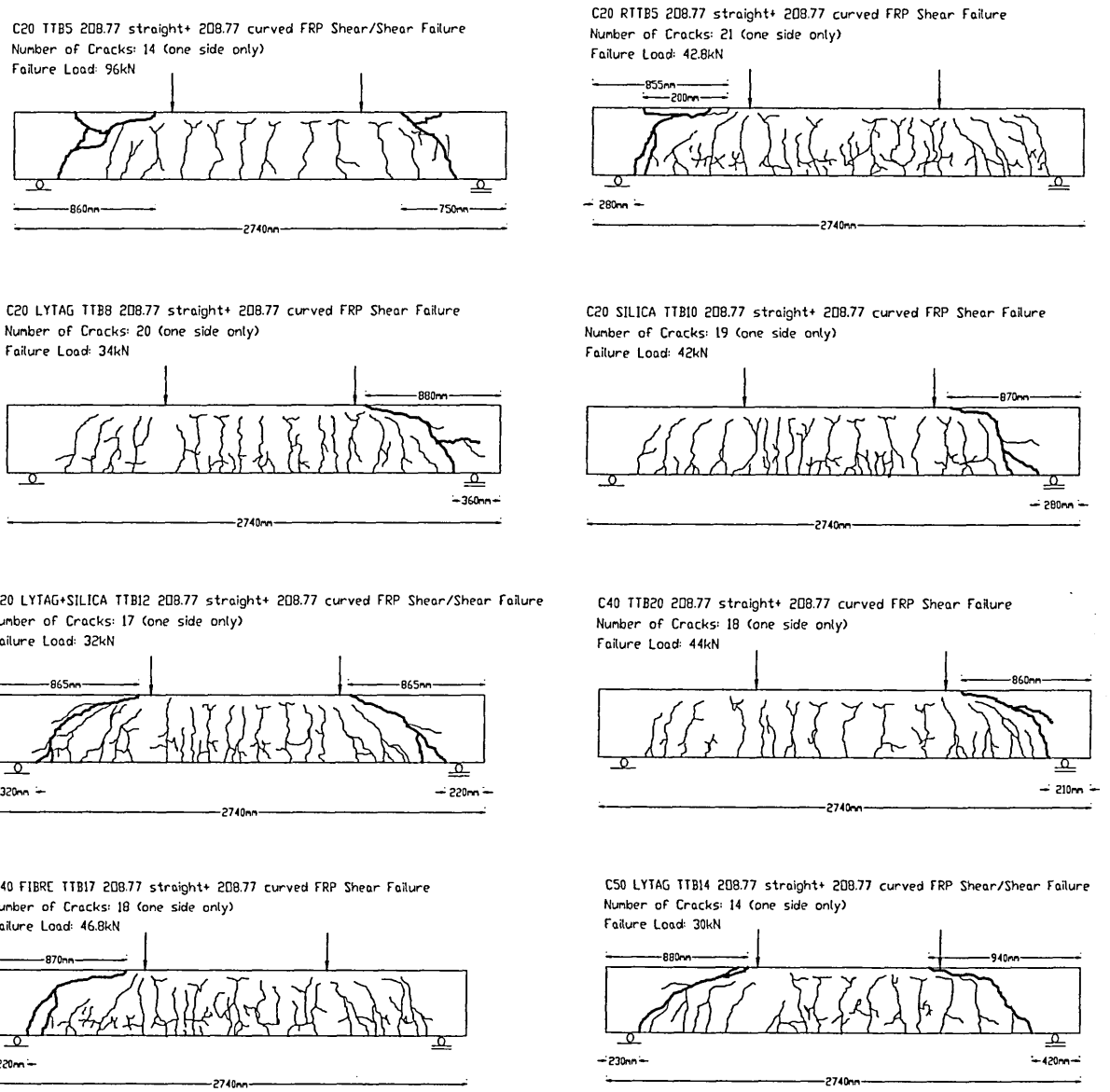

4ϕ13.19 straight and curved profile GFRP rebars in beams of various types of concrete

The crack propagation in the pre and post cracking stages of the beams in this category is very similar to the previous one. The average numbers of cracks in the C20 lightweight and C20 silica added lightweight beams are 24 and 23 respectively. The rest of the types of the beams have a very similar amount of cracking in them (see *Table 6.9*).

Figure 6.13 The crack patterns of the various types of concrete beams reinforced with 4ϕ 13.19 'straight and curved' profile GFRP

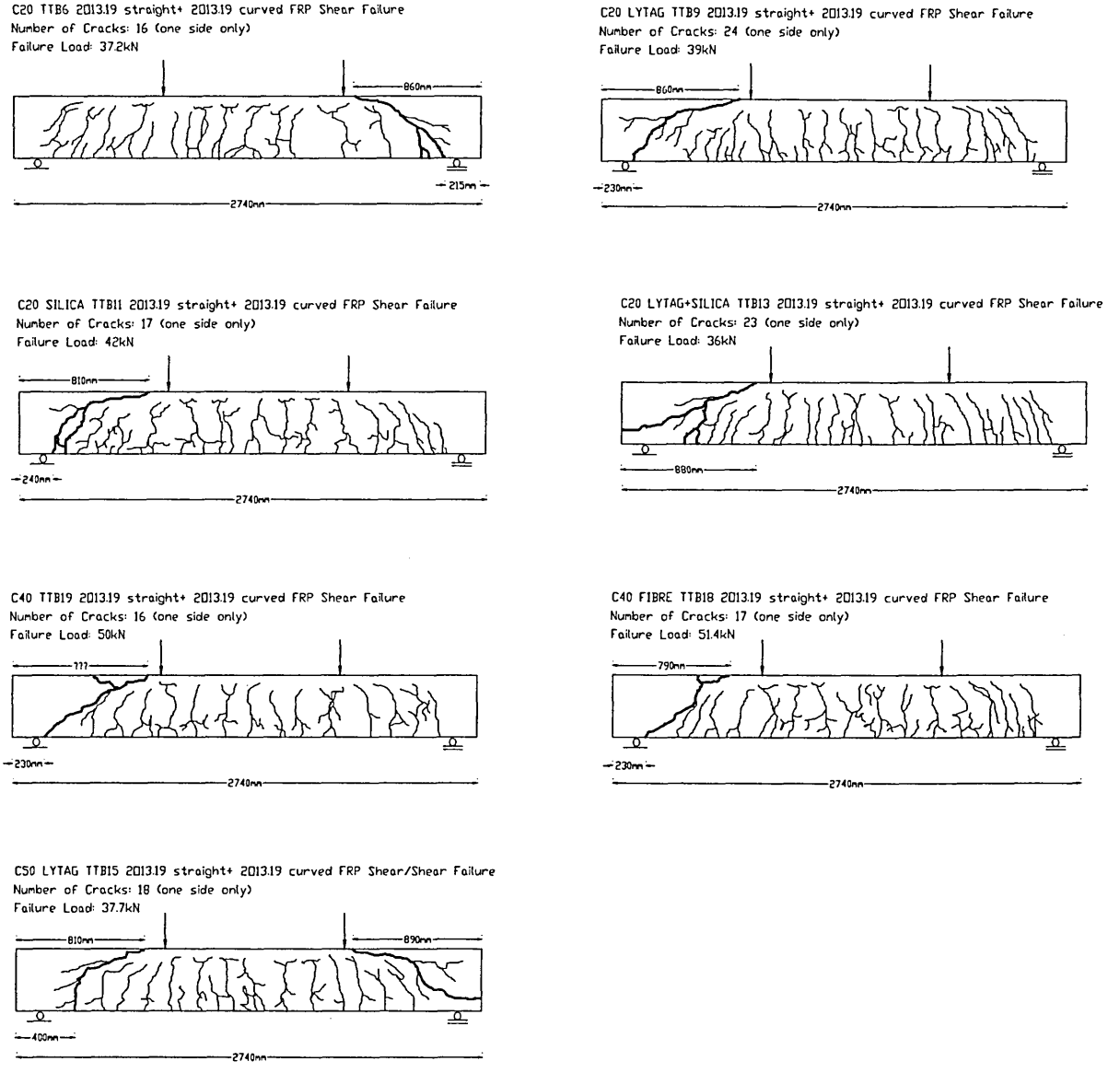

Table 6.9 The summary of average cracks in the beams

	No of cracks at failure							First crack load (kN)						
No of Rebars	C20	C20 LT	C20 SIL	C20 LT SIL	C40	C40 FB	C50 LT	C20	C20 LT	C20 SIL	C20 LT SIL	C40	C40 FB	C50 LT
4Ø8.77	14	20	19	17	18	18	14	6	4	6	4	4	6	6
4Ø13.19	16	24	17	23	16	17	18	4	4	6	4	4	6	6

6.1.9.1 Modes of Failure

A typical 'single shear' failure (shear failure occurring only at the one end of the beam) of a lightweight aggregate concrete beam reinforced with 4<j)13.19 'straight and curved' profile GFRP rebars is shown in *Photo 6.1.* The morphology of beam failures is given in *Table 6.10.* All beams except TTB5 C20, TTB12 C20 lightweight silica added and TTB15 C50 lightweight concrete beam failed in 'double shear' (shear failure occurring at the both ends of the beam) at the ultimate load whereas the rest of the beams failed in 'single shear'. The vertical cracks developed from the bottom surface within the middle section and these were followed by diagonal cracks towards the supports in all cases. The above beams initially failed in shear but still continued to sustain residual load. At this stage, the load increased until shear failure occurred on the opposite end of the beams i.e. 'double shear' failure. It seems that the previously observed rebar rupture failure have been eliminated by the configuration of the rebars.

Photo 6.1 A view of 'single shear' failure of 4(j>13.19 GFRP 'straight and curved' profile reinforced C50 lightweight aggregate concrete beam

Table 6.10 The modes of failure of 4ϕ8.77 and 4ϕ13.19 'straight and curved' profile GFRP reinforced beams of various concrete types

Beam Code	Concrete Grade (Cube Strength MPa)	Rebar No Dia/Type (Profile)	Failure Morphology (Failure Load-kN)
TTB5	C20(43)	4ϕ8.77 GFRP (straight and curved)	**Shear/Shear**- Diagonal tension cracks propagated across the section outside the maximum bending moment region in both sides (96)
RTTB5	C20(44)	4ϕ8.77 GFRP (straight and curved)	**Shear**-Diagonal tension crack propagated across the section outside the maximum bending moment region (42.8)
TTB6	C20(43)	4ϕ13.19 GFRP (straight and curved)	**Shear**-Diagonal tension crack propagated across the section outside the maximum bending moment region (37.2)
TTB8	C20LYTAG(45)	4ϕ8.77 GFRP (straight and curved)	**Shear**-Diagonal tension crack propagated across the section outside the maximum bending moment region (34)
TTB9	C20LYTAG(48)	4ϕ13.19 GFRP (straight and curved)	**Shear**-Diagonal tension crack propagated across the section outside the maximum bending moment region (39)
TTB10	C20Silica(59)	4ϕ8.77 GFRP (straight and curved)	**Shear**-Diagonal tension crack propagated across the section outside the maximum bending moment region (42)
TTB11	C20Silica(51)	4ϕ13.19 GFRP (straight and curved)	**Shear**-Diagonal tension crack propagated across the section outside the maximum bending moment region (42)
TTB12	C20LYTAG + Silica(63)	4ϕ8.77 GFRP (straight and curved)	**Shear/Shear**- Diagonal tension cracks propagated across the section outside the maximum bending moment region in both sides (32)
TTB13	C20LYTAG + Silica(61)	4ϕ13.19 GFRP (straight and curved)	**Shear**-Diagonal tension crack propagated across the section outside the maximum bending moment region (36)
TTB20	C40(61)	4ϕ8.77 GFRP (straight and curved)	**Shear**-Diagonal tension crack propagated across the section outside the maximum bending moment region (44)
TTB17	C40Fibre(56)	4ϕ8.77 GFRP (straight and curved)	**Shear**-Diagonal tension crack propagated across the section outside the maximum bending moment region (46.8)
TTB19	C40(59)	4ϕ13.19 GFRP (straight and curved)	**Shear**-Diagonal tension crack propagated across the section outside the maximum bending moment region (50)
TTB18	C40Fibre(59)	4ϕ13.19 GFRP (straight and curved)	**Shear**-Diagonal tension crack propagated across the section outside the maximum bending moment region (51.4)
TTB14	C50LYTAG(69)	4ϕ8.77 GFRP (straight and curved)	**Shear/Shear**- Diagonal tension cracks propagated across the section outside the maximum bending moment region in both sides (30)
TTB15	C50LYTAG(62)	4ϕ13.19 GFRP (straight and curved)	**Shear**-Diagonal tension crack propagated across the section outside the maximum bending moment region (37.7)

6.1.9.2 Estimation of Flexural Crack Widths

Table 6.11 contains the theoretical and experimental estimations of the maximum crack widths using the equations given in Chapter 4 (see also *Appendix 5*).

The values of maximum crack widths calculated using the equations in BS8110, are comparable with the experimentally estimated values. It seems that the beams reinforced with larger diameter rebars have smaller flexural crack widths than those reinforced with smaller diameter rebars. This could be due to the fact that the larger the area of the rebar the more resistance against the tension in the concrete.

Table 6.11 Estimated crack widths of Part 3 beams

1	2	3	5	6	7
Beam Code	Concrete grade	Rebar No. Dia/Type	[1]*Number of Cracks	**Estimated crack widths (mm)** [2]**BS8110	[3]***Experiment
TTB5	C20	4-08.77F	6	-	-
RTTB5	C20	4-08.77F	11	0.43	0.36
TTB6	C20	4-13.19F	9	0.21	0.21
TTB8	C20 LT	4-8.77F	13	0.34	0.24
TTB9	C20 LT	4-13.19F	12	0.29	0.22
TTB10	C20 SIL	4-08.77F	14	0.42	0.28
TTB11	C20 SIL	4-13.19F	12	0.25	0.19
TTB12	C20 LT SIL	4-08.77F	12	0.29	0.22
TTB13	C20 LT SIL	4-13.19F	13	0.22	0.15
TTB20	C40	4-08.77F	8	0.26	0.30
TTB17	C40 FB	4-08.77F	12	0.42	0.33
TTB19	C40	4-13.19F	7	0.51	0.66
TTB18	C40 FB	4-13.19F	9	0.30	0.31
TTB14	C50 LT	4-08.77F	8	0.24	0.28
TTB15	C50 LT	4-13.19F	9	0.25	0.25

-no accurate strains were obtained

[1]*in the maximum bending moment region

[2]**based upon the formulae

[3]**based upon the dial gauge measurements

6.2 Performance Quotent (Q_p)

The Performance Quotient of the beams was calculated using the formula given in *Appendix 5* and the results for this Part are included in *Table 6.12* column 12. It can be seen in the table that the beams with highest Q_p also have higher load capacity. For the majority of the beams except C20 TTB5 and RTTB5normal, C50 TTB14 and TTB15 lightweight concrete beams, there is not much difference in their Q_p values due to the fact that they have similar load carrying capacities. It should be noted that the high ultimate tensile stress of ϕ8.77 GFRP rebars does influence the Q_p of the beams (compare TTB8 and TTB9). The results indicate that the higher the Q_p of the beam, the better the performance. Also note that Q_p values relate to 'normal' and 'medium' strength concretes and therefore yield higher values than in Chapter 5. Lowest Q_ps are for silica fume and higher grade lightweight concretes. Q_p slightly enhanced by addition of fibres to concrete mix.

6.12 Performance Quotient of Part 3 Beams

1 Beam Code	2 Concrete grade	3 Rebar No. Dia/Type	4 Width b mm	5 Height h mm	6 Rebar Area (mm^2)	7 Beam Self Weight kN	8 Failure Mode	9 Failure Load kN	10 Yield/Ultimate Stress MPa	11 Cube Strength MPa	12 Perform. Quotient	13 Ranking
TTB5	C20	4-08.77F	104	204	242	1.38	Shear/Shear	96	601	43	0.0936	1
RTTB5	*C20*	*4-08.77F*	*104*	*204*	*242*	*1.38*	*Shear*	*42.8*	*601*	*44*	*0.0413*	*2*
TTB6	C20	4-13.19F	104	204	546.56	1.37	Shear	37.2	470.7	43	0.0339	6
TTB8	C20 LT	4-8.77F	104	204	242	1.13	Shear	34	601	45	0.0323	8
TTB9	C20 LT	4-13.19F	104	204	546.56	1.13	Shear	39	470.7	48	0.0320	9
TTB10	C20 SIL	4-08.77F	104	204	242	1.38	Shear	42	601	59	0.0313	10
TTB11	C20 SIL	4-13.19F	104	204	546.56	1.33	Shear	42	470.7	51	0.0330	7
TTB12	C20 LT SIL	4-08.77F	104	204	242	1.12	Shear/Shear	32	601	63	0.0225	13
TTB13	C20 LT SIL	4-13.19F	104	204	546.56	1.14	Shear	36	470.7	61	0.0245	12
TTB20	C40	4-08.77F	104	204	242	1.38	Shear	44	601	61	0.0320	9
TTB17	C40 FB	4-08.77F	104	204	242	1.35	Shear	46.8	601	56	0.0364	3
TTB19	C40	4-13.19F	104	204	545.56	1.38	Shear	50	470.7	59	0.0347	5
TTB18	C40 FB	4-13.19F	104	204	546.56	1.36	Shear	51.4	470.7	59	0.0357	4
TTB14	C50 LT	4-08.77F	104	204	242	1.14	Shear/Shear	30	601	69	0.0196	14
TTB15	C50 LT	4-13.19F	104	204	546.56	1.13	Shear/Shear	37.7	470.7	62	0.0252	11

TTB: New Test Beam includes new geometry of rebars and concrete strengths and types RTTB: Second Repeat of TTB

LT (Lightweight concrete) SIL (Silica added concrete) FB (Glass fibre added concrete) *** note that all the rebar profiles are the combination of 'straight and curved'**

6.3 Conclusions

The performance of normal weight C20 and C40 grade, C20 grade silica added, C20 and C50 lightweight and C20 grade lightweight silica added together with C40 glass fibre added concrete beams reinforced with 'straight and curved' profile of 4ϕ8.77 and 4ϕ13.19 GFRP rebars was studied.

ϕ8.77 GFRP and ϕ13.19 rebars in the beams (except TTB5) reached approximately 67% and 46% respectively, of their ultimate tensile capacity on average (see *Table 6.2*). The 'measured' strains in the rebars suggested that the large diameter rebars deform less than the small diameter rebars at failure and the concrete type does not seem to affect the magnitude of the strains. The 'calculated' strains in the rebars are comparable with the measured (experimental) values for all the beams confirming that the current equations are equally valid even when a different geometry is applied to the rebars (see *Table 6.2*).

The rebar strains obtained in the shear region (left and right hand side) of the beams are similar in magnitude for both straight and curved profiles (see *Figure 6.3*).

The magnitude of the 'measured' concrete strains at the uncracked section is very similar for all types of concrete at a given load up to the appearance of first crack (see *Figure 6.4* and *Figure 6.5*).

The concrete strain distributions obtained from the experiments show a straight line across the section indicating regions of compression and tension (see *Figure 6.6* and *Figure 6.7*).

The results suggest that there is no dominant influential factor operating between different types of concrete beams for the maximum compressive strain (see *Table 6.3*).

The theoretical neutral axis depth of all types of the beams are generally in good agreement with the corresponding measured ones at the cracked section (ultimate). However, it should be noted that the theoretical values are generally less than the

measured ones (see *Table 6.4*). Overall, the results demonstrate that stiffness is enhanced as more rebars/area are put into the concrete indicated by the neutral axis depth shifting less after initial cracking.

In general, all the beams behaved in a very similar manner regardless of the type of concrete. As in Chapter 4 and Chapter 5 the magnitude of the first crack load of the beams is not affected either by the diameter of the rebars and the concrete type or the profile of the rebars i.e. it is between 4kN or 6kN on average (*Table 6.6*).

The lightweight aggregate concrete beams reinforced by either small or medium diameter rebars seem to have lower ultimate load capacity amongst all the beams (see *Table 6.6*). The results suggested that adding 'silica' and 'glass fibres' into the concrete mix could enhance the ultimate load capacity of the beams by 11% (particularly beam reinforced with medium diameter rebars) and 4.5% (on average for the beams reinforced with either small and medium diameter rebars) respectively. The ultimate load capacities of the beams seem to be influenced by the area of rebars (except TTB10 and TTB11) and concrete strength for all the beams.

Generally, theory overestimates the bending moment capacity of the beams at the uncracked and cracked sections compared to those measured (applied). The results suggest that the applied bending moment capacity of the beams reinforced with 4ϕ8.77 and 4ϕ13.19 is approximately 82 % that of the theoretical bending moment at the uncracked section (see *Table 6.6*). The difference between the theoretical and the applied bending moments at the cracked section varies probably depending on the type of concrete and rebar type i.e. the measured values are between 35% and 76% that of the theoretical values (see also *Table 6.6*).

The results suggested that, generally, the shear capacity of the beam increase with increased percentage of reinforcement together with the increase in concrete strength (see *Table 6.7*). The ultimate shear resistance of the concrete beams containing glass fibres is higher than the rest of the beams. The results showed that the ultimate shear resistance of the lightweight concrete beams was less compared to the rest of the beams.

All the beams behaved elasto-plastically up to failure with a change in slope of the load vs deflection curve (see *Figure 6.11*) i.e. the slope is steeper up to the initial crack load and beyond this point the slope decreases. Note that although the rebar behaves elastically close to failure, the concrete does not. The slope in the plastic stage is controlled by the rebar area i.e. the larger the rebar area the steeper the slope.

Generally, the 'measured' deflections are higher than the 'calculated' ones at the uncracked section (see *Table 6.8*). However, they are very similar to each other at the cracked section confirming that the current equations given in BS8110 (see *Appendix 5)* can be used for estimating the deflection of the beams containing 'straight and curved' profile GFRP rebars.

The initiation and the propagation sequence of the cracks in all beams are generally the same i.e. the first crack appears within the maximum bending moment region and subsequently grows to be more prominent and numerous as the load increases.

The values of maximum crack widths calculated using the equations in BS8110, are comparable with the experimentally estimated values for the all types of beams. According to the results, the maximum crack size of the beams range from 0.15mm and 0.66mm depending on the concrete type and rebar diameter (see *Table 6.11*).

The mode of failure is predominantly a shear type regardless of the type of concrete used in the manufacture of the beams. It was also observed that 'double shear' type of failure also occurs with the beams containing 'straight and curved' (optimum) profile GFRP rebars. However, the optimum rebar configuration seems to eliminate the 'catastrophic failure' of the beams observed in the previous Parts of the test programme i.e. there were no beams failed as the result of rebars snapping or concrete exploding.

The results suggested that the high value of Performance Quotient (Q_p) indicates that the load carrying capacity of the beams is also high. The lowest Q_p of 0.0196 was obtained for the lightweight concrete beam (TTB14) reinforced with 4ϕ13.19 rebars

(see *Table 6.12*). The normal weight concrete beams reinforced with 4ϕ8.77 (TTB5 and RTTB5) gave the highest Q_p of 0.096 and 0.0413. Mean values of Q_p were comparable for beams containing both small (ϕ8.77) and medium (ϕ13.19) rebars. Both the highest and lowest Q_p were achieved with small diameter rebars.

CHAPTER 7

7 PART4: NORMAL WEIGHT CONCRETE BEAMS REINFORCED WITH GFRP AND HIGH TENSILE STEEL REBARS WITH GFRP AND MILD STEEL STIRRUPS

7.1 Section Design and Detailing

The dimensions of the beams tested in this Part were the same as in Part1, Part2 and Part3 i.e. approximately 103mm (width) x 203mm (depth) x 2740mm (length). The beams were designed for shear reinforcement using the equations in BS8110 (see *Appendix 5*). Part 1 beam of TB15 was reinforced with 2ϕ8 steel and failed catastrophically in tension and was considered for the design of all the beams in this Part of the investigation. This way, it was also thought that the predominant shear failure of most of the beams could be modified.

The numbers of ϕ6 mild steel and ϕ6.9 GFRP stirrups used in the shear regions of the beams were 10 in each side at 100mm spacing between the stirrups. Although, there was no need to include any stirrups in the maximum bending moment region for resisting shear, four more stirrups were put in this region to control bursting strains (see *Figure 7.1*). The total of 24 stirrups were used in each beam. It was considered that in this way the likelihood of shear failure could be eliminated, thus providing valuable complementary information regarding the flexural capacity of the beams reinforced with both GFRP and steel.

7.2 Experimental and Theoretical Results

7.2.1 Behaviour up to Failure

The results showed so far that the performance of the beams is very much influenced by the configuration and the amount of the rebars used in the beams. The majority of the beams failed in shear mode suggesting that the load capacity of the beams could be enhanced by conventionally reinforcing with stirrups. Consequently, six C20 concrete beams were manufactured and tested under two-point loading. The details and the physical properties of the beams are included in *Figure 7.1* and *Table 7.1* respectively. All six beams had 2ϕ6 mild steel rebar 'top bars' across the compression region of the beams. It was possible to split this Part into three groups. The first group contained beams reinforced with 2ϕ8 and 2ϕ12 high yield steel rebars in the tension region and 24ϕ6 mild steel stirrups (see *Photo 7.1*)

Figure 7.1 Details of Part 4 beams

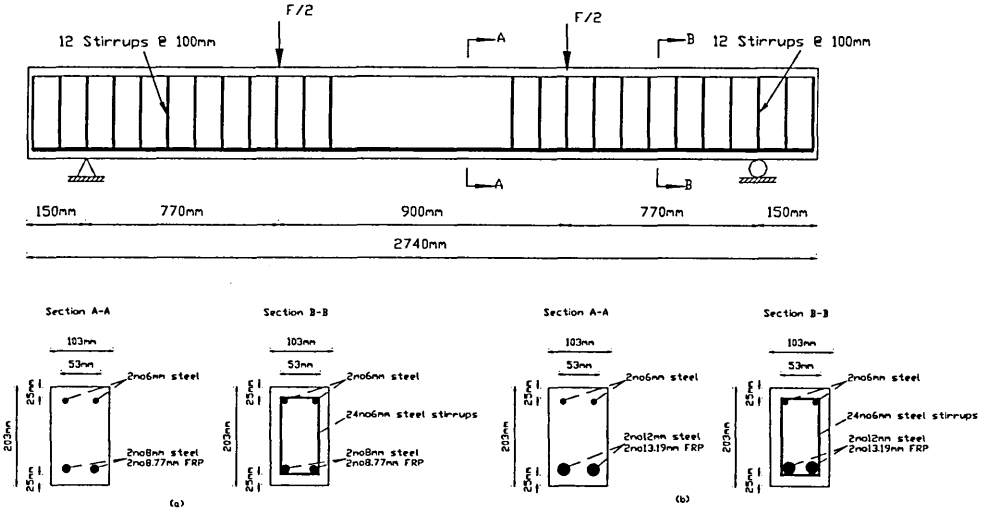

Photo 7.1 A partial view of the group I reinforcement cage (main steel rebars and mild steel stirrups)

In the second group everything was kept the same except 2(j)8.77 and 2(j)13.19 GFRP rebars were used in the tension region (see *Photo 7.2).*

Photo 7.2 A partial view of the group II reinforcement cage (main GFRP rebars and mild steel stirrups

The third group was the same as the second one except 24(|)6.9 GFRP were used (see *Photo 7.3).* The GFRP stirrups were acquired from the company (ICL Ltd.) based in the USA. These stirrups were specially manufactured to meet the beam dimensions. Therefore, they had to be ordered in advance. The reinforcement cages were assembled and placed in the beam mould before casting (see *Photo 7.4).*

Photo 7.3 A partial view of the group III reinforcement cage (main GFRP rebars and stirrups

Photo 7.4 A view of the reinforcement cage placed in the steel mould before casting

The main objectives of this part were to:

- modify the shear failure of the beams using steel/GFRP stirrups.
- observe if GFRP stirrups were capable of increasing the shear resistance of the beams compared with steel stirrups.
- compare the performance of the beams reinforced with GFRP and steel main rebars.
- assess if the load capacity of the beams had been enhanced with stirrups.
- ascertain if a combination of GFRP and steel rebars and stirrups would be applicable.

The concrete strength of C20 (43MPa nominal strength) was selected for this part of the investigation due to its common use in certain applications and also in order to reduce the potential cost of the beam and also to maintain a high performance quotient. Furthermore for GFRP rebar a lower grade of concrete could be permitted for durability purposes.

The analysis of the beams was carried out based on the equations used in Chapter 4, Chapter 5 and Chapter 6. However, the beams in this part were designed for shear reinforcement using BS8110 formulae (see *Appendix 5*). The compression force of the 'top bars' was computed for each beam using rectangular stress block for a doubly reinforced beam. It was found out that the compression force of the 'top bars' is approximately 8% of the ultimate compression force due to the concrete. Therefore, their contribution to concrete resistance in compression is not very significant.

7.2.2 Reinforcement Stresses and Strains in the Maximum Bending Moment Region

The strains along the main and the 'top bars' were measured. *Figure 7.2* shows the rebar strains monitored against applied load. The dotted lines in the graphs represent the strains up to failure. As in the previous parts of the investigation, the strains exhibit linear elastic behaviour up to the initial crack load for both steel and GFRP beams. Once the curve passes the 'elastic limit', the slope continues on a different linear path at a reduced slope for all beams. This was also the case for steel rebars up to the point where the yielding plateau had occurred. The strains obtained from GFRP reinforcing bars are greater than those from the steel reinforcing bars at a similar load. However, it can be seen in the Figure that up to 6kN the strains in small diameter steel rebars combined with mild steel stirrups (TTB22) are comparable with those in small (TTB26 contains GFRP stirrups) and large (TTB25 and TTB27 contain steel and GFRP stirrups respectively) diameter GFRP rebars.

Similar strains were recorded in rebars of similar diameter at a given load indicating consistency of material properties throughout the tests. The strains in the ϕ13.19 GFRP rebars embedded in the beams TTB25 and TTB27 are less than the corresponding values in ϕ8.77 GFRP rebars. This shows that the deformation in the rebars is influenced by the rebar diameter i.e. the bigger the diameter, the less the strain for a given load at the cracked section. It was interesting to see that the strains in the small (ϕ8.77) and large (ϕ13.19) diameter GFRP rebars combined with either mild steel or GFRP stirrups followed a path almost on the same line (see TTB24 and TTB26, TTB25 and TTB27 in *Figure 7.2*).

In summary, the steel and large diameter GFRP main rebars exhibit higher stiffness at the cracked section and the stiffness for rebars of similar diameter with steel or GFRP stirrups at the cracked section is also similar.

Load (kN)

Stresses and strains in the reinforcing bars were calculated based on bending theory (see *Appendix 5*), at the cracked sections (see *Table 7.2*). In the Table, 'calculated' values are based upon substituting the actual (measured) bending moment, second moment of area and the depth of the neutral axis in the theoretical equations (see columns 7 and 10). The 'measured' values were obtained directly from the 'tensile' and 'bending' tests (see columns 6, 8 and 9).

The comparison of data in Table 7.2

- In several cases the maximum 'calculated' values (in column 7), for stresses in steel and GFRP (TTB24) main bars are more than their ultimate tensile stress capacities (in column 6) for the beams of TTB22 ('measured' stress is 85% of 'calculated' stress), TTB23 ('measured' stress is 96% of 'calculated' stress), and TTB24 ('measured' stress is 88% of 'calculated' stress).
- However, the maximum 'calculated' stresses in the GFRP rebars are less than their ultimate tensile stress capacities for the beams of TTB25 ('calculated' stress is 77% of 'measured' stress), TTB26 ('calculated' stress is 97% of 'measured' stress) and TTB27 ('calculated' stress is 69% of 'measured' stress).
- From the bending test, the maximum 'calculated' and 'measured' strains at the cracked section are in reasonably good agreement (see columns 9 and 10).
- The bending test results show that the maximum 'measured' strains in larger diameter (ϕ12) steel rebars are approximately 32% of those in larger diameter (ϕ13.19) GFRP rebars for given ultimate load capacity (compare beams TTB23 and TTB25 in column 14).

Table 7.2 The comparison of tensile stresses and strains in GFRP rebars from the tensile and bending test (using BS8110 equation)

1	2	3	4	5	6	7	8	9	10
Beam Code	Concrete grade	Rebar No. Dia/Type	Stirups No. Dia/Type	Failure Mode	**Maximum Tensile Stresses in the Rebars (MPa)**		**Maximum Tensile Strains in the Rebars**		
					Tensile Test	**Bending Test**	**Tensile Test**	**Bending Test**	
					Measured	*Calculated	Measured	Measured	**Calculated
TTB22	C20	2-08S	24-06S	Compression	523.5	618.51	0.0028	0.00332	0.00333
TTB23	C20	2-12S	24-06S	Compression	497	518.06	0.0026	0.00382	0.00274
TTB24	C20	2-08.77F	24-06S	Compression	601.00	683.94	0.0130	0.01993	0.01487
TTB25	C20	2-13.19F	24-06S	Compression	470.70	364.36	0.0120	0.01194	0.00940
TTB26	C20	2-8.77F	24-06.9F	Compression	601.00	581.03	0.0130	0.01644	0.01264
TTB27	C20	2-13.19F	24-06.9F	Compression	470.70	325.89	0.0120	0.00964	0.00841

7.2.3 Strains in the 'top bars' at the maximum bending moment region

The strains measured in the 'top bars' at the maximum bending moment region of the beams reinforced with 2ϕ8.77 (beam TTB26) and 2ϕ13.19 (beam TTB27) rebars and ϕ6.9 GFRP stirrups followed the trend as shown in *Figure 7.3*. The compressive strains (- ve) recorded in TTB26 and TTB27 up to 4kN and 8kN respectively. Beyond these loads, the bars were under tension (+ ve) and followed almost a straight line up to 30kN. Note that the strain readings beyond this load could not be recorded due to the strain gauges losing their bond with the bars. The change in the status of the strains in the 'top bars' could be due to the location of the strain gauges i.e. the strain gauges attached to the tension face of the 'top bars' reading (+ ve) strains. Possibly, until the main rebars had taken the full tensile forces, the 'top bars' were under the influence of compression i.e. once the cracks were initiated at large flexural loads strains due to curvature would predominant compared with those due to axial compression. It can be seen in the Figure that the 'top bar' strains in beam TTB27 are less than those in beam TTB26 (approximately 45% of beam TTB26 at a load of 30kN).

Figure 7.3 Strains measured in the 'top bars' in the compression zone at the maximum bending moment region

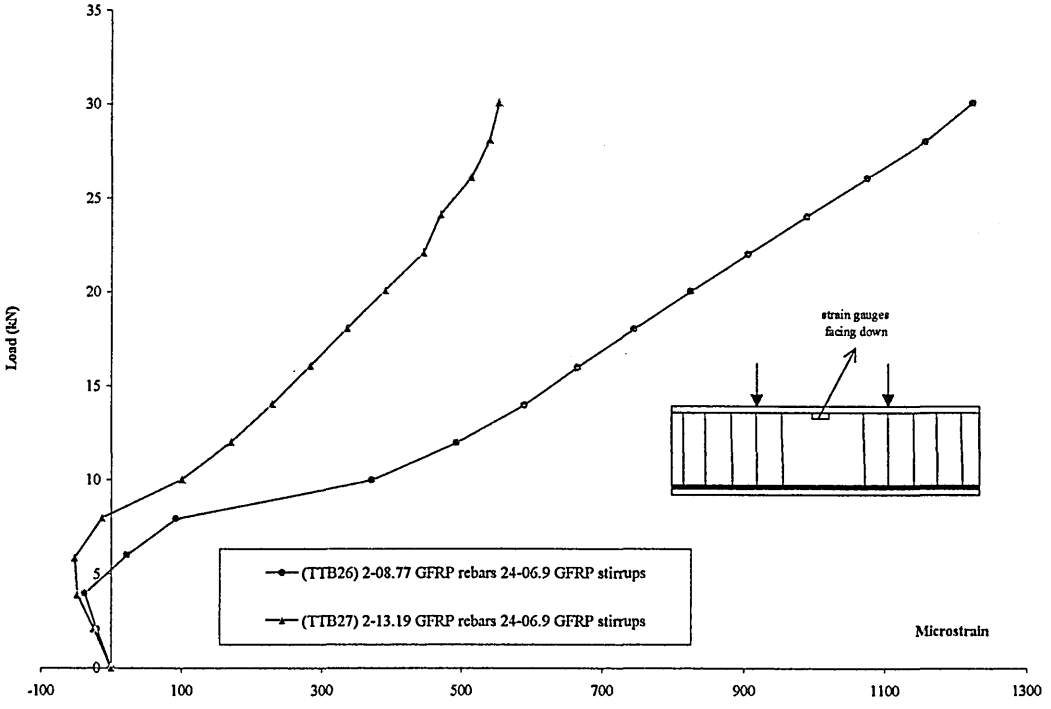

7.2.4 Reinforcement Strains in the Shear Region

Figure 7.4 shows the rebar strains measured in the shear regions (between the loading point and the edge at both ends) of the beams. The strains from the left and the right hand side of the beams follow a similar trend although not identical indicating that the bending applied was consistent in its effect. The results show that the strains in the shear region of the beams reinforced with ([>12 steel rebars and stirrups are less than in the GFRP and <|>8 steel reinforced beams. The slope of strains in the beams reinforced with (j)8 steel and (j>13.19 GFRP together with steel and GFRP stirrups is very similar. Also the defonnation in these rebars is less than in the <J)8.77 GFRP rebars.

Figure 7.4 Rebar strains in the shear region of the beams reinforced with 2(/)8/8.77 and 2ft'12/13.19 steel and GFRP stirrups.

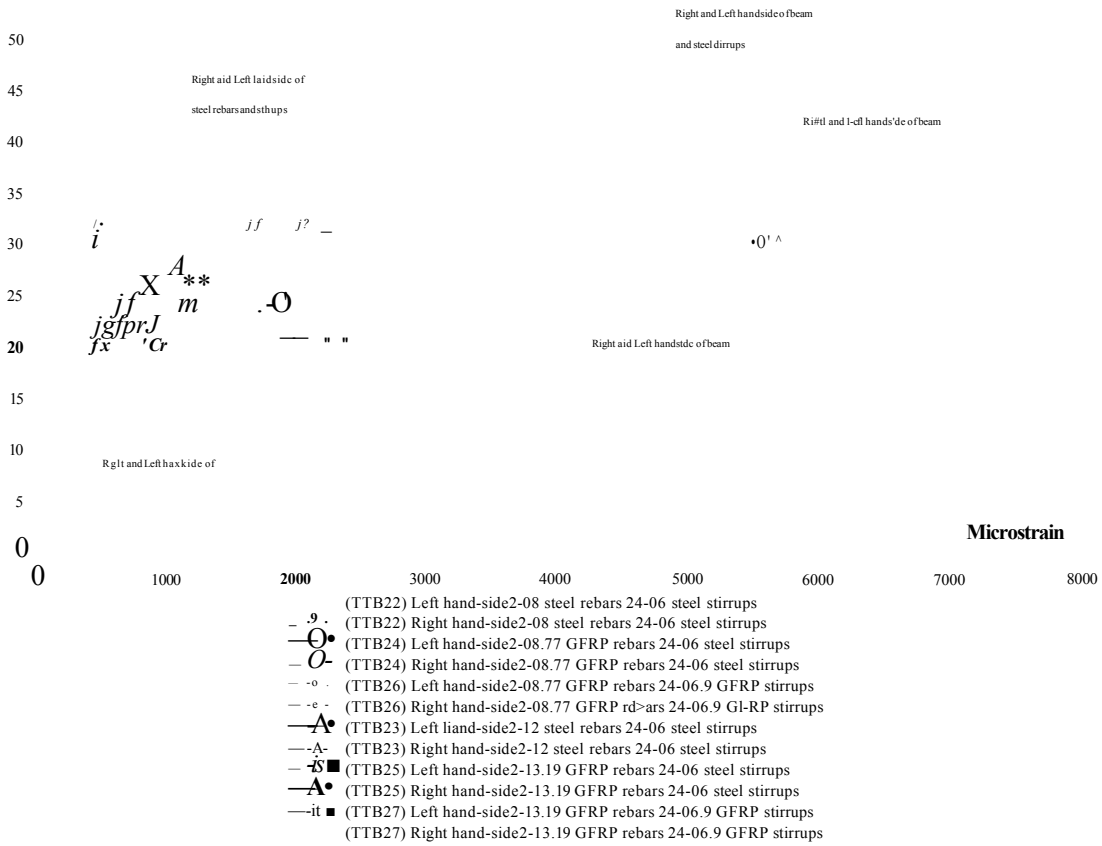

7.2.5 Stirrup strains in the shear region

As it can be seen in *Figure 7.5* and *Figure 7.6* the strains in the stirrups are based on two conditions, compression and tension. Both GFRP and steel stirrups behave in a similar manner owing to the fact that generally strain slope of the steel stirrups was steeper than the GFRP stirrups.

Figure 7.5 The bottom stirrup strains measured in the shear region

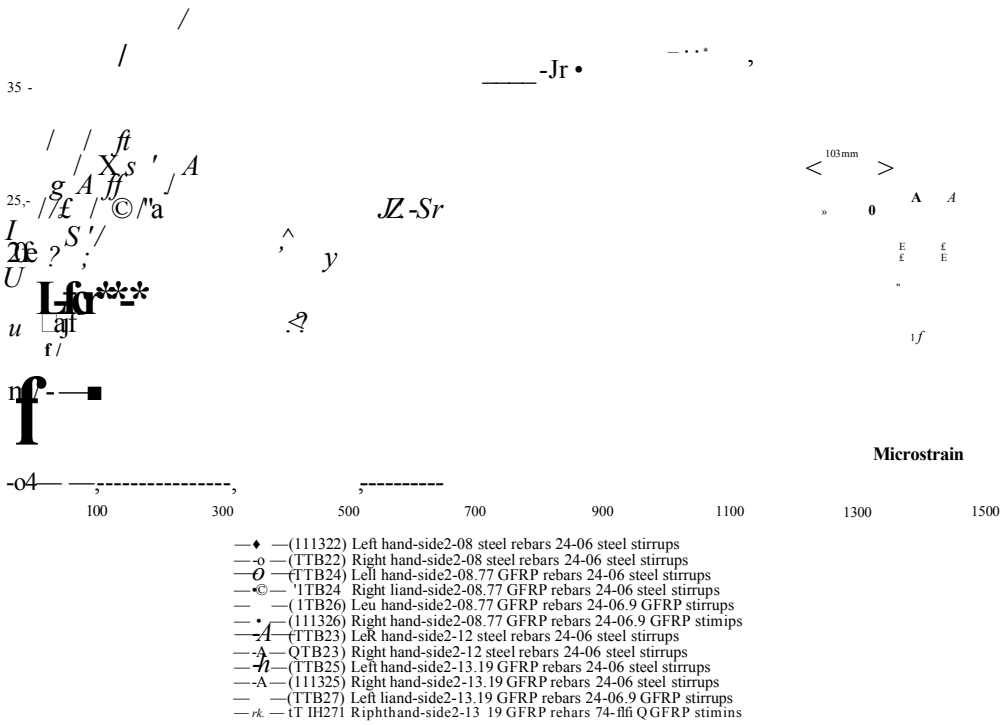

Figure 7.6 The side stirrups strains measured in the shear region

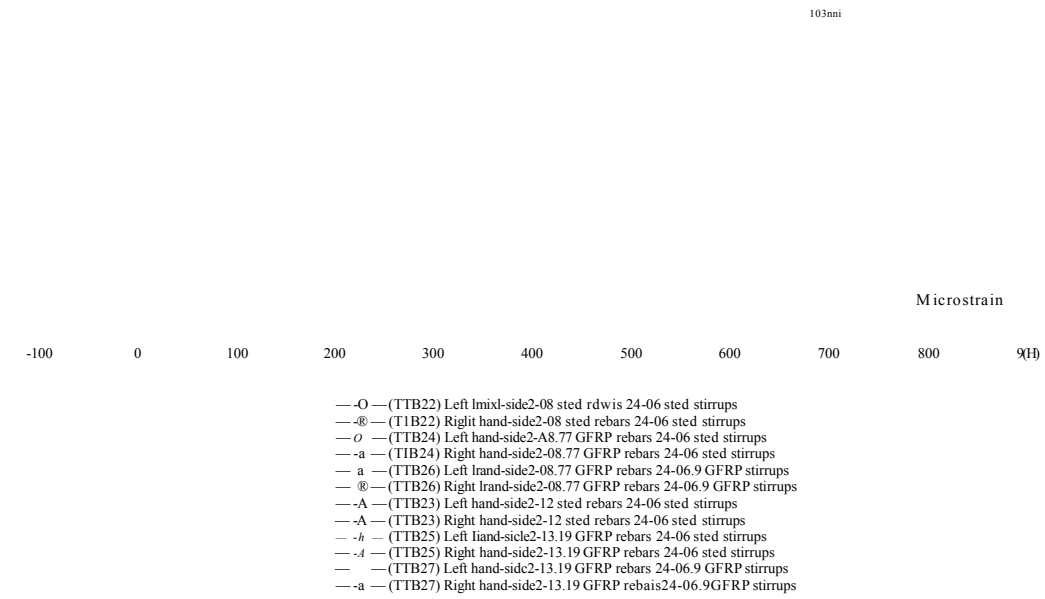

7.2.6 Concrete Strains in Maximum Bending Moment Region

As in the previous Parts of the investigation, the concrete strains were measured (see *Figure 7.7* and *Figure 7.8*) through the depth of the beams over a 900mm gauge length (distance between the two loading points). The concrete strains of the beams reinforced with GFRP main rebar and steel/GFRP stirrups are very similar in magnitude. This indicates that the GFRP stirrups could be used to replace steel stirrups. The dotted lines in the Figure designate the extrapolated strains at failure.

The strain distributions in Figure 7.9 and Figure 7.10 show the linearity of the strains and the changes in neutral axis across the depth of the beam at each load. The concrete strains in the steel reinforced beam increase much less at each load increment compared to GFRP reinforced beam.

Figure 7.7 The concrete strains measured at the maximum bending moment region of C20 concrete grade beams reinforced with small diameter (08 and 08.77) steel and GFRP main rebars and mild steel and GFRP stirrups

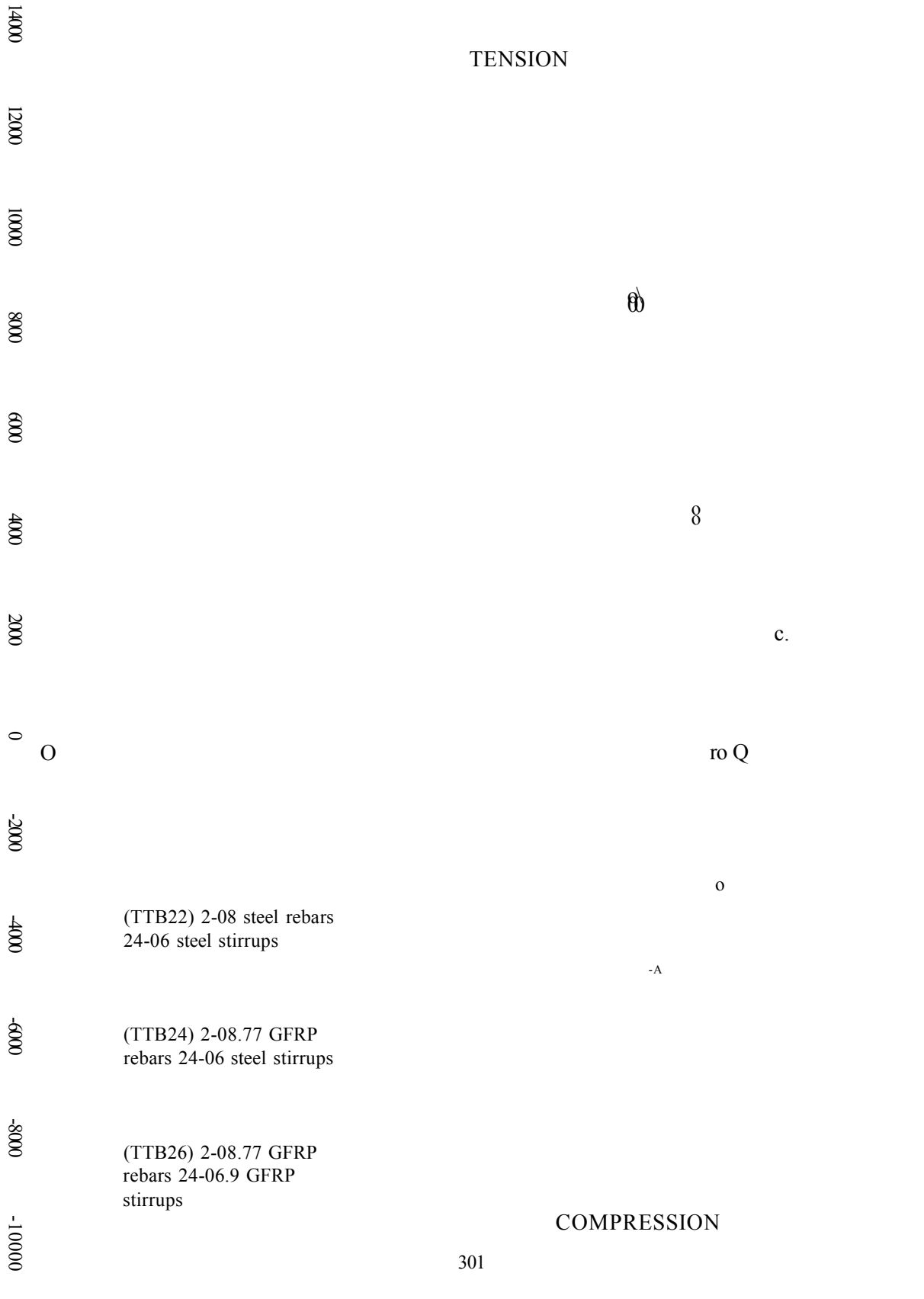

Figure 7.8 The concrete strains measured at the maximum bending moment region of C20 concrete grade beams reinforced with large diameter (pi2 and (pi3.19) steel and GFRP main rebars and mild steel and GFRP stirrups

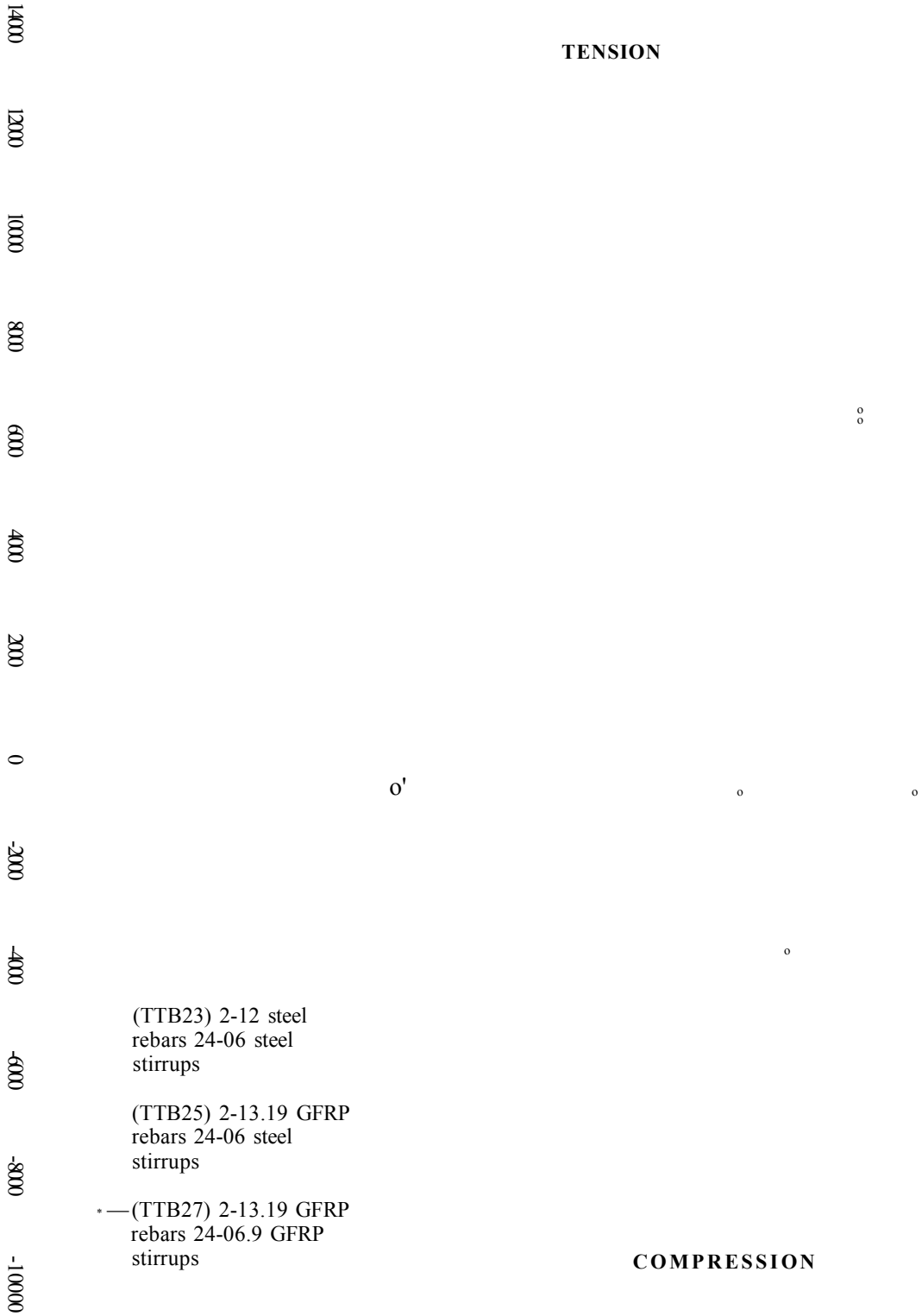

Figure 7.9 An example strain distribution of C20 grade concrete beam reinforced with 2No 12mm steel and 24No 6mm mild steel stirrups

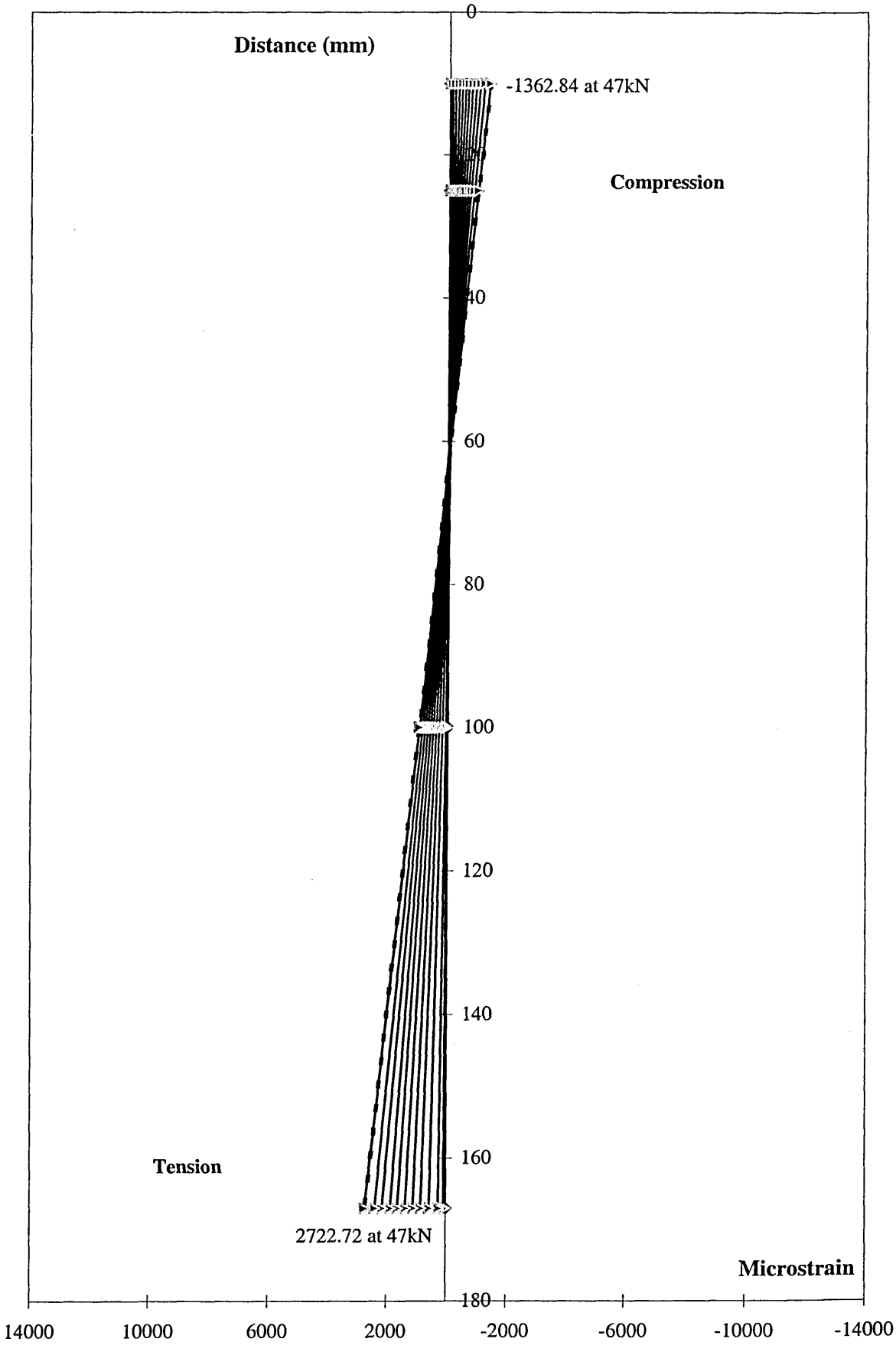

Figure 7.10 An example strain distribution of C20 grade concrete beam reinforced with 2No 13.19mm GFRP and 24No 6.9mm GFRP stirrups

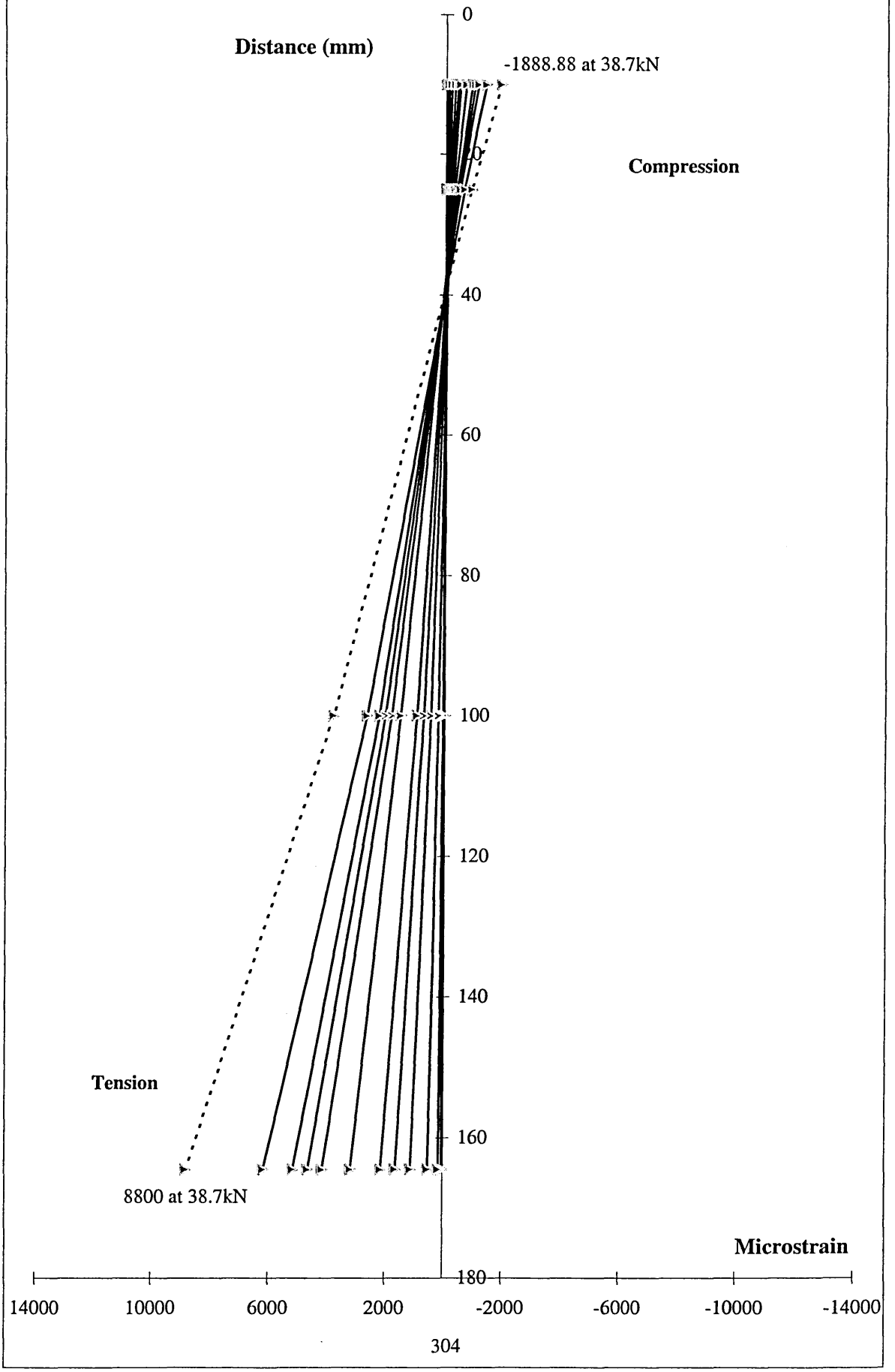

7.2.6.1 Maximum Concrete Compressive Strain

The maximum concrete strains are given in *Table 7.3* for the beams reinforced with steel and GFRP rebars and stirrups. As in Part1, Part2 and Part3 the maximum concrete compressive strains and the neutral axis depth of the beams were determined using the strain distributions (see Figure 7.9 and Figure 7.10). The equation used for calculating the maximum concrete compressive strain is given in *Appendix 5*.

Table 7.3 Extrapolated maximum concrete compressive strains in the beams

1 Beam Code	2 Concrete grade	3 Rebar No. Dia/Type	4 Stirups No. Dia/Type	5 Max. Concrete Comp. strain
TTB22	C20	2-08S	24-06S	0.0014
TTB23	C20	2-12S	24-06S	0.0016
TTB24	C20	2-08.77F	24-06S	0.0028
TTB25	C20	2-13.19F	24-06S	0.0028
TTB26	C20	2-8.77F	24-06.9F	0.0028
TTB27	C20	2-13.19F	24-06.9F	0.0026

The comparison of data in Table 7.3

- The results show that the value of maximum concrete compressive strain in the steel reinforced beams is less than in the GFRP reinforced beams. It should also be noted that the maximum concrete compression strains in the beams reinforced with GFRP tension rebars and steel/GFRP stirrups are similar suggesting that the type of stirrups have no significant effect.
- The average compressive strains in the steel reinforced beams at failure, extrapolated from measured strains on top of the beam, are 0.0015. This is approximately 43% of the maximum design concrete compressive strain given in BS8110.
- The average concrete compressive strains in the GFRP beams are 0.0028 and this is approximately 80% of the maximum design concrete compressive strain given in BS8110.

7.2.6.2 Neutral axis depth (N.A.) at the uncracked and the cracked sections

The 'theoretical' and 'measured' (experimental) neutral axis depths of the beams are given in *Table 7.4*. The values for each beam were calculated using the formula given in *Appendix 5*. The results suggest similar findings as in Part1, Part2 and Part3 of the experimental study.

The comparison of data in Table 7.4

- The 'theoretical' and the 'measured' neutral axis depths at the cracked section of first three cases (TTB22, TTB23 and TTB24) are comparable with each other at failure (see column 6 & 7).
- The percentage difference in neutral axis depths between the beams reinforced with 2ϕ8 steel rebars/mild steel stirrups (beam TTB22) and 2ϕ8.77 GFRP rebars/GFRP stirrups (beam TTB26) is only 9%((32.20*100)/39.40). However, the percentage difference is 28% between 2ϕ8 steel rebars/mild steel stirrups (beam TTB22) and 2ϕ8.77 GFRP rebars/mild steel stirrups (beam TTB24). This means that the neutral axis depth of the beam containing GFRP main rebars and steel stirrups (beams TTB24) increases more than the beams (TTB22 and TTB26) that contain steel/GFRP main rebars and steel/GFRP stirrups (see column 7)
- However, the neutral axis depth of the beam containing ϕ13.19 GFRP main rebars and stirrups (beam TTB27) rebars and stirrups increases more than those reinforced with ϕ12/13.19 main rebars and mild steel/GFRP stirrups (beams TTB23 and TTB25) at failure (see columns 7).

Table 7.4 The experimental and the theoretical neutral axis depth of the beams at the uncracked and cracked sections

1	2	3	4	5	6	7
Beam Code	Concrete grade	Rebar No. Dia/Type	Stirups No. Dia/Type	**Neutral axis depth (mm)** Theory Uncracked	Theory$_{max}$ Cracked	Measured$_{max}$ Cracked
TTB22	C20	2-08S	24-06S	103.50	40.11	39.40
TTB23	C20	2-12S	24-06S	106.09	55.30	60.80
TTB24	C20	2-08.77F	24-06S	102.06	22.49	28.70
TTB25	C20	2-13.19F	24-06S	103.02	29.93	42.20
TTB26	C20	2-8.77F	24-06.9F	102.07	22.77	32.20
TTB27	C20	2-13.19F	24-06.9F	102.48	29.44	38.00

As in Part 1, Part 2 and Part 3 of the investigation, it was observed for all beams that the neutral axis depth increases sharply once the beam cracks become apparent tending towards a constant value all the way to failure (see *Figure 7.11*). The results showed that the neutral axis depth of the beams is primarily influenced by the tension rebar areas and types.

7.2.7 Concrete Strains in Shear Region at the location of tension rebars

The concrete strains at the location of reinforcement (horizontal plane) were measured along a 200mm gauge length in the shear regions. In *Figure 7.12,* dotted lines designate the extrapolated values up to failure. It can be seen in the Figure that the beams reinforced with GFRP rebars and steel/GFRP stirrups are more exposed to the diagonal tension cracks than the ones reinforced with steel rebars and stirrups. This assumption is based upon the slope of the curve i.e. if the slope of the curve is shallow, this could be due to the increase in the number of cracks in the shear region. Also, according to the Figure the beams containing GFRP rebars have larger concrete strains than the steel beams in the shear region. There is also evidence that when the area of rebar increases, the resistance of the beam in the shear regions also increases regardless of type of stirrups used i.e. the slope of the curve is steeper for the beams showing higher resistance to shear.

Figure 7.12 The concrete strains obtained in the shear regions of the beams at the location of tension rebars

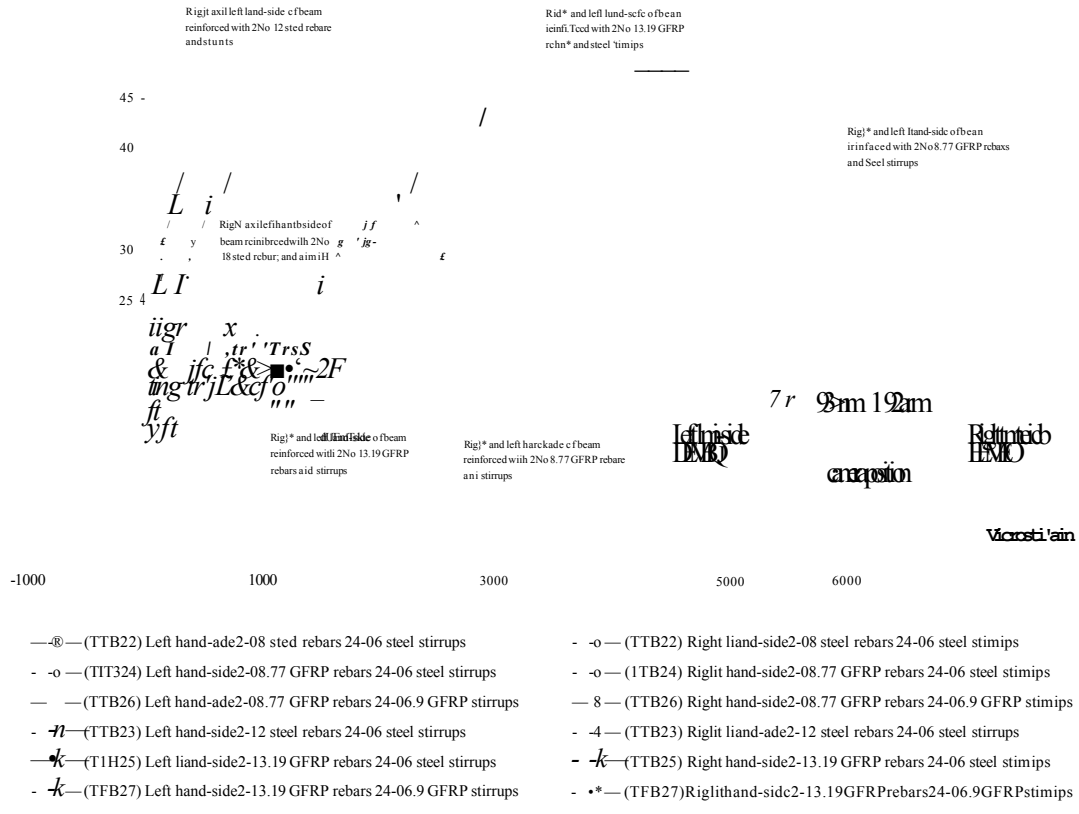

7.2.8 Concrete Strains in the Shear Region at the location of stirrups

The concrete strains obtained at the location of stirrups are very similar to those obtained from the stirrups themselves (see *Figure 7.13).* It can be seen that all the beams are under compression in the shear region on a vertical plane. As the crack openings developed more the strains became tension type. This change to tension takes place with increase in load and possibly because of change in depth of the neutral axis as load increases.

Figure 7.13 The concrete strains obtained in the shear regions of the beams at the location of stirrups

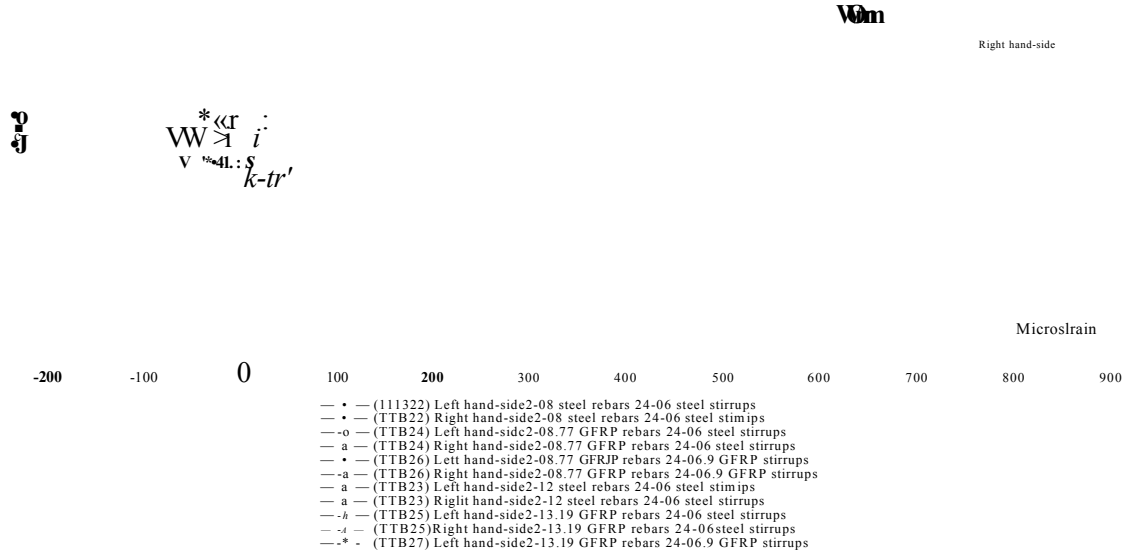

7.2.9 Elastic & Ultimate Load/Moment Capacities

Table 7.5 contains the initial crack and ultimate load capacities together with the 'theoretical' and 'measured' (applied) bending moments of all the beams. Note that the 'initial crack' load in the Table designates the first visible crack observed in the maximum bending moment region (see also *Appendix 5* for the formulae used in the calculations).

The comparison of data in Table 7.5

- It can be seen in column 7 that the initial load capacities of the GFRP reinforced beams combined with either mild steel or GFRP stirrups are 2/3 of the beams reinforced with steel main rebars and stirrups at the uncracked section.
- The beams reinforced with 2ϕ12 (beam TTB23) and 2ϕ13.19 (beam TTB25) GFRP main rebars have exactly the same ultimate load capacity of 47kN (see column 8). Note that both beams contain mild steel stirrups and have the highest ultimate load capacity compared to the rest of the beams.
- It can be seen in column 8, the ultimate load capacities of three beams (beams TTB24, TTB26 and TTB27) are comparable with each other (from 32kN to 38.7kN). The beam (TTB22) reinforced with 2ϕ8 steel main rebars and stirrups has the lowest ultimate load capacity, 24kN, compared to the rest of the beams.
- The theory underestimates the bending moment capacity of all the beams compared to those 'measured' (applied) at the uncracked section.
- Generally, the maximum 'theoretical' bending moments of all the beams with some exceptions are less than those 'measured'.

Table 7.5 Elastic & Ultimate Load/Moment Capacity of Part 4 Beams obtained from theory and experiment

1	2	3	4	5	6	7	8	9	10	11	12
Beam Code	Concrete grade	Rebar No. Dia/Type	Stirups No. Dia/Type	Rebar Area (mm^2)	Tension Rebar %	Initial Crack Load kN	Failure Load kN	**Bending Moment (kNm)** Theory Uncracked	Measured Uncracked	$Theory_{max}$ Cracked	$Measured_{max}$ Cracked
TTB22	C20	2-08S	24-06S	101	0.58	6	24	1.61	2.68	8.18	9.61
TTB23	C20	2-12S	24-06S	226	1.30	6	47	1.58	2.68	16.69	18.47
TTB24	C20	2-08.77F	24-06S	121	0.70	4	35.9	1.59	1.91	11.64	14.19
TTB25	C20	2-13.19F	24-06S	273	1.58	4	47	1.58	1.91	20.10	18.47
TTB26	C20	2-8.77F	24-06.9F	121	0.70	4	32	1.58	1.91	11.57	12.69
TTB27	C20	2-13.19F	24-06.9F	273	1.61	4	38.7	1.56	1.90	19.88	15.26

7.2.10 Ultimate Shear Capacity

The ultimate 'theoretical' and the 'measured' (applied) shear capacity of the beams are given in *Table 7.6.* (see also *Appendix 5* for the formulae used in the calculations). Note that the maximum 'measure' shear capacity of the beams is based upon the ultimate failure load of the beams and their weights does not take into account either the concrete strength or the area of main rebars.

The comparison of data in Table 7.6

- It can be seen in column 9 that the 'theoretical' shear resistances of all the beams are higher than the 'measured' ones. However, the difference between them is not large and in any case of the beams failed in flexural compression consistent with the relative magnitude of bending moment.
- The results also show that the potential shear capacity of the beams generally increases with increased percentage of tension reinforcement (see columns 5 and 9).

Table 7.6 Ultimate Shear Capacity of Part 4 Beams

1	2	3	4	5	6	7	8	9	10
Beam Code	Concrete grade	Rebar No. Dia/Type	Stirups No. Dia/Type	Rebar Area (mm^2)	Tension Rebar %	Shear span/ effective depth	Failure Mode	**Shear Resistance (MPa)** Theory$_{max}$ Cracked	Measured$_{max}$ Cracked
TTB22	C20	2-08S	24-06S	101	0.58	4.58	Compression	0.96	0.61
TTB23	C20	2-12S	24-06S	226	1.30	4.61	Compression	1.25	1.14
TTB24	C20	2-08.77F	24-06S	121	0.70	4.59	Compression	1.02	0.89
TTB25	C20	2-13.19F	24-06S	273	1.58	4.63	Compression	1.34	1.14
TTB26	C20	2-8.77F	24-06.9F	121	0.70	4.62	Compression	1.02	0.80
TTB27	C20	2-13.19F	24-06.9F	273	1.61	4.68	Compression	1.35	0.96

7.2.11 Deflection

The load vs deflection response of all the beams can be seen in *Figure 7.14*. The 'elastic stage' was continued up to the visible crack load of 6 kN for the steel reinforced beams and 4kN for the GFRP reinforced beams. The shape of the load vs deflection curve was similar to previously tested beams. The beams followed a steep straight line with a small increase in deflection up to the initial visible crack load. Beyond the 'elastic stage', the beams reinforced with steel rebars and stirrups displayed a smaller decrease in the slope compared to the ones reinforced with GFRP rebars and steel/GFRP stirrups. The yielding plateau of the steel rebar beams can be seen on the graph. The GFRP beams containing either steel or GFRP stirrups do not exhibit such a plateau but continue on a straight line up to failure. The lines of the beams containing smaller and larger diameter of GFRP rebars and steel/GFRP stirrups follow each other very closely. Note that the beams containing GFRP stirrups have a slightly reduced slope compared with those with the same diameter of rebars and steel stirrups. This could mean that the GFRP stirrups have the potential to replace steel stirrups when a consideration is given to the serviceability of the concrete beams. The Figure also shows that the slope of the 'plastic stage' increases as the area of rebars increases i.e. the beams reinforced with 2ϕ12/13.19 rebars and steel/GFRP stirrups exhibit higher stiffness compared to the beams reinforced with 2ϕ8/8.77 rebars and steel/GFRP.

I t

M
cn

(N >1) p«<n

The comparison of data in Table 7.7

The results suggest that beams containing GFRP main rebars and steel/GFRP stirrups deflect more than the steel reinforced beams at failure. For GFRP reinforced beams, it seems that the rebar diameter plays a more important role in the deflection behaviour of the beams. The smaller the tension rebar diameter the more the beam will deflect at the same load in the 'post-cracked condition (see *Figure 7.14*).

- The 'calculated' deflections are of a comparable order of magnitude as those 'measured' at the uncracked section for the steel reinforced beams (see columns 11 and 12).
- The 'calculated' deflections of the beams containing GFRP main rebars and stirrups are also comparable with those 'measured' at the uncracked section especially the beams containing small diameter GFRP rebars ('measured' deflection is 89% of those 'calculated').
- Generally, the 'measured' and the 'calculated' deflections at the cracked section are of a comparable order of magnitude with each other (see columns 13 and 14). However, the 'calculated' deflections are less than those 'measured'.
- The 'calculated' deflection of the beams containing small and large diameter steel main rebars and mild steel stirrups are 74% and 52% of those 'measured' respectively (see columns 13 and 14) at the cracked section.
- The 'calculated' deflections of the beams containing small and large main GFRP rebars and mild steel stirrups are 94% and 82% of those 'measured' respectively (see also columns 13 and 14) at the cracked section.
- In the case of beam containing small diameter GFRP rebars and stirrups, the 'calculated' deflections at the cracked section are 83% of those 'measured' (see also columns 13 and 14). For the beam containing large diameter GFRP main rebars and stirrups the 'calculated' deflections are 87% of those 'measured'.
- The results suggest that beams containing GFRP main rebars and steel/GFRP stirrups deflect more than the steel reinforced beams at failure. The smaller the tension rebar diameter the more the beam will deflect at the same load in the post-cracked condition (see *Figure 7.14*).

Table 7.7 Theoretical and experimental deflections of Part4 beams

1	2	3	4	5	6	7	8	9	10	11	12	13	14
Beam Code	Concrete grade	Rebar No. Dia/Type	Stirups No. Dia/Type	Rebar Area	Tension Rebar	**Second Moment Area (mm^4)**		**Curvature (1/mm)**		**Deflection (mm)**			
						*Calculated	*Calculated	*Calculated	*Calculated	*Calculated	**$Measured_{max}$	*Calculated	**$Measured_{max}$
				mm^2	%	Uncracked	Cracked	Uncracked	Cracked	Uncracked	Uncracked	Cracked	Cracked
TTB22	C20	2-08S	24-06S	101	0.58	7.67E+07	1.28E+07	1.20E-06	2.27E-05	0.77	0.85	14.60	19.62
TTB23	C20	2-12S	24-06S	226	1.30	7.92E+07	2.38E+07	1.13E-06	2.45E-05	0.73	0.66	15.73	30.29
TTB24	C20	2-08.77F	24-06S	121	0.70	1.49E+08	4.27E+06	5.80E-07	9.72E-05	0.37	0.36	62.51	68.68
TTB25	C20	2-13.19F	24-06S	273	1.58	9.95E+07	7.87E+06	8.70E-07	7.09E-05	0.56	0.38	45.56	55.23
TTB26	C20	2-8.77F	24-06.9F	121	0.70	1.49E+08	4.50E+06	6.00E-07	8.45E-05	0.39	0.44	54.35	65.14
TTB27	C20	2-13.19F	24-06.9F	273	1.61	1.33E+08	7.17E+06	6.28E-07	6.12E-05	0.40	0.60	39.33	45.44

* Column 7-8 using actual n.a depth * Column 9-10 using actual bending moment * Column 11-13 using actual curvature ** Column 12-14 experimental readings

7.2.12 Cracking Behaviour

The beams containing 2φ8/8.77 steel/GFRP rebars and steel/GFRP stirrups

The crack patterns developed in the beams can be seen in *Figure 7.15.* In this category, the beams containing steel rebars have a total of 20 visible cracks whereas the GFRP beams with steel and GFRP stirrups have a total of 15 and 17 visible cracks along the full beam length. The numbers of cracks are less in the GFRP rebars than the steel ones but, there are more branches in the GFRP beams and the cracks are deeper compared to the steel beams.

Figure 7.15 The crack patterns of the concrete beams reinforced with 2φ8/8.77 rebars and steel/GFRP stirrups.

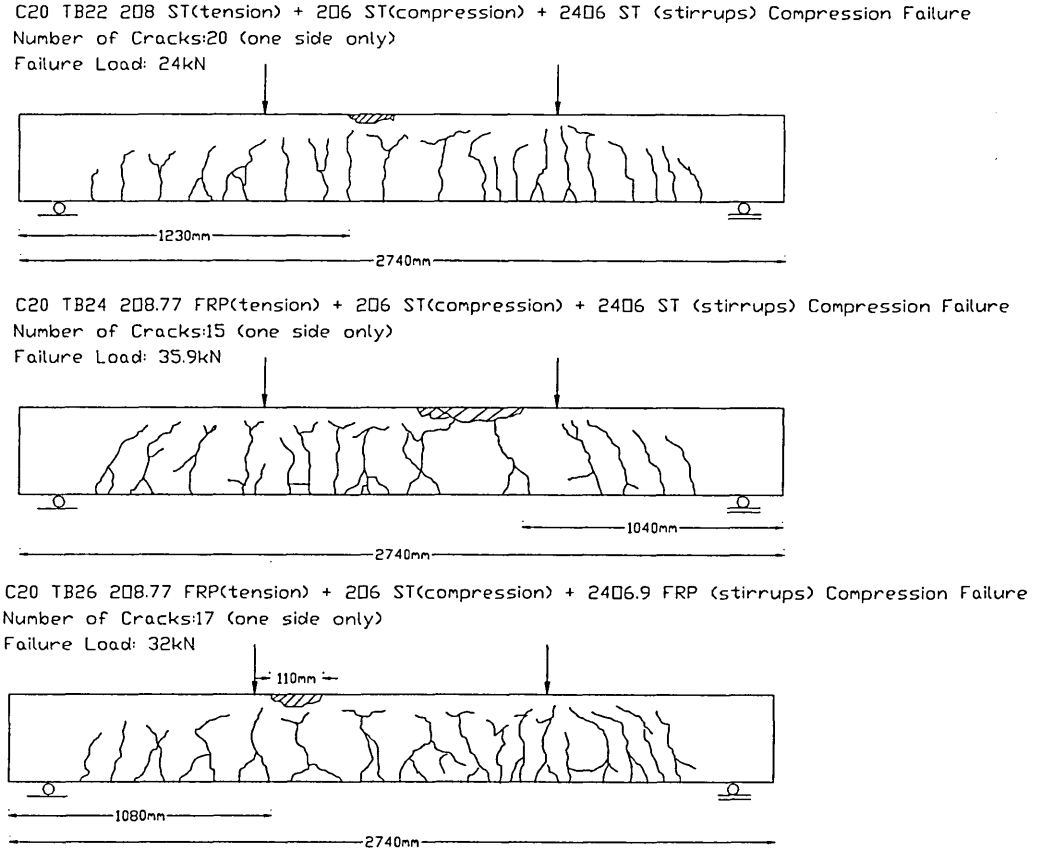

The cracking behaviour of the beams is the same as the rest of the beams tested so far. The first hairline cracks appeared at the maximum bending moment region under 6kN total load in the beams and subsequently grew more prominent and numerous as the load increased.

The beams containing 2φ12/13.19 steel/GFRP rebars and steel/GFRP stirrups

The crack propagation in the pre and post cracking stages of the beams in this category is very similar to the previous category. The average numbers of cracks in the steel beam, GFRP beams with steel stirrups and GFRP beams with GFRP stirrups are 24, 18 and 23 respectively. The crack patterns are very similar in each beam with GFRP beams having more extensions.

Figure 7.16 The cracks patterns of the concrete beams reinforced with 2φ12/13.19 rebars and steel/GFRP stirrups.

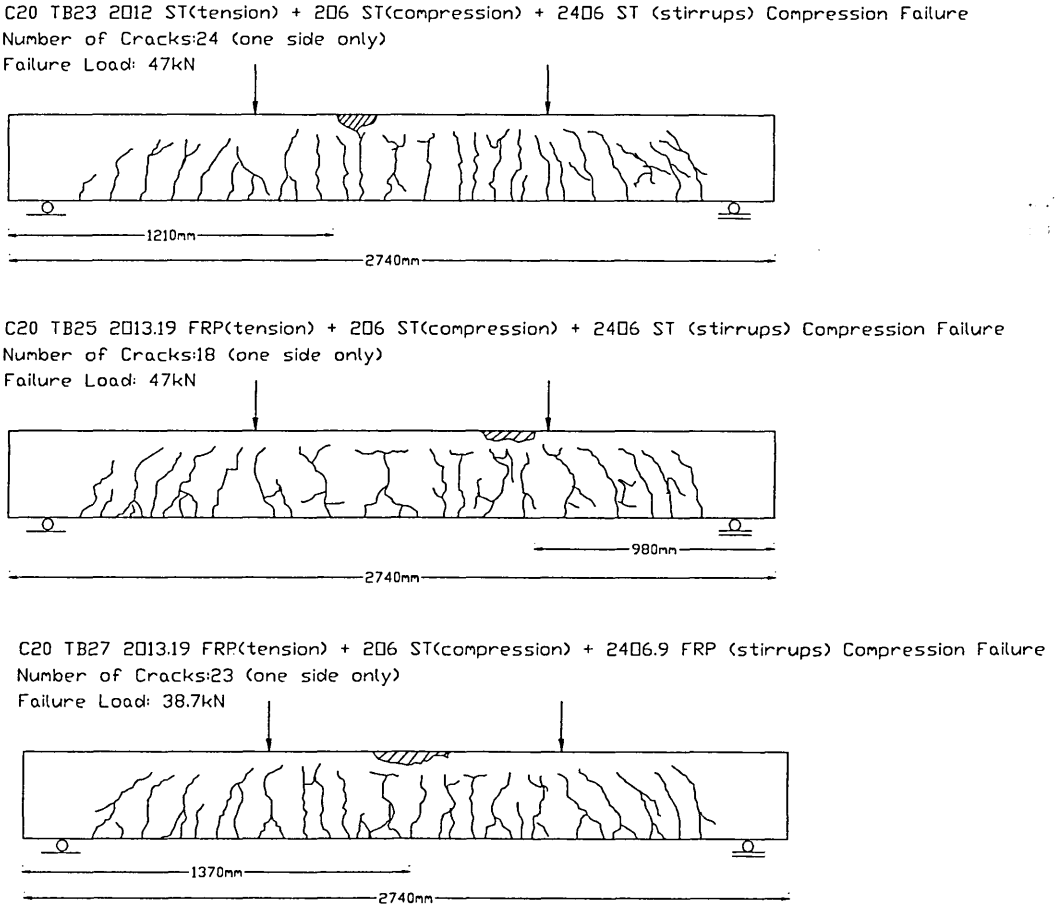

7.2.13 Modes of Failure

Typical failure mode of each beam is shown in *Photo 7.5*. The morphology of beam failures is given in *Table 7.8*. All the beams failed in compression at the maximum bending moment region. As in the previous parts, the vertical cracks were initially developed from the bottom surface within the middle section and these were followed

by diagonal cracks towards the supports in all cases. Also note in the Table that the 'failure morphology' of all the beams can be classified as 'flexural type' but steel beams tended to fail as 'under-reinforced' rather than 'over-reinforced' sections on the bases of steel main rebars reaching their 'yield plateau' and soon after that concrete crushing at the 'top'.

Photo 7.5 A view of 'compression' failure of a beam reinforced with steel/GFRP main bars and steel/GFRP stirrups

Table 7.8 The modes of failure of the concrete beams containing steel/GFRP stirrups

Beam Code	**Concrete Grade (Cube Strength-[MPa)**	**Rebar No Dia/Type**	**Failure Morphology (Failure Load-kN)**
TTB22	C20(43)	2<> 8Steel 24(j)6 Steel links	**Compression-** Steel yielded and concrete crushed in the top edges of the beam (24)
TTB23	C20(44)	2gj) 12Steel 24<j)6 Steel links	**Compression-** Steel yielded and concrete crushed in the top edges of the beam (47)
TTB24	C20(46)	2<j) 8.77GFRP 24cj>6 Steel links	**Compression-** Concrete crushed in the top edges of the beam (35.9)
TTB25	C20(46)	2(j) 13.19GFRP 24(J)6 Steel links	**Compression-** Concrete crushed in the top edges of the beam (47)
TTB26	C20(41)	2<f) 8.77GFRP 24c|)6.9GFRP links	**Compression-** Concrete crushed in the top edges of the beam (32)
TTB27	C20(39)	2(I> 13.19GFRP 24(J>6.9GFRP links	**Compression-** Concrete crushed in the top edges of the beam (38.7)

7.2.14 Estimation of Flexural Crack Widths

Table 7.9 contains the theoretical and experimental estimations of the maximum crack widths using the equations given in *Appendix 5*.

Table 7.9 Estimated crack widths of Part 4 beams

1	2	3	4	5	6	7
Beam Code	Concrete grade	Rebar No. Dia/Type	Stirups No. Dia/Type	[1]*Number of Cracks	**Estimated crack widths (mm)** [2]**BS8110	[3]***Experiment
TTB22	C20	2-08S	24-06S	9	0.07	0.08
TTB23	C20	2-12S	24-06S	14	0.16	0.11
TTB24	C20	2-08.77F	24-06S	11	0.56	0.52
TTB25	C20	2-13.19F	24-06S	9	0.45	0.51
TTB26	C20	2-8.77F	24-06.9F	13	0.56	0.45
TTB27	C20	2-13.19F	24-06.9F	16	0.52	0.33

[1]*in the maximum bending moment region [2]**based upon the formulae [3]***based upon the dial gauge measurements

Also, for this Part, the values of maximum crack widths calculated using the equations in BS8110 are comparable with the experimentally estimated values except beam TTB27. It seems that the beams reinforced with main steel rebar and stirrups have smaller flexural crack widths than the ones reinforced with GFRP rebars and steel/GFRP stirrups whereas those reinforced with smaller diameter GFRP rebars and steel/GFRP stirrups tend to have larger crack widths compared to the ones reinforced with larger diameter GFRP rebars.

7.3 Performance Quotient (Q_p)

The Author proposed another Performance Quotient (Q_p) considering the 'top bars' and the 'stirrups' in the beams. The formula is given below and the results are included in *Table 7.10.* Also, the calculations are given in *Appendix 5.*

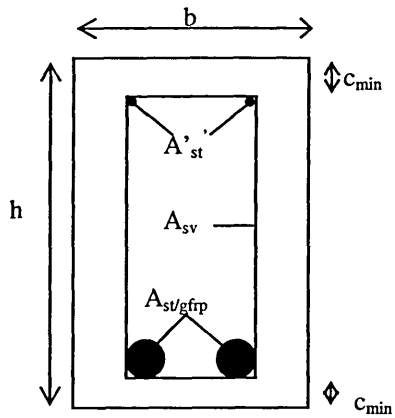

$$Q_p = \frac{1000(F_f + B.S.W)}{f_c(bh - As - As' - neqs) + f_s As + f'_s As' + (f_s . neqs)}$$

$$neqs = \left(\frac{\frac{2L}{SV}(b - 2C\min) + (h - 2C\min)}{L}\right) As''$$

Similar to previously obtained the Q_p of the beams having higher load capacity is also higher for the beams containing mild steel stirrups. According to the results in Table 7.10, the beams (TTB23 & TTB25) reinforced with ϕ12/13.19 diameter steel/GFRP main rebars assembled with mild steel stirrups have a very similar performance quotient suggesting that the ultimate load capacity of these beams and the yield/ultimate stress of the main rebars are also very similar. In the case of beam (TTB24) reinforced with ϕ8.77 diameter GFRP main rebars and mild steel stirrups, the performance quotient is higher than those reinforced with ϕ8 main steel rebars and mild steel stirrups. However, the performance quotient of the beam reinforced with ϕ8.77 and ϕ13.19 main rebars and GFRP stirrups is less than the rest of the beams even though the ultimate load capacity of these beams are very similar in magnitude to beam TTB24. This is due to the fact that the ultimate stress of GFRP stirrups is almost twice of the yield stress of the mild steel stirrups. This suggests that Q_p index of beams containing GFRP main rebars and stirrups having lower value for a higher load capacity when compared with the beams reinforced with GFRP main rebars and mild steel stirrups.

7.4 Conclusions

The performance of C20 normal weight concrete beams reinforced with 2ϕ8, 2ϕ8.77, 2ϕ12, 2ϕ13.19 steel and GFRP main rebars combined with 24ϕ6 mild steel stirrups and 24ϕ6.9 GFRP stirrups, was studied. The main observations and tentative findings of this Part are outlined below.

The results indicated that the maximum tensile stresses and strains in the steel and ϕ8.77 GFRP rebars reach their full tensile capacity whereas with ϕ13.19 GFRP this is approximately 73% of the tensile capacity (see *Table 7.2*). Generally, tensile strains measured in the rebars were influenced by the rebar area i.e. the bigger the area the less the strain at a given load.

The strains of steel main rebars and stirrups in the shear region of the beams are less than those reinforced with GFRP main rebars combined with either steel or GFRP stirrups (see *Figure 7.4*).

Compared with the force sustained by the concrete in the compression zone it was found that the contribution of 2ϕ6 'top bars' against compression was negligible. The results showed that there is a change in the status of strains in the 'top bars' (see *Figure 7.3*) i.e. compressive (-'ve) strains become tensile (+'ve). This could be due to the location of the strain gauges attached to the 'bars' and possible composite to non composite action during loading cycle.

The maximum concrete compressive strain in the beams reinforced with GFRP main rebars and steel/GFRP stirrups is the same suggesting that the type of stirrups has no significant effect (see *Table 7.3*).

There is also evidence that when the area of rebar increases the resistance of concrete in the shear regions at the location of main rebars, also increases regardless of type of stirrups (see *Figure 7.12*). The concrete strains of all the beams at the location of stirrups are initially compressive, however as the crack openings develop the concrete strains become progressively tensile (see *Figure 7.13*).

The results show that the main rebar areas and types primarily influence the neutral axis depth of the beams (see *Figure 7.11*).

The initial load carrying capacity of the beam reinforced with 2ϕ8 steel, 2ϕ8.77 and 2ϕ13.19 GFRP rebars was not affected by either of the stirrup types. The evidence for this is that the same beam with no stirrups tested in Part 1 (Chapter 4) has the same initial crack load of 6kN for the steel and 4kN for the GFRP reinforced beams. However, it seems that the beam reinforced with 2ϕ12 steel rebars was influenced by the stirrups i.e. the initial load capacity of the beam increased from 4kN to 6kN. However, this is not highly significant in view of the fact that this depends on monitoring of visible cracks.

The overall trend for both steel and GFRP reinforced beams is that ultimate load and bending moment capacities can be enhanced with larger diameter of tension rebars. The GFRP and steel stirrups combined with GFRP main rebars are also influential

factors on the enhanced load capacity of the beams (see *Table 4.8* in Chapter 4 and *Table 7.5*).

Load versus deflection behaviour of GFRP reinforced beams containing stirrups also exhibited linear elastic curve up to failure as the beams tested in the previous Parts. The steel reinforced beams exhibited a yielding plateau at failure (*Figure 7.14*).

Generally, the 'measured' and the 'calculated' deflections at the cracked section are of similar orders of magnitude (see *Table 7.7*). However, the 'calculated' deflections are less than those 'measured'. The results suggest that beams containing GFRP main rebars and steel/GFRP stirrups deflect more than the steel reinforced beams at failure

The initiation and the pattern of propagation of the cracks in all the beams are generally the same (see *Figure 7.15* and *Figure 7.16*) although at failure different from that in the majority of beams in the previous parts of the investigation i.e. concrete crushes at the top edge of the beam between the loading points.

It seems that the beams reinforced with main steel rebar and stirrups have smaller flexural crack widths than the ones reinforced with GFRP main rebars and steel/GFRP (see *Table 7.9*).

Using both mild steel and GFRP stirrups has modified the shear failure of the beams to compression (flexural) failure (see *Photo 7.5*). The results suggest that the GFRP rebars can be combined with either mild steel or GFRP stirrups in the beams.

The beams having the highest Performance Quotient (Q_p) generally have the higher load capacity, irrespective of whether the beams containing GFRP or mild steel stirrups (see *Table 7.10*). However, it should be noted that the Q_p indices of beams containing GFRP main rebars and stirrups are lower values as their load capacity when compared with the corresponding beams reinforced with GFRP main rebars and mild steel stirrups.

CHAPTER 8

8 CONCLUSIONS & RECOMMENDATIONS FOR FUTURE RESEARCH

This Chapter contains concluding discussions based on the experimental programme and theoretical (using BS8110 equations) results described in Chapter 3 to Chapter 7. The recommendations for further work are also included at the end of the Chapter.

8.1 Summary Review

A preliminary investigation was undertaken to establish the link designs and material including rebar property. Following the main laboratory testing programme (Part 1) further experiments (Part 2, 3 & 4) were conducted to investigate the behaviour and the performance of concrete beams under two point loading containing various types and grades of concrete in combination with various configurations of steel/GFRP rebars. In Part 1, the performance of steel and GFRP reinforced concrete beams with three different concrete grades, C20, C40 and C60 was examined. This was in relation to the strains in the reinforcing bars and concrete, ultimate load/bending capacities, deflection response, stiffness, performance quotient, ultimate shear capacity, failure modes and cracking behaviour. Following Part 1, the catastrophic failure of some of the GFRP rebars necessitated a formal risk assessment to be completed before the subsequent Parts were undertaken. This was carried out in conjunction with some modification to the monitoring procedure and technique to enable the measurement of performance indicators to proceed safely to an advanced stage up to incipient failure. Part 2 of the investigation was based upon the findings from Part 1 and focused on the GFRP reinforced high strength (C60) concrete beams and the optimisation of rebar configuration. Part 3 was based upon the perceived optimal rebar configuration varying the area of rebars, with different types and strengths of concrete i.e. lightweight aggregate concrete, concrete containing microsilica and chopped glass fibres. Finally, the purpose of the Part 4 was to examine and compare the performance of beams reinforced with steel/GFRP main reinforcing bars combined with steel/GFRP stirrups. Wherever possible, all the performance parameters considered were compared with the existing

recommendations of codes of practice (BS8110) and/or findings from previous research.

The main conclusions of the work are summarized below and the thesis concludes by making recommendations for future research. The work carried out for this research contained a large amount of data and hence in order to focus more clearly upon the critical findings, the Author believed that it would be a good idea to make summary tables selecting only 'top' (higher performance) and 'bottom' (lower performance) three beams from each Part based upon their Performance Quotient (Q_p). Table 8.1, 8.2 and 8.3 contains the summary results of the beams in Part1, Part2 & 3 and Part4 respectively. The ranking of the beams in the Tables helps to interpret the results based upon the loading of the tested beams. The Q_p values in the Tables were calculated using the derived equations in Chapter 4 and Chapter 7 for the beams without and with stirrups respectively. The loading of the beams in the Tables were included in two categories, precracked (when first visible crack/s were apparent) and postcracked (when failure occurred) and based on the ratio of load to deflection.

Table 8.1 Performance Summary of Part 1 Beams

1	2	3	4	5	8	9	6	7	10	11
Beam Code	Concrete grade	Rebar No. Dia/Type	Failure Mode	Rebar Area mm^2	Yield/Ultimate Stress MPa	Cube Strength MPa	Precracked Load (Limit) kN	Postcracked Load (Limit) kN	Performance Quotient (Qp) Actual	Ranking
TB17	C20	2-16S	Shear-Bond	402	467.00	43	6	56.3	0.0539	1
TB13	C20	2-12S	Shear-Bond	226	497.00	40	4	42	0.0461	2
TB14	C20	2-13.19F	Shear-Bond	273	470.70	40	4	31.5	0.0344	3
RBTB16	*C20*	*2-08.77F*	*Shear*	*121*	*601.00*	*47*	*4*	*26*	*0.0265*	*4*
RTB18	*C20*	*2-16.44F*	*Shear*	*425*	*544.00*	*45*	*4*	*26.6*	*0.0242*	*5*
RTB15	*C20*	*2-08S*	*Flexure*	*101*	*523.50*	*50*	*6*	*25.1*	*0.0241*	6
TB9	C40	2-16S	Shear-Bond	402	467.00	61	6	68	0.0483	1
TB1	C40	2-12S	Flexure	226	497.00	55	8	50	0.0414	2
TTB21	C40 FB	2-13.19F	Shear	273	470.70	54	6	36	0.0295	3
TB10	C40	2-16.44F	Shear-Bond	425	544.00	51	5	29	0.0238	4
TB5	C40	2-08S	Flexure	101	523.50	61	6	24	0.0191	5
TB6	C40	2-08.77F	Shear	121	601.00	69	6.8	20	0.0143	6
TB11	C60	2-16S	Shear-Bond	402	467.00	75	9	58	0.0343	1
TB3	C60	2-12S	Flexure	226	497.00	72	8	48	0.0307	2
TB4	C60	2-13.19F	Shear-Bond	273	470.70	79	6	38	0.0224	3
RBTB8	*C60*	*2-08.77F*	*Shear*	*121*	*601.00*	*78*	*6*	*30*	*0.0185*	*4*
TB12	C60	2-16.44F	Shear-Bond	425	544	76.22	5.8	28	0.0164	5
TB7	C60	2-08S	Flexure	101	523.5	73.03	6	24	0.0161	6

Beam Code	Concrete grade	Rebar No. Dia/Type	Failure Mode	Rebar Area mm^2	12 Precracked Deflection (Limit) mm	13 Postcracked Deflection (Limit) mm	14 Stiffness Precracked kN/mm	15 Ranking Precracked	16 Stiffness Postcracked kN/mm	17 Ranking Postcracked
TB17	C20	2-16S	Shear-Bond	402	0.74	15.17	8.1	1	3.7	1
TB13	C20	2-12S	Shear-Bond	226	0.63	17.98	6.3	5	2.3	2
TB14	C20	2-13.19F	Shear-Bond	273	0.51	45.17	7.8	2	0.7	5
RBTB16	*C20*	*2-08.77F*	*Shear*	*121*	*0.97*	*48.38*	*4.1*	*6*	*0.5*	*6*
RTB18	*C20*	*2-16.44F*	*Shear*	*425*	*0.59*	*22.4*	*6.8*	*4*	*1.2*	*4*
RTB15	*C20*	*2-08S*	*Flexure*	*101*	*0.86*	*14.31*	*7.0*	*3*	*1.8*	*3*
TB9	C40	2-16S	Shear-Bond	402	0.75	18.61	8.0	3	3.7	1
TB1	C40	2-12S	Flexure	226	1.18	25.7	6.8	5	1.9	2
TTB21	C40 FB	2-13.19F	Shear	273	0.69	38.34	8.7	2	0.9	4
TB10	C40	2-16.44F	Shear-Bond	425	0.41	33.23	12.2	1	0.9	4
TB5	C40	2-08S	Flexure	101	0.87	13.94	6.9	4	1.7	3
TB6	C40	2-08.77F	Shear	121	2.18	47.97	3.1	6	0.4	5
TB11	C60	2-16S	Shear-Bond	402	0.94	13.2	9.6	1	4.4	1
TB3	C60	2-12S	Flexure	226	1.16	18.79	6.9	3	2.6	2
TB4	C60	2-13.19F	Shear-Bond	273	1.22	56.72	4.9	4	0.7	5
RBTB8	*C60*	*2-08.77F*	*Shear*	*121*	*1.71*	*56.55*	*3.5*	*5*	*0.5*	*6*
TB12	C60	2-16.44F	Shear-Bond	425	1.91	31.23	3.0	6	0.9	4
TB7	C60	2-08S	Flexure	101	0.65	13.67	9.2	2	1.8	3

steel reinforced beam
GFRP reinforced beam

Table 8.2 Performance Summary of Part 2 & 3 Beams reinforced with GFRP rebars

1	2	3	4	5	6	7	8	9	10	11	12	
Beam Code	**Concrete grade**	**Rebar No. Dia/Type**	**Rebar Profile**	**Failure Mode**	**Rebar Area (mm^2)**	**Yield/Ultimate Stress MPa**	**Cube Strength MPa**	**Precracked Load (Limit) kN**	**Postcracked Load (Limit) kN**	**Performance Quotient (Qp) Actual**	**Ranking**	
TTB7	C60	4-13.19F	straight & curved	Shear	546.56	470.7	70	4	54	0.0325	1	
TTB2	C60	4-08.77F	straight & curved	Compression	242	601	78	6	52	0.0300	2	
RTRIAL	*C60*	*3-08.77F*	*curved*	*Shear*	*181.5*	*601*	*74*	6	*38*	*0.0236*	3	*Part 2*
TTB1	*C60*	*3-08.77F*	*straight & curved*	*Shear*	*181.5*	*601*	*78*	6	*35.2*	*0.0209*	4	
TTB4	C60	3-08.77F	straight	Shear	181.5	601	77	5.6	34	0.0205	5	
TTB3	C60	2-08.77F	curved	Shear-Rupture	121.00	601	78	6	27.2	0.0166	6	
RTTB5	*C20*	*4-08.77F*	straight & curved	*Shear*	*242*	*601*	*44*	*6*	*42.8*	*0.0413*	*1*	
TTB17	C40 FB	4-08.77F	straight & curved	Shear	242	601	56	6	46.8	0.0364	2	
TTB18	C40 FB	4-13.19F	straight & curved	Shear	546.56	470.7	59	6	51.4	0.0357	3	*Part3*
TTB13	C20 LT SIL	4-13.19F	straight & curved	Shear	546.56	470.7	61	4	36	0.0245	4	
TTB12	C20 LT SIL	4-08.77F	straight & curved	Shear/Shear	242	601	63	4	32	0.0225	5	
TTB14	C50 LT	4-08.77F	straight & curved	Shear/Shear	242	601	69	6	30	0.0196	6	

						13	14	15	16	17	18	
Beam Code	**Concrete grade**	**Rebar No. Dia/Type**	**Rebar Profile**	**Failure Mode**	**Rebar Area (mm^2)**	**Precracked Deflection (Limit) mm**	**Postcracked Deflection (Limit) mm**	**Stiffness Precracked kN/mm**	**Ranking Precracked**	**Postcracked kN/mm**	**Ranking Postcracked**	
TTB7	C60	4-13.19F	straight & curved	Shear	546.56	0.52	42.97	7.7	2	1.3	1	
TTB2	C60	4-08.77F	straight & curved	Compression	242	1.57	48.27	3.8	3	1.1	2	
RTRIAL	*C60*	*3-08.77F*	*curved*	*Shear*	*181.5*	*0.7*	*54.68*	8.6	1	0.7	3	*Part 2*
TTB1	*C60*	*3-08.77F*	*straight & curved*	*Shear*	*181.5*	2.71	*67.84*	2.2	4	0.5	4	
TTB4	C60	3-08.77F	straight	Shear	181.5	2.58	62.45	2.2	4	0.5	4	
TTB3	C60	2-08.77F	curved	Shear-Rupture	121.00	2.76	72.12	2.2	4	0.4	5	
RTTB5	*C20*	*4-08.77F*	straight & curved	*Shear*	*242*	*1.1*	*45.85*	5.5	*5*	0.9	*5*	
TTB17	C40 FB	4-08.77F	straight & curved	Shear	242	0.73	44.8	8.2	2	1.0	4	
TTB18	C40 FB	4-13.19F	straight & curved	Shear	546.56	0.67	33.97	9.0	1	1.5	1	*Part3*
TTB13	C20 LT SIL	4-13.19F	straight & curved	Shear	546.56	0.6	24.85	6.7	4	1.4	2	
TTB12	C20 LT SIL	4-08.77F	straight & curved	Shear/Shear	242	0.54	32.36	7.4	3	1.0	4	
TTB14	C50 LT	4-08.77F	straight & curved	Shear/Shear	242	0.73	24.96	8.2	2	1.2	3	

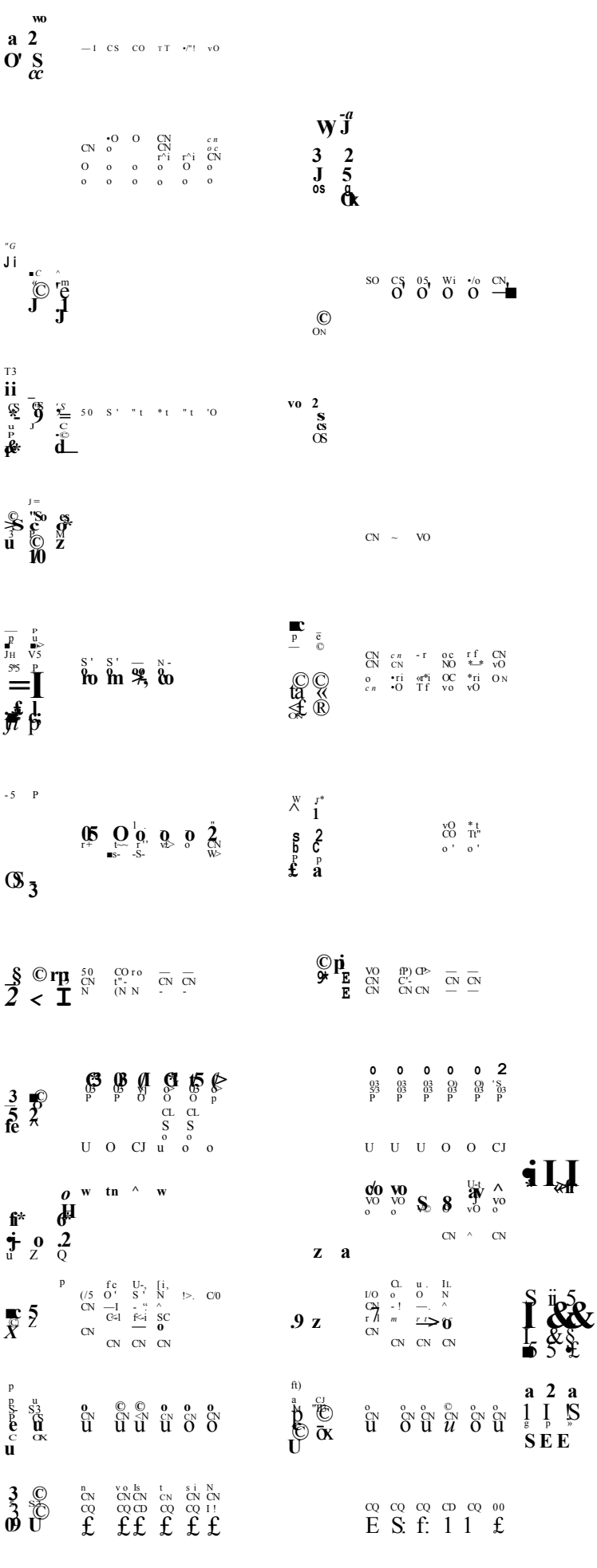

Table 83 Performance Summary of Pari 4 Beams

8.2 Conclusions

The conclusions drawn herein are based upon the key findings throughout the experimental study.

Precracked Load Capacity

1. Generally, the precracked crack load capacity of all the beams having the dimensions of 103mm x 203mm x 2740mm and tested in Part 1 to Part 4 was approximately 4kN to 6kN minimum regardless of rebar type.
2. The precracked crack load capacity of Part 1 beams reinforced with both steel and GFRP main rebars, increased between 34% and 50% with increased concrete grade for a given rebar diameter (see column 6 in Table 8.1 for Part 1). However, concrete grade did not seem to influence the precracked load capacity of the beams reinforced with small diameter (ϕ8) steel rebars.
3. The precracked load capacity of the beams reinforced with 'straight only', 'curved only' and 'straight and curved' GFRP rebar profiles was very similar in magnitude (4kN to 6kN). This suggests that the beams are not sensitive to the geometry of rebars within the precracked limit of the beams for a given concrete grade and rebar diameter (see column 9 in Table 8.2 for Part2).
4. The precracked load capacity of the beams did not seem to be influenced by the stirrup types for the beams reinforced with steel and GFRP main rebars for a given concrete grade and rebar diameter (compare column 6 in Table 8.1 for Part1 with column 10 in Table 8.3 for Part4).

Postcracked (Ultimate) Load Capacity

5. For all grades of concrete, the ultimate load capacity of the beams reinforced with larger (ϕ16) and medium (ϕ12) diameter 'straight profile' steel rebars was higher than the beams reinforced with ϕ8.77, ϕ13.19, ϕ16.44 diameter 'straight profile' GFRP rebars and ϕ8 diameter steel (see column 7 in Table 8.1 for Part 1).
6. The ultimate load capacity of the beams reinforced with both steel and GFRP rebars increased between 3% and 18% with increasing concrete grade for a given rebar diameter and failure mode (see column 7 in Table 8.1 for Part 1). However, concrete grade did not seem to affect the ultimate load capacity of the beams

reinforced with small diameter (ϕ8) steel and large diameter (ϕ16.44) GFRP rebars.

7. The ultimate load capacity of the steel reinforced beams increased between 40% and 60% with increased rebar area for a given concrete grade and failure mode. This was also the case for the GFRP reinforced beams but with a smaller percentage between 21% and 36% i.e. less sensitive to the rebar area (see column 7 in Table 8.1 for Part 1). It should be noted that the beams reinforced with larger diameter (ϕ16.44) GFRP rebars had a very similar ultimate load capacity to those reinforced with smaller diameter (ϕ8.77) GFRP rebars.
8. The ultimate load capacity of the beams seemed to be influenced by the profile of the GFRP rebars. The beams containing 'curved only' profile rebars failed at a load 4% and 11% more than those reinforced with 'straight only' profile rebars for a given concrete grade, rebar area and failure mode (see column 10 in Table 8.2 for Part2).
9. The beams reinforced with 'straight and curved' profile GFRP rebars (see column 10 in Table 8.2 for Part 2) have reached the highest ultimate load capacity with increased concrete strength (compare column 10 in Table 8.2 for Part 2 and Part 3) for a given rebar diameter/area and failure mode.
10. The ultimate load capacity of the C40 glass fibre added concrete beams reached a higher value (51.4.kN and 46.8) than the rest of the beams in Part 3 (see column 10 in Table 8.2) for a given rebar geometry. Also in Part3, C20 lightweight and microsilica added lightweight concrete beams seemed to be approximately 25% lower than the C20 normal grade concrete beams for a given rebar area, concrete grade and failure mode. Generally, lightweight aggregate concrete beams had a lower load capacity compared to normal grade concrete beams.
11. The ultimate load capacity of the beams reinforced with GFRP main rebars and stirrups was approximately 10% less than those reinforced with steel stirrups for a given concrete grade, rebar diameter and failure mode (see column 11 in Table 8.3 for Part 4). Generally, the beams containing medium diameter (ϕ12 and ϕ13.19) main steel or GFRP rebars combined with steel/GFRP stirrups had the highest load capacity amongst all the beams in Part 4.
12. The ultimate flexural load capacity of the beams reinforced with GFRP main rebars and steel stirrups was approximately 30% more than those reinforced with

GFRP main rebar only (failed in shear in Part1). This was approximately 20% for the beams reinforced with GFRP main rebars and stirrups (compare column 11 in Table 8.3 with column 7 in Table 8.1).

13. The beams containing stirrups had higher load capacities compared to those reinforced with two main rebars only. However, the beams reinforced with novel geometry of GFRP rebars ('straight and curved' profile) achieved higher load capacity than those containing stirrups with increased rebar area and concrete grade (compare column 11 in Table 8.3 for Part 4 with column 10 Table 8.2 Part 3). This could offer a potential for the fact that the GFRP rebars could be used more efficiently having this type of profile with a consequent saving on materials and assemblage time.

Precracked Stiffness

A high value of stiffness in both pre and postcracked cases, generally, indicates that the beam deflected at a low value for a given load.

14. Steel reinforced C20 and C60 beams exhibited higher stiffness than the beams reinforced with GFRP rebars (see column 15 in Table 8.1 for Part 1).
15. The stiffness of the beams reinforced with 'straight and curved' profile GFRP rebars had higher stiffness than the rest of the beams in Part 2 for a given concrete grade (see column 16 in Table 8.2).
16. The stiffness of the beam containing 'straight' profile GFRP rebars was approximately 60% of the one reinforced with 'curved only' profile GFRP rebar for a given concrete grade and rebar diameter/area (compare column 14 in Table 8.1 for Part 1 with column 15 in Table 8.2 for Part2).
17. C40 glass fibre added, C50 lightweight aggregate and C20 silica added lightweight aggregate concrete beams containing 'straight and curved' profile GFRP rebars had higher stiffnesses than the rest of the beams in Part 3 (see column 16 in Table 8.2).
18. The beam reinforced with 2ϕ8.77 GFRP main rebars with steel stirrups had the highest stiffness (see column 17 in Table 8.3 for Part4). The beams reinforced with 2ϕ12 steel main rebars with steel stirrups and 2ϕ8.77 GFRP main rebars with GFRP stirrups had the same stiffness.

19. The stiffness of the C20 grade concrete beams containing steel and GFRP stirrups were higher compared to those without stirrups for a given rebar diameter/area (compare column 14 in Table 8.1 for Part 1with column 16 in Table 8.3 for Part 4). GFRP reinforced beams contained steel stirrups exhibited higher stiffnesses than those contained GFRP stirrups.

Postcracked Stiffness

Generally, the beams reinforced with GFRP rebars deflected more than the steel reinforced beams. However, in the further test programmes (Part 2, Part 3 and Part4) it was found that the rate of increase in deflection at each load increment could be influenced by using different areas of reinforcement and configurations. The following conclusions based upon the test results can be drawn.

20. All the steel reinforced beams had higher stiffnesses than the beams reinforced with GFRP rebars (see column 17 in Table 8.1 for Part 1 and column 19 in Table 8.3 for Part 4).
21. The stiffness of the beams reinforced with steel or GFRP rebars with and without stirrups increased with increased rebar diameter/area for all concrete grades for a given failure mode (see column 17 in Table 8.1, column 18 in Table 8.2 for Part 2 & 3 and column 19 in Table 8.3 for Part 4).
22. C40 with glass fibre added concrete beam had the highest stiffness of the beams in Part 3 for a given rebar profile and failure mode (see column 18 in Table 8.2).
23. The beams containing steel/GFRP stirrups exhibited higher stiffnesses for a given main rebar type and diameter (compare column 16 in Table 8.1 for Part 1 with column 18 in Table 8.3 for Part 4).

Rebar strain capacity

24. The tensile recovery of the GFRP rebars under load versus extension curves was remarkable owing to the fact that the recoverable energy in the GFRP rebars was elastic rather than plastic as for steel rebars. This could indicate that the GFRP rebars have potential to perform better in post yield state in seismic design applications.
25. The strains measured from both steel and GFRP main rebars in the tension region of the beams suggested that the large diameter rebars deformed less than the small diameter rebars at failure and the concrete type did not seem to affect the magnitude of the rebar strains.
26. Generally, the maximum tensile stresses and strains in the steel rebars and small diameter (ϕ8.77) GFRP reached almost their full tensile capacity throughout the investigation.

Failure mode

27. Shear failure was to be the dominant type for GFRP reinforced beams. However, using either mild steel or preformed GFRP stirrups could modify this to tensile or compressive type of failure mode. The shear failure is not necessarily the worse type considering some of the beams containing steel main rebars failed in flexure catastrophically and ruptured.
28. The beams reinforced with GFRP rebars and which failed in shear-rupture were changed the 'failure type' with using larger area of rebars having different profiles or using steel/GFRP stirrups.

Crack patterns & widths

29. The initiation and the sequence of the crack development were very similar in all the beams. The first crack appeared within the maximum bending moment region and subsequently grown to be more prominent and numerous along the span as the load increased. In comparison with beams reinforced with 'straight profile' steel rebars, the cracks in GFRP reinforced beams were observed to be deeper with larger gaps between the adjacent cracks (Part 1). However, beams reinforced with 'curved profile' GFRP rebars seemed to have more shear cracks compared to the beams reinforced with 'straight profile' GFRP rebars (Part2). The beams

reinforced with combination of 'straight and curved' profile GFRP rebars developed more cracks but the gaps between them seemed to be reduced (Part3). The overall crack pattern of the beams containing mild steel/GFRP stirrups (Part4) was similar to the other Parts, however, the final appearance was governed by the compression failure.

30. The crack widths in the GFRP reinforced beams were observed to be larger compared to the steel reinforced beams at failure. The results showed that the dial gauge used to measure the concrete strains within the maximum bending moment region of all the beams could be adopted for estimating the flexural crack widths which are comparable with those calculated using BS8110 formulae.

Performance Quotient

31. The following mathematical expressions have been derived for determining the performance (Performance Quotients, Q_ps) of concrete beams reinforced with either steel or GFRP main rebars combined with or without stirrups. The interpretations of Q_p values are governed mainly by the ultimate load capacity, however, the concrete grade and the yield/ultimate strength of the rebar also affect the magnitude of Q_p.

For beams containing main rebars only in the tension region:

$$Q_p = \frac{1000\ (\text{Failure Load} + \text{Beam Self Weight})}{f_c\,(bh - A_{st\,/\,gfrp}) + f_{st\,/\,gfrp}\,A_{st\,/\,gfrp}}$$

For beams containing main rebars in the tension region and combined with stirrups:

$$Q_p = \frac{1000(\text{Failure Load} + \text{Beam selfweight})}{f_c\left[bh - A_{st\,/\,gfrp} - A'_{st} - n_{eqs}\right] + \left[f_{st\,/\,gfrp} \times A_{st\,/\,gfrp} + f'_{s_{top}} \times A'_{st} + (f_{yv} \times n_{eqs})\right]}$$

$$n_{eqs} = \left(\frac{L_{eqs}}{L_s}\right) \times A''_{sv}$$

$$L_{eqs} = \frac{2L_s}{s_v}\{(b - 2c_{\min}) + (h - 2c_{\min})\}$$

30. The performance of the beams reinforced with ϕ16 and ϕ12 steel rebars was in the top rank whereas the beams contained ϕ8 steel rebars were in the bottom rank

amongst all the beams for all concrete grades (see column 11 in Table 8.1 for Part 1).

31. The beams reinforced with ϕ13.19 and ϕ8.77 GFRP rebars had the top rank performance amongst all the beams reinforced with GFRP rebars except for C40 concrete grade (see also column 11 in Table 8.1 for Part 1).
32. Q_p values of the beams reinforced with either steel or GFRP rebars suggested that better or similar performance could be achieved with low grade concrete (C20) and with less rebar area (compare TB13 and TB9 in column 10 of Table 8.1).
33. The beams reinforced with 4ϕ13.19 and 4ϕ8.77 GFRP 'straight and curved' profile rebars had the top rank performances amongst all the beams tested in Part 2 (see column 12 in Table 8.2 for Part 2). Their Q_p values were very similar due to the fact that they also had a similar load capacity but the beam reinforced with smaller diameter rebars failed in compression.
34. The beams containing 'curved only' profile GFRP rebars reached higher performance ranking with increased load capacity, compared to those that contained 'straight only' profile steel/GFRP rebars for a given diameter/area and concrete grade (C60) (compare column 11 in Table 8.2 for Part 2 and column 10 in Table 8.1 for Part 1, also TTB3 with TB7).
35. The highest ranking performance was achieved with C20 concrete beams that contained 4ϕ13.19 and 4ϕ8.77 'straight and curved' profile GFRP rebars in Part 3 (see column 12 in Table 8.2).
36. The lowest performance ranking occurred with lightweight aggregate concrete beams in Part 3 (see column 12 in Table 8.2). However, the performance of the lightweight concrete beams containing microsilica was better than the beams containing only lightweight aggregate. The beams reinforced with ϕ13.19 and ϕ8.77 GFRP rebars had a very similar performance value (see column 11 in Table 8.2).
37. The performance of the beams reinforced with main steel/GFRP rebars increased with using steel/GFRP stirrups for a given main rebar area. Although more rebar material was used in these beams, the failure mode was modified from shear to compression type (compare Table 8.1 with Table 8.3 for C20 concrete grade).

38. The beams reinforced with ϕ12 steel and ϕ13.19 GFRP rebars and steel stirrups had the highest rank performance amongst the other beams in Part 4 (see column 13 in Table 8.3)

Reliability of the existing code

39. The existing code of practice (BS8110) is a reliable source for assessing and predicting the performance of GFRP reinforced beams. However, when designing concrete elements containing GFRP rebars, a higher material factor (γ_m) should be considered since the load versus extension characteristic of GFRP rebars exhibits linear behaviour up to brittle failure i.e. concrete element may not give any warning prior to failure. In addition, changing (increasing) load factor in design to compensate for potentially more 'brittle' behaviour of GFRP should also be considered. Alternatively, using the optimum (novel) rebar geometry proposed in design (i.e. main rebars having 'straight and curved' profile) would modify failure mode to less catastrophic ('softer') forms.

Proposed Model

40. The theoretical values of performance parameters i.e. bending moment, ultimate shear capacity, deflection etc have been calculated using the formulae in the current code of practice, BS8110 and compared with the experimental data wherever possible. The study showed that the existing code, within certain limits is a reliable source, for assessing and predicting the performance of GFRP reinforced beams. However, direct substitution is unlikely in practice because of the difference in mechanical properties of the two materials. Traditional reinforced design relies upon the yielding of steel as the primary cause of failure (under-reinforced design concept). Whereas, when using GFRP an alternative design philosophy must be adopted in which a 'softer' compression or shear type failure condition must be induced either through a 'soft' compression or shear type failure but still maintaining structural continuity. Consideration should also be given to the serviceability design. GFRP's lower elastic modulus will affect deflection in design. Although crack width is also one of the serviceability requirements and provides additional warning of failure prior to compression

failure of concrete, it is suggested that due to GFRP's corrosion resistant characteristics this would not be a significant consideration in design except for aesthetic reasons.

41. The beams manufactured in this investigation would be ideally suited for use as small structural precast components such as a prefabricated concrete lintel containing either 'straight and curved' GFRP rebars or GFRP main rebars combined with steel/GFRP stirrups. It is suggested that these configurations of rebars will enable the concrete element to fail in 'softer' shear or compression types of failures. Also, there is a potential use of GFRP reinforced elements in short span concrete members where deflection would not be the major concern.

8.3 Summary of Key Findings

- In general, increasing concrete strength had a small effect upon load capacity of the beams. Overall, steel reinforced beams had a greater load capacity than the GFRP reinforced beams. However, for flexural failure GFRP reinforced beams displayed a greater capacity to absorb energy than steel for similar loads but exhibited reduced stiffness at any given load although this was enhanced by the inclusion of glass fibres in the mix.
- The beams reinforced with GFRP main rebars demonstrated larger deflection than those reinforced with steel. In general, the results showed load capacity increases with increase in main rebar area. Deflection is the limiting criterion for serviceability design of GFRP reinforced beams and hence the potential use of GFRP rebars should be recommended for small/short span concrete elements.
- Overall, the crack widths in the GFRP reinforced beams were observed to be larger and deeper compared to the steel reinforced beams. However, this would not be the major concern for serviceability design due to non-corrodible nature of GFRP rebars.
- Failure of the steel reinforced beams was predominantly in 'flexure' for the more lightly reinforced sections and in 'shear-bond' for those with the largest areas of reinforcement. GFRP reinforced beams exhibited mostly 'shear-bond' type failure with the exception of the most lightly reinforced high strength concrete beam. The failure mode was altered to 'double shear' and 'compression' types of failures

by using combination of 'straight and curved' profile GFRP main rebars and mild steel/GFRP stirrups respectively.

- Experimental measurements generally agreed with the corresponding theoretical and quasi-theoretical values derived from fundamental principles and conventional design considerations. However, the theory generally overestimated the bending moment and shear resistance capacity and underestimated the neutral axis depth and deflection.
- A mathematical expression has been derived for the development of the concept of a 'performance quotient' as a useful efficiency comparator for the beams of different types and composition.

8.4 Recommendations for Future Work

The following may constitute important points for further research into the performance of GFRP reinforced concrete elements:-

1. This study could provide useful amount of data for 'shear' failure of the beams reinforced with GFRP rebars.
2. This investigation has examined the differences in rebar type, configuration and concrete types and strength. It would be desirable to assess the effects of beams having deeper depths and shorter shear span on the shear performance.
3. Using Scanning Electron Microscope (SEM) in order to determine the bond between concrete and the GFRP rebars. However, the attention should be paid to cutting of the samples to the appropriate size with as less disturbance as possible to the bond between the rebar and the concrete.
4. New performance indices can be developed based upon deflection, energy absorbtion capacity or fatigue of the beams.

Appendix Table of Contents

LIST OF PUBLICATIONS

1. A paper published in the 'Proceedings of International Conference, Concrete in Mankind', Dundee, Scotland, 1996.

2. An abstract published in 'The Institution of Structural Engineers Young Researcher's Conference', London, UK, 1999.

3. A poster presented in 'Science & Engineering Technology (SET200) in House of Commons', London, UK, 2000.

Typical Tensile Properties of Single Fibres (after Weidmann[1])

Material	Density (kg/m^3)	Tensile Modulus (GPa)	Tensile Strength (MPa)
natural fibres			
cotton	1520	6-20	300-800
silk	1340	8-13	300-650
wool	1300	3-4	100-200
synthetic fibres			
nylon 6	1130	0.7	330
nylon 6,6	1140	1-5	400-750
PET(Polyethylene terephthalate)	1380	12-19	600-800
PP(Polypropylene)	910	6.4	600
PAN(Polyacrylonitrile)	1140	7	380
high performance fibres			
aramid (Kevlar 29) (Kevlar 49)	1400 1440	60 124	2800 3100
Polythelene (SPECTRA 900)	970	120	2600
carbon	1760-1960	265-520	1900-2800
inorganic fibres			
E-glass	2550	72	3400
C-glass	2490	69	2800
S-glass	2490	87	4600
A-glass	2500	68	2400
zirconia	5600	100	700
alumina	2800	100	1000
boron	2600	380	3800
asbestos	2500	160	2100
silicon carbide	2500	410	4000
metallic			
steel	7860	210	3000

The Comparison of Selected High Performance Fibres (after Yang[5])

	Kevlar Fibre	Carbon Fibre	High strength Polyethylene Fibre	S 2-glass Fibre
Physical properties				
Density (kg/m^3)	1440	1800	970	2480
Melt temperature (^0C)	550	4000	147	1200
Tensile strength (MPa)	2300-3400	4000	2600-3000	4800
Tensile modulus (GPa)	55-143	400	120-171	85
Performance Parameters				
Tensile strength	good	very good	very good	poor
Tensile modulus	good	very good	very good	poor
Toughness	good	poor	good	poor
Compressive properties	poor	very good	good	good
Shear properties	poor	good	good	good
Light stability	poor	good	good	good
Creep	good	good	very poor	good
Flame resistance	good	very good	very poor	very good
Moisture regain	poor	good	good	good
Non-abrasiveness	good	poor	good	poor
Lightweight	good	poor	very good	poor
Thermal properties	good	very good	very poor	very good
Solvent resistance	good	very good	poor	very good
Impact resistance	very good	poor	good	poor
Adhesion	poor	good	very poor	poor

Grading curve for coarse aggregate

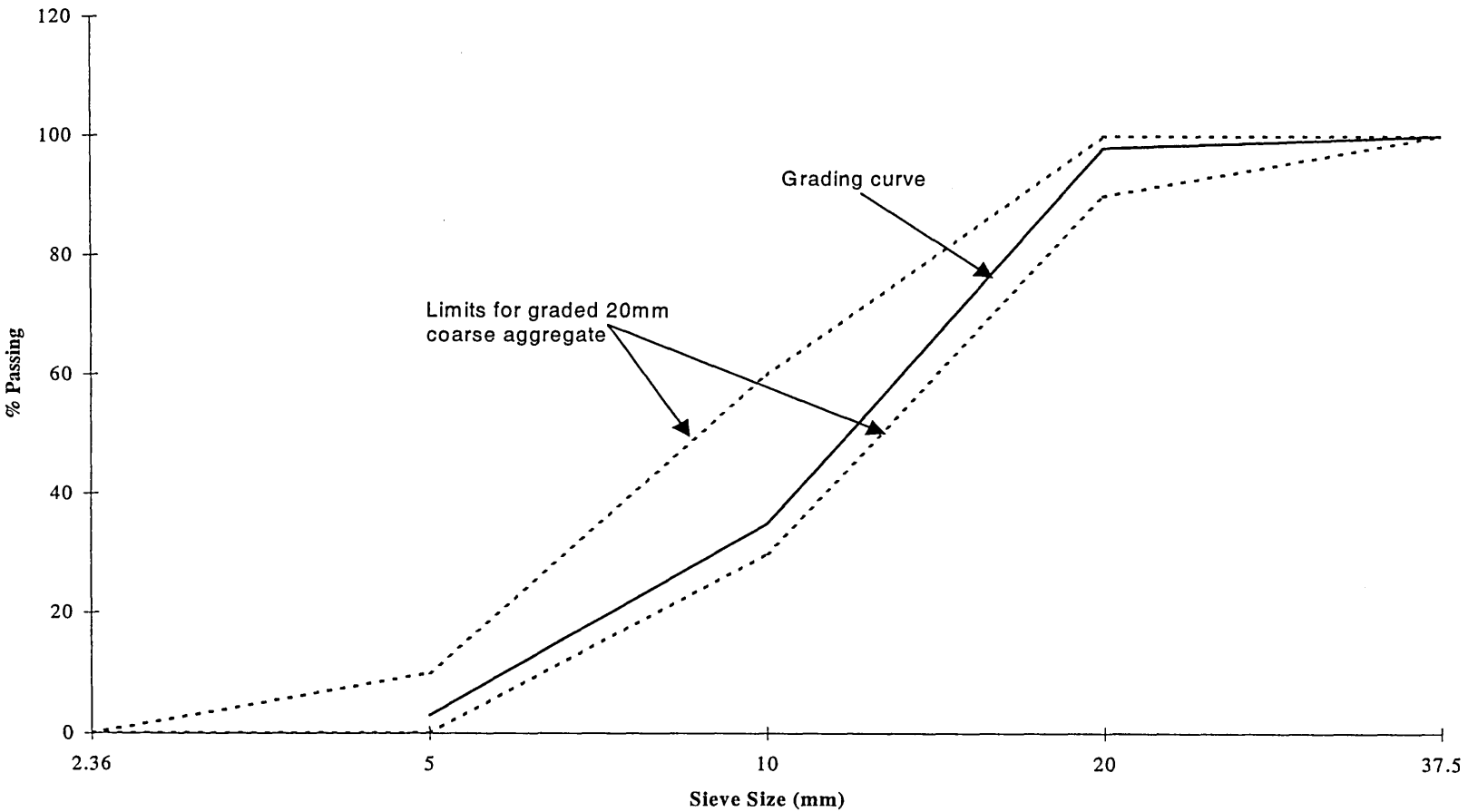

Grading curve for lightweight aggregate

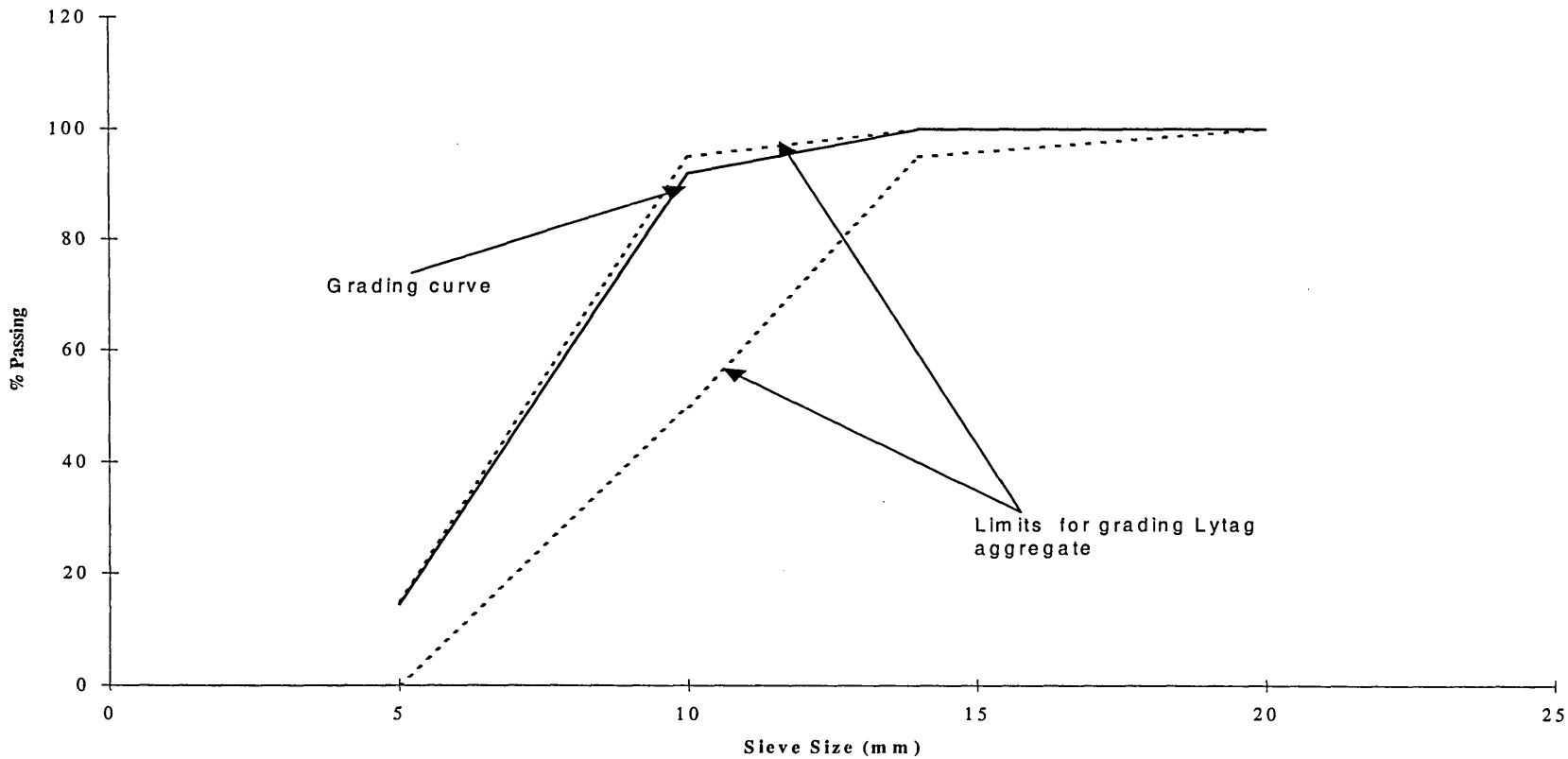

Grading curve for fine aggregate

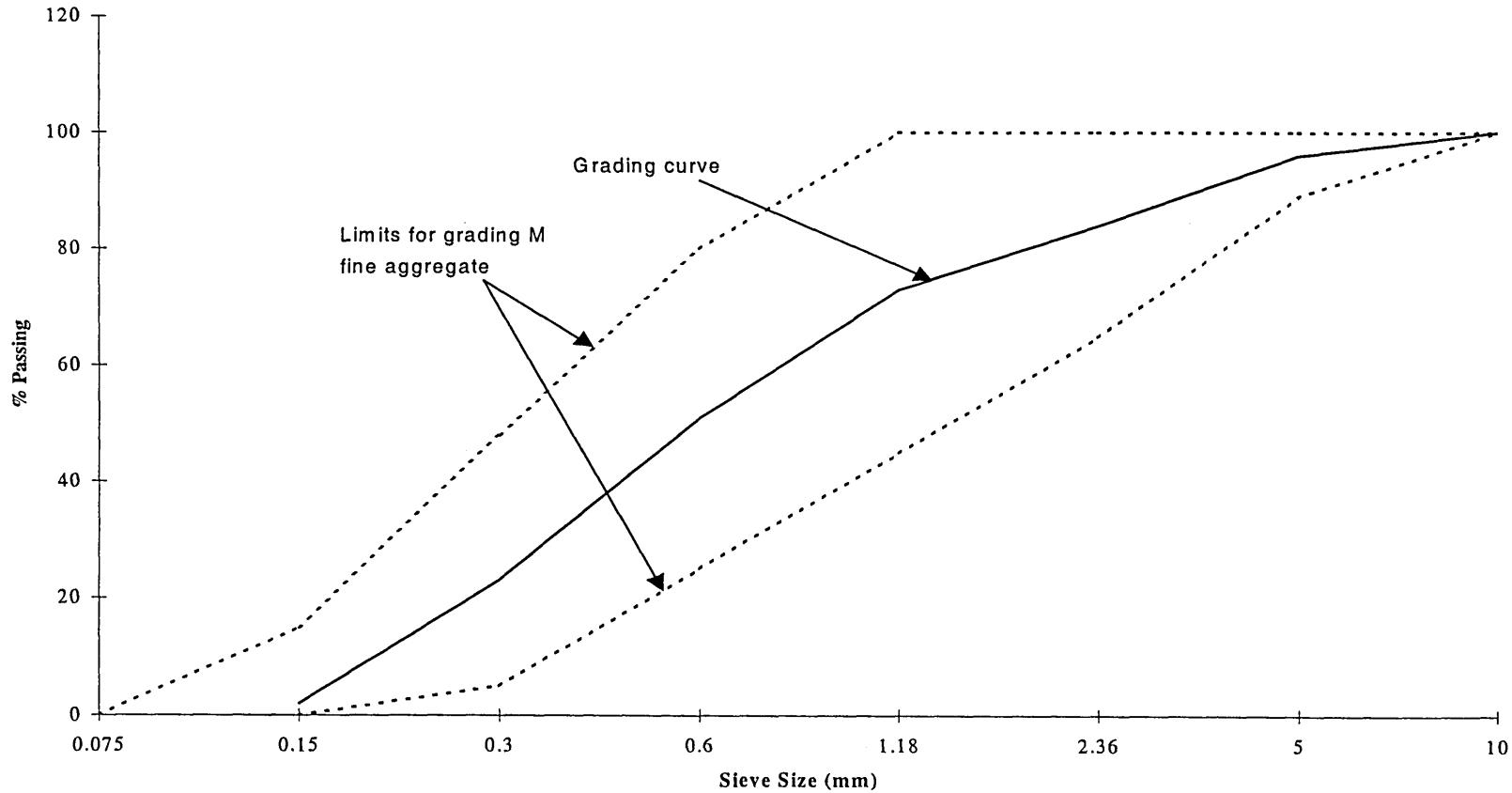

A representative stress vs strain curve of C20 grade concrete cylinder 1 used for determination of concrete modulus of elasticity

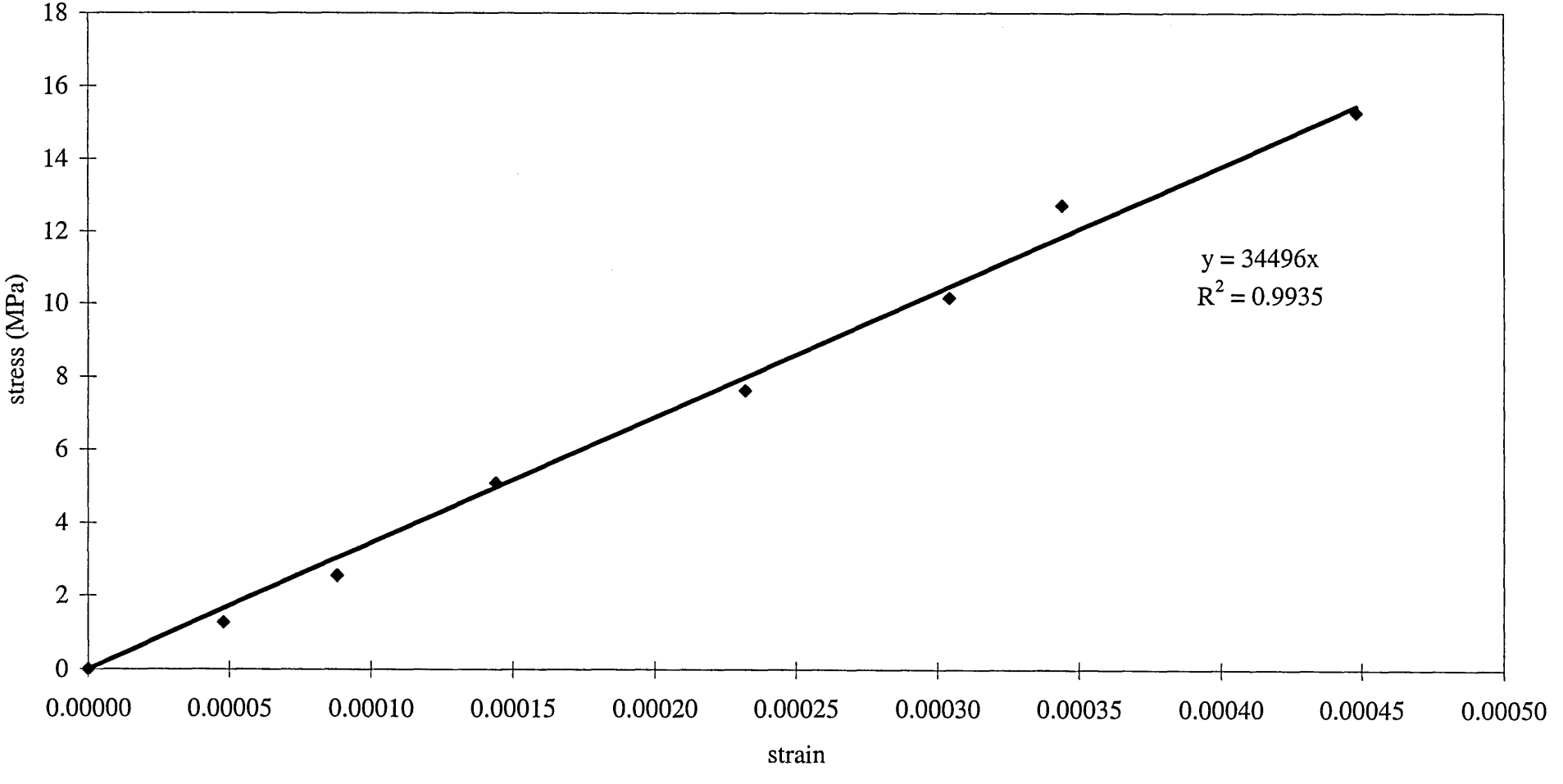

xxx

SAMPLE CALCULATIONS

1. *Neutral Axis Depth (χ_{theo}) based upon BS8110 equations*

C20, TB15 reinforced with 2∅8 Steel rebars in the tension region.....(1)
C20, TB16 reinforced with 2∅8.77 GFRP rebars in the tension region.....(2)

uncracked:

$$\frac{\chi_{theo\,uncr}}{d} = \frac{\alpha_e\rho + \frac{1}{2}\left(\frac{h}{d}\right)^2}{\alpha_e\rho + \left(\frac{h}{d}\right)} = \left[\frac{(5.636\times0.00483) + \frac{1}{2}\left(\frac{203}{174}\right)^2}{(5.636\times0.00483) + \left(\frac{203}{174}\right)}\right]\times174 = \underline{\underline{103.15}}\,\text{mm}.....(1)$$

$$\frac{\chi_{theo\,uncr}}{d} = \frac{\alpha_e\rho + \frac{1}{2}\left(\frac{h}{d}\right)^2}{\alpha_e\rho + \left(\frac{h}{d}\right)} = \left[\frac{(1.366\times0.00578) + \frac{1}{2}\left(\frac{203}{173.61}\right)^2}{(1.366\times0.00578) + \left(\frac{203}{173.61}\right)}\right]\times173.61 = \underline{\underline{101.98}}\,\text{mm}.....(2)$$

$$\alpha_e = \left(\frac{E_{st}}{E_c}\right) = \left(\frac{186}{33}\right) = 5.636.....(1) \qquad \alpha_e = \left(\frac{E_{gfrp}}{E_c}\right) = \left(\frac{45.09}{33}\right) = 1.366.....(2)$$

$$A_{st} = \frac{\pi D^2}{4} = \frac{2\times3.141\times8^2}{4} = 100.53\text{mm}^2 \sim 101\,\text{mm}^2.....(1)$$

$$A_{gfrp} = \frac{\pi D^2}{4} = \frac{2\times3.141\times8.77^2}{4} = 120.81\text{mm}^2 \sim 121\,\text{mm}^2.....(2)$$

$$d = h - (\text{cover} + \frac{D}{2}) = 203 - (25 + \frac{8}{2}) = 174\,\text{mm}.....(1)$$

$$d = h - (\text{cover} + \frac{D}{2}) = 203 - (25 + \frac{8.77}{2}) = 173.61\,\text{mm}.....(2)$$

$$\rho = \left(\frac{A_{st}}{bh}\right) = \left(\frac{101}{103\times203}\right) = 0.00483.....(1) \quad \rho = \left(\frac{A_{gfrp}}{bh}\right) = \left(\frac{121}{103\times203}\right) = 0.00578.....(2)$$

cracked:

$$\frac{\chi_{theo\,cr}}{d} = \sqrt{\alpha_e\rho(2+\alpha_e\rho)} - \alpha_e\rho \qquad \alpha_e\rho = 5.636\times0.00483 = 0.02722.....(1)$$

$$= \left[\sqrt{(0.02722)\times(2+(0.02722))} - 0.02722\right]\times174 = \underline{\underline{36.13}}\,\text{mm}.....(1)$$

$$\frac{\chi_{theo\,cr}}{d} = \sqrt{\alpha_e\rho(2+\alpha_e\rho)} - \alpha_e\rho \qquad \alpha_e\rho = 1.366\times0.00578 = 0.00789.....(2)$$

$$= \left[\sqrt{(0.00789)\times(2+(0.00789))} - 0.00789\right]\times173.61 = \underline{\underline{20.48}}\,\text{mm}.....(2)$$

Neutral Axis Depth (χ_{actual}) based upon experimental strains

C20, TB15 reinforced with 2∅8 Steel rebars in the tension region.....(1)
C20, TB16 reinforced with 2∅8.77 GFRP rebars in the tension region.....(2)

$$\varepsilon_{c1}x-\varepsilon_{c2}x=\varepsilon_{c1}a_2-\varepsilon_{c2}a_1 \Rightarrow x_{actual_{uncr/cr}}=\frac{(\varepsilon_{c1}a_2-\varepsilon_{c2}a_1)}{(\varepsilon_{c1}-\varepsilon_{c2})}$$

uncracked:

$$x_{actual_{uncr}}=\frac{(\varepsilon_{c1}a_2-\varepsilon_{c2}a_1)}{(\varepsilon_{c1}-\varepsilon_{c2})}=\frac{[(118.14\times25)-(91.29\times10)]}{(118.14-91.29)}=\underline{\underline{76\text{mm}}}.....(1)$$

$$\left.\begin{array}{ll}\varepsilon_{c1}=118.14(\text{measured}) & \varepsilon_{c2}=91.29(\text{measured})\\ a_1=10\text{mm} & a_2=25\text{mm}\end{array}\right]\text{at 6kN.....(1)}$$

$$x_{actual_{uncr}}=\frac{(\varepsilon_{c1}a_2-\varepsilon_{c2}a_1)}{(\varepsilon_{c1}-\varepsilon_{c2})}=\frac{[(88.64\times25)-(24.16\times10)]}{(88.64-24.16)}=\underline{\underline{30.62\text{mm}}}.....(2)$$

$$\left.\begin{array}{ll}\varepsilon_{c1}=88.61(\text{measured}) & \varepsilon_{c2}=24.16(\text{measured})\\ a_1=10\text{mm} & a_2=25\text{mm}\end{array}\right]\text{at 4kN.....(2)}$$

cracked:

$$x_{actual_{cr}}=\frac{(\varepsilon_{c1}a_2-\varepsilon_{c2}a_1)}{(\varepsilon_{c1}-\varepsilon_{c2})}=\frac{[(865.47\times25)-(528.94\times10)]}{(865.47-528.94)}=\underline{\underline{48.58\text{mm}}}.....(1)$$

$$\left.\begin{array}{ll}\varepsilon_{c1}=865.47(\text{measured}) & \varepsilon_{c2}=528.94(\text{measured})\\ a_1=10\text{mm} & a_2=25\text{mm}\end{array}\right]\text{at 23kN.....(1)}$$

$$x_{actual_{cr}}=\frac{(\varepsilon_{c1}a_2-\varepsilon_{c2}a_1)}{(\varepsilon_{c1}-\varepsilon_{c2})}=\frac{[(1469.59\times25)-(331.15\times10)]}{(1469.59-331.15)}=\underline{\underline{29.36\text{mm}}}.....(2)$$

$$\left.\begin{array}{ll}\varepsilon_{c1}=1469.59(\text{measured}) & \varepsilon_{c2}=331.15(\text{measured})\\ a_1=10\text{mm} & a_2=25\text{mm}\end{array}\right]\text{at 22kN.....(2)}$$

2. ***Second Moment of Area (SMA) of Transformed Section (I_{actual}) based upon the experimental neutral axis depth(χ_{actual}) used in BS8110 equations***

C20, TB15 reinforced with 2∅8 Steel rebars in the tension region.....(1)
C20, TB16 reinforced with 2∅8.77 GFRP rebars in the tension region.....(2)

uncracked :

$$\frac{I_{actual\,uncr}}{bd^3} = \frac{1}{12}\left(\frac{h}{d}\right)^3 + \frac{h}{d}\left(\frac{\chi_{actual\,uncr}}{d} - \frac{h}{2d}\right)^2 + \alpha_e\rho\left(1 - \frac{\chi_{actual\,uncr}}{d}\right)^2$$

$$I_{actual\,uncr} = \left[\frac{1}{12}\left(\frac{203}{174}\right)^3 + \frac{203}{174}\left(\frac{76}{174} - \frac{203}{2\times174}\right)^2 + 0.02722\times\left(1 - \frac{76}{174}\right)^2\right]\times(103\times174^3)$$

$$I_{actual\,uncr} = \underline{\underline{90.10\times10^6}}\,mm^4 \text{ at } 6kN.....(1)$$

$$I_{actual\,uncr} = \left[\frac{1}{12}\left(\frac{203}{173.61}\right)^3 + \frac{203}{173.61}\left(\frac{30.62}{173.61} - \frac{203}{2\times173.61}\right)^2 + 0.00789\times\left(1 - \frac{30.62}{173.61}\right)^2\right]\times(103\times173.61^3)$$

$$I_{actual\,uncr} = \underline{\underline{180\times10^6}}\,mm^4 \text{ at } 6kN.....(2)$$

cracked :

$$\frac{I_{actual\,cr}}{bd^3} = \frac{1}{3}\left(\frac{\chi_{actual\,cr}}{d}\right)^3 + \alpha_e\rho\left(1 - \frac{\chi_{actual\,cr}}{d}\right)^2$$

$$I_{actual\,cr} = \left[\frac{1}{3}\left(\frac{48.58}{174}\right)^3 + 0.02722\left(1 - \frac{48.58}{174}\right)^2\right]\times(103\times174^3) = \underline{\underline{11.60\times10^6}}\,mm^4 \text{ at } 23kN.....(1)$$

$$I_{actual\,cr} = \left[\frac{1}{3}\left(\frac{29.36}{173.61}\right)^3 + 0.00789\left(1 - \frac{29.36}{173.61}\right)^2\right]\times(103\times173.61^3) = \underline{\underline{3.81\times10^6}}\,mm^4 \text{ at } 22kN.....(2)$$

3. *Theoretical (M_{theo}) Bending Moment based upon BS8110 equations*

C20, TB15 reinforced with 2∅8 Steel rebars in the tension region.....(1)
C20, TB16 reinforced with 2∅8.77 GFRP rebars in the tension region.....(2)

uncracked :

$$M_{theo_{uncr}} = f_{st\,/\,gfrp} A_{s\,/\,gfrp}\left(d - \frac{\chi_{theo_{uncr}}}{3}\right) \text{based on rebar}$$

$$M_{theo_{uncr}} = 119.38\times10^{3}\times101\times10^{-6}\times\left(0.174 - \frac{0.10315}{3}\right) = \underline{\underline{1.68}}\text{kNm.....(1)}$$

$f_{st} = 119.38\text{MPa}$ (from the tensile test at 6kN)

$$M_{theo_{uncr}} = 65.53\times10^{3}\times121\times10^{-6}\times\left(0.17361 - \frac{0.10198}{3}\right) = \underline{\underline{1.11}}\text{kNm.....(2)}$$

$f_{gfrp} = 65.53\text{MPa}$ (from the tensile test at 4kN)

cracked :

$$M_{theo_{cr}} = f_{st\,/\,gfrp} A_{st\,/\,gfrp}\left(d - \frac{\chi_{theo_{cr}}}{3}\right) \text{based on rebar}$$

$$M_{theo_{cr}} = 523.5\times10^{3}\times101\times10^{-6}\times\left(0.174 - \frac{0.03613}{3}\right) = \underline{\underline{8.56}}\text{kNm.....(1)}$$

$f_{st} = 523.5\text{MPa}$ (from the tensile test at failure)

$$M_{theo_{cr}} = 601\times10^{3}\times121\times10^{-6}\times\left(0.174 - \frac{0.02048}{3}\right) = \underline{\underline{12.13}}\text{kNm.....(2)}$$

$f_{gfrp} = 601\text{MPa}$ (from the tensile test at failure)

4. *Actual (M_{actual}) Bending Moments based upon the Bending Moment Diagram(BMD)*

C20, TB15 reinforced with 2∅8 Steel rebars in the tension region.....(1)
C20, TB16 reinforced with 2∅8.77 GFRP rebars in the tension region.....(2)

uncracked :

$$M_{actual\,uncr/cr} = \frac{\frac{F_{initial}}{2}(L-e)}{2} + \frac{wL^2}{8}$$ (see Shear Force (SF) and BMD on next page)

$$M_{actual\,uncr} = \frac{6\times(2.44-0.9)}{4} + \frac{0.48\times 2.44^2}{8} = \underline{\underline{2.67}}\text{kNm at 6kN.....(1)}$$

$$w\,(\text{kN/m}) = \frac{b\times h\times beam\,length\times \rho_{concrete}\times 9.81\times 10^{-3}}{beam\,length}$$

$$w = \frac{0.103\times 0.203\times 2.770\times 2340\times 9.81\times 10^{-3}}{2.770} = 0.48\text{kN/m}$$

$$M_{actual\,uncr} = \frac{4\times(2.44-0.9)}{4} + \frac{0.48\times 2.44^2}{8} = \underline{\underline{1.90}}\text{kNm at 4kN.....(2)}$$

$w = 0.48$kN/m

cracked :

$$M_{actual\,cr} = \frac{\frac{F_{max}}{2}(L-e)}{2} + \frac{wL^2}{8}$$

$$M_{actual\,cr} = \frac{23\times(2.44-0.9)}{4} + \frac{0.48\times 2.44^2}{8} = \underline{\underline{9.21}}\text{kNm at 23kN.....(1)}$$

$$M_{actual\,cr} = \frac{28\times(2.44-0.9)}{4} + \frac{0.48\times 2.44^2}{8} = \underline{\underline{11.13}}\text{kNm at 28kN.....(2)}$$

SHEAR FORCE (SF) & BENDING MOMENT DIAGRAMS (BMD) OF THE BEAMS

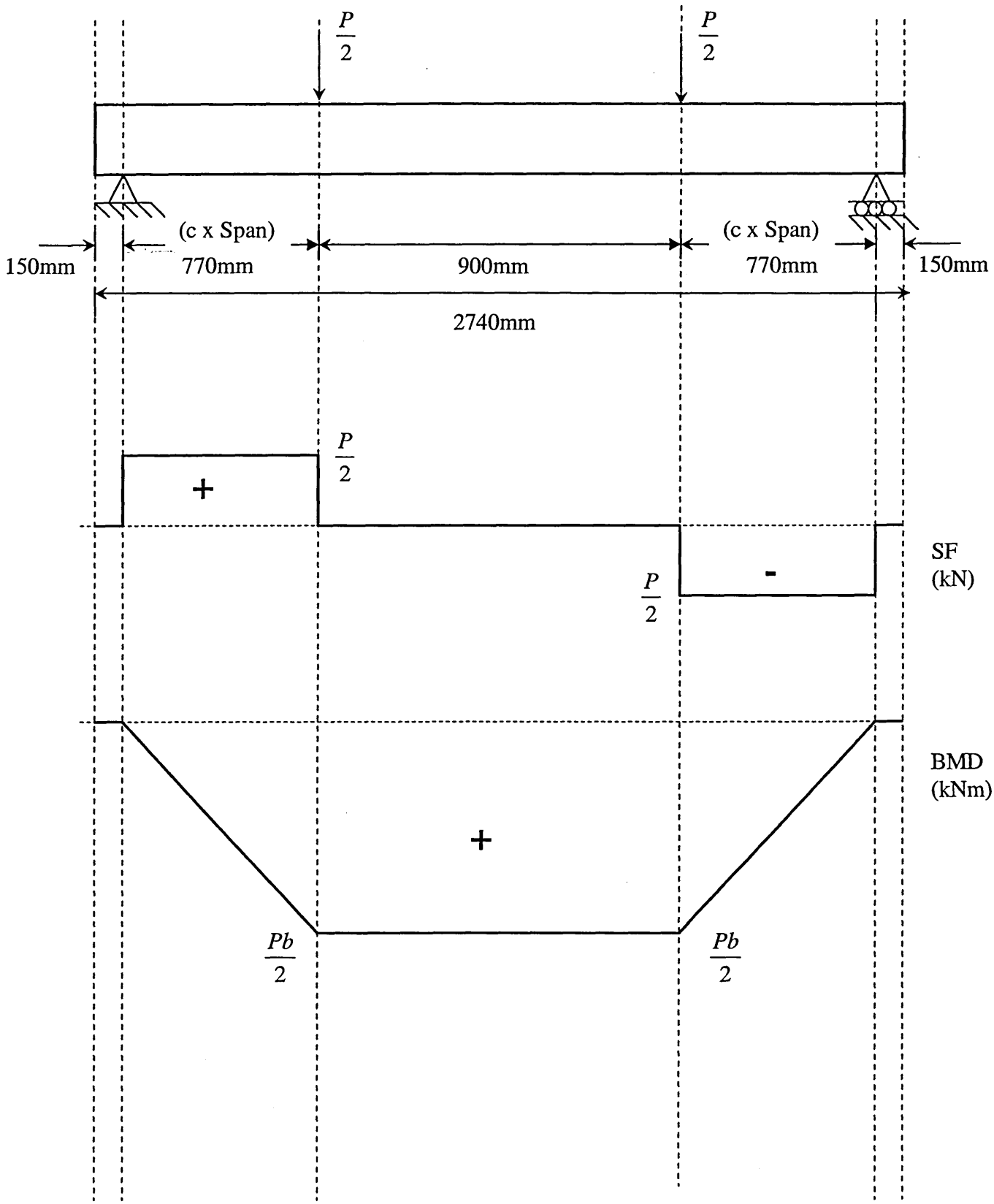

5. ***Curvature of the Beams ($1/r_{actual}$) based upon the actual bending moment (M_{actual}) and SMA (I_{actual}) used in BS8110 equations***

C20, TB15 reinforced with 2∅8 Steel rebars in the tension region.....(1)
C20, TB16 reinforced with 2∅8.77 GFRP rebars in the tension region.....(2)

uncracked:

$$\left(\frac{1}{r_b}\right)_{actual_{uncr}} = \frac{M_{actual\,uncr}}{E_c I_{actual\,uncr}}$$

$$\left(\frac{1}{r_b}\right)_{actual_{uncr}} = \frac{2.67\times10^6}{33\times10^3\times90.72\times10^6} = \underline{\underline{8.91\times10^{-7}}}\,(1/mm).....(1)$$

$$\left(\frac{1}{r_b}\right)_{actual_{uncr}} = \frac{1.90\times10^6}{33\times10^3\times179.87\times10^6} = \underline{\underline{3.20\times10^{-7}}}\,(1/mm).....(2)$$

cracked:

$$\left(\frac{1}{r_b}\right)_{actual_{cr}} = \frac{M_{actual\,cr} - \frac{bd^2}{3}\times\frac{\left(\frac{h}{d}-\frac{\chi_{actual\,cr}}{d}\right)^3}{\left(1-\frac{\chi_{actual\,cr}}{d}\right)}}{E_c I_{actual\,cr}}$$

$$\left(\frac{1}{r_b}\right)_{actual_{cr}} = \frac{9.21\times10^6 - \frac{103\times174^2}{3}\times\frac{\left(\frac{203}{174}-\frac{48.58}{174}\right)^3}{\left(1-\frac{48.58}{174}\right)}}{33\times10^3\times12.89\times10^6} = \underline{\underline{1.93\times10^{-5}}}\,(1/mm).....(1)$$

$$\left(\frac{1}{r_b}\right)_{actual_{cr}} = \frac{11.13\times10^6 - \frac{103\times173.61^2}{3}\times\frac{\left(\frac{203}{173.61}-\frac{29.36}{173.61}\right)^3}{\left(1-\frac{29.36}{173.61}\right)}}{33\times10^3\times4.31\times10^6} = \underline{\underline{6.95\times10^{-5}}}\,(1/mm).....(2)$$

6. ***Deflection of the Beams (Δ_{actual}) based upon the actual curvature ($1/r_{actual}$)used in BS8110 equations***

C20, TB15 reinforced with 2Ø8 Steel rebars in the tension region.....(1)
C20, TB16 reinforced with 2Ø8.77 GFRP rebars in the tension region.....(2)

uncracked :

$$\Delta_{actual_{uncr}} = K \times L^2 \times \frac{1}{r_{b_{actual_{uncr\,/\,cr}}}}$$

$K = 0.125 - \frac{c^2}{6}$ (based on the shape of BMD)

$K = 0.125 - \frac{0.315^2}{6} = 0.108$ (constant for all beams)

$$\Delta_{actual_{uncr}} = KL^2 \frac{1}{r_{b_{actual_{uncr}}}}$$

$\Delta_{actual_{uncr}} = 0.108 \times 2440^2 \times 8.91 \times 10^{-7} = \underline{0.57\text{mm}}$.....(1)

$\Delta_{theo_{uncr}} = 0.108 \times 2440^2 \times 3.20 \times 10^{-7} = \underline{0.21\text{mm}}$.....(2)

cracked :

$$\Delta_{actual_{cr}} = KL^2 \frac{1}{r_{b_{actual_{cr}}}}$$

$\Delta_{actual_{cr}} = 0.108 \times 2440^2 \times 1.93 \times 10^{-5} = \underline{12.41\text{mm}}$.....(1)

$\Delta_{theo_{cr}} = 0.108 \times 2440^2 \times 6.95 \times 10^{-5} = \underline{44.69\text{mm}}$.....(2)

7. ***Stresses (σ_{actual}) and strains (ε_{actual}) in rebars from the two point loading test based upon the actual bending moment (M_{actual}), the actual neutral axis depth (x_{actual}) and the actual SMA (I_{actual})used in BS8110 equations***

C20, TB15 reinforced with 2∅8 Steel rebars in the tension region.....(1)
C20, TB16 reinforced with 2∅8.77 GFRP rebars in the tension region.....(2)

uncracked:

$$\sigma_{st/gfrp\,actual_{uncr}} = \alpha_e \frac{M_{actual_{uncr}}}{I_{actual_{uncr}}} x_{actual_{uncr}} \quad \text{where } \alpha_e = \frac{E_{st/gfrp}}{E_c}$$

$$\sigma_{st\,actual_{uncr}} = 5.636 \times \frac{2.67\times10^6}{90.72\times10^6} \times 76 = 12.61\text{N/mm}^2 = 12.61\times10^6\,\text{N/m}^2 = \underline{12.61\text{MPa}}.....(1)$$

$$\sigma_{gfrp\,actual_{uncr}} = 1.366 \times \frac{1.90\times10^6}{179.87\times10^6} \times 30.62 = 0.44\text{N/mm}^2 = 0.44\times10^6\,\text{N/m}^2 = \underline{0.44\text{MPa}}.....(2)$$

cracked:

$$\sigma_{st/gfrp\,actual_{cr}} = \alpha_e \frac{M_{actual_{cr}}}{I_{actual_{cr}}} (d - x_{actual_{cr}})$$

$$\sigma_{st\,actual_{cr}} = 5.636 \times \frac{9.21\times10^6}{12.89\times10^6} \times (174 - 48.58) = 505.06\text{N/mm}^2$$

$$= 505.06\times10^6\,\text{N/m}^2 = \underline{505.06\text{MPa}}.....(1)$$

$$\sigma_{gfrp\,actual_{cr}} = 1.366 \times \frac{11.13\times10^6}{4.31\times10^6} \times (173.61 - 29.36) = 508.84\text{N/mm}^2$$

$$= 508.84\times10^6\,\text{N/m}^2 = \underline{508.84\text{MPa}}.....(2)$$

uncracked:

$$\varepsilon_{st/gfrp\,actual_{uncr}} = \frac{\sigma_{st/gfrp\,actual_{uncr}}}{E_{st/gfrp}}$$

$$\varepsilon_{st\,actual_{uncr}} = \frac{12.61\times10^6}{186\times10^9} = \underline{0.00007}.....(1) \quad \varepsilon_{gfrp\,actual_{uncr}} = \frac{0.44\times10^6}{45.09\times10^9} = 1.....(2)$$

cracked:

$$\varepsilon_{st/gfrp\,actual_{cr}} = \frac{\sigma_{st/gfrp\,actual_{cr}}}{E_{st/gfrp}}$$

$$\varepsilon_{st\,actual_{cr}} = \frac{505.06\times10^6}{186\times10^9} = \underline{0.0027}.....(1) \quad \varepsilon_{gfrp\,actual_{cr}} = \frac{508.84\times10^6}{45.09\times10^9} = 0.0112.....(2)$$

8. ***Maximum concrete compressive strain (ε_{co}) based upon the measured strains in the beams***

C20, TB15 reinforced with 2∅8 Steel rebars in the tension region.....(1)
C20, TB16 reinforced with 2∅8.77 GFRP rebars in the tension region.....(2)

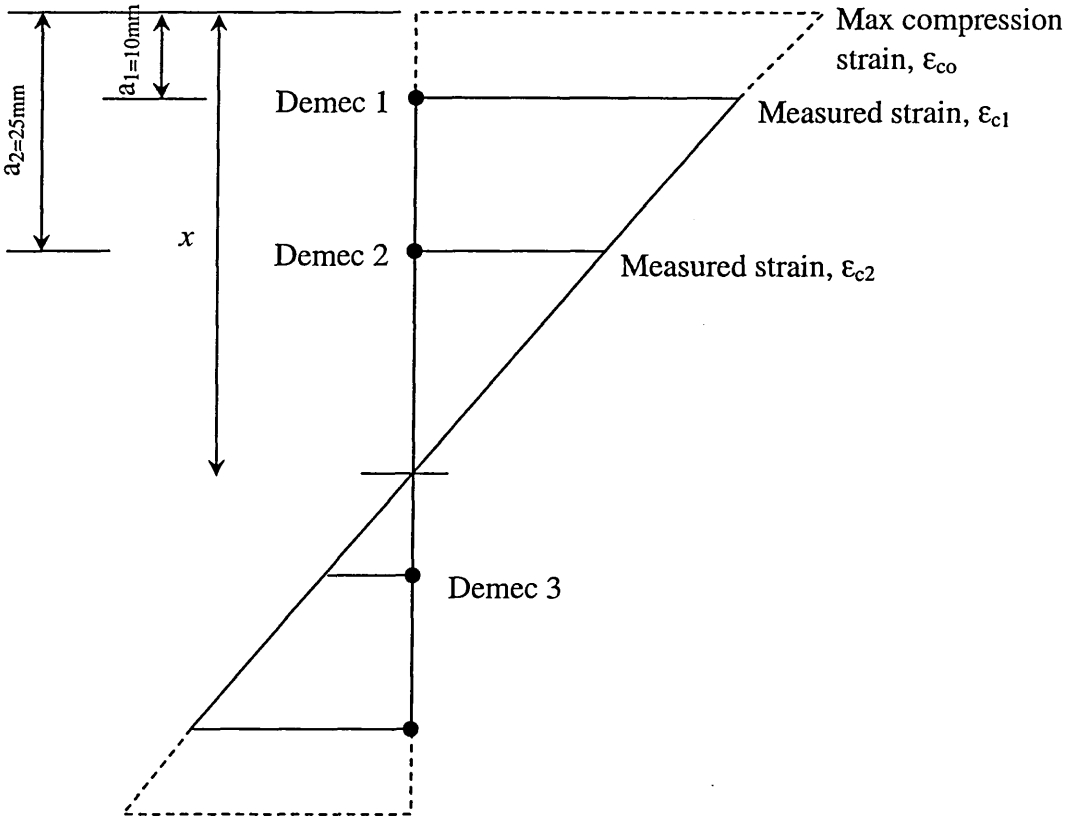

$$\frac{\varepsilon_{c1}}{\varepsilon_{co}} = \frac{(x_{actual\,cr} - a_1)}{x_{actual\,cr}} \Rightarrow (\text{max.compressive strain})\ \varepsilon_{co} = \frac{\varepsilon_{c1} x_{actual\,cr}}{(x_{actual\,cr} - a_1)}$$

$$\varepsilon_{co} = \frac{865.47\times10^{-6}\times48.58}{(48.58-10)} = \underline{0.00109}.....(1)$$

$$\varepsilon_{co} = \frac{2044.22\times10^{-6}\times29.36}{(29.36-10)} = \underline{0.0031}.....(2)$$

9. ***Shear strength (v_{max})of the beams based upon BS 8110 equation***

C20, TB15 reinforced with 2∅8 Steel rebars in the tension region.....(1)
C20, TB16 reinforced with 2∅8.77 GFRP rebars in the tension region.....(2)

Theoretical shear strength :

$$v_{\max_{theo}} = k_1 k_2 0.79\left(\frac{100A_{st/gfrp}}{bd}\right)^{1/3}\left(\frac{400}{d}\right)^{1/4} \text{ where } k_1 = 1 \text{ and } k_2 = \left(\frac{f_c}{25}\right)^{1/3}$$

where f_c not $\rangle 40MPa$

$$v_{\max_{theo}} = 1\times\left(\frac{40}{25}\right)^{1/3}\times 0.79\times\left(\frac{100\times 101}{103\times 174}\right)^{1/3}\times\left(\frac{400}{174}\right)^{1/4} = \underline{0.94\text{MPa}}.....(1)$$

$$v_{\max_{theo}} = 1\times\left(\frac{40}{25}\right)^{1/3}\times 0.79\times\left(\frac{100\times 121}{103\times 173.61}\right)^{1/3}\times\left(\frac{400}{173.61}\right)^{1/4} = \underline{1.00\text{MPa}}.....(2)$$

Actual *shear strength* :

$$v_{actual} = \frac{1000(\text{Failure load} + \text{Beam selfweight})}{2bh}$$

$$v_{actual} = \frac{1000\times(23+1.32)}{2\times 103\times 203} = \underline{0.58\text{MPa}}.....(1)$$

$$v_{actual} = \frac{1000\times(28+1.32)}{2\times 103\times 203} = \underline{0.70\text{MPa}}.....(2)$$

10. Determination of number of stirrups required for the beams based on the shear resistance

C20, TB15 reinforced with 2∅8 Steel rebars in the tension region.....(1)

minimum stirrups for whole length of beam:

$0.5v_{\max_{theo}} \langle v_{actual} \langle \left(v_{\max_{theo}} + 0.4\right)$ BS8110, Table 3.8

$0.5 \times 0.94 \langle 0.58 \langle \left(0.94 + 0.4\right)$

$0.47 \langle 0.58 \langle 1.34$.....(1)

the cross sectional area of the two legs of the stirrups:

$$A_{sv} \geq \frac{0.4 b_v s_v}{0.87 f_{yu}} \qquad \text{BS8110, Table 3.8}$$

$$\therefore s_v = \frac{0.87 f_{yu} A_{sv}}{0.4 b_v}$$

$$s_v = \frac{0.87 \times 250 \times 28.27}{0.4 \times 103} = 149mm$$

However maximum spacing of links should not exceed 0.75d

$$\therefore s_{v_{\max}} = 0.75d = 0.75 \times 168 = 126mm \text{.....(1)}$$

$$\therefore \text{The number of stirrups } (n_s) = \frac{L_{shearspan}(mm)}{s_{v_{\max}}} = \frac{920}{126} = 7.30 \approx 8 \text{ stirrups .....(1)}$$

11. ***Estimation of crack widths in the beams based upon BS 8110 equation***

C20, TB15 reinforced with 2∅8 Steel rebars in the tension region.....(1)
C20, TB16 reinforced with 2∅8.77 GFRP rebars in the tension region.....(2)

$$w_{\max theo} = \frac{3a_{cr}\varepsilon_m}{1+2\left(\frac{a_{cr}-c_{\min}}{h-x_{cr}}\right)}$$

$$a_{cr} = \sqrt{\left(c_{\min}+\frac{D}{2}\right)^2 \times 2} - \frac{D}{2}$$

$$a_{cr} = \sqrt{\left(25+\frac{8}{2}\right)^2 \times 2} - \frac{8}{2} = 37.01\text{mm}.....(1)$$

$$a_{cr} = \sqrt{\left(25+\frac{8.77}{2}\right)^2 \times 2} - \frac{8.77}{2} = 37.17\text{mm}.....(2)$$

$$\varepsilon_m = \varepsilon_{c4}(\text{at DEMEC4}) - \varepsilon_{c3}(\text{at DEMEC3})$$

$$\varepsilon_m = 0.00346 - 0.00109 = 0.00237.....(1)$$
$$\varepsilon_m = 0.0182 - 0.0075 = 0.0107.....(2)$$

$$w_{\max theo} = \frac{3\times 37.01\times 0.00237}{1+2\times\left(\frac{37.01-25}{203-48.58}\right)} = \underline{\underline{0.23\text{mm}}}.....(1)$$

$$w_{\max theo} = \frac{3\times 37.17\times 0.0107}{1+2\times\left(\frac{37.17-25}{203-29.36}\right)} = \underline{\underline{1.05\text{mm}}}.....(2)$$

12. ***Estimation of crack widths in the beams using a dial gauge***

C20, TB15 reinforced with 2∅8 Steel rebars in the tension region.....(1)
C20, TB16 reinforced with 2∅8.77 GFRP rebars in the tension region.....(2)

$$\varepsilon_{c3,c4} = \frac{w_{L_{1,2}}}{Gauge\ Length\ (G.L.)} \Rightarrow w_{L_1} = \varepsilon_{c3} \times (G.L.) \text{ and } w_{L_2} = \varepsilon_{c4} \times (G.L.)$$

$$w_{L_1} = 0.00109 \times 900 = 0.98\text{mm}.....(1)$$
$$w_{L_2} = 0.00346 \times 900 = 3.11\text{mm}.....(1)$$
$$w_{L_1} = 0.0075 \times 900 = 6.75\text{mm}.....(2)$$
$$w_{L_2} = 0.0182 \times 900 = 16.38\text{mm}.....(2)$$

$$w_{L_{average}} = \frac{w_{L_2} - w_{L_1}}{no.\ of\ cracks\ in\ \max imum\ bending\ moment\ region}$$

$$w_{L_{average}} = \frac{3.11 - 0.98}{10} = \underline{\underline{0.213\text{mm}}}.....(1)$$
$$w_{L_{average}} = \frac{16.38 - 6.75}{5} = \underline{\underline{1.93\text{mm}}}.....(1)$$

13. ***Performance Quotient (Q_p) for concrete beams without stirrups***

C20, TB15 reinforced with 2∅8 Steel rebars in the tension region.....(1)
C20, TB16 reinforced with 2∅8.77 GFRP rebars in the tension region.....(2)

$$Q_p = \frac{1000(Failure\ Load + Beam\ selfweight)}{f_c(bh - A_{st\,/\,gfrp}) + (f_{st\,/\,gfrp} \times A_{st\,/\,gfrp})}$$

$$Q_p = \frac{1000 \times (23 + 1.32)}{41 \times (103 \times 203 - 101) + (523.5 \times 101)} = \underline{\underline{0.0268}}.....(1)$$
$$Q_p = \frac{1000 \times (28 + 1.32)}{41 \times (103 \times 203 - 121) + (601 \times 121)} = \underline{\underline{0.0317}}.....(2)$$

Performance Quotient (Q_p) for concrete beams with stirrups

C20, TTB22 reinforced with 2∅8 Main Steel rebars and 24∅6 Mild Steel stirrups and *2∅6 Mild Steel* 'top rebars'...(1)

C20, TTB26 reinforced with 2∅8.77 Main GFRP rebars and 24∅6.9 GFRP stirrups and *2∅6 Mild Steel* 'top rebars'...(2)

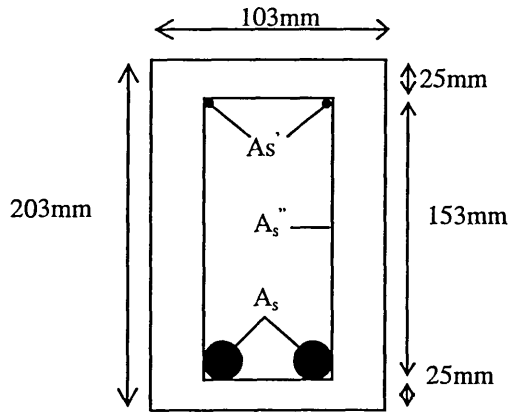

$$Q_p = \frac{1000(F_f + \text{BSW})}{f_c\,(bh - A_s - A_s' - [(\frac{\frac{2L}{S_v}(b-2c_{\min}) + (h-2c_{\min})}{L})As'']) + f_s A_s + f'_s A_s' + f'_s [\left(\frac{\frac{2L(b-2c_{\min})}{Sv} + (h-2c_{\min})}{L}\right) As'']}$$

neqs neqs

b= Breadth of the beam section (mm)

h= Depth of the beam section (mm)

Cmin= Minimum cover to the reinforcement (mm)

L=Length of the beam (mm)

As= Cross sectional area of the main rebars (mm^2)

As' = Cross sectional area of the top bars (mm^2)

neqs=Equivalent cross sectional area of stirrups (mm^2)

Sv= Spacing between the stirrups (mm)

f_c = Cube strength (MPa)

f_s = Yield/ ultimate(GFRP) tensile strength of main rebars (MPa)

f_s'= Yield /ultimate (GFRP) tensile strength of stirrups(MPa)

F_f= Failure Load (KN)

B.S.W.= Beam self weight (KN)

$$Q_p = \frac{1000(F_f + B.S.W)}{f_c(bh - As - As' - neqs) + f_s As + f'_s As' + (f_s .neqs)}$$

TTB22

f_c=43 MPa

b= 103 mm

h= 203 mm

L=2740 mm

Sv= 100 mm

Cmin= 25mm

F_f= 24 KN

B.S.W.= 1.36 KN

f_s= 528.74 MPa

f_s'=304 MPa

As =$\pi D^2/4 = 2\pi.8^2/4 = 101\ mm^2$

As' = $\pi D^2/4 = 2\pi.6^2/4 = 56.54\ mm^2$

As''= $\pi D^2/4 = \pi\ 6^2/4 = 56.5\ mm^2$

$$neqs = (\frac{\frac{2L}{SV}(b - 2C\min) + (h - 2C\min)}{L})As'' = [\frac{2.24[9103 - 2.25) + (203 - 2.25)}{2740}]56.5 = 204mm^2$$

$$Q_p = \frac{1000(24 + 1.36)}{43(103x203 - 101 - 56.54 - 204) + (528.74x101) + (304x56.54) + (304x204)} = 0.0249$$

TTB26

f_c= 41 MPa

b = 103 mm

h= 203 mm

L= 2740 mm

Sv= 100 mm

Cmin= 25 mm

F_f = 32 KN

B.S.W.= 1.35 KN

f_s= 601 MPa

f_s'= 581 MPa

As= 121 mm^2

As'=56.54 mm^2

$As'' = 2\pi(6.9)^2/4 = 74.78\ mm^2$

$$neqs = \frac{2.24[103-50) + (203-50)}{2740}]74.78 = 270mm^2$$

$$Q_{p2} = \frac{1000(32+1.35)}{41(103x203-121-56.54-270)+(601x121)+(304x56.54)+(581x270)} = 0.0307$$

The crack patterns of the C20 grade concrete beams reinforced with 2ϕ8.77/8 GFRP/steel rebars

C20 TB15 208 ST Flexure Failure
Number of Cracks: 20 (one side only)
Failure Load: 23kN

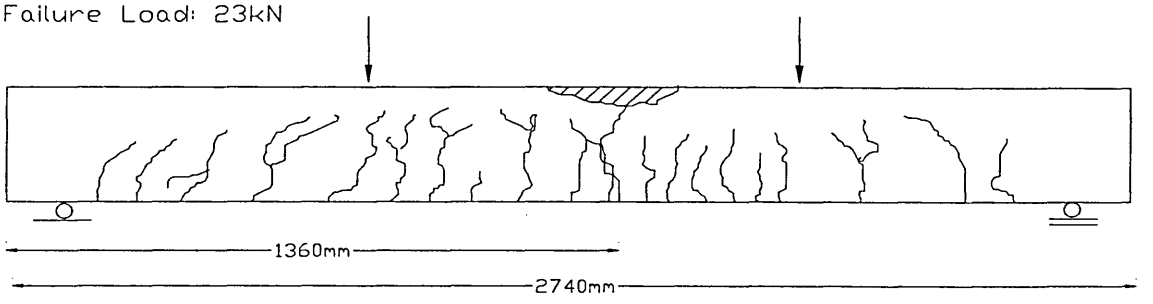

C20 RTB15 208 ST Flexure Failure
Number of Cracks: 18 (one side only)
Failure Load: 25.1kN

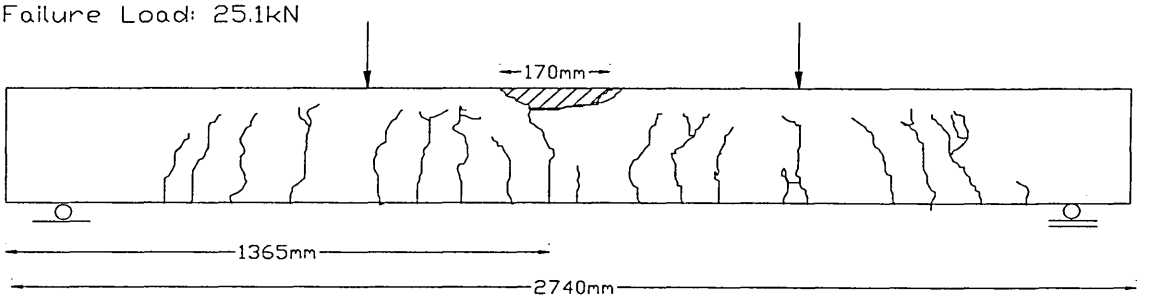

C20 TB16 208.77 FRP Flexure Failure
Number of Cracks: 9 (one side only)
Failure Load: 28kN

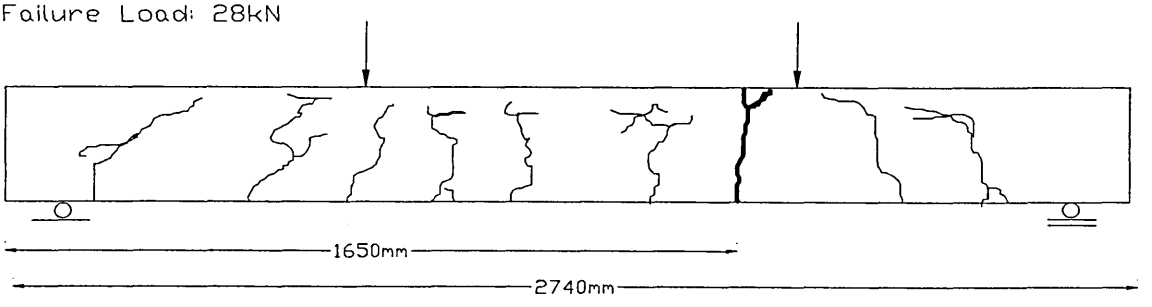

C20 RTB16 208.77 FRP Shear Failure
Number of Cracks: 9 (one side only)
Failure Load: 24kN

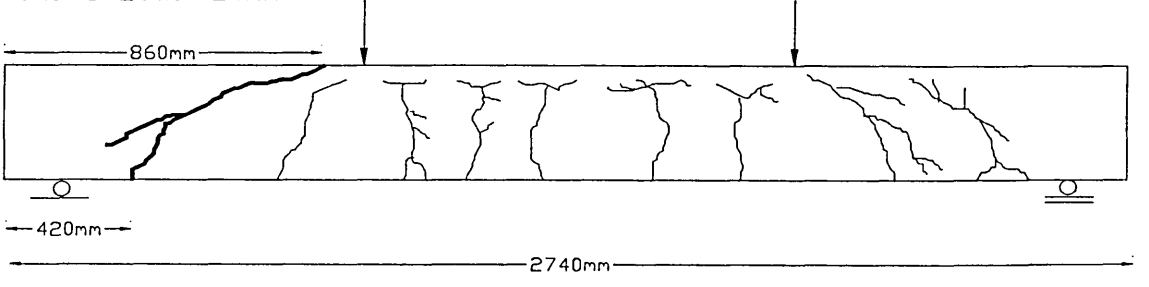

The crack patterns of the C40 grade concrete beams reinforced with 2ϕ8.77/8 GFRP/steel rebars

C40 TB5 2Ø8 ST Compression Failure
Number of Cracks:23 (one side only)
Failure Load: 24kN

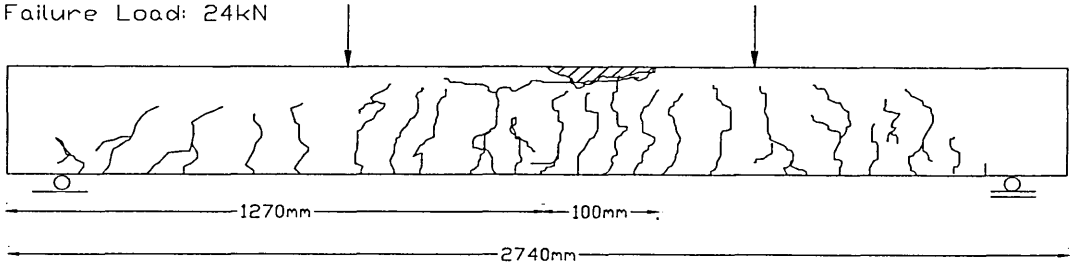

C40 TB6 2Ø8.77 FRP Shear Failure
Number of Cracks:9 (one side only)
Failure Load: 20kN

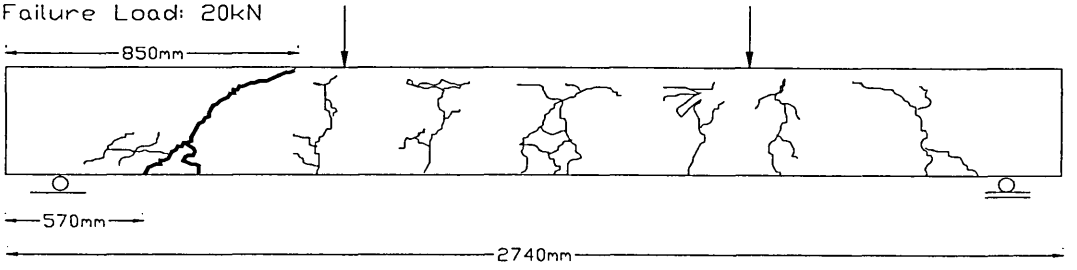

C40 RTB6 2Ø8.77 FRP Shear Failure
Number of Cracks: 10 (one side only)
Failure Load: 22kN

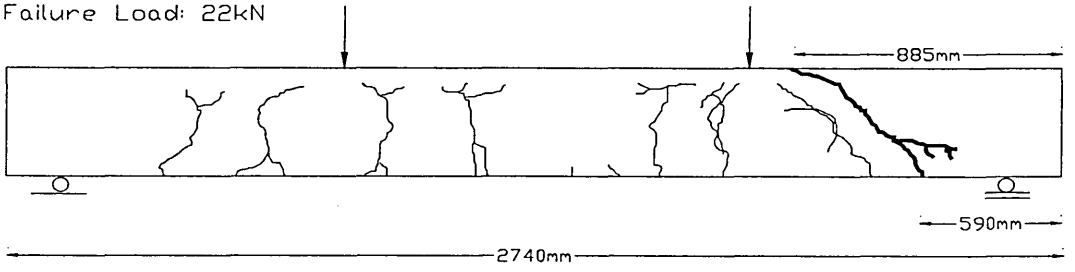

C40 FIBRE TTB16 2Ø8.77 FRP Shear Failure
Number of Cracks: 12 (one side only)
Failure Load: 33.6kN

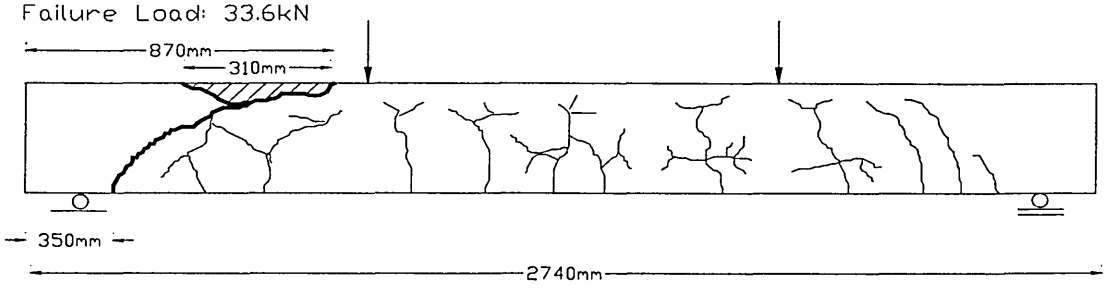

The crack patterns of the C60 grade concrete beams reinforced with 2ϕ8.77/8 GFRP/steel rebars

C60 TB7 2□8 ST Compression Failure
Number of Cracks:18 (one side only)
Failure Load: 24kN

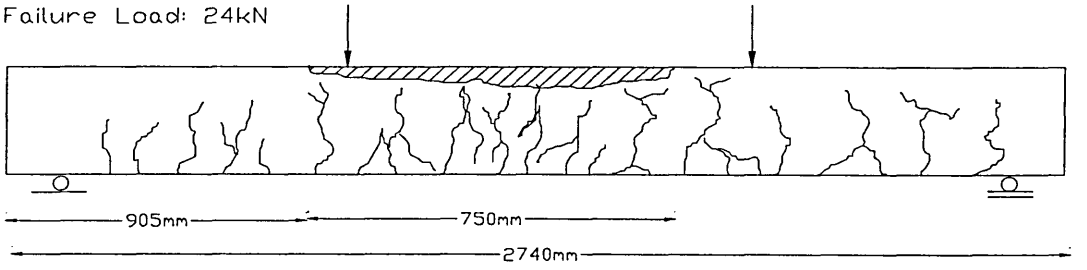

C60 TB8 2□8.77 FRP Tension Failure
Number of Cracks:9 (one side only)
Failure Load: 26kN

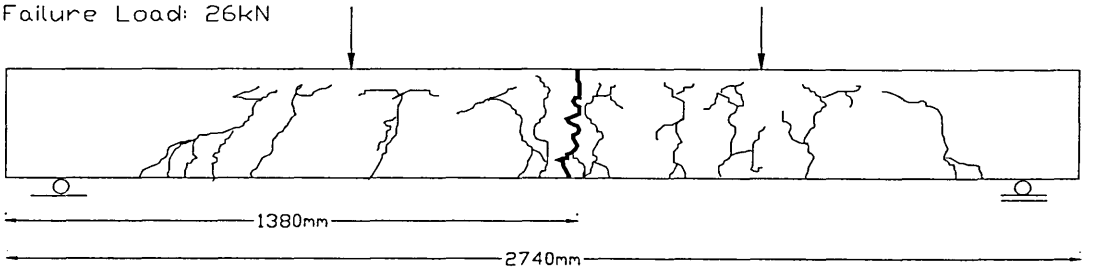

C60 RTB8 2□8.77 FRP Shear Failure
Number of Cracks: 8 (one side only)
Failure Load: 26.4kN

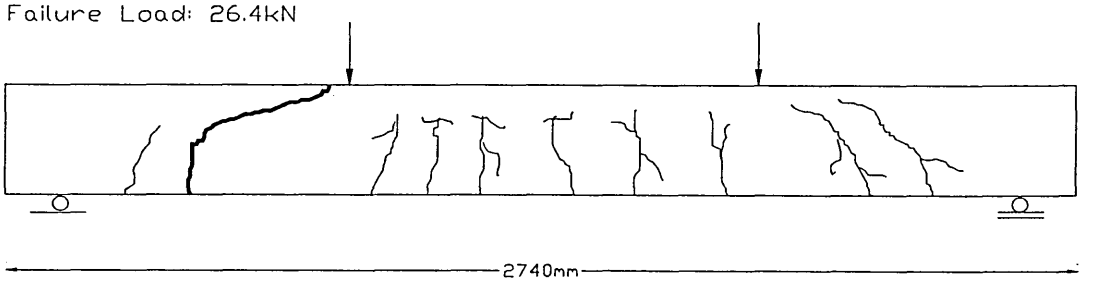

The crack patterns of the C20 grade concrete beams reinforced with 2ϕ13.19/12 GFRP/steel rebars

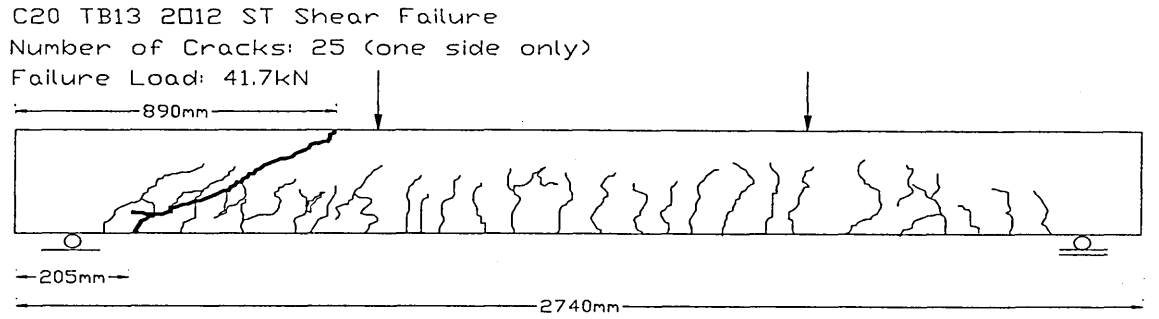

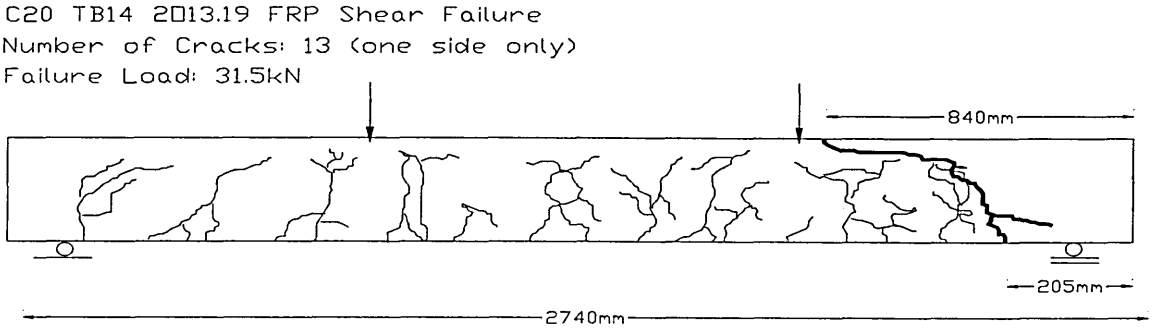

The crack patterns of the C60 grade concrete beams reinforced with 2ϕ13.19/12 GFRP/steel rebars

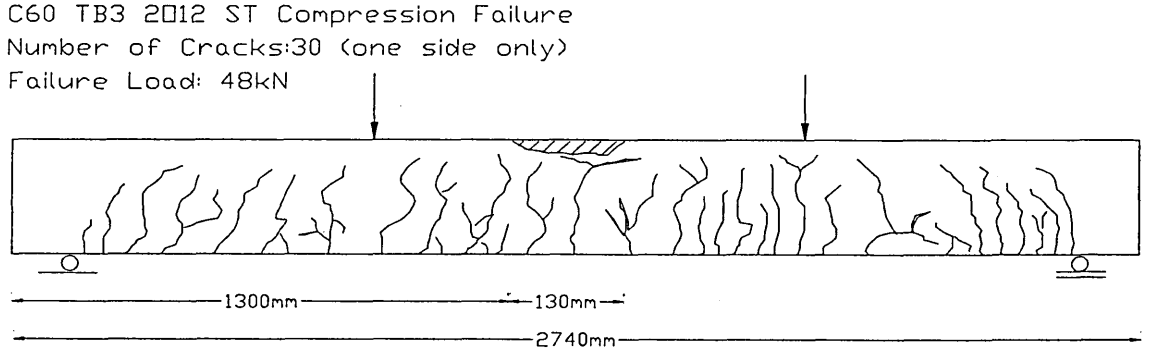

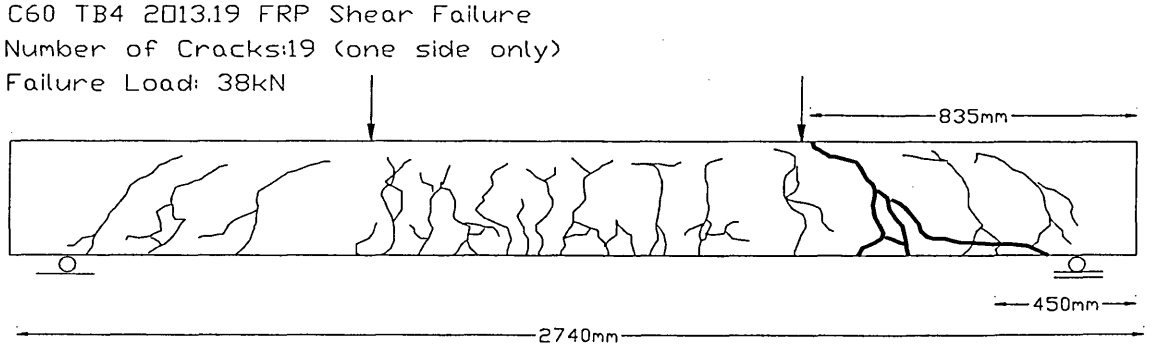

The crack patterns of the C40 grade concrete beams reinforced with 2ϕ13.19/12 GFRP/steel rebars

C40 TB1 2Ø12 ST Compression Failure
Number of Cracks:25 (one side only)
Failure Load: 50kN

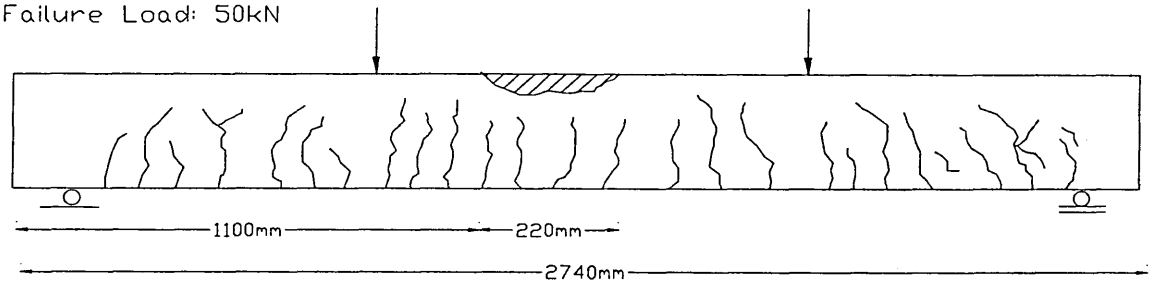

C40 RTB1 2Ø12 ST Compression Failure
Number of Cracks:26 (one side only)
Failure Load: 51kN

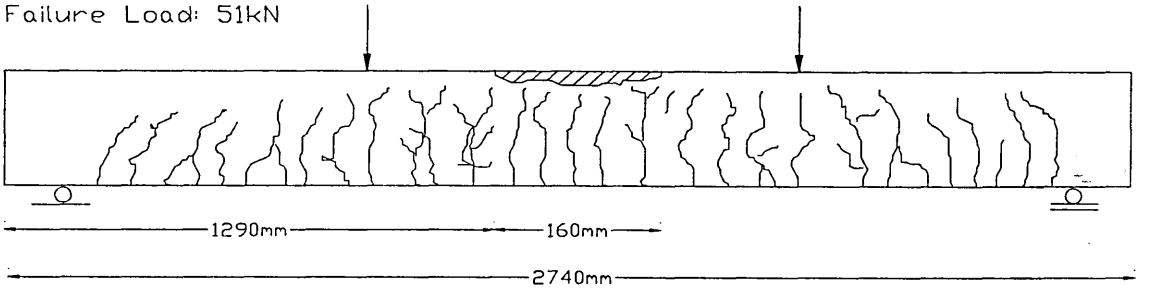

C40 TB2 2Ø13.19 FRP Shear Failure
Number of Cracks:16 (one side only)
Failure Load: 34kN

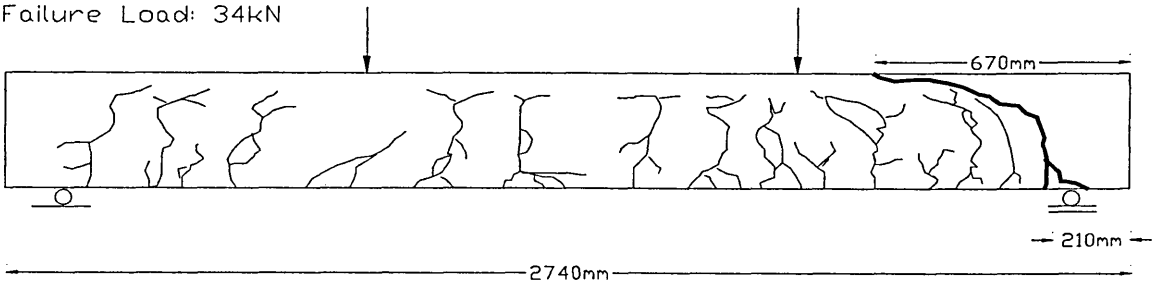

C40 FIBRE TTB21 2Ø13.19 FRP Shear Failure
Number of Cracks: 18 (one side only)
Failure Load: 36kN

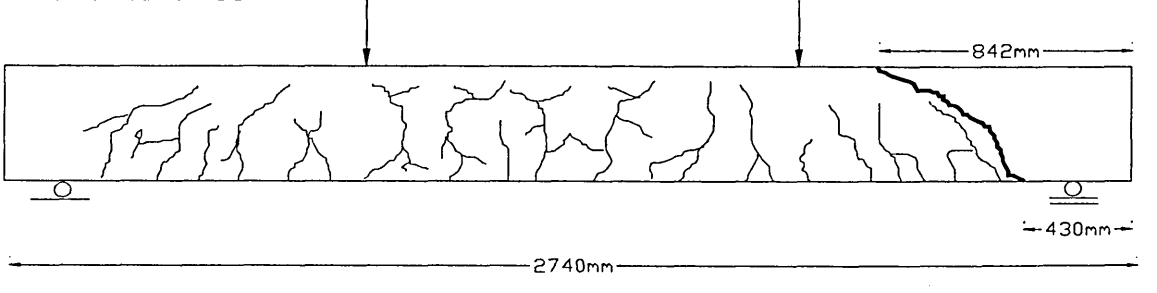

The crack patterns of the C20 grade concrete beams reinforced with 2ϕ16.44/16 GFRP/steel rebars

C20 TB17 2□16 ST Shear Failure
Number of Cracks: 27 (one side only)
Failure Load: 56.3kN

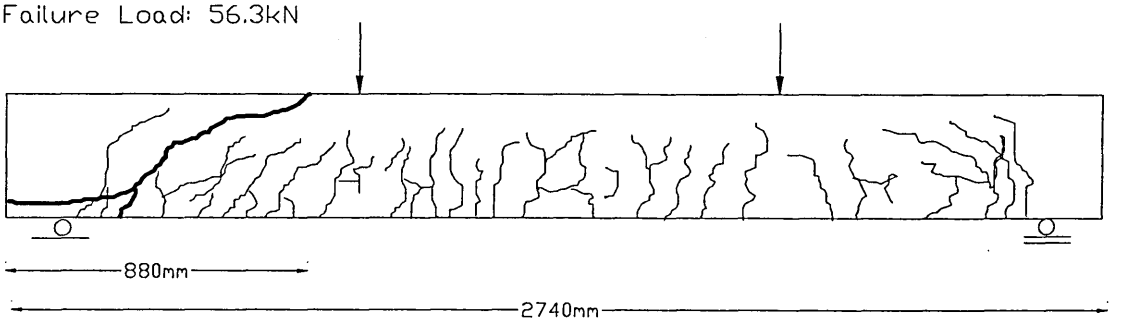

C20 TB18 2□16.44 FRP Shear Failure
Number of Cracks: 10 (one side only)
Failure Load: 30kN

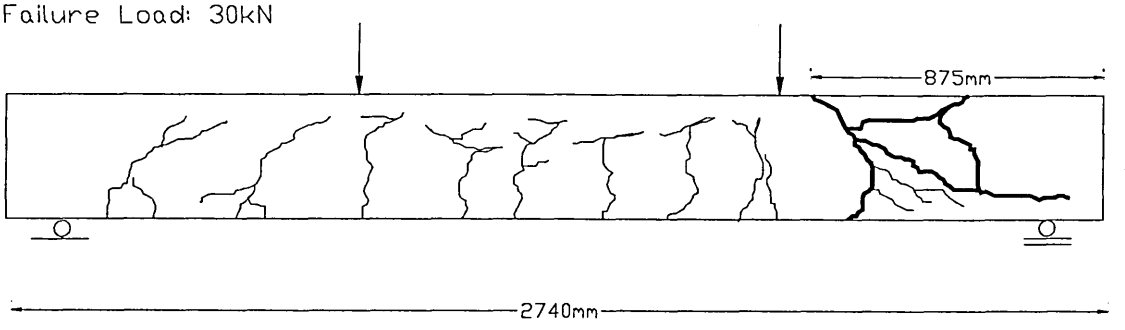

C20 RTB18 2□16.44 FRP Shear Failure
Number of Cracks: 10 (one side only)
Failure Load: 26.6kN

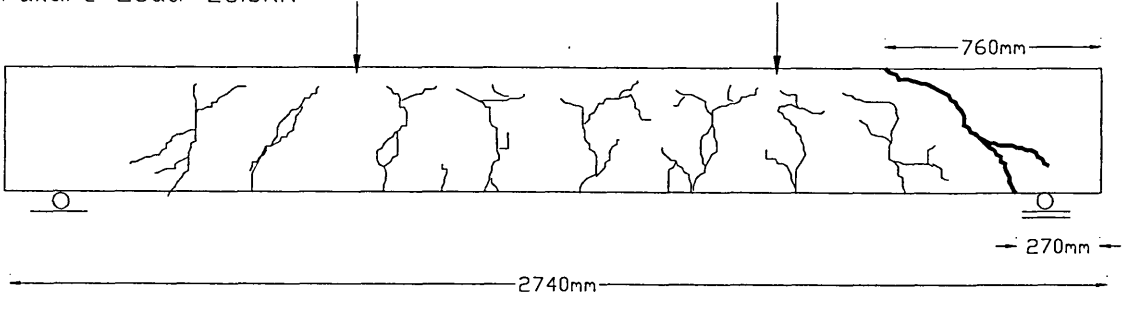

The crack patterns of the C40 grade concrete beams reinforced with 2ϕ16.44/16 GFRP/steel rebars

C40 TB9 2Ø16 ST Shear Failure
Number of Cracks: 29 (one side only)
Failure Load: 67kN

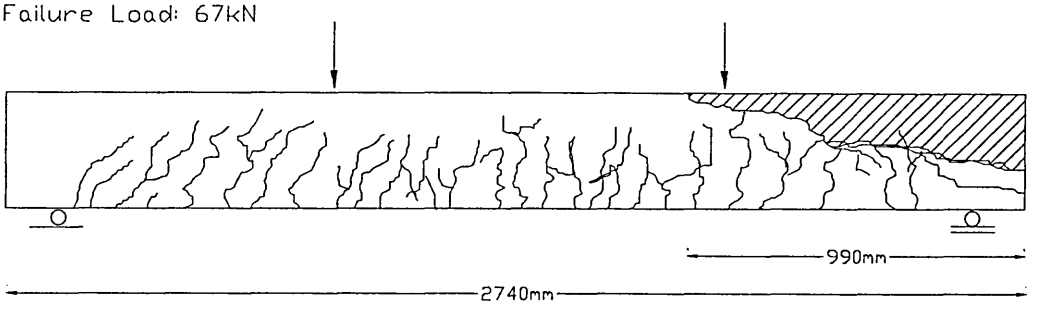

C40 TB10 2Ø16.44 FRP Shear Failure
Number of Cracks: 9 (one side only)
Failure Load: 29kN

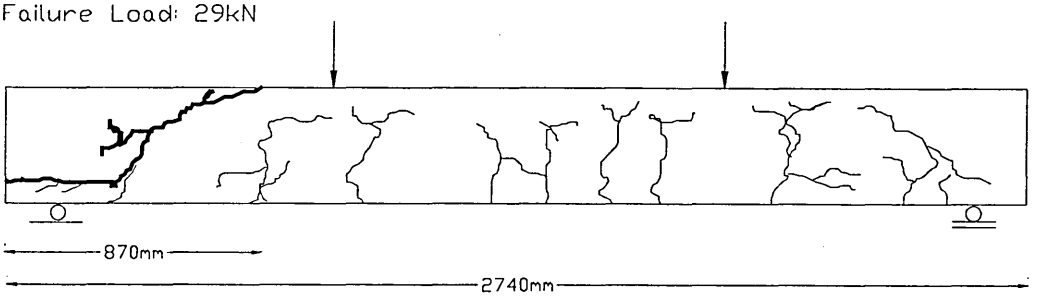

The crack patterns of the C60 grade concrete beams reinforced with 2ϕ16.44/16 GFRP/steel rebars

C60 TB11 2Ø16 ST Shear Failure
Number of Cracks: 39 (one side only)
Failure Load: 61.8kN

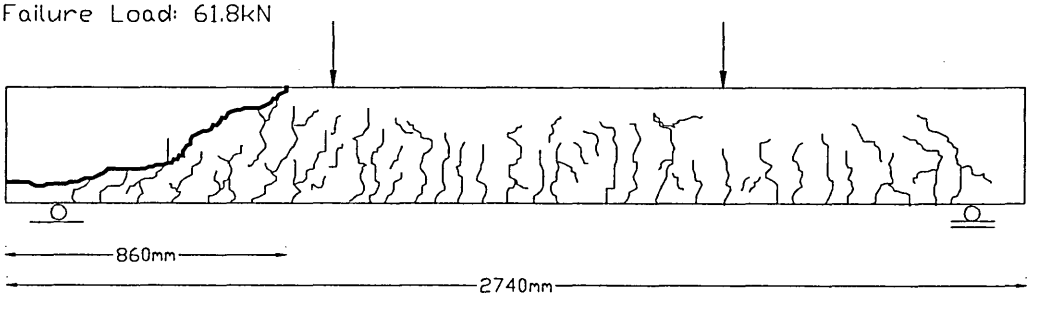

C60 TB12 2Ø16.44 FRP Shear Failure
Number of Cracks: 8 (one side only)
Failure Load: 28kN

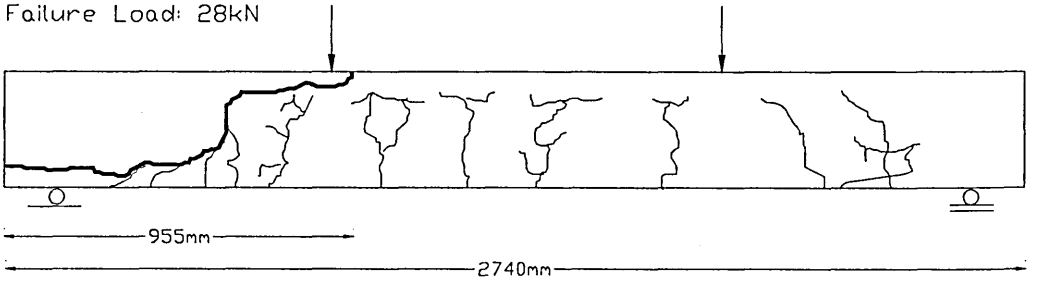

Geometrical definition of the GFRP rebars used in Part 5 and 6.

The configurations i.e. curved profile rebars used in Part 5 and 6 can be defined as a mathematical expression. The curved profile can be treated as a parabolic shape* and hence the length of each segment on the parabola can be defined to obtain the total length of the rebar and its location along the rebar length.

*shape: combination of the curved profiles from the shear regions.

$y = ax^2 - bx - c$

a) $x = 0$ $y = 0$ 1)

b) $x = L$ $y = 0$ 2)

c) $x = L/2$ $y = h$ 3)

from 1) $c = 0$

from 2) $0 = aL^2 - bL \longrightarrow b = aL$

from 3) $h = a(L^2/4) - b(L/2) \longrightarrow a = -4h/L^2$

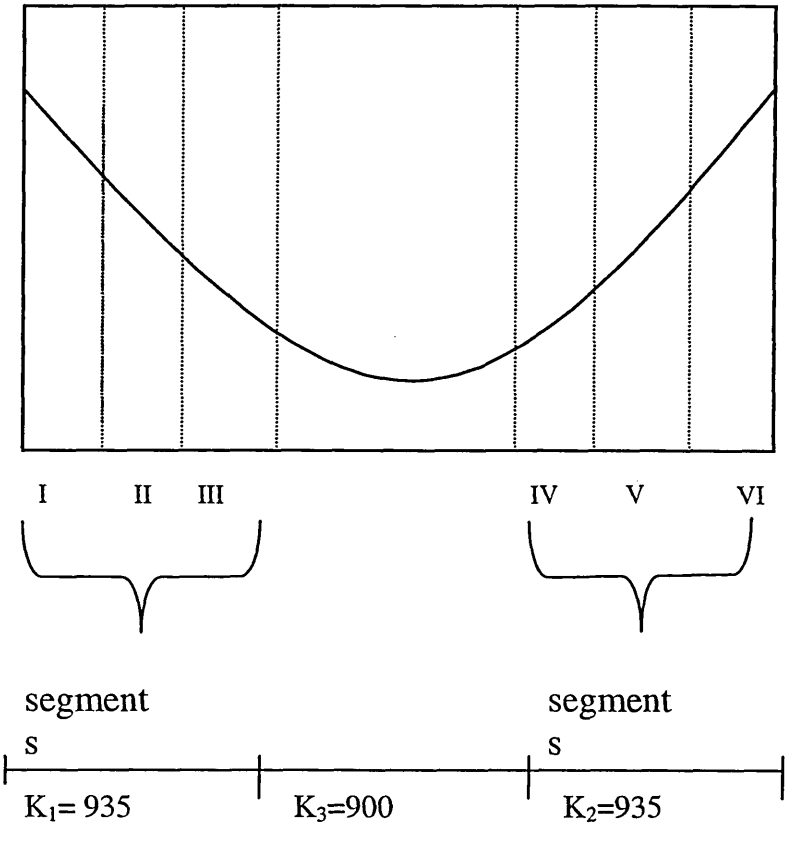

∴ Parabola can be defined as

$y = ax^2 - bx - c$

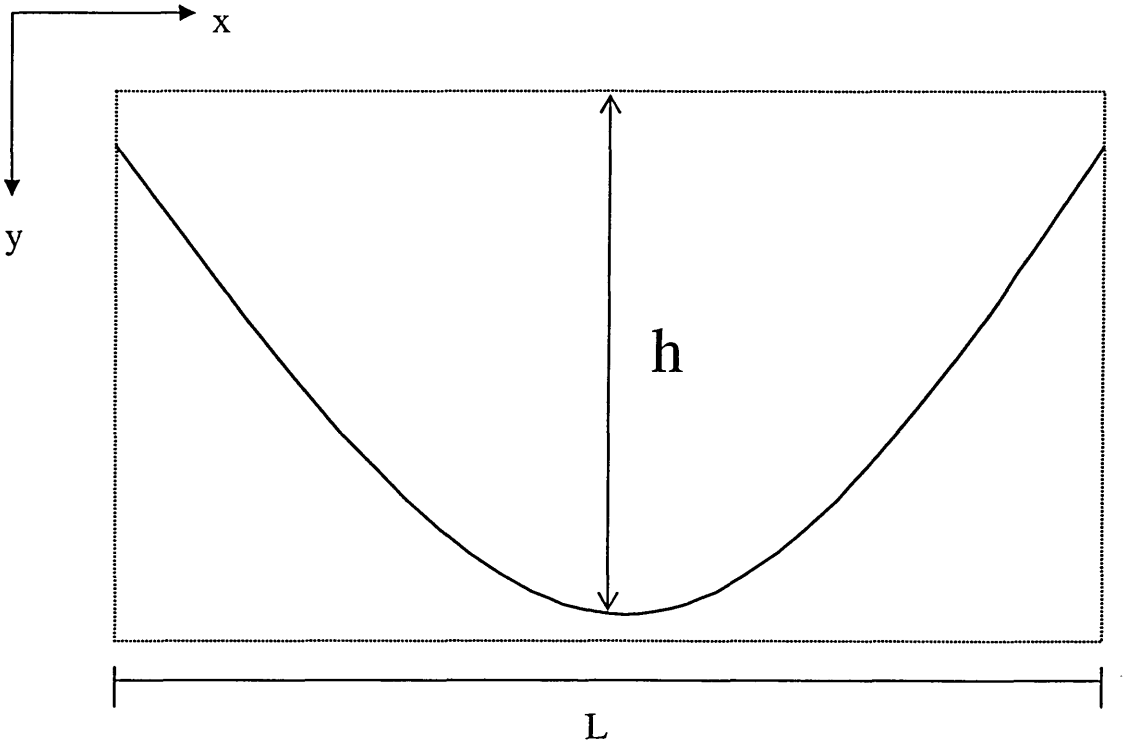

Substitute a, b and c into the above

$$y = \frac{-4h}{L^2}x^2 + \frac{4hLx}{L^2} - 0$$

$$y = \frac{-4h}{L^2}(Lx - x2)$$

Constant boundary conditions are as follows.

When	$x = k_1$	$y = h$	$k_1 = 935$ mm	$h = 203$mm
	$x = k_1 + k_3$	$y = h$	$k_3 = 900$ mm	

Length of curved profile can be derived as follows

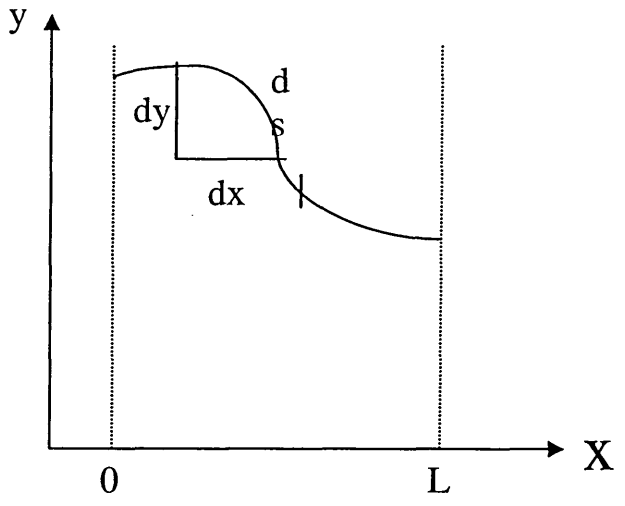

$y = ax^2 + bx$

$ds = \sqrt{dx^2 + dy^2}$ 1)

$y = ax^2 + bx$ differentiate

$dy = (2ax + b)\,dx$

substitute dy into 1)

$$ds = \sqrt{dx^2 + (2ax+b)^2 dx^2} \qquad \int ds = \int \sqrt{(2ax+b)^2 + 1}\, dx$$

$$\int ds = = \int_{x=0}^{x=l} \sqrt{(2ax+b)^2 + 1} dx$$

Integral solved in DERIVE math software programme

$$S = \frac{Ln\{[\sqrt{(b^2+1)}-1]x[\sqrt{4a^2L^2+4abL+b^2+1)+2al+b]}\}}{4a} + [\frac{b}{4a}+\frac{L}{2}][\sqrt{(4a^2L^2+4abl+b^2+1)}] - \frac{[b\sqrt{(b^2+1)}]}{4a}$$

A PRELIMINARY INVESTIGATION INTO THE COMPARATIVE PERFORMANCE OF FRP AND STEEL REINFORCEMENT IN MEDIUM AND HIGH STRENGTH CONCRETE

C Ellis

E M Ulas

Sheffield Hallam University

UK

ABSTRACT. This paper presents the preliminary findings of an investigation into the performance of medium to high strength concrete beams containing comparable areas of fibreglass-reinforced plastic(FRP) and high tensile steel reinforcing bars. Failure of the steel reinforced beams was predominantly in flexure for the more lightly reinforced sections and in shear-bond for those with the largest areas of reinforcement whereas the FRP reinforced beams exhibited mostly shear-bond type failure with the exception of the most lightly reinforced high strength concrete beam which failed in flexure. In general, increasing concrete strength had a marginal effect upon ultimate load capacity. The development of the concept of a 'performance quotient' is proposed as an efficiency comparator for elements of different types and composition.

Keywords: Fibreglass-reinforced plastic reinforcing bars(FRP), high tensile steel, medium strength concrete, high strength concrete, flexure, shear-bond, performance quotient.

Mr C Ellis is a Senior Lecturer in the School of Construction, Sheffield Hallam University. His main research interests are in the mechanical properties and optimisation of the performance and application of environmentally beneficial materials.

Mr E M Ulas is a Research Student in the School of Construction, Sheffield Hallam University. He is currently carrying out research into the behaviour and use of fibre-glass reinforced plastic reinforcement in concrete.

Appropriate Concrete Technology. Edited by R K Dhir and M J McCarthy. Published in 1996 by E & FN Spon, 2–6 Boundary Row, London SE1 8HN, UK. ISBN 0 419 21470 4.

INTRODUCTION

The current interest in non-ferrous reinforcement for use in concrete has occurred mainly as the result of the extensive problems associated with the degradation of existing buildings and structures resulting from the corrosion of steel rebar in adverse service environments[1]. Design practice for enhancing the durability of reinforced structures involves matching the assessed exposure with an appropriate amount of protection in terms of concrete grade and cover to rebar [2], [3]. This often produces a concrete with a performance potential in excess of that required for sustaining imposed service loads.

The use of fibre-reinforced polymers in concrete is not new[4] but improved manufacturing techniques and modified morphology have enabled a more efficient use of materials to produce elements which in strength and specific energy relative to performance excel that for ferrous reinforcement [5], [6]. Furthermore the reinstatement or strengthening of structures may provide another opportunity for the use of FRP in lieu of steel [7], [8]. Although, as with steel, at elevated temperatures and during exposure to fire, loss in structural integrity of FRP reinforced concrete elements could occur mainly because of the susceptibility of the resin component in the rebar.

This paper presents results from the first stage of an investigation into the behaviour of medium to high strength concrete beams reinforced with FRP and high tensile steel rebars and examines their comparative behaviour in the context of models currently used for conventional reinforced concrete design in the UK.

EXPERIMENTAL DETAILS

Materials

Concrete:-Portland cement (42.5) with uncrushed fine aggregate(M sand) and coarse aggregate (20-5mm gravel).

Reinforcement:- Steel and FRP reinforcement details are contained in Table 1

Table 1 Specified Reinforcement Details

REBAR TYPE	DENSITY kg/m^3	STRENGTH MPa	ELASTIC MODULUS GPa	BAR SIZES mm
High Tensile Steel	7,850	460 (Yield)	210	8, 12, 16
FRP	2,045	695(Ultimate)	50	8.8, 13.2, 16.4

Concrete Properties and Mix Proportions

Details of grades, mean strengths,W/C ratios and mix proportions are shown in Table 2.In addition, all concretes had slumps within the range 30 - 60mm.

CONCRET

GRADE (Nominal)

C40

C60

Manufactu

Two concr FRP) were specimens

Test Cube:

3 No. 100r test beam i

Beams cor

One beam FRP bars v

Testing of

Cubes wer capacity cc

Beams we displaceme displaceme rebar(A_r) ; Details and

Models

In general minor vari

Table 2 Concrete Properties & Mix Proportions

CONCRETE GRADE (Nominal)	MEAN STRENGTH MPa	W/C	MIX PROPORTIONS W	C	FA	CA
C40	59	0.39	155	400	735	1170
C60	75	0.29	175	615	415	1250

Manufacture & Curing of Test Specimens

Two concrete grades(C40 and C60), three Bar sizes and and two rebar types (steel and FRP) were investigated giving a total of 12 No. mixes for all combinations. Details of test specimens manufactured and curing are given below.

Test Cubes

3 No. 100mm side test cubes were manufactured from each mix and cured adjacent to the test beam in the laboratory. The results are in Table 3, column 7

Beams composition

One beam 103mm(breadth) x 203(depth) x 2,740mm(length) containing 2 No. steel or FRP bars was manufactured from each mix; further details shown in Figure 1.

Testing of Concrete Specimens

Cubes were tested at 42/43 days. and compression tests were carried out in a 3000kN capacity compression testing machine in accordance with BS1881 Part 116.

Beams were tested 42/43 days in four point bending in stroke control mode. A displacement transducer placed at mid-span enabled a continuous record of load versus displacement to be made. In order for failure mode transitions to be observed as area of rebar(A_r) and concrete grade were changed no specific shear reinforcement was included. Details and dimensions of testing configuration are also shown in Figure 1.

FAILURE MODELS AND MECHANISMS

Models

In general these follow the basis of design for steel reinforced members in BS8110 with minor variations and are summarised below with appropriate explanation (3).

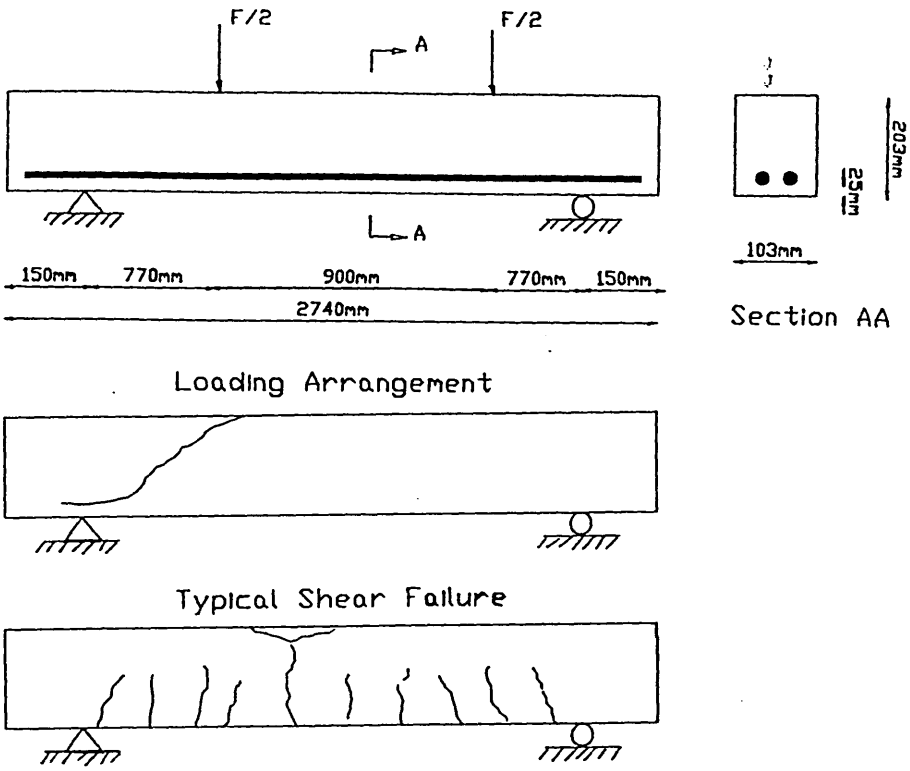

Figure 1 Beam Dimensions and Failure Modes

Ultimate Bending Moment(M_u)

The ultimate theoretical bending moment(M_u) = $C\,z = T\,z$, where

Force in concrete stress block (C) = $0.67f_c\,b\,d\,0.9x$, Force in rebar (T) = $f_y\,A_s$ Lever Arm (z) = (d - $0.45x$) , Depth to rebar(d) = 178mm , Beam width(b) = 103mm

Neutral axis depth(x) & Lever Arm(z)

For flexural failure in an under-reinforced section then at ultimate load and equating forces in concrete stress block (omitting materials factor, γ_m) with those in steel at yield gives:

$$0.67f_c\,b\,d\,0.9x = f_y\,A_s \quad \text{hence} \quad x = \frac{f_y\,A_s}{0.603f_c\,b\,d\,0.9}$$

$$\text{thus} \quad z = d - \frac{f_y\,A_s}{0.603f_c\,b\,d\,0.9}$$

Therefore
rebar stre
FRP whe
moment c

Resistanc

After BS
follows:
$v_{s(max)}$

where k_1

Failure m

Sketches c
cracks em
cases. In s
ultimate cc

Flexure fa
by crushin
ultimate m
its lever a
which app

M_u' =

thus;

Shear and
between lo
from a loa
rebar-concr
shear stress

vs =

Performan

To assess th
or energy e
influences a
the authors

Therefore the the ultimate moment(M_u) may be calculated from concrete cube strength(f_c) rebar strength(f_y) and area of rebar(A_s). It should be noted however that when applied to FRP where area of rebar is A_f this model equation is likely to give an underestimate of the moment capacity as there is minimal yield of this material at failure.

Resistance to Shear (vs)

After BS8110 (cl 3.4.5.4,Pt 1), but omitting the materials factor (γ_m). is expressed as follows:

$$v_{s(max)} = k_1 k_2 0.79 (100 A_f/(b d)^{1/3}(400/d)^{1/4}$$

where $k_1 = 1.0$ and $k_2 = (f_c/25)^{1/3}$ where fc not > 40MPa

Failure mechanisms

Sketches of the two principal failure mechanisms are shown in Figure 1. Initially vertical cracks emanating from the bottom surface within the middle section preceded failure in all cases. In some cases these were followed by inclined cracks towards the supports. At the ultimate condition beams failed in two alternate modes.

Flexure failure:- resulted from yielding of the steel or sudden rupture of the FRP followed by crushing of concrete in the compression zone within the mid-span section The actual ultimate moment (M_u') is calculated on the basis of the maximum load at failure(F in kN) its lever arm 0.770m and takes into account the self weight of the beam(kN) and span(m) which approximates to:

$$M_u' = \frac{\text{Failure Load x Lever Arm}}{2} + \frac{\text{Beam self-weight x Span}}{8}$$

thus; $M_u' = 0.385\,F + 0.40$ kNm

Shear and Shear-Bond failure:- namely Type I resulted from simple diagonal shear between load point and support and Type II by shear-bond failure; along a line emanating from a loading point and passing diagonally across the section then horizontally along the rebar-concrete interface between one loading point and a support (9). The average failure shear stress across section(vs) was taken as approximately:

$$vs = \frac{1000\,(F + \text{Beam self-weight})}{2\,b\,d} = 0.545(F + 1.3)\ \text{MPa}$$

Performance Quotient (Q_P)

To assess the efficiency of the beam in resisting load it is useful to relate cost (in real terms or energy equivalence) to strength(6). As an alternative to obviate the effect of capricious influences associated with market and manufacturing factors which vary from time to time, the authors propose a quotient relating the load capacity with the load bearing potential

based upon a measure of the strength of component materials and their average cross-sectional area throughout the beam. This may be expressed as:

$$Q_P = \frac{1000\,(F + 1.3)}{f_c\,(b\,d - A_r) + f_r\,A_r}$$

where A_r = area of rebar

f_c = concrete strength

f_r = rebar strength

RESULTS AND DISCUSSION

Table 3 contains details of the beam references and experimental programme together with rebar details in columns 1- 4. Results from the experimental work and those from the theoretical models are contained in columns 5 to 14.

Failure modes

All steel rebar beams failed in flexure except those with 16mm diameter rebars(TB9 & TB11 - shear-bond mode) whereas FRP rebar beams failed in shear-bond with the exception of C60 beam with 8.8mm diameter bars (TB8 - flexural rupture of bars) and C40 with 8.77mm diameter bars (TB6 - simple shear). See column 5.

Failure Load

Failure loads suggest that the steel rebar beams were more sensitive to rebar area and less sensitive to concrete grade than those reinforced by FRP, however cognisance must be taken of failure mode in this respect. See column 6.

Actual and Predicted Failure Mode and Capacity

The design models for steel rebar beams were consistent with the test results including the transition from flexural to shear failure as area of rebar was increased (see TB5,TB1 and TB9). When applied to FRP beams these overestimated shear capacity but underestimated flexural capacity (TB8); the latter finding contrasts with some recent work by Brown and Bartholomew [10]. See colunms 5,6 & 10 - 13.

Performance Quotient

For flexural failure the Performance Quotient for steel and FRP reinforced beams (TB5 & TB8) were comparable although not for the shear type failures. See column 14.

LOAD VERSUS DEFLECTION BEHAVIOUR

Load versus deflection behaviour for C40 concrete with 8mm steel rebars (TB5) compared with C60 concrete with 8.8mm FRP(TB8) rebars are shown in Figure 2. This suggests that although the FRP reinforced concrete displays a higher deflection at a similar failure load , the toughness of the 'FRP' beam (indicated by the area under the Load vs Deflection curve) is much higher than that for the steel beam of a similar performance quotient for flexural failures.

Table 3 Summary of beam properties and performance

Table 3 Summary of beam properties and performance

1	2	3	4	5	< 6	Column 7	Number 8	> 9	10	11	12	13	14
Beam Code	Concrete grade	Rebar No. Dia/Type	Area Rebar mm2	Failure Mode	Failure Load kN	fc Cube Str. MPa	NA Depth mm	Lever Arm mm	Mu' Actual kNm	Mu Theor kNm	vs Actual MPa	vs(max) Theor MPa	Perform. Quotient Actual
TB5	C40	2-08S	101	Flexure	24	61	12	173	9.64	8.01	0.57	0.93	0.01863
TB1	C40	2-12S	226	Flexure	50	55	31	164	19.65	17.08	1.20	1.21	0.0411
TB9	C40	2-16S	402	Shear-Bond	68	61	49	156	26.58	28.85	1.63	1.47	0.04794
TB6	C40	2-08.77F	121	Shear	20	69	20	169	8.10	14.20	0.48	0.98	0.01369
TB2	C40	2-13.19F	273	Shear-Bond	34	57	54	154	13.49	29.23	0.81	1.29	0.02531
TB10	C40	2-16.44F	425	Shear-Bond	29	51	93	136	11.57	40.13	0.69	1.50	0.02216
TB7	C60	2-08S	101	Flexure	24	73	10	173	9.64	8.02	0.57	0.93	0.01574
TB3	C60	2-12S	226	Flexure	48	72	23	168	18.88	17.44	1.15	1.21	0.03044
TB11	C60	2-16S	402	Shear-Bond	58	75	40	160	22.73	44.77	1.39	1.47	0.0339
TB8	C60	2-08.77F	121	Flexure	26	72	19	170	10.41	14.24	0.62	0.98	0.01678
TB4	C60	2-13.19F	273	Shear-Bond	38	79	39	161	15.03	30.49	0.91	1.29	0.02127
TB12	C60	2-16.44F	425	Shear-Bond	28	76	62	150	11.18	44.24	0.67	1.50	0.01543

Key:

Steel rebar(S) FRP rebar(F)

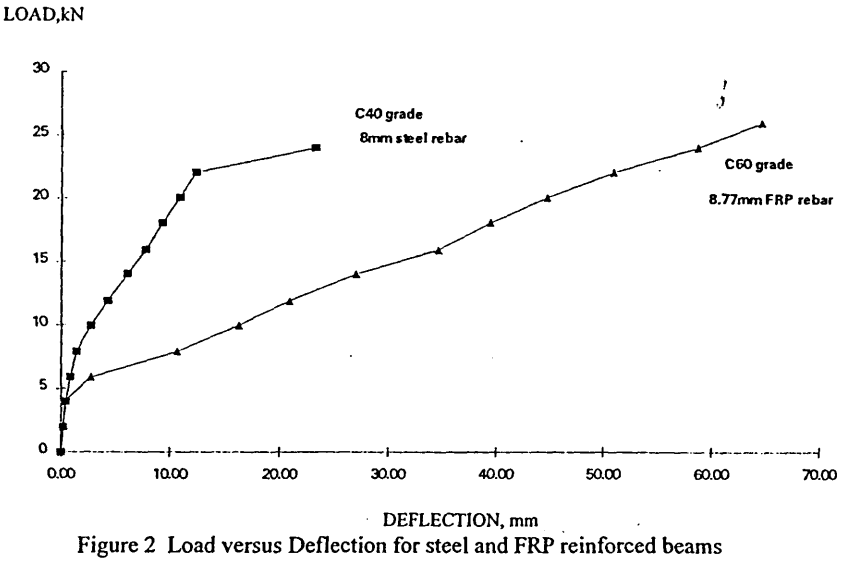

Figure 2 Load versus Deflection for steel and FRP reinforced beams

Figue 3 shows a similar curve comparing 16mm steel rebars with 16.44mm FRP rebars for C60 concrete (TB11 & TB12) and indicates that shear-bond failure tends to favour the perfomance of the steel rebar beam compared with the FRP rebar beam.

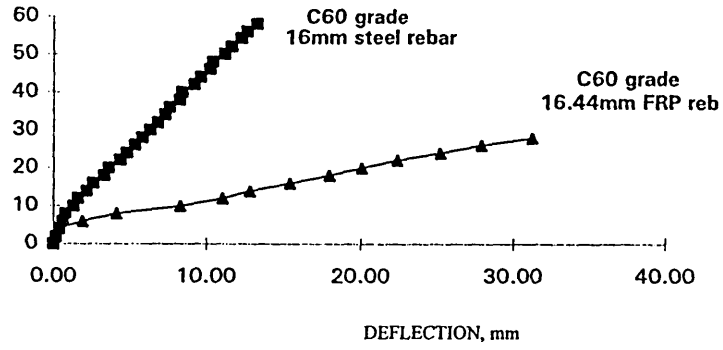

Figure 3 Load versus Deflection for steel and FRP reinforced beams

PRACTICAL IMPLICATIONS OF RESULTS

The results suggest that performance of the FRP beams containing the higher areas of tension reinforcement could be greatly enhanced by improving shear-bond capacity hence utilising their maximum flexural strength capability. Certain properties of FRP should enable this to be attained more economically than with steel rebar. It is proposed to explore new design strategies in future stages of the investigation.

CONCLUSIONS

1. The mode of failure appears to be influenced by rebar type and area although concrete grade was a confounding factor for FRP reinforced beams.

2. Conventional design models for steel reinforced concrete may require modification for FRP rebar beams especially for shear failure.

3. For flexural failure FRP beams display a greater capacity to absorb energy than steel for similar load capacity, although they exhibit reduced stiffness.

4. A performance quotient relating load capacity to 'section potential' for similar geometry may be a useful efficiency comparator.

5. The development of a design strategy for improving shear-bond performance without significantly increasing rebar area could be applied to FRP beams to enhance their performance.

ACKNOWLEDGMENTS

The authors wish to express their gratitude to International Composties and International Gratings Ltd for the provision of materials and technical advice and information and also to Sheffield Hallam University for provision of facilities and in particular the invaluable assistance of the technical staff in the School of Construction.

REFERENCES

1. CLARKE J.L. Alternative Materials for the Reinforcement and Prestressing of Concrete, First Edition1993, 201pp.

2. BRITISH STANDARDS INSTITUTION, BS 5328:1991 Concrete. Guide to Specifying Concrete. Part 1.

3 BRITISH STANDARDS INSTITUTION, BS 8110:1985 Structural Use of Concrete.Part 1.

4. NAWY, E.G. et al. Behaviour of Fiberglass Reinforced Concrete Beams, Journal of Structural Division ASCE, September 1971, pp2203-2215.

5. ERKI, M.A. & RIZKALLA, S.H. FRP Reinforcement for Concrete Structures, Concrete International, June 1993, pp48-53.

6. BRITISH CEMENT ASSOCIATION.UK Cement Manufacture and the Environment. 13pp.

7. SAADATMANESH, H. Fiber Composites for New and Existing Structures, ACI Structural Journal, V91, No 3, May-June 1994, pp346-354.

8. LARRALDE, J. et al. Fiberglass Reinforced Plastic Rebars in Lieu of Steel Rebars, ASCE 7th Annual Structures Congress, San Francisco, California, May 1989, pp1-8.

9 MARTIN, L.H. et al. Concrete Design to BS 8110,Edward Arnold,London 1989. 477pp

10. BROWN, V.L. & BARTHOLOMEW, C.L. FRP Reinforcing Bars in Reinforced Concrete Members, ACI Materials Journal, V90, No 1, January-February 1993, pp34-39.

STRU

ABSTRA
applicatio
University
This paper

Keywor

Dr Khos
Catholic
Naradov
London,
research
widely an

Mr Alex
Federal U
at the san

Mr Hum
Sc. stude

Dr Norm
Federal U
Catholic
Marie Cu
concrete.

Appropriat
by E & FN

THE INSTITUTION OF STRUCTURAL ENGINEERS

YOUNG RESEARCHERS' CONFERENCE

1999

23RD MARCH 1999

11, Upper Belgrave Street, LONDON SW1X 8BH.

Name of delegate : **Esref Ulas** **Abstract No. 37**
Establishment : **Sheffield Hallam University**

Project Title : **Investigation Into the Performance of Fibre Reinforced Plastic(FRP) Reinforcement Used in Concrete Elements**

Corrosion of steel reinforcement has always been a major problem for concrete construction, particularly, located in aggressive environments such as marine structures, bridges, chemical plants. Fibre composites have become popular in the civil engineering field in recent years. The area of research and development of fibre composites in the concrete industry has been related to corrosion resistance fibre reinforced plastic(FRP) reinforcing bars.

The project investigates and assesses the performance and the efficiency of concrete beams reinforced with relatively low cost glass fibre reinforced plastic rebars in comparison with beams reinforced with conventional steel using a variety of rebar configurations and materials. As a preliminary investigation, a number of singly reinforced rectangular beams using different type and diameter of reinforcing bars with different grades of concrete, have been manufactured and tested under two point bending.

The results obtained from the experimental work so far, indicate that the potential contribution of the fibre reinforced plastic rebars to the flexural and shear capacities of concrete need to be identified and defined more clearly and there are some advantages in the use of novel rebar geometry in enhancing beam properties.

Further investigative work focuses upon the evolution of models to accurately describe the behaviour of enhanced performance elements with a view to incorporating the findings into standards of codes of practice for concrete design using FRP rebars with state of the art materials currently use in construction.

A comparison with steel as a reinforcement in concrete elements

FOCUS

This poster presents the methodology and findings from an ongoing programme of investigation into the comparative performance of Fibre Reinforced Plastic (FRP) and steel reinforced concrete The diameter sizes of the reinforcing bars are shown in Photo !

Photo 1 The »ize of Steel and FRP bars

The focus in this instance is on the applications to medium (C40) and high strength CfiO) concrete beams under different loading regimes.

BACKGROUND

During the past decade, increasing interest has been shown in the utilisation of alternative or complementary materials to steel for use as reinforcement in concrete. Several factors such as cost, utility, inferior engineering properties have militated against their widespread use.

The advent of pultrudcd glass-libre reinforced polyester (FRP) bars of relatively low cost suggests a potential for use in situations where there is a serious risk of corrosion and in other specialised applications such as the avoidance of radio wave interference.

METHODOLOGY

Sending Test Set up

Two-point bending test was conducted in the laboratory. The beams were subjected to two equal loads symmetrically placed on the mid-span as shown in Photo 2. The beam details in conjunction with the reinforcement arrangements are included in Figure I

Photo 2 Two-point bending (esc up

L ,. ___

Figure 1 The beam details and the reinforcement arrangements

Test Regime

An automatic data acquisition system was used to monitor loading, mid-span deflection and deformations of both concrete and the reinforcements see Photo 3).

Photo 3 (from right to left) The control panel, plotter for load vs deflection response and computer data store

The load applied to the beam was increment of 2kN. The behaviour of the beams, in terms of crack patterns, load-dctlection histories, failure mode and load carrying capacities were monitored during the test.

MATERIAL DATA

Mechanical Properties *of* Materials:

REINFORCEMENT

Propertlos (Units)	Types		
	Steel	j	FRP
Strength (MPa)	".160	:	"695
Elastic Modulus (GPa)	210		50
Density (kg/ml)	7050		2045

"Yield strength "Ultimate tensile

Tabic I The typical mechanical properties of steel and FRP reinforcements used In this study

CONCRETE

	Properties (Units)			Mix Proportions	
Nominal Grades	Strength (MPa)	Density (kg/ml)	w/c	FA %	Density (kg/rrr*)
C40	60	2396	0.42	39	429
C60	75	2435	0.29	25	615

w/c (water cement ratio) rA (Fine Aggregate)

Table 2 The properties and mix proportions of the concrete erodes used In this study

RESULTS AND ANALYSIS

Crack patterns and failure inodes

L *J U -*

Figure 2 Typical cracks and shear failure observed in FRP reinforced beams

Figure 3 Typical cracks and flexural failure observed in steel reinforced beams

Photo 4 Instantaneous catastrophic tension of C-40 Grade 208mm steel reinforced beam

Figure 4 Typical load versus deflection beha concrete beams reinforced with FRP and .tc

CONCLUSION

- The numbers of cracks in FRF reinforced b less and deeper than the steel reinforced bea (see Figure 2 & 3).
- The mode of failure appears to be influence type and area although concrete grade was a confounding factor for FRF reinforced bean
- For flexural failure FRF reinforced beams di greater capacity to absorb energy than steel ones for similar load capacity, nevertheless, t reduced stiffness (see Figure 4).

  Deflection of FRF reinforced beams is large: steel reinforced beams due to lower modulu; elasticity of FRP bars.

MAIN CONTRIBUTION

The development of a design strategy for enhar performance of FRF beams e.g. by improving li capacity relative to concrete quality and bar are: investigated and it shows potential for field appl

Esref Ulas
School of Environment and Developt
The Centre for the Built Environmer
Supervised by Cliff Ellis

§ > | *Sheffield Hallam Univers*